IMPORTANCE OF ACTIVE SITES IN COAL CHAR AND CARBON GASIFICATION

L. R. Radovic, P. L. Walker, Jr. and R. G. Jenkins

Department of Materials Science and Engineering
The Pennsylvania State University, University Park, PA 16802

INTRODUCTION

A fundamental understanding of the kinetics of coal gasification requires the knowledge of the role of (a) carbon active sites, (b) inherently present catalysts and (c) diffusivity of the reactant gases within the pores of the (usually) rapidly devolatilized char (1). The pressing need for design data for the new generations of coal gasification processes probably justifies the great number of essentially empirical kinetic studies that provide useful correlations, but in which the above factors are lumped into overall empirical parameters (e.g., reactivities) which cannot be related to measurable physical properties of the chars. The predictive capabilities of such correlations and the possibility of their extrapolation are uncertain, at best. A parallel effort is needed in order to obtain more fundamental kinetic parameters.

Many coal researchers have not fully realized the relevance, to the kinetics of coal gasification, of studies performed on relatively pure and highly crystalline materials such as graphitized carbon blacks and graphite. A recent comprehensive review by Essenhigh (2) emphasizes the value of these studies in helping to understand coal reactions. The purpose of this paper is to provide experimental evidence for the usefulness (and necessity of application!) of the concept of active sites in understanding the gasification behavior of lignite chars.

EXPERIMENTAL

A North Dakota lignite (3) was pretreated with HCl and HF in order to remove essentially all the inorganic constituents (4). Chars were prepared by both slow and rapid pyrolysis in N_2 (99.99% purity). Slow pyrolysis (10 K/min) was performed in a conventional horizontal-tube furnace at temperatures between 975 and 1475 K and residence (soak) times up to 1 h at final temperature. Rapid pyrolysis (~ 10^4 K/s) was effected in an entrained-flow reactor (5,6) at 1275 K. The residence time was varied between 0.3 s and 5 min. The reactivity of the various chars and carbons of increasing crystallinity, from Saran char to SP-1 graphite, was determined by isothermal thermogravimetric analysis (TGA) in 0.1 MPa air. Weight changes were recorded continuously as a function of time. The maximum slope of the burn-off vs. time plot (R_{max}) was used as a measure of gasification reactivity. In a series of preliminary runs, discussed in detail elsewhere (6), appropriate reaction conditions were selected to eliminate interparticle and intraparticle heat and mass transfer limitations. The reported rates are, therefore, thought to be intrinsic, chemically controlled values.

Elemental analyses were performed on the chars in order to determine their C/H ratios and thus the extent of their devolatilization. Physical adsorption of CO_2 at 298 K was measured and micropore volumes were determined using the Dubinin-Radushkevich equation (7). The concentration of carbon active sites (active surface area) was measured by oxygen chemisorption on the chars at 375 K and 0.1 MPa air (6,8).

RESULTS

Table 1 gives the C/H ratio, micropore volume and oxygen chemisorption capacity of the demineralized (Dem) lignite and selected Dem-chars. Unless otherwise noted

Table 1

SELECTED PROPERTIES OF DEMINERALIZED LIGNITE AND CHARS PRODUCED UNDER DIFFERENT PYROLYSIS CONDITIONS

Sample	C/H (atomic, daf)	Micropore Volume (cm^3(STP)/g)	Oxygen Chemisorption Capacity (wt% oxygen)
Dem-Coal	1.2	--[a]	--
R - 0.3 s[b]	3.8	93[c]	7.2
R - 1.2 s	--	98	5.4
R - 1.8 s	7.2	107	4.3
R - 5 min	13	104	2.3
S - 0 h[d]	5.8	--	--
S - 30 min	--	98	--
S - 1 h	11	--	1.6
S - 1 h (975 K)	--	--	3.4
S - 1 h (1475 K)	--	--	0.72

[a]Not determined

[b]R = rapid pyrolysis

[c]At 298 K (near critical temperature for CO_2) the density of liquid CO_2 is about 1.0 g/cm^3. Thus the liquid volume is about 0.2 cm^3/g.

[d]S = slow pyrolysis

in parentheses, all char samples were prepared at 1275 K. Figure 1 shows the effect of pyrolysis residence time at 1275 K on the subsequent reactivity of the char. Significant char deactivation is observed with increasing pyrolysis severity. A similar effect is observed by increasing the temperature of pyrolysis. Figure 2 shows the Arrhenius plots of reactivity for chars and carbons of increasing purity and crystallinity. The Saran char was prepared by slow pyrolysis of Saran at 1225 K for 3 h.

DISCUSSION

The demineralized lignite can be considered as the most convenient "model compound" for studying the uncatalyzed coal char gasification reactions at a fundamental level. It contains about 2000 ppm of impurities, compared to about 8% in the original lignite. This is still a relatively high level of potential catalysts when compared to carbons of higher purity also used in this study: spectroscopically pure natural graphite (SP-1, Union Carbide Corp.), with < 6 ppm; graphitized carbon black (V3G, Cabot Corp.), with < 120 ppm; Saran char (Dow Chem. Co.) with < 100 ppm. However, most of the remaining inorganics are present in the form of relatively poorly dispersed discrete minerals (such as clays and pyrite) which are not thought to be very efficient in catalyzing char gasification in air (9).

Even though the weight loss during rapid pyrolysis at 1275 K is essentially complete after about 1 s (6), it is seen in Table 1 that the evolution of hydrogen is a relatively slow process. There exists a qualitative correlation between the decrease in char reactivity and the increase in C/H ratio of the chars. It is also seen in Table 1 that the micropore volume of the Dem-chars is relatively high, of the same order of magnitude as for typical carbonaceous adsorbents (~ 0.3 - 0.4 cm^3/g). Accordingly, the total surface area is also expected to be high. The oxygen chemisorption capacity, calculated from the amount of CO and CO_2 evolved upon the decomposition of the carbon-oxygen complexes, is seen to decrease by a factor of about ten with increasing severity of pyrolysis.

Table 2 summarizes and integrates the reactivity and surface characterization results. Total surface area (TSA) was calculated using the Polanyi-Dubinin approach (10), by assuming that micropore volume is approximately equal to the monolayer capacity. It is concluded that if this is a measure of the true total surface area, then TSA is not a relevant reactivity parameter. A difference in observed rates (per unit mass) of about five orders of magnitude (column 4) is reduced only by about two orders of magnitude when TSA is taken into account (column 5).

Oxygen chemisorption capacity was transformed into active surface area (ASA) by assuming that each chemisorbed oxygen atom occupies about 0.08 nm^2 (11). The values are given in column 3 of Table 2. Rate constants per unit ASA are given in column 6. It is seen that a difference in observed reactivities of Dem-chars of a factor of twelve is reduced to within a factor of three when expressed on this basis. The value of ASA for the Saran char was obtained under conditions similar to those used in this study. In the case of V3G, chemisorption was effected at 575 K and 65 Pa O_2, also in the absence of gasification. It is assumed that the value of oxygen content thus obtained is also a measure of ASA. For SP-1 graphite the geometric edge area was taken as ASA. It is seen that differences in observed reactivities of about five orders of magnitude between the most reactive Dem-char and the least reactive SP-1 graphite are reduced to within one order of magnitude when their ASAs are taken into account. The relatively small differences in the rate constants in column 6 are attributed to the effects of catalysis. It is seen that lower values are consistently obtained for chars (carbons) of higher purity. Also, in lignite chars which have been subjected to more severe pyrolysis conditions the dispersion of the inherent catalyst (CaO) was shown to be lower (6). Catalysis is expected to play a greater role in chars which have undergone milder heat treatment. This is, indeed, suggested by the relatively high rate constants of the short-residence-time and low-temperature chars.

CONCLUSIONS

The oxygen chemisorption capacity of demineralized lignite chars at 375 K and 0.1 MPa air gives an indication, at least from a relative standpoint, of the concentration of carbon active sites in them. It certainly provides an index of their gasification reactivity. The commonly observed and heretofore empirically treated coal char deactivation with increasing severity of pyrolysis conditions was thus correlated with a decrease in a measurable fundamental property of the chars: carbon active surface area. The importance of the concept of carbon active sites in gasification reactions was also illustrated for carbons of increasing crystallinity from a Saran char to SP-1 graphite. Total surface area, as estimated by the Polanyi-Dubinin approach, was shown not to be a relevant reactivity parameter.

ACKNOWLEDGEMENTS

This work was supported by the Gas Research Institute on Contract No. 5014-363-0235.

REFERENCES

1. Walker, P. L., Jr., Fuel 60, 801 (1981).

2. Essenhigh, R. H., "Fundamentals of Coal Combustion," in "Chemistry of Coal Utilization," 2nd Suppl. Vol. (M. A. Elliott, Ed.), Wiley, New York, 1981, p. 1153.

3. Penn State/DOE Coal Data Base, PSOC-246, Coal Research Section, The Pennsylvania State University.

4. Morgan, M. E., Jenkins, R. G. and Walker, P. L., Jr., Fuel 60, 189 (1981).

5. Scaroni, A. W., Walker, P. L, Jr. and Essenhigh, R. H., Fuel 60, 71 (1981).

6. Radovic, L. R., "Importance of Catalysis and Carbon Active Sites in Lignite Char Gasification," Ph.D. Thesis, The Pennsylvania State University, 1982.

7. Dubinin, M. M., Chem. Rev. 60, 235 (1960).

8. Radovic, L. R., Walker, P. L., Jr. and Jenkins, R. G., "Importance of Carbon Active Sites in the Gasification of Lignite Chars," Fuel, in press.

9. Tomita, A., Mahajan, O. P. and Walker, P. L., Jr., ACS Preprints, Fuel Chemistry Division 22(1), 4 (1977).

10. Mahajan, O. P. and Walker, P. L., Jr., "Porosity of Coals and Coal Products," in "Analytical Methods for Coal and Coal Products," Vol. I (C. Karr, Ed.), Academic Press, New York, 1978, p. 125.

11. Laine, N. R., Vastola, F. J. and Walker, P. L., Jr., J. Phys. Chem. 67, 2030 (1963).

12. Taylor, R. L., "Low-Temperature Gasification and Chemisorption Studies of the Carbon-Oxygen Reaction," Ph.D. Thesis, The Pennsylvania State University, 1982.

Table 2

SURFACE AREAS AND REACTIVITIES OF DEM-CHARS AND CARBONS OF INCREASING PURITY AND CRYSTALLINITY

Sample	TSA (m^2/g)	ASA (m^2/g)	R_{700} (g/g/h)	R_{700} (g/m^2TSA/h)x10^3	k_{700} (g/m^2ASA/h)x10^3
R - 0.3 s	630	225	1.8	2.9	8.0
R - 1.8 s	730	133	0.94	1.3	7.1
R - 5 min	710	73	0.30	0.42	4.1
S - 30 min	665	--[a]	0.28	0.42	--
S - 1 h	--	50	0.25	--	5.0
S - 1 h (975 K)	--	108	1.2	--	11
S - 1 h (1475 K)	--	25	0.15	--	6.0
Saran char	1,224[b]	50[b]	0.15	0.12	3.0
CB-Monarch 700	206	--	0.05	0.24	--
GCB-V3G	63[b]	< 1[b]	~2×10^{-4}[c]	0.0032	> 0.2
SP-1 graphite	1.8	< 0.1	~2×10^{-5}[c]	0.011	> 0.2

[a]Not determined

[b]Data taken from Ref. 12

[c]Extrapolated value

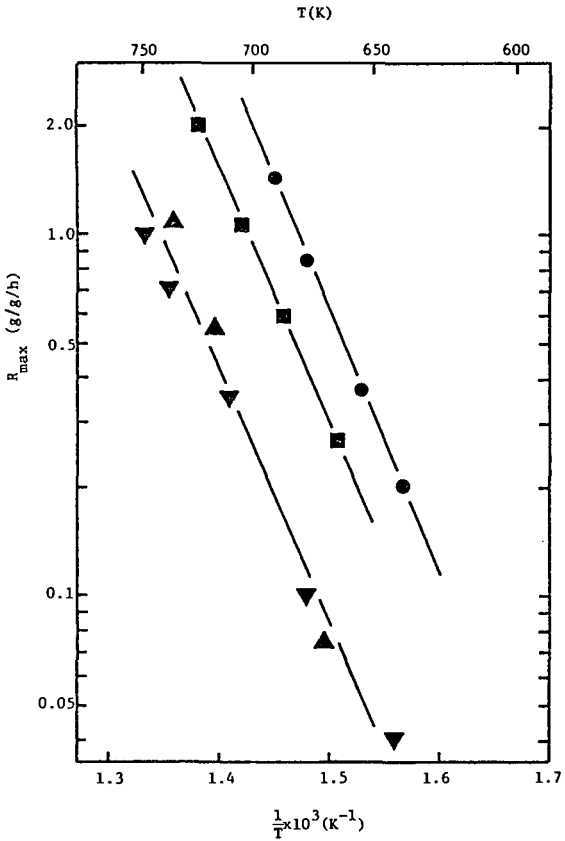

Figure 1

Effect of Pyrolysis Residence Time Between 0.3 s and 1 h on the Reactivity of Dem-Char. Pyrolysis Temperature, 1275 K (0.1 MPa Air):
● R - 0.3 s; ■ R - 1.8 s; ▲ R - 5 min; ▼ S - 1 h

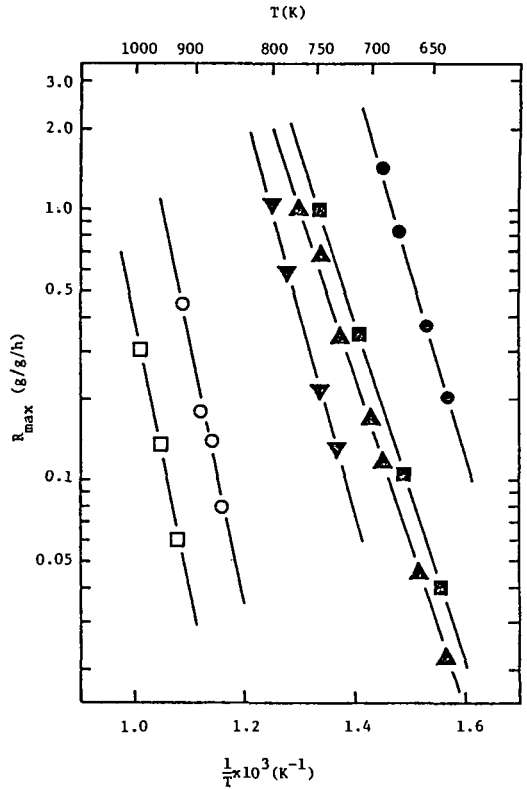

Figure 2

Arrhenius Plots of Reactivity of Chars and Carbons of Varying Degree of Crystallinity and Purity (0.1 MPa Air):
● R - 0.3 s; ■ S - 1 h; ▲ Saran Char; ▼ Carbon Black (Monarch 700); ○ Graphitized Carbon Black (V3G); □ SP-1 Graphite

TRANSIENT KINETIC STUDIES OF CHAR REACTIONS IN A GRADIENTLESS REACTOR SYSTEM -- CO_2 GASIFICATION

O. Sy and J. M. Calo

Division of Engineering
Brown University
Providence, Rhode Island 02912

1. INTRODUCTION

Although a voluminous literature exists concerning the study of coal char-gas reaction systems, the understanding of the actual mechanisms and the roles of heat and mass transport in the overall conversion process, are still far from complete. One difficulty in determining intrinsic reaction mechanisms in many previous studies can be at least partially attributed to the use of "steady-state" conditions. The results of such experiments can be explained equally well by a few plausible models which all yield roughly the same overall gasification rate. Discrimination among candidate models is difficult under these conditions, and there is no guarantee that the model finally selected actually reflects the true mechanism over a wide range of operating conditions. Also, "steady-state" rate measurements reveal relatively little concerning the detailed sequence of elementary steps that constitutes the intrinsic reaction mechanism.

In addition to difficulties in model discrimination, the types of laboratory reactors which have been used in coal gasification kinetic studies may have also contributed to data interpretation problems that are well known for heterogeneous catalytic systems [e.g., see (1-3)].

The primary objective of the current work is to overcome most of these problems in order to develop a fundamental description of the reaction mechanisms of the heterogeneous coal char-gas reactions using an experimental system and techniques which allow the elementary steps to be better identified. More specifically, the approach involves the application of a "gradientless" reactor system coupled with a supersonic, modulated molecular beam mass spectrometer, and transient response techniques to char gasification kinetic studies. The transient behavior of a reaction system as it proceeds from one steady-state to another upon perturbation of system state variables exhibits characteristics reflective of the nature of the detailed kinetic mechanism. Furthermore, in addition to transient data, the usual steady-state results are available as well. Thus the transient response method is employed as an aid in model discrimination, mechanism determination, and, ultimately, parameter estimation.

The use of an internal recycle, "gradientless" reactor serves a dual purpose: (1) it simplifies the mathematical analysis of the transient data due to the resultant lumped parameter description of the transient response; and (2) it significantly reduces the influence of interphase mass and heat transport gradients. The principal advantages of this type of reactor over other common reactor types have been well documented in the literature [e.g., see (3-11)].

Finally, in order to obtain the transient data, the reactor must be coupled to a responsive analytical technique which allows continuous measurement of the transient product concentrations. Mass spectrometry is one such technique compatible with the transient response method. On-line mass spectrometry has been employed by several researchers in studies of the devolatilization of coal under vacuum conditions (12-14). Rapid sampling while operating at the high pressures relevant to the present study can be accomplished by allowing the product gases after pressure letdown to expand through a sonic orifice as a supersonic, adiabatic free jet into a differentially-pumped vacuum system. The rapid expansion into the vacuum "freezes" the relative compositions of the product gases when the sampled gas attains molecular flow. By skimming the core of the jet, a molecular beam can be formed. The resultant beam is further modulated to discriminate between the in-

stantaneous behavior of the beam species and the same species in the background of the mass spectrometer vacuum envelope (15,16).

The adaptation of these techniques to the current purpose is set forth below. The char-carbon dioxide reaction system is used to illustrate the efficacy of the approach. Other char-gas reaction systems and related studies are being pursued in a similar manner.

2. EXPERIMENTAL

2.1. System Description

A schematic of the experimental apparatus developed for the current transient kinetic studies is presented in Figure 1. Essentially, it consists of: (a) a continuous gas flow, fixed solids, "gradientless" (Berty-type) reactor; (b) an automatic switching gas addition valve network for generating concentration perturbations under conditions of constant flowrate, temperature, and pressure; and (c) a supersonic, modulated, molecular beam mass spectrometer for measuring the transient behavior of the concentrations of the product gases.

A typical experimental run might proceed in the following manner. Steady-state is first established with inert gas (e.g., argon) flowing through the reactor (maintained at the desired temperature and pressure), and with reactant gas (e.g., carbon dioxide) flowing through the purge line. At time zero, the inert gas is instantaneously replaced by the reactant gas now flowing through the reactor, and the reaction is thereby initiated. The switching is done in such a manner as to insure the same volumetric flowrate through the reactor, in spite of the change in gas species. This results in a well-defined step function increase of the reactant to the reactor. The transient response of the reaction system to this perturbation is then monitored with the beam sampling system at the reactor exit.

The experimental system has been designed to operate at conditions relevant to commercial coal gasification conditions (e.g., up to 500 psi at 1400°F, and even higher pressures at lower temperatures, as determined primarily by the manufacturer's specifications for the reactor). Also, the reactor space time (the ratio of the reactor gas phase volume to the volumetric flowrate) can be varied over the range 0.01 - 1.0 min.

The preceeding, necessarily brief description is intended to convey only a general overview of the apparatus and its mode of operation. For a thorough discussion of the important and interesting details of the development of the apparatus, and the adaptation of transient kinetic techniques to char gasification, see reference (17).

2.2. System Performance

Reactor mixing performance curves were obtained by imposing step changes in the reactor feed from argon to carbon dioxide at constant volumetric flowrate, pressure, and temperature, and recording the resultant transient response. Due to considerable adsorption of test gases by the char, nonporous 3 mm glass beads were used in the basket for these studies. The resultant data were all clearly exponential, in accordance with well-mixed reactor behavior, and the corresponding time constants were close to expected values. The total gas mixing volume deduced from these experiments was found to be 241.4 cm^3, which is quite reasonable in view of the fact that the total internal reactor volume is 275 cm^3, of which approximately 30 cm^3 is presumed to be dead volume located beneath the impeller.

In order to assess the relative influence of interphase heat and mass transfer on intrinsic chemical kinetic rates, the reactor internal recycle ratio, R, and superficial velocity, v_o, through the char bed were determined by measuring the pressure drop across the char bed in the same manner as described by Berty (18); i.e., $R = A\ v_o/q$, where A is the cross-sectional area of the basket (20.27 cm^2) and q is the volumetric flowrate at reactor conditions. For typical experimental conditions with space time τ = 15 s, free gas volume V_g = 220 cm^3 (V_g = 241.4 cm^3 - W/ρ_s, where W is the weight of dry char in the basket, ρ_s is the solid density and 241.4 cm^3 is the total free gas volume in the reactor from the glass beads experiments), and impeller speed of 2800 RPM, the superficial gas velocity deter-

mined from our calibration is v_o = 13.72 cm/s (0.45 ft/s). With a flowrate of q = 14.67 cm^3/s the recirculation ratio is R = 19, which is sufficient to guarantee good mixing and gradientless operation.

The influence of interphase mass transfer limitation on measured kinetics for a particular set of experimental conditions can be assessed from the Damkohler number, $Da = k_1 C_{so}(1-\theta)/k_m a_m/RT)$, which is the ratio of the reaction rate, (as represented by the kinetic rate constant for the oxygen-exchange reaction; see below), and the effective interphase mass transfer coefficient for CO_2 which can be estimated from the j-factor for interphase mass transfer, j_D (e.g., see (19),p.395). For the experimental conditions used in the current work, it was found that $1 \times 10^{-6} < Da < 9 \times 10^{-4}$. Since Da<<1, the reaction is definitely not limited by interphase mass transport. The relative importance of intraphase diffusion is considered in the Discussion.

The interphase heat transfer limitation can also be evaluated from the Damkohler number by making use of the Chilton-Colburn analogy between mass and heat transfer in packed beds (e.g., see (19), p. 396). For typical reaction conditions, assuming a heat of reaction of +41.23 kcal/g mol for the overall CO_2 - char gasification reaction, the estimated temperature difference between the surface of the char, T_s, and the bulk fluid, T_b, is $5 \times 10^{-6} < (T_b - T_s)/T_b < 4 \times 10^{-3}$. Thus, for a high operating temperature like 972 K, $(T_b - T_s)$ can be as large as 4°C. Actual temperature differences between the solid and gas in the char bed are expected to be less than this due to radiation. Therefore, it can be conservatively stated that the interphase heat transfer limitation is not significant in the current studies.

Based upon the preceeding performance data and numerical estiamtes, the particle size of the activated coconut (Fischer) char selected for the experiments reported on here was > 14 mesh. With an average particle diameter of about 1.6 mm, the resultant superficial velocity through the char bed at maximum impeller RPM should effectively eliminate interphase heat and mass transfer gradients, and provide a relatively high internal recycle ratio for space times in the range of 12 to 20s, that were found to be optimum for the current experiments.

3. KINETIC MODELING

The general treatment of transient kinetic models is outlined by Bennett (20) and Cutlip et al. (21). In essence, the transient mass balances for the species in the reaction system yield a set of differential equations which defines the model for the particular mechanism assumed. Integration of this system of equations results in the transient curves of the various species, which can then be used for parameter sensitivity studies, and also for parameter estimation by comparison with corresponding experimental data.

In order to illustrate this approach, consider the simple two-step mechanism:

$$CO_2 + C_f \xrightarrow{k_1} CO + C[O] \qquad \text{R1)}$$

$$C[O] \xrightarrow{k_2} CO + C_f \qquad \text{R2)}$$

which is imbedded in all known CO_2 gasification kinetic mechanisms, and was found to adequately represent the data in the current work.

If C_{so}, C_o, x, θ, and P_i represent, respectively, the active site concentration in g mol/g mol C, the initial total g mol of carbon, the fractional conversion, the fractional surface coverage of the complex, and the partial pressure of species i in the gas phase, the following rate expressions result for the preceeding mechanism:

$$r_1 = C_{so}C_o(1-x)[k_1(1-\theta)P_{CO_2}] \qquad 1)$$

$$r_2 = C_{so}C_o(1-x)[k_2\theta] \qquad 2)$$

Assuming a gradientless reactor, a mass balance on each species yields:

$$CO_2: \qquad \frac{dP_{CO_2}}{dt} = \frac{P_{CO_2}(1-\delta)_f - P_{CO_2}}{\tau} - \frac{r_1 RT}{V_g} \qquad 3)$$

CO_2: $$\frac{dP_{CO}}{dt} = \frac{(r_1 + r_2)}{V_g} - \frac{P_{CO}}{\tau} \quad 4)$$

C[O]: $$\frac{d\theta}{dt} = \frac{r_1 \; r_2}{C_{so}C_o(1-x)} + \frac{\theta r_2}{C_o \; (1-x)} \quad 5)$$

C: $$\frac{dx}{dt} = \frac{r_2}{C_o} \quad 6)$$

Inert gas (Ar): $$P_{Ar} = P_{CO_{2f}} - P_{CO_2} - P_{CO} \quad 7)$$

where $\delta = \frac{r_2 RT\tau}{V_g P_{CO_{2f}}}$ (due to the increase in gas volume upon reaction)

P_t = total system pressure, atm

$P_{CO_{2f}}$ = partial pressure of CO_2 in the feed (also total pressure of reactor if feed is pure CO_2), atm

τ = V_g/q; reactor space time evaluated at reactor conditions, min

V_g = reactor gas phase volume, cm^3

q = volumetric flowrate at reactor conditions, cm^3/min

T = reaction temperature, K

R = universal gas constant, $atm.cm^3/K.g\ mol$

The units for the rate parameters are $k_1 = [min^{-1}atm^{-1}]$ and $k_2 = [min^{-1}]$. The initial conditions for a pure CO_2 feed at time t = 0 are:

$$P_{CO_2} = P_{CO} = \theta = x = 0$$
$$P_{Ar} = P_t \quad 8)$$

Equations 1 through 8 constitute the model for the reaction system with dependent variables P_{CO_2}, C_{CO}, P_{Ar}, θ, and x, and parameters C_{so}, k_1, and k_2.

From simulated CO transient response results, it was found that the active site concentration, C_{so}, has a pronounced effect on the production of CO, but the shape of the transient curve remains relatively unchanged. However, the shape and position in time of the "overshoot" of the CO responses for both mechanisms are quite sensitive to the kinetic rate parameters k_1 and k_2. The effects of k_1 and k_2 are qualitatively illustrated in Figure 2. It is noted that the "overshoot" is due to large values of k_1, while the "leveling-off" is associated with large k_2 values.

Once the raw data (i.e., transient curves of the modulated signals for m/e = 44 and 28) are corrected to yield the net CO production curve due to reaction (from the fragmentation coefficient measured for CO_2), and then converted to CO partial pressure data (from the relative sensitivity measured for CO and CO_2), the next step is to determine a best parameter set for the proposed mechanism. This is done by minimizing the least squares objective function,

$$\phi = \sum_{k=1}^{\ell} \sum_{i=1}^{\eta} [(\hat{y}_{ik} - \hat{y}_{ik})/y_{ik}]^2 \quad 9)$$

(where the subscript ik represents the ith variable at time k, with:

i = i,...,n; the number of variables used in the optimization process,

k = i,..., ; the time intervals

y_{ik} = experimental point (partial pressure data),

$\hat{y}_{ik}$ = predicted value from the model,

using a Marquardt-type technique (22), coupled with a Green's function method (23) to determine the necessary first order sensitivity coefficient matrix, $\underset{\sim}{S} = \partial y/\partial \underset{\sim}{\beta}$. In essence, the parameter estimation procedure consists of solving the equations resulting from minimizing the objective function, Equation 9, based on local linearization of the model about the initial guess parameter set, $\underset{\sim}{\beta}^{o}$. This solution yields the vector of parameter changes, Δb_i, which in turn gives the next best estimate of the parameter set to minimize ϕ. This procedure is repeated until the objective function meets an acceptable preset tolerance. In the current work only one variable, P_{CO}, was used in the optimization of the objective function for parameter estimation from the experimental transient data. This was done because this variable is the most sensitive to the particular model used, while P_{CO_2} and P_{Ar} are less so.

4. RESULTS

The CO transient responses for the experimental runs conducted with two particle sizes of activated coconut (Fischer) char are presented in Figures 3 and 4. In these figures, the characteristic "overshoot" of the oxygen-exchange reaction, R1, as well as the "leveling-off" of the transient curves due to the carbon gasification reaction, R2, are clearly evident. As predicted by transient response simulations, smaller space times result in a sharper "overshoot" and a lower quasi-steady-state level of CO at longer times. Higher temperatures favor greater CO production but the "overshoot" becomes progressively less sharp.

The inhibition effect of pressure on gasification is not clearly evident in these figures, but becomes more so upon analysis of the quasi-steady-state gasification rate attained after "leveling-off" of the transient curves. From the stoichiometry of the overall reaction:

$$C + CO_2 \rightleftharpoons 2\ CO \qquad \text{R3)}$$

For continuous pure CO_2 gas feed, the "steady-state" gasification rate is given by

$$W_{ss} = \frac{-1}{} \frac{dC}{dt} = \frac{1}{2C} \frac{d[CO]}{dt} = \frac{P_{CO_{ss}}}{2C_o(1-x)RT} \simeq \frac{P_{CO_{ss}} q}{2C_o RT} \qquad 10)$$

for negligibly small carbon conversion (i.e., $x \simeq 0$).
Equation 10 can be rearranged to

$$\left(\frac{P_{CO_2}}{W}\right)_{ss} = \left(\frac{2C_o RT}{q}\right) \left(\frac{P_{CO_2}}{P_{CO}}\right)_{ss} \qquad 11)$$

The $(P_{CO_2}/P_{CO})_{ss}$ in this expression can be evaluated from the quasi-steady-state values obtained at the end of the transient period. A plot of the right-hand side of Equation 11 versus P_{CO_2} at constant temperature is presented in Figure 5. The observed linear dependence of the gasification rate on CO_2 partial pressure suggests a "steady-state" rate expression of the form:

$$\frac{P_{CO_2}}{W_{ss}} = \frac{1}{j_1} + \frac{P_{CO_2}}{j_2} \qquad 12)$$

or

$$W_{ss} = \frac{j_1 P_{CO_2}}{1 + (j_1/j_2)P_{CO_2}} \qquad 13)$$

Equation 13 is the same steady-state rate form observed by Ergun (24), with $j_1 = k_1 C_{s_o}$ and $j_2 = k_2 C_{s_o}$, and clearly shows the inhibiting effect of pressure on the gasification rate.

Several models were fit to the transient data: the Blackwood and Ingeme model (25), seven parameters; the Shaw model (26), five parameters; the Mentser and Ergun mechanism (27), five parameters; the Ergun mechanism (24), four parameters; and the two-step mechanism found appropriate in the current work (three parameters). Due to the low levels of CO present in the reactor under the current experimental

conditions, only the latter model fits the data accurately since the others all have CO reaction paths which are superfluous for our data.

The resultant parameter values for the two-step mechanism exhibited distinct Arrhenius temperature dependence. Numerical fits of all the data as a function of temperature yielded the following expressions:

$$k_1 = 6.13 \times 10^{11} \exp\left|\frac{-55,500}{RT}\right| \quad min^{-1}atm^{-1} \qquad 14)$$

and $$k_2 = 9.98 \times 10^{9} \exp\left|\frac{-44,800}{RT}\right| \quad min^{-1} \qquad 15)$$

Also, for the first time in the same experiment, the concentration of active carbon sites expressed as g mol/g mol C, was determined for the coconut char to be:

$$C_{so} = 1.70 \times 10^{-9} \exp\left|\frac{27,000}{RT}\right| \qquad 16)$$

This indicates that the active site concentration has a negative "activation energy". In other words, at higher temperatures, initially active sites become deactivated; viz.,

$$\underset{\text{active}}{C_f} \longrightarrow \underset{\text{inactive}}{C_i} \qquad R4)$$

This deactivation phenomenon agrees with some of the findings of Duval (28) and Blackwood et al. (29), which are discussed further below.

It is of interest to compare the values of the activation energies obtained in the present study for the two steps, R1 and R2, with corresponding values reported in the literature. Table I summarizes the results of previous investigators. It is evident that the apparent activation energy for the two common kinetic steps varies considerably from one study to another; with E_1' ranging from -27 to +76 kcal/g mol and E_2' from -17 to +93 kcal/g mol. This variation can be at least partially attributed to differences in experimental data analysis techniques, as well as the particular reaction mechanism assumed.It should also be noted that in all these studies, the rate parameters are reported as the product of the active site concentration , C_{so}, and the intrinsic rate constant, k. Hence, the apparent activation energies also reflect any variation of C_{so} with temperature. In other words, the difference in the types of char and experimental conditions can account for the wide range of activation energies evident in Table I. As indicated by Johnson (30), C_{so} is expected to decrease with increasing coal rank. In fact, this general trend is substantiated in the case of k_2C_{so} by the large activation energies observed for the high purity carbon (e.g., Ceylon graphite, Spheron 6 carbon, activated carbon, and graphite) used by Ergun (24) and Mentser and Ergun (27), vis-a-vis the much smaller temperature coefficients found for coconut char by Gadsby et al. (31), Long and Sykes (32), and also in the current work.

Differences in activation energies can also be attributed to presumably catalytic impurities in the char. This effect is especially pronounced (for k_2C_{so}) in the work of Long and Sykes (32) with coconut char where E_2' changed from 38 to 66 kcal/g mol upon removal of mineral impurities with hydrochloric and hydrofluoric acids.

On the other hand, Mentser and Ergun (27) argued that the constant activation energies obtained in their work with different forms of high purity carbon were due to a constant number of active sites, C_{so}, independent of temperature, and thus reflected the true activation energies for the reaction steps. This hypothesis is not at all unreasonable since C_{so} should not decrease indefinitely with coal rank, but rather the active site concentration should attain some constant asymptotic value for the high purity carbons. If the activation energies reported by Mentser and Ergun are the "true" temperature coefficients for R1 and R2 (with E_1 = 53.0 kcal/g mol and E_2 = 58.0 kcal/g mol), then their results agree reasonably well with the intrinsic activation energies found in the current work (E_1 = 55.5 kcal/g mol and E_2 = 44.8 kcal/g mol).

Other differences in E_1' and E_2' are probably numerical in origin. For instance, Golovina (33) fitted several simplified forms of the same gasification rate expression to data (i.e., due to possible changes in mechanism at various conditions), and reported different E' values for three different regimes of pressure and temperature. However, the negative activation energies obtained are indicative of improper analysis of kinetic data. In addition, the fact that the same rate form can give rise to different apparent activation energies in different temperature regimes but over the same pressure range (see Table I , as reported by Golovina, also argues against the inherent validity of the proposed rate expression and the reaction rate - controlling zone claimed by the investigator.

The effect of intraphase mass transport resistance on the rate constants is now addressed. First, there was no discernible difference in the gasification rate behavior of the 1.6 mm and 2.68 mm coconut char particles. Also, the resultant model parameters for the two-step mechanism exhibit essentially the same temperature dependence for both particle sizes. However, chars generally exhibit a polymodal pore size distribution with most of the internal surface area available in pores of molecular dimensions (super micropores) (34). Thus, even though the insensitivity to particle size indicates no bulk diffusional limitation (i.e., in the macropores), if diffusion in the micropores were the limiting resistance to char gasification, particle size would not necessarily have any effect; i.e., the characteristic size of the microporous material in both particle sizes is similar. In addition, micropore diffusion is known to be activated (35). Thus if its rate is comparable to the kinetic rate, or rate-controlling, its activation energy would be included in the overall apparent activation energy.

The diffusion parameter (diffusion time constant) of CO_2 in the micropores of WYODAK 35 x 60 char at 800°C is given by Debelak and Malito (36) as $D/r^2 = 1.68$ min^{-1} for fresh char (i.e., x = 0). The coconut char gasification rate at 800°C and 1 atm in pure CO_2, as given by Equation 13 with the rate parameters reported here, is $1.16 \times 10^{-3} min^{-1}$. Thus, if the microporous structure of the WYODAK and coconut chars are at all similar, the observed gasification rate is too small by three orders-of-magnitude to be micropore diffusion-controlled. Even at the highest possible constant asymptotic gasification rate (i.e., at high pressure) of $4.02 \times 10^{-3} min^{-1}$ at 800°C, the reaction is still definitely reaction rate-controlled.

Based on these observations, it is concluded that the activation energies for the parameters k_1 and k_2 found in the present study are intrinsic and in agreement with the general trend reported in the literature.

The negative "activation energy" exhibited by the active site concentration is consistent with the results of Duval (28), who presented strong evidence that active sites on a graphitic lattice disappear spontaneously with reaction temperature by a process termed thermal "healing" or "annealing". Thus, in effect, active sites are subjected to two modes of depletion: reaction with a gas phase molecule and thermal neutralization. Boulangier (37) also noted the same effect in carbon - CO_2 and carbon-steam systems. A similar trend was reported by Blackwood et al. (29) and Johnson (30) in studies of the effects of coal-char preparation temperatures. Blackwood et al. (29) correlated their results for hydrogen gasification rate constants in terms of $k = k^* \exp(E_p/RT_p) \exp(-E_g/RT_g)$, where T_g and T_p are the gasification and char preparation temperatures, respectively. For brown coal chars gasified in hydrogen at 25 atm with $T_p = T_g$, these workers found $E_p = 20$ kcal/g mol. It is noted that there is a direct analogy between $T_p = T_g$ in these char reactivity studies and conditions in the current work whereby the coconut char was held at the reaction temperature in an argon atmosphere for relatively long periods of time prior to imposing the concentration step change to reactant CO_2. Thus, the temperature dependence of C_{so} found by Blackwood et al. (29) agrees well with that found by Duval (28) and in the present study. Blackwood et al. (29) proposed that the decreasing reactivity with increasing temperature is due to rearrangement of the carbon structure into a more stable ring

lattice, thereby reducing the availability of free π electrons for the formation of complexes at edges, and stabilizing previously unstabilized bonds.

6. CONCLUDING REMARKS

The efficacy of applying the experimental apparatus and transient response techniques to heterogeneous char-gas reactions has been successfully demonstrated for CO_2 gasification. This approach promises to be a valuable tool for determining mechanisms and rate parameters for direct use in modeling, design, and analysis of new or existing gasification and related systems. A similar approach is being taken in studying gasification reactions with other gases and mixtures.

ACKNOWLEDGEMENT

The authors gratefully acknowledge the support of the U. S. Department of Energy under Grant Nos. DE-FG22-80PC30211 and DE-FG22-81PC40786. However, any opinions, findings, conclusions, or recommendations expressed herein are those of the authors and do not necessarily reflect the views of DOE.

REFERENCES

(1) Carberry, J. J., Ind. Eng. Chem. 56, 39 (1964).
(2) Bennett, C. O., Cutlip, M. B., and Yang, C. C., Chem. Eng. Sci. 27, 2255 (1972).
(3) Mahoney, J. A., J. Catal. 32, 247 (1974).
(4) Kobayashi, H., and Kobayashi, M., Catal. Rev.-Sci. Eng. 10, 138 (1974).
(5) Bennett, C. O., Ibid. 13, 121 (1976).
(6) Yang, C. C., Cutlip, M. B., and Bennett, C. O., in Catalysis, Hightower, J. W., Ed., vol. 1, Proceedings of the Fifth International Symposium Congress on Catalysis, p. 14-279, Miami, Fla. (1972).
(7) Berty, J. M., Preprint No. 41F, 70th Annual Meeting of AIChE, New York, N. Y., Nov. 13-17, 1977.
(8) Tajbl, D. G., Simons, J. B., and Carberry, J. J., Ind. Eng. Chem. Fund. 5, 171 (1966).
(9) Paspek, S. C., Varma, A., and Carberry, J. J., Chem. Eng. Edn. 14, 78 (1980).
(10) Halladay, J. B., and Mrazek, R. V., J. Catal. 28, 221 (1973).
(11) Brown, C. E., and Bennett, C. O., AIChE J. 16, 817 (1970).
(12) Joy, W. K., Ladner, W. R., and Pritchard, E., Fuel 49, 26 (1970).
(13) Juntgen, H., and van Heek, K. H., Ibid. 47, 102 (1968).
(14) Meyer, R. T., and Lynch, A. W., High Temp. Sci. 4, 283 (1972).
(15) Fenn, J. B., and Anderson, J. B., Fourth International Symposium on Rarified Gas Dynamics, Section 8, p. 311, Toronto (1964).
(16) Calo, J. M., and Bailey, A. D., Rev. Sci. Instrum. 45, 1325 (1974).
(17) Sy, O., "Transient Kinetic Studies of Char-Gas Reactions in a Gradientless Reactor: CO_2 Gasification," Masters Dissertation, Princeton University, May 1982.
(18) Berty, J. M., Chem. Eng. Progr. 70, 78 (1974).
(19) Smith, J. M., Chemical Engineering Kinetics, McGraw Hill, N. Y. (1981).
(20) Bennett, C. O., AIChE J. 13, 890 (1967).
(21) Cutlip, M. B., Yang, C. C., and Bennett, C. O., Ibid. 18, 1073 (1972).
(22) Marquardt, D. W., J. Soc. Ind. Appl. Math. 11, 431 (1963).
(23) Kramer, M. A., J. M. Calo, and H. Rabitz, Appl. Math Model. 5, 432 (1981).
(24) Ergun, S., J. Phys. Chem. 60, 480 (1956).
(25) Blackwood, J. D., and Ingeme, A. J., Aust. J. Chem. 13, 134 (1960).
(26) Shaw, J. T., Fuel 56, 134 (1977).
(27) Mentser, M., and Ergun, S., U. S. Bur. Mines Bull. 644 (1973).
(28) Duval, X., J. Chim. Phys. 47, 339 (1950).
(29) Blackwood, J. D., McCarthy, D. J., and Cullis, B. D., Aust. J. Chem. 20, 1561, 2525 (1967).
(30) Johnson, J. L., Kinetics of Coal Gasification, Wiley, N. Y. (1979).
(31) Gadsby, J., Long, F. J., Sleightholm, P., and Sykes, K. W., Ibid. A193, 357 (1948).
(32) Long, F. J., and Sykes, K. W., J. Chim. Phys. 47, 362 (1950).

(33) Golovina, E. S., Carbon 18, 197 (1980).
(34) Gan, H., Nandi, S. P., and Walker, P. L., Jr., Fuel 51, 272 (1972).
(35) Walker, P. L., Jr., Fuel 59, 809 (1980).
(36) Debelak, K. and Malito, J. T., "Effective Diffusivity in Coals as a Function of Conversion," presented at the 56th Colloid and Surface Science Symposium, Blacksburg, VA, June, 1982.
(37) Boulangier, F., Duval, X., and Letort, M., Proceedings of the Third Conference on Carbon, p. 257, Permagon Press, N. Y. (1959).

TABLE I.
Comparison of Kinetic Parameters from Different Investigators

Reference	Carbon Type	T(°C)	P(atm)	$k_1C_{so} = A_1\exp(-E'_1/RT)$ $A_1(min^{-1}atm^{-1})$	E'_1(kcal/gmol)	$k_2C_{so} = A_2\exp(-E'_2/RT)$ $A_2(min^{-1})$	E'_2(kcal/gmol)
1. (31)	coconut char	700-850	0.01 - 1	7.6×10^9	58.8	2.4×10^3	28.7
2. (32)	coconut char	700-800	0.07 - 0.2	7.6×10^9	58.8	3.6×10^3	38.0
	with impurities extracted			3.8×10^{10}	68.4	2.3×10^8	66.0
3. (24)	activated carbon	(a) 700-1000	1	-	-	8.5×10^8	59.0
	activated carbon	(b) 900-1150	1	-	-	8.28×10^7	59.0
	ceylon graphite	(c) 1000-1400	1	-	-	1.55×10^7	59.0
4. (29)	coconut char	790-870	2-40	2.7×10^{11}	76.0	1.13×10^{12}	76.0
5. (27)	Spheron 6	750-850	1	1.54×10^6	53.0	5.15×10^7	58.0
6. (30)	high volatile bituminous coal char (Pittsburgh seam)	870-980	1-35	3.56×10^3	28.4	3.42×10^{10}	65.0
7. (33)	graphite	1380-1530	1	4.7×10^8	75.0	-	-
		"	3-10	4.7×10^8	75.0	23.5	18.0
Note:		"	2-40	4.7×10^8	75.0	1.9×10^6	56.5
		1730-1927	1	3.8×10^{-4}	-27.0	-	-
$A_1 = \left\lvert \frac{g}{cm^2 min\ atm} \right\rvert$		"	3-10	3.8×10^{-4}	-27.0	67.2	24.5
		"	20-40	3.8×10^{-4}	-27.0	0.17	-3.0
$A_2 = \left\lvert \frac{g}{cm^2 min} \right\rvert$		2030-2330	1	9.5×10^2	40.0	-	-
		"	3-10	9.5×10^2	40.0	7.1×10^{-3}	-17.0
		"	20-40	9.5×10^2	40.0	3.0	12.5
8. (38)	summary of various chars	-	-	-	32.5 to 61.7	-	17.9
9. Present Work	activated coconut char	680-770	8-30	1.0×10^3	28.5	17.0	17.9

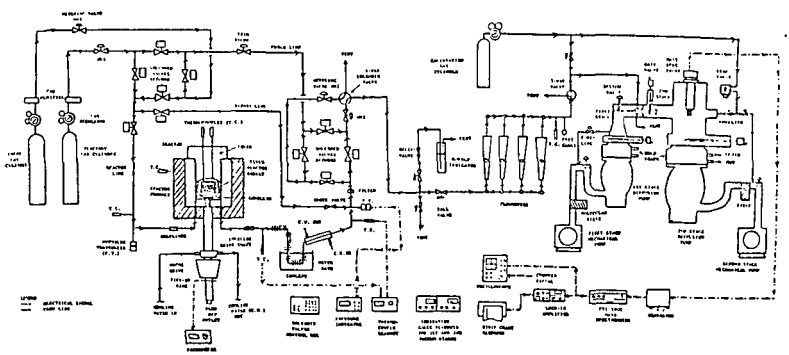

Figure 1. Schematic of the experimental apparatus for transient kinetic studies.

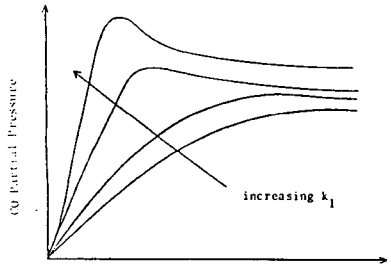

(a) Effect of Parameter k_1

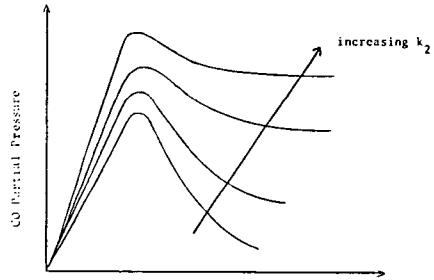

(b) Effect of Parameter k_2

Figure 2. Sensitivity of CO transient response to parameters k_1 and k_2 - qualitative behavior.

Figure 3. Experimental transient response of CO partial pressure versus model predictions for CO_2 gasification of activated coconut char using the two-step mechanism (1.6 mm, 36.1925g, 4.3 cm bed height).

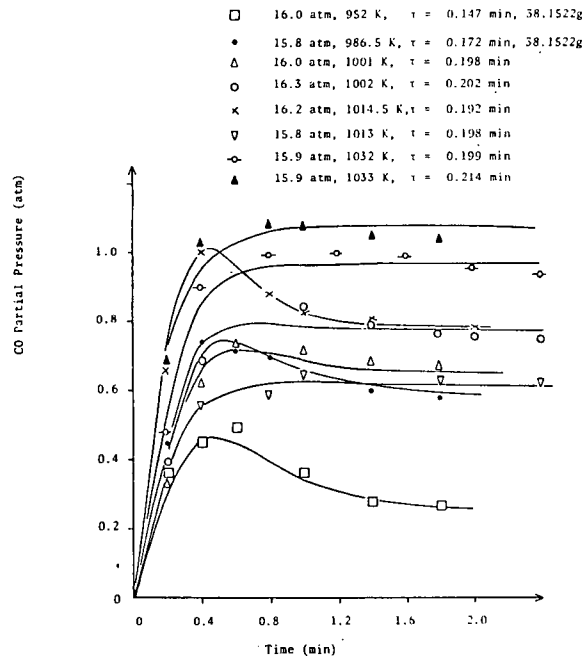

Figure 3 Experimental transient response of CO partial pressure and model predictions for CO_2 gasification of activated coconut char using the two-step mechanism (2.68 mm, 39.0369g, 4.3 cm bed height).

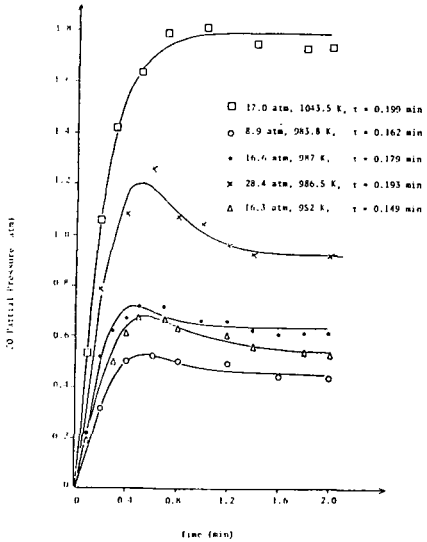

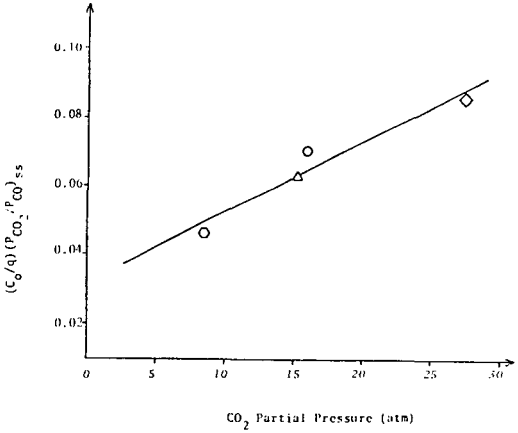

Figure 5. Quasi-steady-state gasification rate as a function of CO_2 partial pressure: (a) 2.68 mm activated coconut char, 38.0369g, 4.3 cm bed height; ○ P = 8.9 atm, τ = 0.16 min; ○ P = 16.6 atm, τ = 0.18 min; ◇ P = 28.4 atm, τ = 0.19 min; (b) 1.6 mm activated coconut char, 38.1522g, 4.3 cm. bed height; △ P = 15.8 atm, τ = 0.17 min.

REACTION OF HIGH VELOCITY ATOMIC OXYGEN WITH GRAPHITE

G. S. Arnold, R. R. Herm, and D. R. Peplinski

Chemistry and Physics Laboratory,
The Aerospace Corporation
El Segundo CA, 90245

Atmospheric bombardment of a spacecraft in low Earth orbit (LEO) presents a regime of gas-surface chemistry which has been the subject of very little laboratory investigation. The predominant atmospheric species in LEO (200-800 km) is ground state, neutral atomic oxygen (1). Although the ambient temperature is not extremely high ($\sim 10^3$ K), the 8 km sec^{-1} orbital velocity of the spacecraft causes oxygen atoms to strike the satellite's surfaces with an average collision energy of 5×10^2 kJ $mole^{-1}$ ($\sim$ 5 eV). At the altitude at which the space shuttle operates ($\sim$ 240 km) the flux of atomic oxygen striking surfaces normal to the craft's velocity vector is of the order of 8×10^{14} cm^{-2} sec^{-1}.(1) The phenomenology of oxygen atom-surface interactions at such a collision energy is completely unstudied in the laboratory. The lack of experimentation in this area owes not to any assumption that such chemistry is fundamentally uninteresting, but rather reflects the difficulties inherent in reproducing in the laboratory the 8 km sec^{-1} impact velocity.

The details of oxygen atom surface interactions at orbital velocity are of particular interest for the prediction of the integrated effects of long-term exposure of materials to the LEO atmosphere. The unique opportunity which the shuttle orbiter provides to recover a variety of materials from LEO has highlighted the need for such an understanding. Organic polymers, including polyimides, polyesters, and polyurethanes, have been observed to erode at significant rates (2). A silver surface 2100Å thick was completely oxidized (3). Osmium and graphite surfaces exposed to the atmosphere were completely removed (3,4).

The reaction of atomic oxygen with graphite:

$$C_c + O_g \xrightarrow{\varepsilon_1} CO_g \qquad \Delta H^o = -\ 360 \text{ kJ mole}^{-1} \qquad (1)$$

is well known and so initially one does not find the removal of graphite surfaces by atmospheric oxygen to be particularly surprising (5). The rate at which graphite was removed was, however, quite unexpected. On the third shuttle flight (STS-3), a graphite surface estimated to be 10^{-4} in. thick was completely removed. The total time of direct exposure of the surface to the atmosphere was approximately 9 hours. If reaction 1 were responsible for the removal of the graphite, then it must have been occurring with a probability in excess of 0.8 per oxygen atom collision.

Reference 5 reports that the variation with surface temperature of the probability of reaction 1, ε_1, for the case of oxygen atoms impacting at thermal velocities is given by:

$$\varepsilon_1 = 0.63\ e^{-1160/T}. \qquad (2)$$

The temperature of the graphite exposed on STS-3 is expected not to exceed 420K, a temperature at which the Arrhenius expression given above predicts a value of ε_1 of 0.04. Even though the estimate of reaction probability on orbit is based on data which are somewhat less precise than might be desirable, the difference between prediction and observation is substantial.

Such a discrepancy in predicted and observed reaction probabilities indicates the possibility that the high translational energy of oxygen atoms striking graphite surfaces on orbit results in the enhancement of the probability that an oxygen atom removes a carbon atom on impact (as compared to the thermal oxidation of graphite by

O atoms). It is instructive to note that if one includes the translational energy of the atomic oxygen in one's accounting, channels for the removal of carbon atoms in addition to reaction 1 are at least thermodynamically allowed. Two of these reactions are:*

$$2C_c + O^*_g \rightarrow CO_g + C_g \qquad \Delta H = -125 \text{ kJ mole}^{-1} \tag{3}$$

and

$$3C_c + O^*_g \rightarrow CO_g + C_{2g} \qquad \Delta H = -8.9 \text{ kJ mole}^{-1}. \tag{4}$$

Thus the oxidation of graphite was selected as the initial subject for investigation in a new facility constructed specifically for the study of high energy oxygen atom surface chemistry. In addition to providing further insight into a gas-surface interaction of great fundamental and practical interest, such experimentation serves as the prototype for the investigation of the oxidation of spacecraft materials by high energy atomic oxygen.

Figure 1 shows a schematic representation of the beam apparatus designed for the investigation of high energy oxygen atom surface chemistry. The vacuum system is comprised of four chambers. The first three are stainless steel boxes, 18 in. cubed, sealed with Buna-N "O-Rings". The first is pumped by an unbaffled 16 in. oil diffusion pump (Varian VHS-400). Each of the second and third chambers is pumped by a 10 in. oil diffusion pump (Consolidated Vacuum Corp.), topped with a liquid nitrogen cooled trap (Mt. Vernon Research Corp.), and an electro-pneumatically operated, viton-sealed gate valve (Vacuum Research Manufacturing Corp.). The fourth chamber uses crushed metal seals and is pumped by a high-speed turbomolecular pump (Balzers TPU 510).

The oxygen atom beam source (described below) is housed in chamber 1. The source is recessed into chamber 1 in order to minimize the distance from source to target thereby delivering the maximum available beam flux to the target. A Beam Dynamics Inc. model 2 nickel skimmer, 0.90 mm orifice diameter, connects chambers 1 and 2. Chambers 2 and 3 act as buffers to aid in the reduction of pressure between the source and the target. A beam chopper and beam flag which aid in the characterization of the beam are mounted in chamber 2. The second chamber also provides space for installation of a low resolution slotted disk velocity filter, which may be used when it is desirable to prevent light from the beam source from falling upon the target.

The solid target is contained in the fourth chamber, which is recessed into the third chamber to minimize source to target distance. A quadrupole mass spectrometer (Extranuclenar Laboratories) is provided for characterization of the atomic beam and also for identification of the volatile products of bombardment of the target.

The production of a beam of neutral atomic oxygen of sufficient velocity and intensity for this program requires advances in the state-of-the-art of beam source technology. Indeed, one major reason for the scarcity of experimental data on atomic oxygen-surface interactions at high energies (~ 5 eV) is the difficulty in building a reliable, fast, high-intensity O atom beam source. Figure 2 shows the source constructed here to achieve such a beam. The source is a modified, commercially available plasma torch. The modifications include attachments for a water-cooled nozzle, through which the atomic beam expands into the vacuum system, and exhaust channels to dispose of excess torch gas. The torch operates in the non-transferred mode, i.e., the electric arc is confined within the torch. A plasma is formed in

* O^* indicates translational excitation of 480 kJ mole^{-1}.

helium by a dc arc. A small amount of O_2 (~ 2% of the total gas flow) is injected downstream of the arc into the gas flow, where it is thermally dissociated into oxygen atoms by the hot helium. The high temperature and the isentropic expansion provide for the oxygen atom velocity, which results in a supersonic beam. A similar source has been reported by Air Force Geophysics Laboratories (6).

The arc source has been tested with pure He, He/O_2 mixtures, $He/Ar/O_2$ mixtures, and Ar/O_2 mixtures as a function of torch power. Tests with O_2 indicate that oxidation of electrodes does not take place even at high torch current levels. He, Ar, O_2, and O atom beams have been detected using the mass spectrometer. Conversion of molecular oxygen into atoms is determined from relative mass peak signals (measured by the quadrupole mass spectrometer), I_O/I_{O_2}, by the formula of Miller and Patch (7).

$$y = \frac{N_O}{N_{O_2}} = P \left(\frac{\sigma_{O_2}}{\sigma_O}\right) \left(\frac{1}{\eta} \frac{I_O}{I_{O_2}} - 1\right) \qquad (6)$$

where N_O/N_{O_2} is the inferred number density ratio of O to O_2, P is the probability of dissociative ionization, σ_{O_2} / σ_O is the ratio of electron impact ionization cross sections, I_O/I_{O_2} is the ratio of mass spectrometer signals of O and O_2 with the torch on, and η is the I_O/I_{O_2} ratio with the torch off. The per cent dissociation is given by:

$$\%D = 100\ y/(y + 2).$$

As one can see from figure 3, the per cent dissociation of O_2 into O ranges from ~ 30 to 48% for a 2.55% O_2 in Ar mixture, to ~ 15 to ~ 19% for various O_2 in He/Ar mixtures. These per cent dissociation translate into source temperatures of 3000-3200°K for O_2 in Ar, and 2700-2850°K for O_2 in He/Ar mixtures. Although not shown, tests made using pure He also show a lower dissociation. The greater efficacy of argon in dissociating O_2 probably owes to increased energy deposition in Ar, which flows more slowly through the torch (0.63 STP ℓ sec^{-1} Ar, 2.1 STP ℓ sec^{-1} He).

Results will be reported of measurements of the rate of volatilization of graphite by high velocity atomic oxygen in order to determine if the apparent enhancement of this rate on orbit is real. Mass spectral measurement of the products of high velocity O atom bombardment of carbon will be described as well.

References

1. A. E. Hedin, Tables of Thermospheric Temperature, Density and Composition Derived from Satellite and Ground Base Measurements, Laboratory of Planetary Atmospheres, Goddard Space Flight Center, Volumes 1, 2, and 3 (January 1979).

   A. E. Hedin, C. A. Reber, G. P. Newton, N. W. Spencer, H. C. Brinton, H. G. Mazer, and W. E. Pottes, "A Global Thermospheric Model Based on Mass Spectrometer and Incoherent Scatter Data MSIS 2, Composition," J. Geophys. Res. 82, 2148-2156 (1977).

   A. E. Hedin, J. E. Salah, JH. V. Evans, C. A. Reber, G. P. Newton, H. W. Spencer, D. C. Kayser, D. Alcayde, P. Bauer, L. Cogger, and J. P. McClure, "A Global Thermospheric Model Based on Mass Spectrometer and Incoherent Scatter Data 1, N_2 Density and Temperature," J. Geophys. Res. 82, 2139-2147 (1977).

2. Lubert J. Leger, "Oxygen Atom Reactions with Shuttle Materials at Orbital Altitudes," NASA TM 58246, May 1982.

3. R. Linton, NASA MSFC, private communication.

4. G. B. Murphy and S. D. Shawhan, "Initial Results: The Measurements of the Shuttle's plasma environment on STS-3," 12th Space Simulation Conference, Pasadena CA. 17-19 May 1982.

5. Chul Park, "Effect of Atomic Oxygen on Graphite Ablation," AIAA Journal 14, 1640 (1976) and references cited therein.

6. J. A. Silver, A. Freedman, C. E. Kolb, A. Rahbee and C. P. Dolan, "A supersonic nozzle beam source of atomic oxygen produced by electric discharge heating," Accepted for Publication, Rev. Sci. Instrum.

7. D. R. Miller and D. F. Patch, "Design and Analysis of a High Intensity Fast Oxygen Atom Source Rev. Sci. Instrum. 40, 1566 (1969).

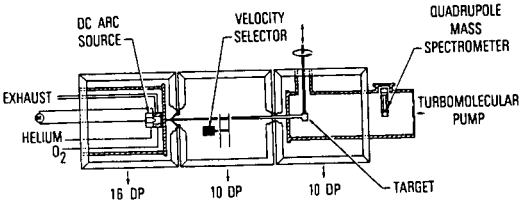

Figure 1. High energy oxygen atom surface chemistry apparatus.

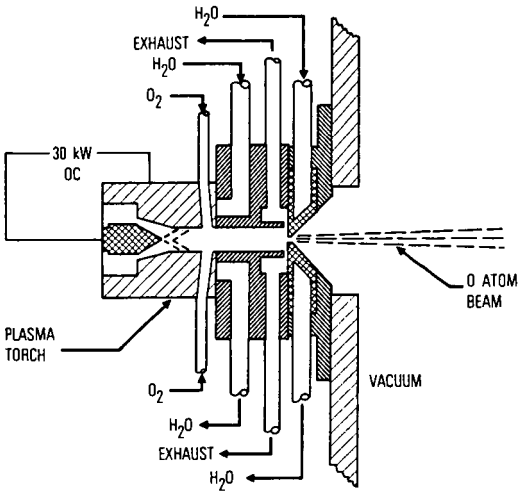

Figure 2. DC plasma arc atomic beam source.

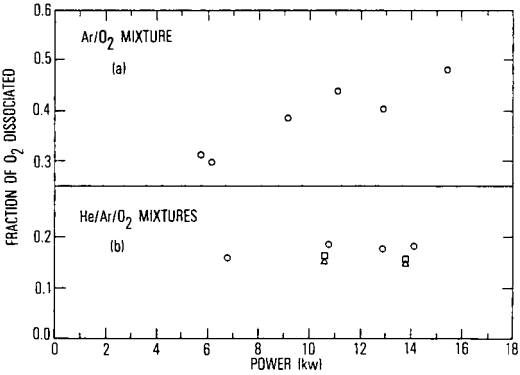

Figure 3.

Dissociation efficiency for O_2 in gas mixtures as a function of arc source power consumption: (a) 2.55% O_2 in Ar, (b) (O) 2.2% O_2, 5.9% Ar, 91.9% He; (ø) 1.5% Ar, 92.6% He; and (Δ) 2.9% O_2, 5.9% Ar, 91.2% He.

Structure Changes During Carbon Methanation Reactions

J. Sentiesteban*, S. Fuentes* and M.J. Yacaman**

*Instituto de Fisica UNAM, Mexico, 20 DF

**Physics Department, West Virginia University

1. INTRODUCTION

The reaction of carbon methanation on graphite surfaces containing platinum particles was studied using electron microscopy, gas chromatography and thermogravimetry. In the electron microscope, the weak beam thickness fringes (1) and topographic refraction images(2) were used. In addition the STEM microdiffraction technique to obtain crystallographic information from individual particles (3) was employed.

2. ACTIVITY RESULTS

Figure 1 shows the results for the activity for methane production as function of the temperature. Below 700°C the methane concentration is undetectable. It starts to increase at this temperature and a maximum is obtained at 800°C. At 850°C the reaction approaches the thermodynamic equilibrium and the concentration is reduced. However at 900°C it increases again. The TEM showed that at this temperature channeling on the graphite surface starts to be produced.(3) Below this temperature the particles produced only pits in the surface.. Figure 2 shows a topographic image of the channels. Irregular large particles are extremely active in this reaction since they produce large channels and therefore remove more carbon from the surface. The weak beam image picture shows that the particles are very rough in shape. They

are flat platelets with a thickness of about 100 Å. A typical example is shown in Figure 3. It was found that well faceted particles did not produce any channeling and therefore they were inactive for the reaction. Particles in the size range below 100 Å produced regular channels moving along <1150> directions of the graphite in most cases, in agreement with the findings of Baker et.al[3] and Tomita and Tamai[4]. However large irregular particles produced irregular channels not oriented along specific directions. The channeling always started along edges or steps on the graphite surface. The activation energy and reaction rate was determined by chromatography in the 700-800°C range and by thermogravimetry in 800-900° interval. The reason for this was that at high temperatures, the methane was decomposed in the post-reaction zone, producing an error in the chromatographic measurements. The values found were 43.5±4 KCal/mol and 0.0415 gr(CH_4) / hr gr(PT) for the activation energy and reaction velocity respectively in the 700-800°C interval and 44.0±4 KCal/mol and 0.026 gr(CH_4) / hr gr(PT) for the 800-900°C interval. These results suggest that the reaction mechanism is the same for the whole range of temperatures. Microdiffraction experiments indicated that particles had an FCC structure corresponding to a cubo-octahedron. However in many cases a complex pattern was obtained not corresponding to an FCC structure. This was probably a carbide or an oxide. It was not possible to identify this phase univocaly and more experiments are being carried out. The reaction appears to be produced on the interface Pt-graphite and is always related to pitting or channeling. The rate determining step seems to be the break of the C-C bond on the graphite surface. The main rate of the catalyst is to reduce the activation energy for the breaking of the C-C bond. The ability of the particles to remove carbon seems to be related to its surface roughness.

REFERENCES

1. M.J. Yacaman and T. Ocana, Phys. Stat. Sol. A) 42, 571 (1977).
2. A. Gomez, P. Hernandez and M.J. Yacaman, Surf. and Interf. Anal. 4, 120 (1982).
3. R.T.K. Baker, R.D. Sherwood and J.A. Dumesic, J.Catal 66, 56 (1980).
4. A. Tomita and Y. Tamai, J. Catal. 27, 293 (1972).

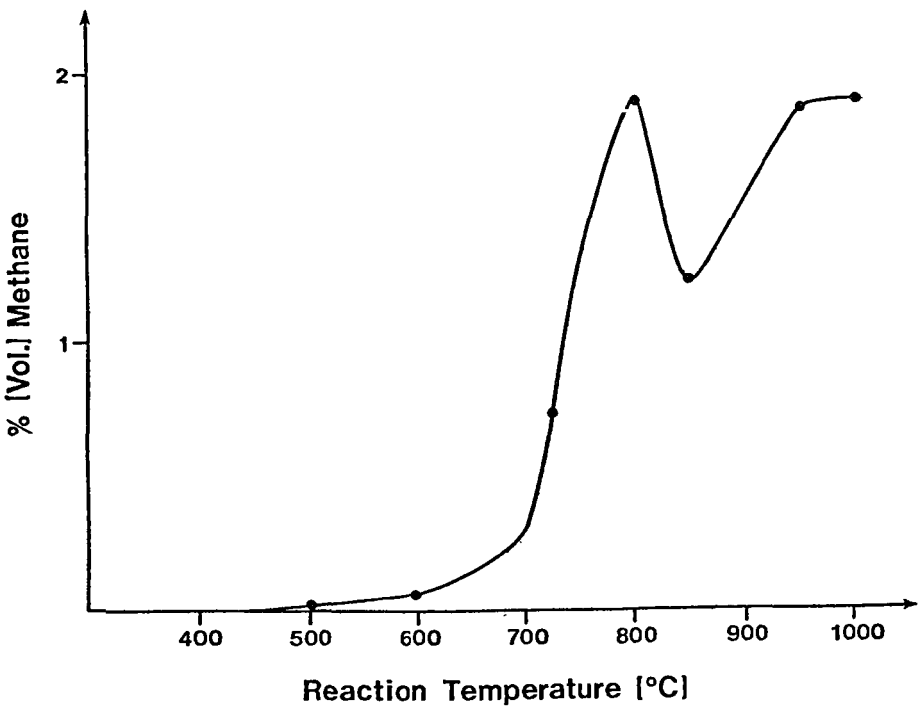

Figure 1. Concentration of methane as a function of the temperature.

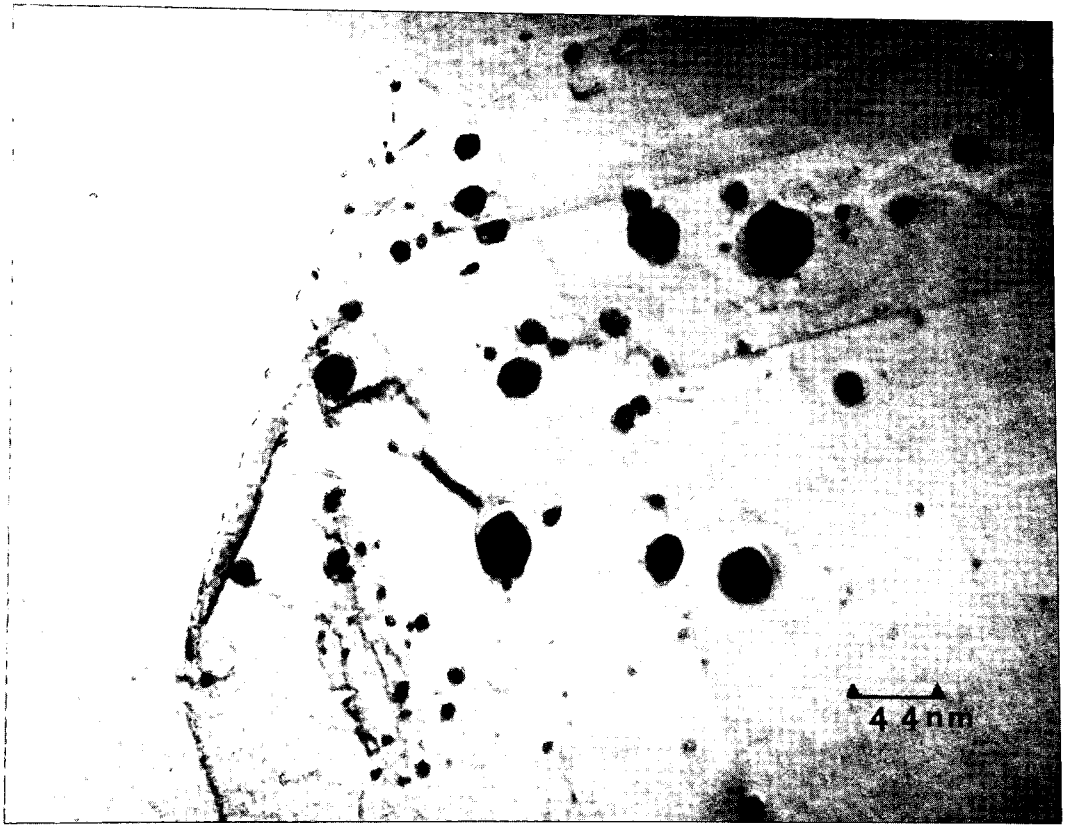

Figure 2. Topographic image of channeling in graphite surfaces.

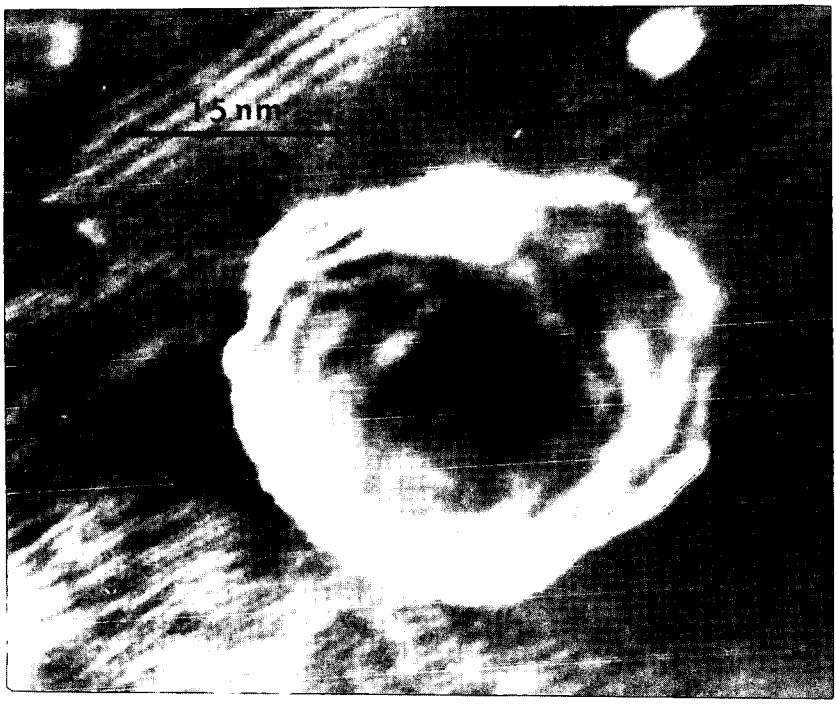

Figure 3. Weak beam image of a large particle showing rough surfaces.

DIRECT INVESTIGATION OF REACTING COALS BY DIFFUSE REFLECTANCE INFRARED SPECTROMETRY

Peter R. Griffiths, Shih-Hsien Wang, Issam M. Hamadeh,
Paul W. Yang and David E. Henry

Department of Chemistry, University of California,
Riverside, California 92521

Introduction

A few years ago we showed that it was possible to measure the diffuse reflectance (DR) infrared spectrum of solids at high signal-to-noise ratio (SNR) with no sample preparation required other than pulverization (1). The key factors in our design were the use of a Fourier transform infrared (FT-IR) spectrometer incorporating a mercury cadmium telluride (MCT) detector, and the design of a highly efficient optical configuration for collecting diffusely reflected radiation and passing it to the detector. At that time, we suggested that the study of coal might be among the more important applications of DR spectrometry, although we initially believed that in order for good spectra to be obtained it was necessary to grind the samples with about ten times their weight of an alkali halide diluent (2). Subsequently, we demonstrated that equally good spectra could be obtained when no diluent was added, and several applications of DR infrared spectrometry to coal chemistry were described in a recent publication from this laboratory (3). Today it is possible to obtain commercial accessories for DR spectrometry for most commonly used FT-IR spectrometers from at least four different sources.

In view of the structural information potentially obtainable from the infrared spectra of neat powdered coals, we have studied the feasibility of monitoring the chemical changes which occur while reactions are taking place. This work necessitated two instrumental developments before truly useful data could be obtained. These were the construction of a cell and optical configuration suitable for the study of gas-solid reactions at high temperature and the further refinement of the assignment of infrared spectra of coals, especially after resolution enhancement.

Optics and Cell

The first DR infrared spectra measured during a reaction were described by Niwa *et. al.* (4,5). Their spectra were measured on a grating spectrometer and had a very low SNR. Subsequently (6), we described a small cell for controlling the atmosphere around a heated powder which could be installed in the optics reported in our first paper on DR spectrometry (1). Although the spectra measured with this cell had a far higher SNR than those of Niwa *et. al.*, the cell still had several disadvantages, in that it had to be very small, its temperature could not be raised above about 200°C, and temperatures had to be estimated rather than measured directly. The optical efficiency was reduced by the window geometry and, in addition, a substantial fraction of the radiation reaching the detector had never interacted with the sample, leading to a high level (∿20%) of stray light.

Subsequently, a superior cell was introduced by Harrick Scientific Corporation (Ossining, N.Y.) with improved upper temperature limits, optical efficiency and stray light specifications. However, this cell still had one significant drawback for the study of reacting coals, in that it had only one inlet/outlet gas line, so that if tars were formed they would condense on the windows, completely obscuring the infrared beam from the detector.

To circumvent this problem and to permit improved operating specifications, a completely redesigned cell was constructed. Separate inlet and outlet gas lines were installed; the use of a wide-bore outlet tube permitted a vacuum of 10^{-4} torr to be obtained. The base of the sample cup is fritted so that inert or reactive gases can be drawn through the sample, preventing tar deposits on the window. The

input beam and diffusely reflected output beam are passed through a single 50cm diameter KCl window. The sample is heated by a nichrome wire coiled around the cup. The temperature of the sample can be measured by a thermocouple inserted into the powdered coal, and temperatures up to 600°C (1100°F) have been reached, which should allow the study of most important reactions of coals. To avoid overheating, the body of the cell is water-cooled.

To accomodate this cell, we designed a fundamentally different optical configuration for DR infrared spectrometry, which permits a large cell to be installed with little or no loss in optical efficiency. If a non-absorbing sample (such as powdered KCl) is placed in the cell, the SNR of the interferogram measured with an FT-IR spectrometer operating at full throughput (0.06 cm^2 steradian) with a medium-range MCT detector (λ_{max}=15μm) can be so large in the region of the centerburst that the dynamic range of the analog-to-digital converter may be exceeded unless a screen is placed in the beam. This cell and optics are described in details in the Ph.D. dissertation of Hamadeh (7), and are shown schematically in Figure 1.

Resolution Enhancement

Absorption bands in the infrared spectra of coals may be rather broad, so that detailed chemical information may be masked by the overlap of neighboring bands. Conversion of the spectrum to the second, or even the fourth, derivative has permitted the separation of small shoulders in the spectra of coals (3,6,8) but the interpretation of second- and fourth-derivative spectra is made difficult by the possibility that secondary lobes from intense sharp peaks may be mistaken for a real spectral feature in complex spectra. An alternative, and we believe preferable, technique for resolution enhancement where the effect of secondary lobes should be minimized is Fourier self-deconvolution (FSD). Here the absorption spectrum is converted to its Fourier transform, multiplied by an exponential function, and truncated if necessary to remove the high frequency noise components. The inverse transform then yields a spectrum in which the width of all spectral features has been reduced (9). Care must be taken, however, to avoid the use of an exponent in the multiplier which is too large since side-lobes will be generated which are analogous to those of second-derivative spectra.

To illustrate the potential of Fourier self-deconvolution in coal spectrometry, the progressive resolution enhancement of the spectrum of an oxidized low volatility bituminous coal in the region of the carbonyl stretching bands is shown in Figure 2. In the upper spectrum it can be seen that side-lobes have been generated and the noise level of the spectrum is increased to the point that it is difficult to distinguish a real feature from a noise spike. We have recently developed a technique to determine the optimum level of resolution enhancement consistent with an acceptable noise level and side-lobes (10), and we believe that the degree of resolution enhancement of all spectra shown or used in subsequent sections of this paper is quite conservative, and could probably have been improved upon if there optimization procedures had been applied rigorously.

Spectral Assignments

This increased resolution leads to some benefits and some problems. The benefits are obvious when the newly resolved bands can be unequivocally assigned to definite vibrational modes. For example, the spectra of most coals contain two bands between 3000 and 2800 cm^{-1}; these may be assigned to the symmetric and asymmetric stretching modes of aliphatic C-H groups. Each band often shows evidence of being composed of two unresolved or partially resolved components which can be completely resolved by FSD; these components can be assigned to vibrations of methylene and methyl groups. By studying the ratio of the intensities of these bands, the relative rates of reaction of CH_2 and CH_3 groups can be monitored, for example during air oxidation (vide infra).

The disadvantage of the enhanced information content is encountered when the newly resolved spectra cannot be interpreted with certainty. In Figure 2, as many as nine bands may be resolved in the carbonyl stretching region alone. Some of these, e.g. the two anhydride bands at 1845 and 1775 cm^{-1}, are easily assigned. Others, especially the bands between 1735 and 1675 cm^{-1}, are much less easy to assign with any degree of certainty.

We are hoping to increase the certainty of these band assignments by correlating the infrared spectra with both solution-phase ^{1}H and solid-phase ^{13}C NMR spectra. The correlating of solution-phase ^{1}H spectra of that fraction of each coal soluble in pyridine-d_5 with the diffuse reflectance spectrum of the solute remaining after complete evaporation of the solvent is certainly useful, but one can never be sure that the structure of the coal remains unchanged after solvent elimination. The SNR of CP-MAS ^{13}C NMR spectra measured on a 60 MHz spectrometer was too low to permit useful conclusions to be made, and we are hoping that spectra to be measured on a 90 MHz spectrometer with a wide magnet gap prove more helpful.

Low Temperature Oxidation

The potential of DR spectrometry for monitoring coal reactions will be illustrated by the low temperature (150°C) air oxidation of a low volatile bituminous coal. This reaction is very slow - much slower than the types of reactions which we ultimately hope to study (which can have half-lives of only a few seconds) - but the data still give a good indication of the type of results which can be obtained. Deconvolved spectra measured at different times after oxidation was initiated are shown in Figure 3. The increase in absorption around 1700 and 1250 cm^{-1} is evident, showing that oxygen reacts to form both double and single carbon-oxygen bands, with C=O formation being the more rapid reaction. The existence of anhydride groups is not obvious in the early spectra, but the 1845 cm^{-1} band builds up rapidly after a few days, indicating that oxidation to carboxylic acids is an initial step, followed by condensation of neighboring $-CO_2H$ groups when their concentration is sufficiently high.

The increase in aromaticity can be inferred from a plot of the ratio of the intensity of the aromatic C-H stretching band at 3070 cm^{-1} to that of the symmetric methyl stretching band (2872 cm^{-1}) against time of oxidation, see Figure 4. The mechanism of this reaction can be inferred from a plot of the ratio of the intensities of the asymmetric methylene and methyl stretching mode against time of oxidation, see Figure 5. The faster rate of disappearance of CH_2 groups indicates that one possible mechanism by which aromaticity is increased is by oxidative dehydrogenation of hydroaromatic methylene groups:

A:

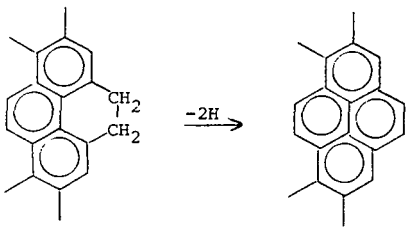

or B:

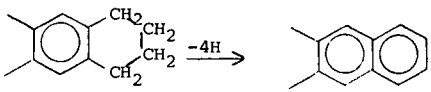

In Reaction A, an aromatic ring with two neighboring C-H groups would be formed whereas in Reaction B the newly formed aromatic ring would have four neighboring C-H groups. It is possible to determine which reaction has the higher probability by studying the spectral region between 950 and 650 cm^{-1}. Three strong bands of approximately equal intensity may be observed in this region, at approximately 880, 815 and 760 cm^{-1}. These bands are due to the aromatic out-of-plane C-H deformations, and may be assigned as follows, after Bellamy (11):

880 cm^{-1} band: Isolated C-H groups, i.e. 1,2,3,4,5-pentasubstituted ring; 1,2,3,5 and 1,2,4,5-tetrasubstituted ring; 1,2,4, trisubstituted ring (in conjunction with 815 cm^{-1} band).

815 cm^{-1} band: Two neighboring C-H groups, i.e. 1,2,3,4-tetrasubstituted ring; 1,2,4-trisubstituted ring (in conjunction with 880 cm^{-1} band); para-dissubstituted ring.

760 cm^{-1} band: Four neighboring C-H groups, i.e. ortho-substituted ring.

An increase in the intensity of the 815 cm^{-1} band relative to that of the 760 cm^{-1} band on dehydrogenation would indicate that Reaction A is favored over Reaction B, and vice versa. In Figure 6, it is shown that the rate of increase of the 760 cm^{-1} band is greater than that of the 815 cm^{-1} band, indicating that Reaction B is favored. It is noteworthy that this type of conclusion also gives an indication of the structure of low volatility bituminous coals, since the dimethylene structural unit in the reactant for Reaction A has been generally believed to be more prevalent in coals of this rank than the tetramethylene hydroaromatic unit in the reactant for Reaction B.

Conclusions

We believe that these data indicate the feasibility of monitoring structural changes occurring during reactions such as oxidation, pyrolysis and hydrogenation, with or without catalysts present, in situ by diffuse reflectance infrared spectrometry. Our current cell allows reactions to be studied at temperatures as high as 600°C. Reaction products may be continuously swept out of the cell, permitting characterization by a wide range of other instrumental techniques. Reactions occurring at high pressure are less easy to monitor at this time, but it should not be too difficult to redesign the cell so that pressures to 1000 psig are permissible.

References

1. M. P. Fuller and P. R. Griffiths, Anal. Chem., 50, 1906 (1978).
2. M. P. Fuller and P. R. Griffiths, Amer. Lab., 10(10), 69 (1978).
3. M. P. Fuller, I. M. Hamadeh, P. R. Griffiths and D.E. Lowenhaupt, Fuel, 61, 529 (1982).
4. M. Niwa, T. Hattori, M. Takahashi, K. Shirai, M. Watanabe and Y. Murakami, Anal. Chem., 51, 46 (1979).
5. T. Hattori, K. Shirai, M. Niwa and Y. Murakami, Anal. Chem., 53, 1129 (1981).
6. P.R. Griffiths and M. P. Fuller, in Advances in Infrared and Raman Spectroscopy, Vol. 9, (R. Clark and R. Hester, eds.), Wiley-Interscience, New York (1982), pp. 63-12
7. I. M. Hamadeh, Ph.D. dissertation, Ohio University, Athens, Ohio (1982).
8. P. C. Painter, R. W. Snyder, M. Starsinic, M. M. Coleman, D. W. Kuehn and A. Davis, Appl. Spectrosc., 35, 475 (1981).
9. J. K. Kauppinen, D. J. Moffatt, H. H. Mantsch and D. G. Cameron, Appl. Spectrosc., 35, 271 (1981).
10. W. J. Yang and P. R. Griffiths, unpublished results (1982).
11. L. J. Bellamy, "The Infrared Spectra of Complex Molecules," Chapman and Hall, London (1954).

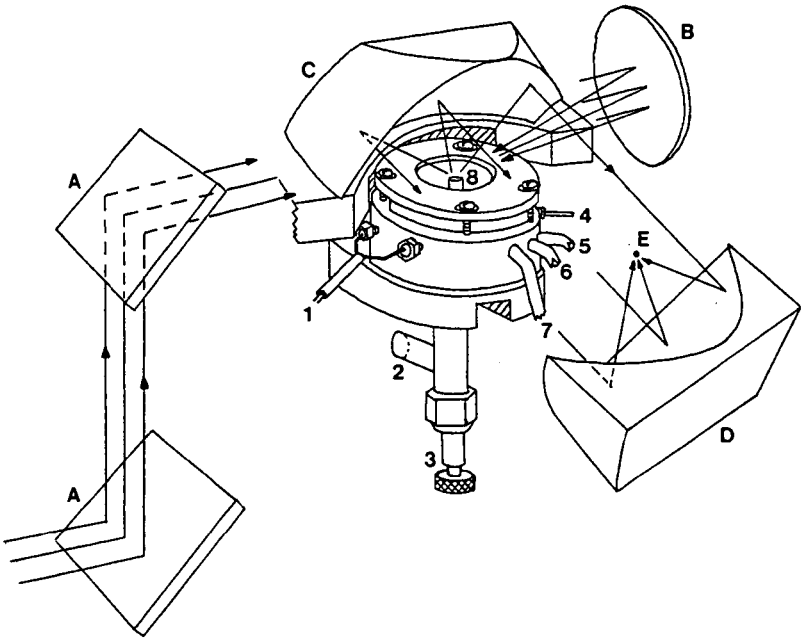

Figure 1: Schematic of cell designed for the study of gas-solid reactions. The level of the collimated beam from the interferometer is raised by the two plane mirrors (A) and focused onto the sample by the off-axis paraboloidal mirror (B). The diffusely reflected beam is collected and collimated by the paraboloidal mirror (C) and refocused by the other segment of the same paraboloidal blank (D) onto a downward-looking MCT detector at E. The components of the cell are as follows: (1) Heater leads, (2) Line to vacuum pumps, (3) Screw for sample removal, (4) Gas inlet line, (5) (6) Water inlet and outlet lines, (7) Manometer connection, (8) Sample.

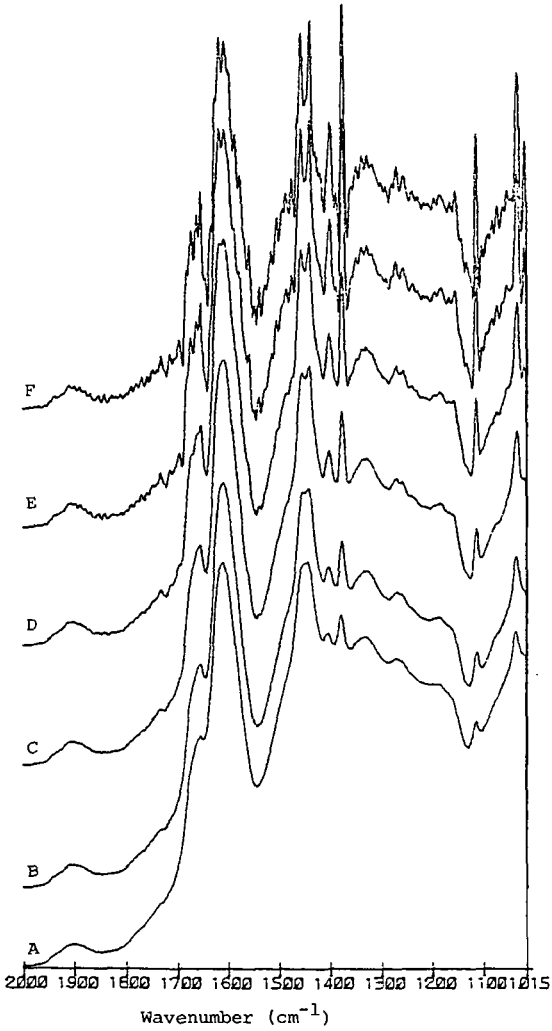

Figure 2: Effect of progressive resolution enhancement of the DR spectrum of a low volatility bituminous coal. The original spectrum is the lowest trace (A). Spectra used in this paper were computed with the parameter used for spectrum D.

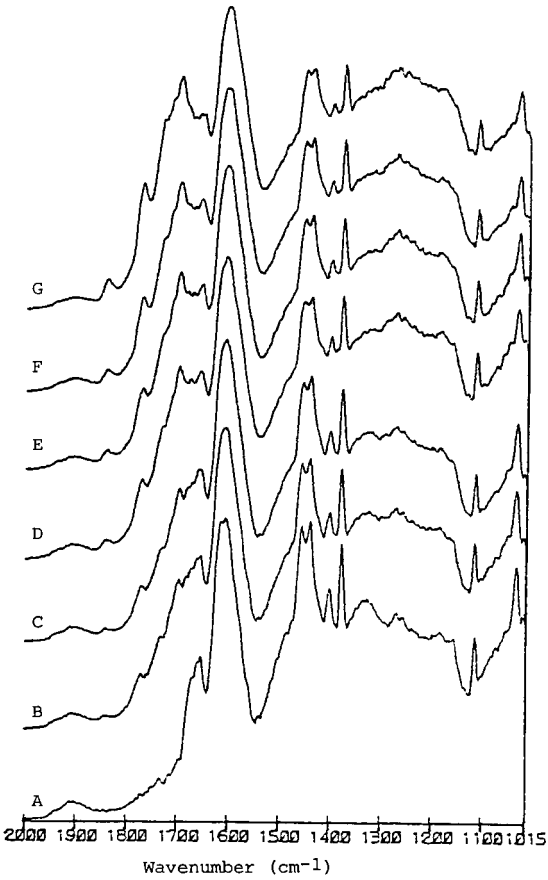

Figure 3: Resolution-enhanced spectra of a low volatility coal subjected to 150°C air oxidation for (A), 0; (B), 2; (C), 4; (D), 6; (E); 8; (F), 10; (G), 12 days.

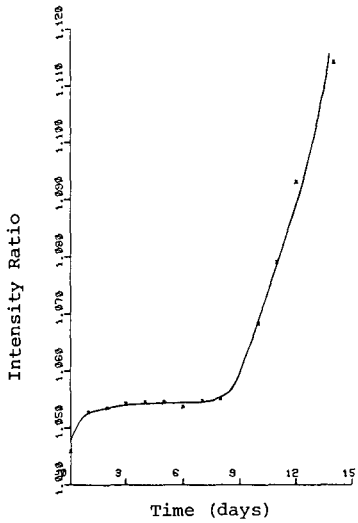

Figure 4

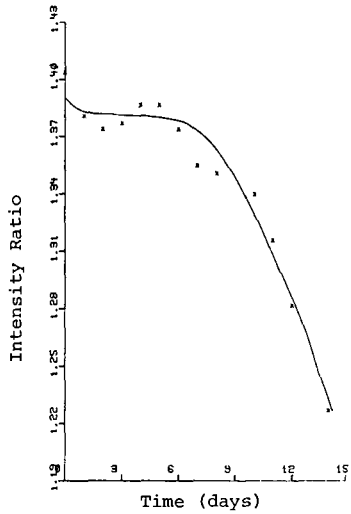

Figure 5

Figures 4, 5 and 6: Plots of ratio of band intensities in the DR spectra of a low volatility coal (PSOC 620, Bedford Co., PA) against time of oxidation at 150°C.

Figure 4: Aromatic C-H stretch (3070 cm^{-1}) vs symmetric methyl stretch (2872 cm^{-1});

Figure 5: Asymmetric methylene stretch (2920 cm^{-1}) vs asymmetric methyl stretch (2962 cm^{-1});

Figure 6: 760 cm^{-1} aromatic C-H out-of-plane deformation vs 815 cm^{-1} band.

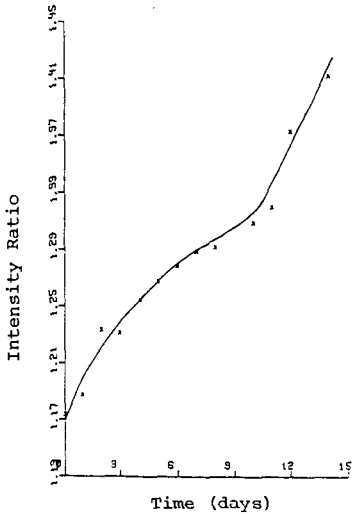

Figure 6

THE IDENTIFICATION AND CHEMISTRY OF SPECIES RESULTING FROM THE RAPID PYROLYSIS OF SMALL COAL PARTICLES IN VACUUM AND IN THE PRESENCE OF REACTIVE GASES

R.H. Hauge, L. Fredin, J. Chu and J.L. Margrave

Department of Chemistry, Rice University, Houston, Texas 77251

INTRODUCTION

The various experiments in this study are designed to produce data from reactors which emphasize the early stages of coal gasification and its reactions with auxiliary gases by bringing the coal quickly up to reaction temperature under conditions where highly reactive gas phase intermediates can exit rapidly from the reaction zone. They are then deposited on a 15K reflective surface with a large excess of inert gas where further reaction is rapidly quenched. The products when isolated in a non-interactive solid such as nitrogen, argon, or even dry air exhibit well-defined spectra which allow the precise measurement of isotopic shifts and peak positions. Free radicals and other reactive species can be detected by characteristic infrared spectra. The presence of intermediates is also monitored with a fast time response quadrupole mass spectrometer. The combination of mass spectrometry and matrix isolation infrared spectroscopy serves as an effective probe for the existence of transient gaseous reaction intermediates.

The types of data obtained from the studies include:

(1) Structural data for new species and suggested reaction pathways from isotopically-substituted reactants.

(2) Information on the dependence of various gas products formed on rates of heating, reactant gases, and coal particle size.

The question as to whether the reactions of particular primary building blocks of coal lead to specific products is studied by adding the molecular species, i.e., various polycyclic aromatics (PCA's) to the coal or as a reactant gas and noting the effect on product distribution.

EXPERIMENTAL

A new matrix isolation system has been designed to allow both mass spectrometric and matrix isolation infrared studies of highly reactive transient species. Close coupling with differentially pumped systems permits the detection of species evolving from samples exposed to pressure pulses of various gases up to one atmosphere. The system is integrated into a high resolution Fourier transform spectrometer which covers the spectral range from the far i.r. to the near i.r. (100 microns to 1 micron). The design has seventy available deposition surfaces. This large number of surfaces is very valuable in attempts to detect small changes which occur due to changed reactor conditions. The increased accuracy of infrared difference spectroscopy can be used to great advantage with a large number of samples which result from small changes in reactor conditions. The combination of mass spectrometric and matrix isolation spectra greatly increase the likelihood of positive species identification. Three quartz crystal

infrared. Results from this study are presented in Figure 5.

At 146C, coal devolatilization can be characterized by evolution of CO_2, CH_4, H_2O, and CO. At an increased temperature of 326C, light hydrocarbon gases such as C_2H_4 and C_2H_6 are observed along with CH_4, CO_2, CO and H_2O. Most of these light hydrocarbons are devolatilized between 326 and 605C. A similar behavior has been noted by Solomon and co-workers. /1,2/ At 1038C, a new peak at 1525 cm^{-1} appears which has not yet been identified.

An interesting observation is that CO_2 seems to reach maximum yield at low temperatures and remains relatively constant at higher temperatures. However, CO appears to increase with higher temperatures and does not reach a maximum at the highest temperature studied.

Rapid Pyrolysis of Illinois #6

Studies of rapid pyrolysis of coal granules, using the pulsed flow reactor and the coal granule inlet valve described in Figure 3 indicate results similar to those for slow pyrolysis. However, rapid pyrolysis of Illinois #6 powder gives a much more complex IR spectrum with two new peaks appearing at 1180 and 1328 cm^{-1}. These two peaks are predominant and always occur simultaneously. Their relative intensities are always the same, indicating that they are due to a single species.

A comparison of rapid pyrolysis of Illinois #6 granules versus powders is illustrated in Figure 6.

Two other coals beside Illinois #6 were studied, Western Kentucky and Upper Freeport as shown in Figure 7. Western Kentucky is a high moisture and high oxygen content coal while Upper Freeport is a low moisture and low oxygen content coal. Both types of coal gives results similar to Illinois #6 when their powders are rapidly pyrolyzed. Absorptions at 1180 and 1328 cm^{-1} are predominant over the methane absorption for both coals studied. This indicates that the species responsible for 1180 and 1328 cm^{-1} is common to all coals during rapid pyrolysis.

Rapid Pyrolysis of Oxidized Illinois #6

Illinois #6 powder was oxidized by heating in an oven at 190C. Samples taken after one hour and after 18 hours of heating were rapidly pyrolyzed through the pulsed flow reactor. Figure 8 shows the predominant gaseous products to be CO_2, CO and H_2O, as expected for oxidized coal. Slight traces of CH_4 and the species responsible for 1180 and 1328 cm^{-1} are also observed. This indicates that the presence of the unidentified intermediate species is not dependent upon the extent of oxidation of the coal samples. It is, however, reduced in yield which indicates the species is not due to oxidation of the coal sample.

Rapid Pyrolysis of Illinois #6 with D2016 and D2018

The effect of gaseous water on rapid pyrolysis of Illinois #6 granules was studied by the addition of D2016 and D2018. Gaseous deuterated water was pre-mixed with argon and pulsed through the reactor immediately after coal granules were dropped into the hot reactor zone. Results, shown in Figure 9, suggest that oxygen from

mass monitors are mounted on the cold trapping block. They serve as very sensitive quantitative monitors of the beam density striking the trapping surface. A detailed schematic of the MI-MS apparatus is shown in Figures 1 and 2.

Figure 3 presents a schematic diagram of a pulsed flow reactor for coal granules and coal powders. The reactor contains three sections. The first section, A, contains the coal granule inlet valve. The second section, B, contains the hot reactor zone, resistively heated through a nichrome wire wrapped around the outside of the quartz tube. It is separated from the cold (15K) copper matrix isolation surface by a small amount og quartz wool inserted in the tube. Coal granules are introduced into the hot reactor zone by simply dropping them in through valve A. A two-way valve is then pulsed open which causes an inert gas, argon, to carry the gaseous products through the quartz wool and onto the 15K copper surface of the matrix isolation apparatus. Approximately 15 grains of coal were used for each trapping.

The third section, C, is used for introduction of coal powders into the hot reactor zone. It contains a flutted glass column, separated from the hot reactor zone by two two-way valves. The inert carrier gas, argon, is let in from the bottom, passing the frit, creating a simulated fluidized bed of coal powder. Coal powder along with the inert gas is pulsed into the hot reactor zone by sequentially pulsing open each of the two-way valves. Gaseous products are carried by the excess inert gas onto the 15K matrix isolation surface to be studied by infrared spectroscopy. Usually 50-100 pauses of coal powder were used for each trapping.

PULSED FLOW VERTICAL HEATER REACTOR

A schematic drawing of the vertical heater reactor is shown in Figure 4. This reactor is very similar to the pulsed flow reactor described in Figure 3, except that the design allows the gaseous products to be trapped directly onto the matrix surface without formation of tars along the sides of the tube as in the case for the previous reactor. The hot reactor zone is placed in the matrix isolation chamber. It consists of a quartz tube with a small opening near the bottom of the tube which is inserted into a vertical tantalum heater. The tantalum heater also has a small opening on the side facing the matrix isolation surface. A small piece of quartz wool is placed into the quartz tube so that it just covers the opening. This prevents particles from being blown onto the matrix surface and keeps them in the hot reactor zone.

Coal powder is pulsed into the heater in the same way as described for the previous pulsed flow reactor. In general, pyrolysis is carried out over a temperature range of 120 to 1000 C, in vacuo. Argon has been used as the inert carrier and matrix gas.

RESULTS

Slow Pyrolysis of Illinois #6 Powder

Coal particles (250 mesh) are placed in the vertical quartz tube described in Figure 4 and slowly heated from 146C to 1038C. Gaseous products obtained at different intervals of temperature are trapped with argon, introduced from a separate inlet tube, onto the 15K copper matrix isolation surface and subsequently examined through

the water ends up as CO and CO_2, as seen by the presence of CO^{18} and $CO^{16}O^{18}$ in the reaction with D_2O^{18}. However, no deuterated methane is evident in either reactions.

DISCUSSION

To date our work has shown that the product gaseous species from pyrolysis are very dependent on coal particle size. As might be expected, the larger particles tend to produce the smaller alkanes and alkenes as a result of secondary pyrolysis. Rapid pyrolysis of the smaller particles produces new species which are thought to be more representative of the species resulting from initial bond breaking steps. One species in particular produces strong features at 1328 and 1180 cm^{-1}. Insufficient reference data has prevented the identification of this species as yet but it is hoped that studies of model compounds and additional mass spectrometric information will allow identification of this significant reaction intermediate. It is also clear that improved control of particle size and the amount of coal injected per pulse will greatly aid our interpretation of product distributions. Of course, this also applies to studies of reactions with gases such as water, hydrogen and carbon dioxide. Preliminary work with a small gas recirculating system in which selected coal particle sizes are entrained with reactant and inert gases indicates that a much improved pulsed coal injection system is possible. It is expected that considerable additional data of product distributions correlated to particle size, temperature and reactant gas will be available in the near future.

REFERENCES

1. P.R. Solomon, "The Evolution of Pollutants During Rapid Devolatilization of Coal", Rep. R76-952588-2, United Technologies Research Center, East Hartford Conn. 1977, Rep. NSF/RA-770422, NTISPB, 278496/AS, 1977.

2. Adv. in Chem. Series, 192, Coal Structure, Ed. M.L. Gorbaty and K. Ouchi, Chap. 7, "Coal Structure and Thermal Decomposition", P.R. Solomon.

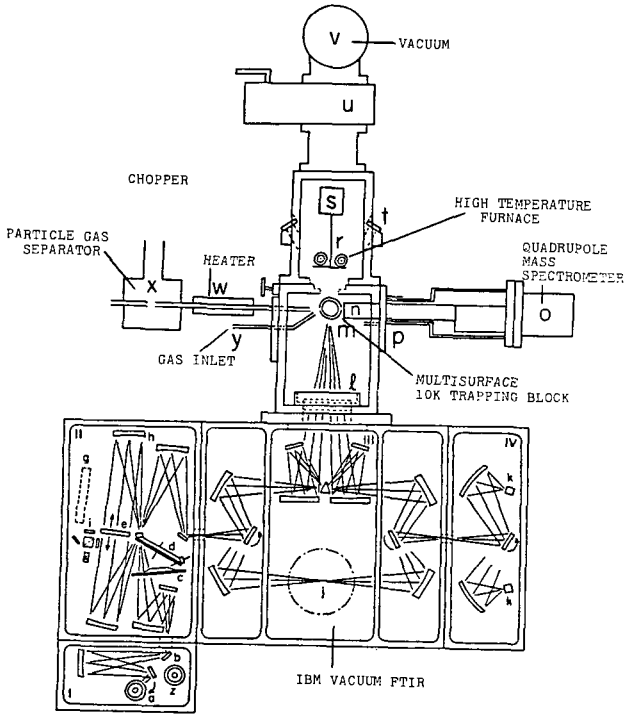

FIGURE 1

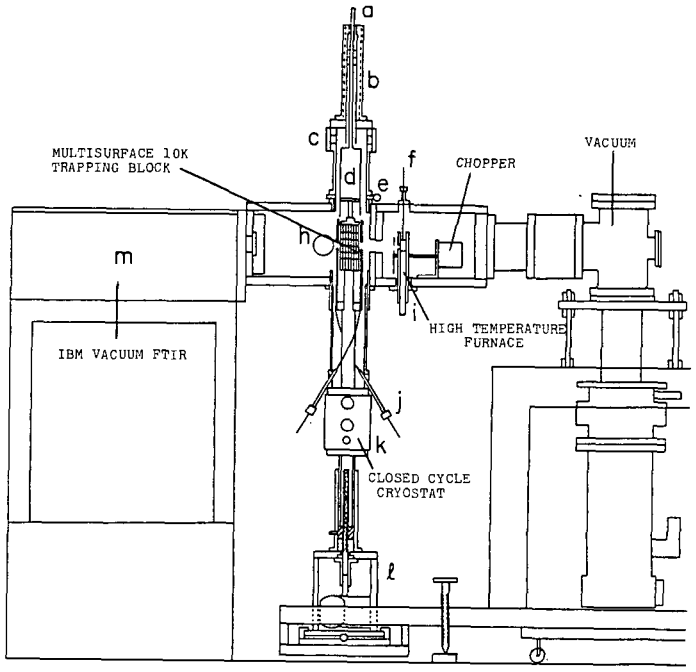

FIGURE 2

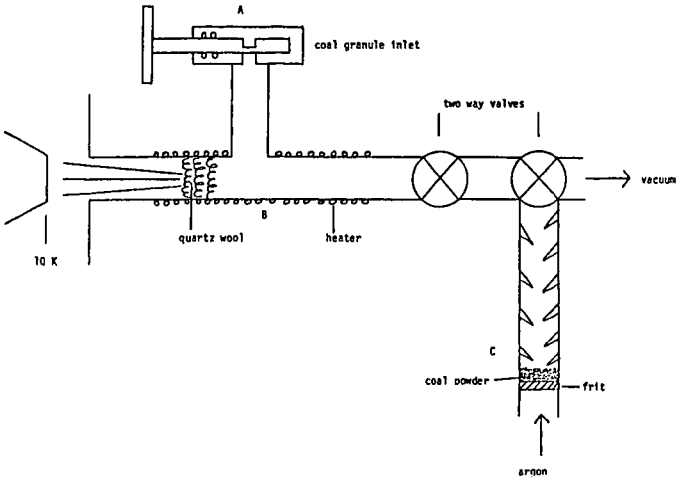

Fig. 3. PULSED FLOW REACTOR

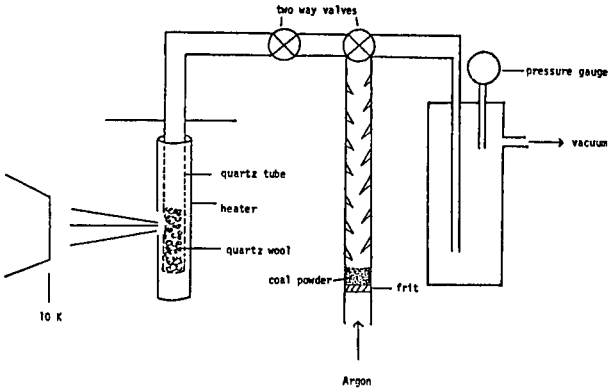

Fig. 4. PULSED FLOW VERTICLE HEATER REACTOR

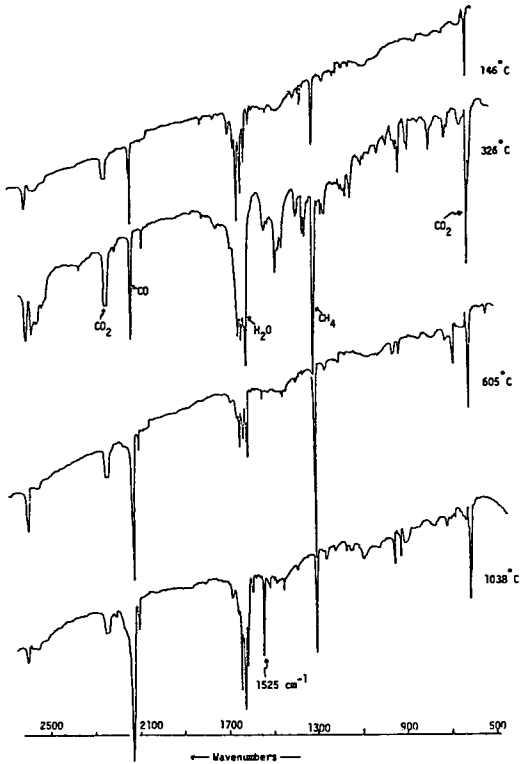

Fig. 5. Slow Pyrolysis of Illinois #6 Powder

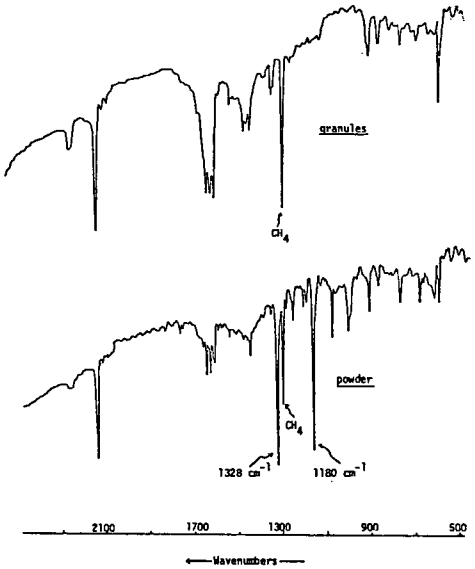

Fig. 6. Rapid Pyrolysis of Ill. #6 at ~1000°C

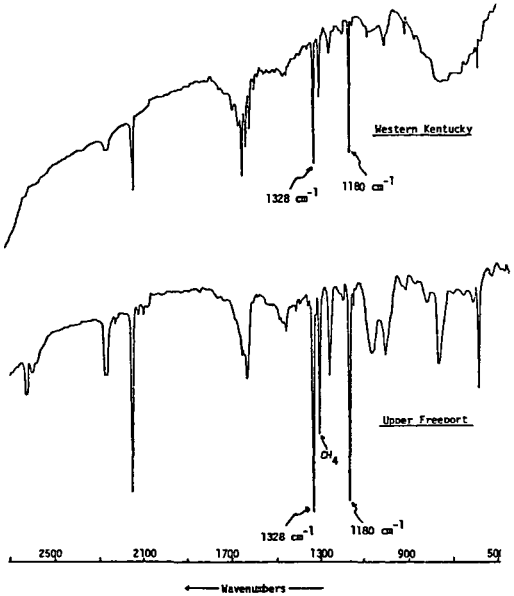

Fig. 7. Rapid Pyrolysis of Other Coals at 1000°C

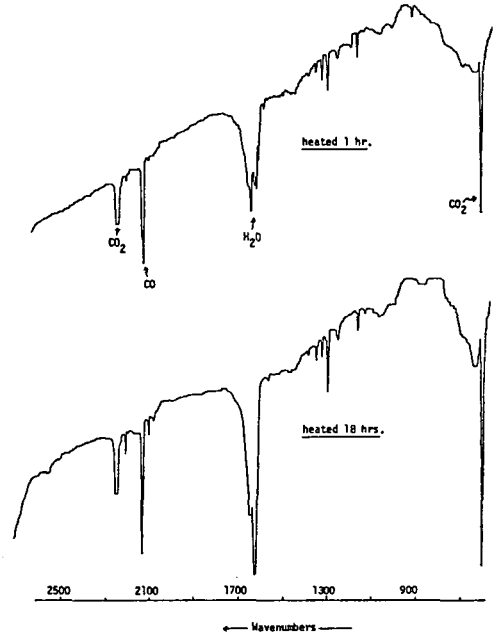

Fig. 8. Rapid Pyrolysis of Oxidized Ill. #6

Fig. 9. Rapid Pyrolysis of Ill. #6 with D_2O^{16} & D_2O^{18}

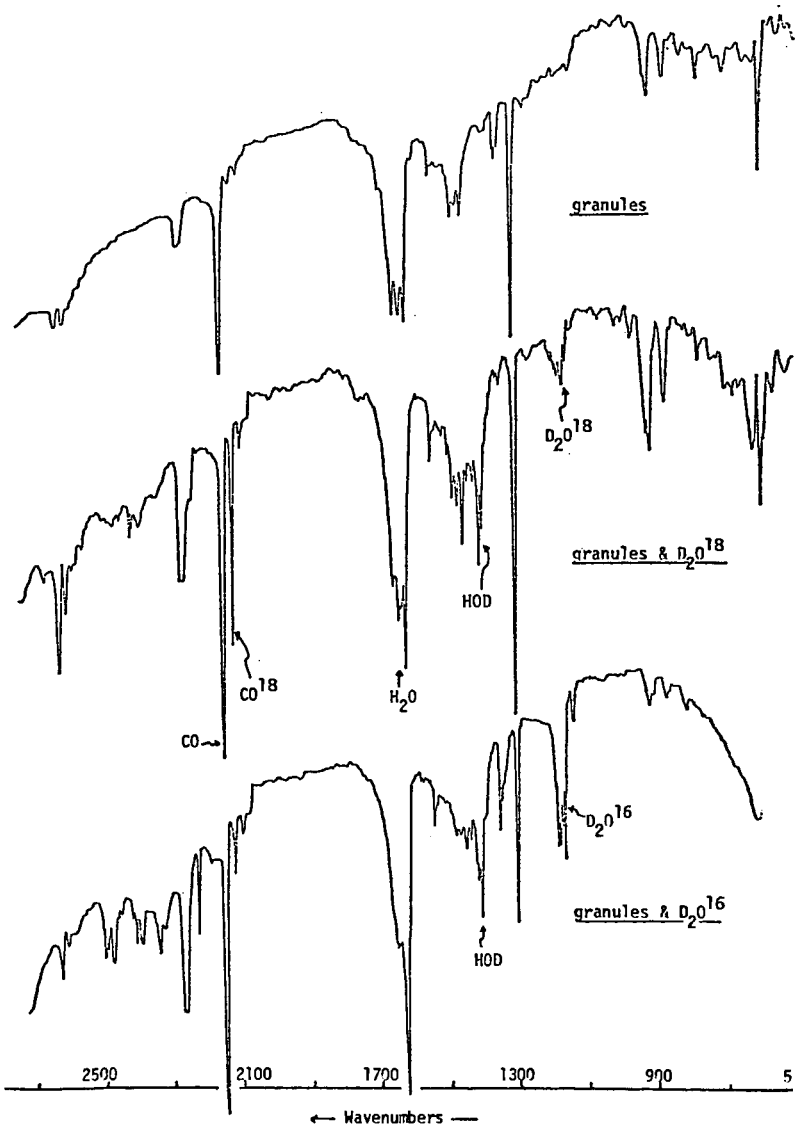

CHEMISTRY AND STRUCTURE OF COALS: AIR OXIDATION STUDIES RELATED TO FLUIDIZED BED COMBUSTION

E. L. Fuller, Jr., N. R. Smyrl, R. W. Smithwick III, and C. S. Daw*

Oak Ridge Y-12 Plant
Union Carbide Corporation,
Nuclear Division
Oak Ridge, Tennessee 37830

Efficient use of coals as feedstocks and thermal energy requires comprehensive understanding of the physical and chemical structure of the starting materials and the changes wrought in the processing steps. Diffuse Reflectance Infrared Fourier Transform (DRIFT) spectroscopy is being developed[1,2] as a facile, nondistructive, rapid, highly informative means of measuring and monitoring the chemical structure of coals

Figure 1 shows how well the DRIFT technique can be used to rank coals with respect to the hydroxyl content and hydrocarbon type and content for unweathered powders of the greater maturity increasing from top to bottom. Figure 2 shows the wealth of information as related to carbonyl content, polynuclear aromaticity and mineral type and mineral content for the various coal powders and the simulated end members of the coalification process (cellulosic fibers and graphite). Figure 3 is an example where the changes due to oxidation are readily discerned. This partial oxidation involved loss of the aliphatic hydrogen (2800-3000 cm^{-1}) and simultaneous carbonyl formation (1600-1900 cm^{-1}) with little or no loss of hydroxyl (3600-2000 cm^{-1}), aromatic hydrogen (3200-3000 cm^{-1}), polynuclear carbon (1650-1550 cm^{-1}), nor polyaromatic hydrogen (900-700 cm^{-1}). Studies of catalytic effects due to inorganic constituents are facilitated by DRIFT as shown in Figure 4 where quantitative measures are obtained for the amount and nature of argillic components inherent in and/or admixed with the run of the mine coals.

The DRIFT technique uses the coal as a solid piece and/or as powder with no mulling agents (CCl_4), support medium (KBr), or other extraneous materials that can contribute erroneous spectral features and serve as barriers for <u>in situ</u> reaction studies. Figures 5 and 6 illustrate the additional information that one can obtain by noting spectral changes wrought on oxidation. The dehydrogenation process involves oxidation of only the aliphatic hydrocarbon initially and only at the latter stages the oxygen attack involves unsaturated olefinic and aromatic species

(3035 cm^{-1}). Also there is little or no loss of phenolic, carboxyl alcoholic, etc. entities (3650-2400 cm^{-1}) until the later stages of reaction. Figure 6 shows more details of the oxygen insertion process where the initial oxidation forms somewhat isolated carbonyls (1705 cm^{-1}) with higher degrees of reaction progressively forming analogs of carboxylic acids (1745 cm^{-1}), acid anhydrides (1775 cm^{-1}) and organic carbonates (1845 cm^{-1}) as a synergetic continum of oxygen enrichment prior to the final evolution as gaseous carbon dioxide. Steady state conditions seem to prevail where the process proceeds continuously at the steady state concentrations noted in the upper difference spectrum. DRIFT spectroscopy uniquely allows one to monitor the concentration of virtually all of the entities required to fully elucidate the oxidation mechanism proposed by batch techniques.[3,4] Additional details of interpretation and experimental techniques are given elsewhere.

Mercury porosimetry, vapor sorption, microscopy, and helium picnometry aid appreciably in our heat and mass transport modelling under conditions relevant to fluidized bed reactors of the Tennessee Valley Authority. The original rigid structure of the coal swells and expands as volatile bubbles grow and flow out of the tarlike mass where the -3+4 mesh particles are introduced into the hot (1500°F) reactor. The volatiles burn vigorously and the residual char slowly burns away to leave residual ash. Data will be given to show the nature of the porosity (internal/external, open/closed, macro/micro, etc.) as determined by the various techniques and the relevance to existing and proposed processes.

ACKNOWLEDGMENTS

The Oak Ridge Y-12 Plant is operated by Union Carbide Corporation's Nuclear Division for the Department of Energy under U.S. Government Contract W-7405-eng-26. *C. S. Daw is located at the Oak Ridge National Laboratory.

REFERENCES

1. Smyrl, N. R. and Fuller, E. L., Jr.; *Chemistry and Structure of Coals: Diffuse Reflectance Infrared Fourier Transform (DRIFT) Spectroscopy of Air Oxidation* in Coal-Coal Products: Analytical Characterization Techniques edited by E. L. Fuller, Jr., American Chemical Society, 1982.

2. Fuller, M. P., Hamadeh, I. M., Griffiths, P. R., and Lowenhaupt, D. E.; *Diffuse Reflectance Infrared Spectrometry of Powdered Coals*, Fuel, 61, 529 (1982).

3. Bouwman, R. and Frericks, I.; *Low Temperature Oxidation of a Bituminous Coal: Infrared Spectroscopic Study of Samples from a Coal Pile*, Fuel, 59, 309 (1980).

4. Keifer, J. R., Novicky, M., Akhtar, M. S., Chughtai, A. R., and Smith, D. M.; *The Nature and Reactivity of Elemental Carbon (Soot) Surface as Revealed by Fourier Transform Infrared (FTIR) Spectroscopy*, Pro Intnl. Soc for Opt. Eng., 289, 184 (1981)

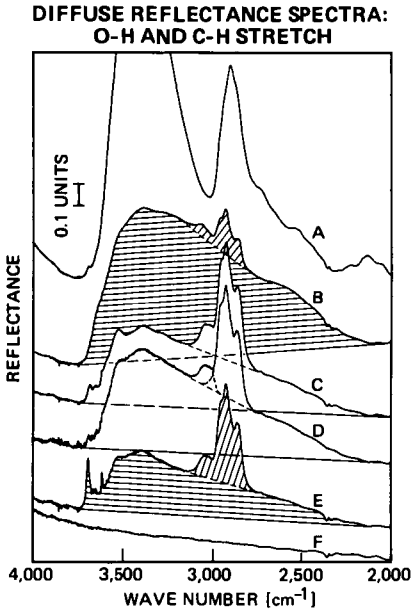

Figure 1. Hydrogen stretch region of DRIFT spectra of; A. cellulosic fibers, B. Lignite, C. Subbituminous Coal, D. C-bituminous coal, E. A-bituminous coal, and F. Graphite. All samples are equilibrated with 30 ppm moisture in the argon purge.

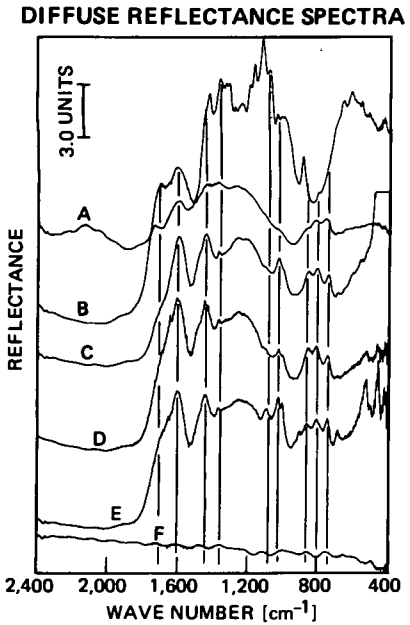

Figure 2. Low energy DRIFT Spectra: Legend Same as Figure 5. Vertical lines (left to right) denote characteristic bands for (1) carbonyl, (2) polynuclear aromatic rings, (3) methylene, (4) mineral, and (5) aromatic hydrogen groups, respectively.

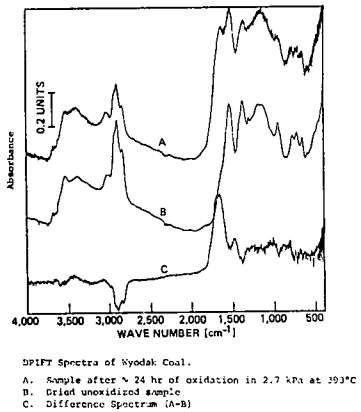

Figure 3. DRIFT Spectra. A. Partially oxidized coal powder 1 hour, 2.7 kPa of air at 395°C. B. Original coal powder dried in vacuum at 400°C. C. A-B with no scaling factor to show the changes due to oxidation.

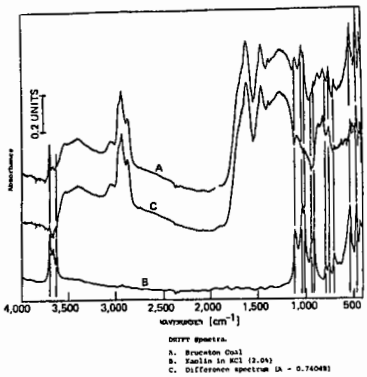

Figure 4. Correction for Minerals. A. DRIFT spectrum for powdered coal. B. DRIFT spectrum of 20% kaolin dispersed in powdered KCl. C. A-0.7404B for each of the individual 3600 data points.

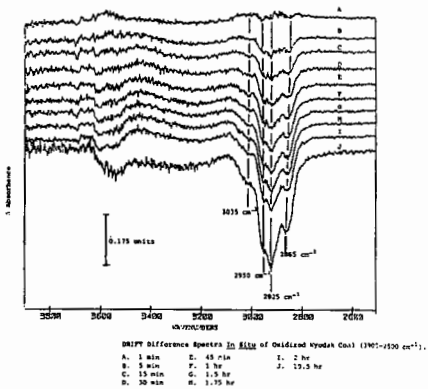

Figure 5. DRIFT Difference Spectra for ca 19 hours continuous oxidation of coal. These difference spectra show the loss of hydrogen from C-H and, in later stages, OH units of coal.

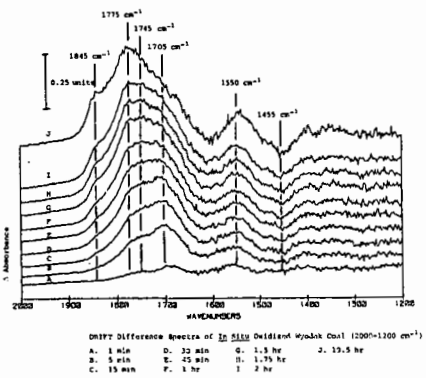

Figure 6. DRIFT Difference Spectra for Carbonyl Region. The amount and nature of the oxygenated specie changes markedly. A general increase in carbonyls is noted and shift to higher frequencies is evident.

Solid-Solid Contacting in Catalyzed Gas-Char Reactions

D. C. Baker

Shell Development Company
Houston, TX 77001

and

A. Attar

Department of Chemical Engineering
North Carolina State University, Raleigh, NC 27650

Introduction

Coal char samples that are used for gas-carbon reaction studies can possess a wide range of porosities depending upon preparation techniques. In general, the char may be classified as non-porous, slightly porous, or highly porous. The total particle reaction rate is a summation of the intra-particle reaction rate and the external surface reaction rate and is dependent upon the type of char under investigation, viz.

$$r_{meas} = (\eta A^{int} + A^{ext}) r_{true} \tag{1}$$

where r_{meas} is the measured total particle reaction rate, r_{true} is the true reaction rate, A^{int} and A^{ext} are the internal and external surface areas, respectively, and η is the effectiveness factor.

Further elaborations on the total particle reaction rate arise in gas-carbon reactions when reaction at specific sites warrants the inclusion of an internal and external active site density, C_t, and when r_{true} applies to a complex reaction path such as gasification, viz. char-CO_2 gasification,

$$r_{meas} = (\eta A^{int} C_t^{int} + A^{ext} C_t^{ext}) \frac{k_1(CO_2)}{1 + \frac{k_1}{k_3}(CO_2) + \frac{k_{-1}}{k_3}(CO)} \tag{2}$$

It is often difficult to determine when the effectiveness factor is approximately unity for complex reaction paths, consequently rate expressions simpler than equation (2) are often used. For example, Jalan and Rao[1] assumed a first order reaction rate with respect to CO_2 during char-CO_2 gasification. Also note that in the case of equation (2) only "apparent" activation energies can be obtained from Arrhenius plots of r_{meas} vs. 1/T since k_1, k_{-1}, and k_3 all depend on T, and even this approach is invalid if the surface areas and site densities are not constant with respect to temperature and the time duration of the experiment.

When a solid catalyst is introduced onto char, the catalyst contacting with char must be considered since it may be (a) limited to a small portion of the external char surface area, (b) contacted with the entire external char surface area, but excluded from internal pores, or (c) contacted with the entire external and internal char surface areas. The consequences of catalyst contacting on measured reaction rates and measured activation energies need to be realized when interpreting experimental data since these measurements often are taken as the main basis for speculating on catalytic mechanisms.[2-4]

Analysis

It has been proposed that certain catalysts in gas-carbon reactions act only to increase the density of active sites (i.e. C_t in equation (2)).[5] Assuming this type of catalysis prevails, Table 1 summarizes, for several initial reaction conditions and for several conditions of catalyst contacting, the changes in measured reaction rates and measured activation energies which occur when a solid catalyst is introduced onto char. As shown in Table 1, the initial uncatalyzed reaction conditions may be in the regime of kinetic control ($\eta=1$), intra-particle diffusional control ($\eta<1$), or external diffusional control (i.e. proportional to the difference in bulk and surface concentrations and film thickness). When a solid catalyst is introduced, the catalyzed reaction conditions depend on the porosity of the char and the extent of catalyst contacting (i.e. catalyst penetrates internal pores or catalyst excluded from internal pores). The interplay between initial uncatalyzed reaction conditions and extent of catalyst contacting during catalytic gasification can lead to measured activation energies increasing, decreasing, or remaining constant with catalyst application. An interesting case is where the measured activation energy increases with the introduction of a solid catalyst. In such a case a slightly porous char has an uncatalyzed total particle reaction rate initially made up of nearly equivalent external and internal (diffusion controlled) reaction rates. Introduction of a catalyst, which is excluded from internal pores but which contacts the entire external surface area, can lead to the external surface reaction rate overwhelming the intra-particle reaction rate and consequently increasing the measured activation energy.

In reviews of catalyzed gas-carbon reactions, it is often noted that the measured activation energy may decrease with introduction of a catalyst as the system becomes diffusion controlled.[6] However, similar physical reaction considerations are usually not given to the case where the measured activation energy increases with introduction of a catalyst. Measured activation energies have been reported to increase, decrease, and remain constant for catalyzed gas-carbon reactions relative to the uncatalyzed reactions.[2-5,7] It is interesting to note that catalyst contacting alone may explain these differences.

Results Using Non-porous Char

In a recent study, Baker[8] presented results on the catalyzed char-CO_2 surface exchange of oxygen. Such a system was originally studied

by Orning and Sterling.[9] The char that was used in this study was nonporous thereby eliminating the need for considerations of both intraparticle reaction rates and internal catalyst contacting. By employing a unique pulsing technique, the CO_2 molecules could be followed through a char-packed microdifferential reactor without the use of radioactive tracers which were extensively used in earlier studies.[9-12] The experimental system is depicted in Figure 1. Proper choice of pulse size, pulse residence time, and reactor temperature and pressure, permitted measurements of the char-CO_2 oxygen exchange reaction for uncatalyzed char, as well as char catalyzed with alkali and alkaline earth carbonates, viz.

$$CO_2(g) + C_f \xrightarrow{k_1} CO(g) + C_o \qquad (3)$$

where C_f is a free active exchange site which can accept oxygen from gaseous CO_2 and C_o is an oxygen occupied active exchange site. The total density of active exchange sites is given by

$$C_t = C_o + C_f \qquad (4)$$

Figure 2 presents some of the data from the study. A detailed discussion and analysis is provided by Baker[8] and by Baker and Attar.[13] By initially purging the system with CO, all the active sites were converted to free active sites. Consequently, the reaction rate at low surface oxide formation is given by

$$r_{meas} = A^{ext} C_t^{ext} k_1 (CO_2) \qquad (5)$$

which allows direct measurement of $k_1(T)$. Since negligible gasification occurred, the surface area and active site density, as given in equation (5), remained constant throughout the experiments.

The data which are plotted in Figure 2 indicate the possibility that the activation energy for k_1 at low surface oxide formation, 214 kJ/mole, is the same for catalyzed and uncatalyzed char. Mentser and Ergun determined a similar value of 222 kJ/mole for uncatalyzed carbon black.[14] At high surface oxide formation the back reaction cannot be neglected, viz.

$$CO + C_o \xrightarrow{k_{-1}} CO_2 + C_f \qquad (6)$$

and this leads to curvature in the Arrhenius data.[a] The differences in measured reaction rates for different catalysts is attributed to differences in the density of active sites, C_t^{ext}. Surface areas, A^{ext}, were essentially equivalent for all samples.

At present, the data do not allow discrimination between the degree of catalyst contacting at the char surface for the various carbonates (calcium, sodium, and potassium) and their intrinsic capability to generate active sites on the char surface. However, the data do point out some similarities between catalyzed and uncatalyzed gas-char reactions which are not accounted for in many of the proposed catalytic gasification mechanisms that are based mainly on differences in measured "apparent" activation energies.

---

a Statistically meaningful data could only be obtained at conversions of >3% and the back reaction became noticeable at conversions of 10%, thus limiting the conversion range for activation energy determinations.

Conclusions

Solid-solid contacting may affect the measured reaction rate and measured activation energy during catalyzed gas-carbon reactions. The measured activation energy may increase, decrease, or remain constant with the introduction of a solid catalyst. Data for a non-porous char indicated an identical first step in catalyzed and uncatalyzed char gasification. That is, CO_2 exchanged oxygen with the char surface, apparently at active site locations. The activation energy for this reaction, 214 kJ/mole, was similar for catalyzed and uncatalyzed char, however, the reaction rates differed by orders of magnitude. The catalytic effect for the alkali and alkaline earth carbonates was attributed to differences in the density of active sites. Whether the different catalyzed rates were due to different degrees of external contacting or to true differences in catalytic properties was not resolved in this study.

REFERENCES

1. Jalan, B. P. and Y. K. Rao, Carbon, 16, 175-184, 1978.
2. Veraa, M. J. and A. T. Bell, Fuel, 57, 194-200, 1978.
3. McKee, D. W., Carbon, 17, 419-425, 1979.
4. McKee, D. W., Fuel, 59, 308-314, 1980.
5. Otto, K., L. Bartosiewicz and M. Shelef, Fuel, 58, 565-572, 1979.
6. McKee, D. W., Physics and Chemistry of Carbon (Ed. P. L. Walker, Jr.), 16, 1-118, 1981.
7. Guzman, G. L. and E. E. Wolf, Ind. Eng. Chem. Process Des. Dev., 21, 25-29, 1982.
8. Baker, D. C., Ph.D. Dissertation, Univ. of Houston, 1981.
9. Orning, A. A. and E. Sterling, J. Phys. Chem., 58, 1044-1047, 1954.
10. Bonner, F. and J. Turkevich, J. Am. Chem. Soc., 73, 561-564, 1951.
11. Ergun, S., J. Phys. Chem., 60, 480-485, 1956.
12. McKee, D. W. and J. T. Yates, J. Catalysis, 71, 308-315, 1981.
13. Baker, D. C. and A. Attar, submitted for publication to Fuel.
14. Mentser, M. and S. Ergun, U.S. Bur. of Mines, Bull. No. 664, 1973.

Table 1. Changes in Measured Rate (r_m) and Activation Energy (E_m) with Catalyst Application to Char

Initial Reaction Conditions		Non-Porous Char	Slightly Porous Char		Highly Porous Char	
			Catalyst Penetrates Internal Pores	Catalyst Excluded From Internal Pores	Catalyst Penetrates Internal Pores	Catalyst Excluded From Internal Pores
Kinetic Control	r_m	Increase				No Change
	E_m	No Change or Decrease				
Intraparticle Diffusional Control	r_m	NA	Increase			
	E_m		Decrease	Increase	Decrease	
External Diffusional Control	r_m	No Change				
	E_m					

NA - Not Applicable

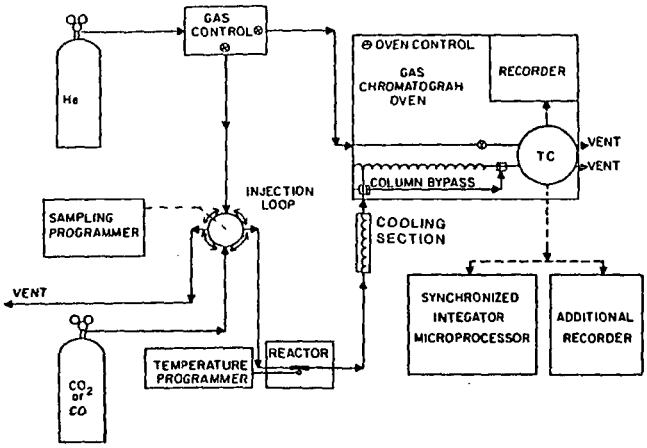

FIGURE 1

SYSTEM FOR STUDYING CHAR-CO_2 SURFACE EXCHANGE OF OXYGEN[8]

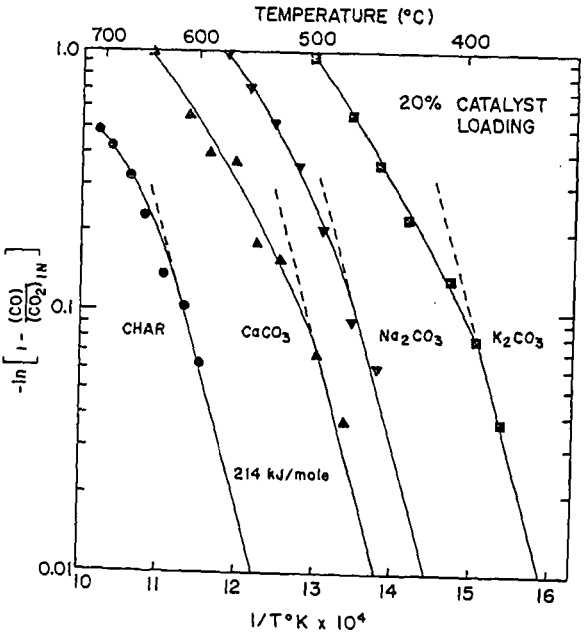

FIGURE 2

ARRHENIUS-TYPE DATA FROM CHAR-CO_2 SURFACE EXCHANGE OF OXYGEN[8]

A STUDY OF THE ROLE OF ALKALI METAL SALTS AS CHAR GASIFICATION CATALYSTS BY KNUDSEN CELL MASS SPECTROMETRY

Bernard J. Wood, Robert D. Brittain, and K. H. Lau

Materials Rsearch Laboratory, SRI International
333 Ravenswood Avenue, Menlo Park, CA 94025

INTRODUCTION

Although there is much current interest (1, 2)in the high-temperature reaction of oxidizing gases with carbons admixed with alkali metal salts, there is no consensus on the chemical mechanisms that comprise the process. There is general agreement that the carbon and the salt chemically interact at modest temperatures to form a catalytically active state or reactive intermediate for the oxidation reaction. The nature of this state or intermediate, however, is disputable. To search for the identity of this intermediate and to elucidate its role in catalyzing the gasification or oxidation of carbon, we have employed Knudsen cell mass spectrometry to examine the gaseous species in equilibrium with carbon-alkali metal salt admixtures at elevated temperatures.

EXPERIMENTAL

Knudsen cell mass spectrometry is a technique which reveals the gaseous species in equilibrium with a solid or liquid phase, alone or in the presence of added gases. The material of interest is loaded into the Knudsen cell, a small cylindrical container made of refractory material, with an orifice that is a very small fraction of the cell's total surface area. The cell is situated in a high vacuum system so that the orifice is in line-of-sight with a mass spectrometer ion source. An electrical resistance heating element permits the cell to be heated to high temperatures. Gaseous species formed in the cell, or introduced through an inlet tube, collide, on the average, thousands of times with the contents of the cell before they escape through the orifice. Consequently, these species can be considered to be in chemical and thermal equilibrium with the solid/liquid phases in the cell when they emerge from the orifice and are detected by the mass spectrometer. A shutter, which can be moved over the orifice, permits the cell effusate to be distinguished from the ambient gases in the vacuum system. The general experimental technique and our apparatus have been described in the literature (3, 4). In our experiments we used 100 mg samples of pure alkali metal salts or of salts admixed with Illinois No. 6 coal char or Spheron-6 channel black in Knudsen effusion cells fabricated from platinum and from graphite. We determined the relative partial pressures of vapor components by measuring their ion intensities with ionizing energies 3 to 3.5 eV greater than their respective appearance potentials, to avoid contributions to the ion signals by alternative fragmentation processes in the mass spectrometer. The absolute vapor pressure of each species was calculated by the equation,

$$P = k(I^{+})(T)/\sigma \qquad 1)$$

where T is the Temperature in Kelvins, σ is the relative ionization cross-section, and k is an instrumental constant.

The particular systems of interest in this study were K_2CO_3 mixed with Spheron-6 or char, Cs_2CO_3 mixed with Spheron-6, and KBr mixed with Spheron-6. The effects of added H_2O, CO_2, CO on vapor species abundances above the K_2CO_3 admixtures were investigated in separate runs. The relative abundances of the vapor species above the pure alkali metal salts in platinum cells, were also determined.

RESULTS

Equilibrium Gaseous Species

Pure Salts

On the basis of the observed ions and their relative intensities (Table 1), we conclude that the major vapor species over $K_2CO_3(s)$ are $K_2CO_3(g)$, $K(g)$, $CO_2(g)$, and $O_2(g)$. The neutral $K_2O(g)$ appears only at high temperature in negligible amount. The vaporization processes of K_2CO_3, in the observed temperature range can be written as follows:

$$K_2CO_3(s) = 2K(g) + CO_2(g) + 1/2O_2(g) \qquad 2)$$

$$K_2CO_3(s) = K_2CO_3(g) \qquad 3)$$

The enthalpy, ΔH, for Reaction 2 was calculated from the temperature dependence of the intensities of the gaseous ions. The value obtained, 247 (+/- 5) kJ/mol, is in agreement with the value of 251 kJ/mol calculated from JANAF data (5). The derived enthalpy of Reaction 3 was 291 kJ/mol.

The vaporization of Cs_2CO_3 was found to proceed by analogous reactions:

$$Cs_2CO_3(s) = 2Cs(g) + CO_2(g) + 1/2O_2(g) \qquad 4)$$

$$Cs_2CO_3(s) = Cs_2CO_3(g) \qquad 5)$$

Enthalpies of vaporization were calculated from the temperature dependence of Cs^+ and $Cs_2CO_3^+$ in the temperature range 930 to 1051 K. For Reaction 4 the experimental enthalpy was ΔH = 240.3 (+/- 3) kJ/mol compared to 248.7 kJ/mol calculated from the JANAF tables (5). The enthalpy of the sublimation reaction was 251.9 (+/- 3) kJ/mol.

Carbon-Salt Admixtures

Over an admixture of K_2CO_3 and coal char (8 wt% K, mole ratio K/C = 0.029), observed in the temperature range 723 to 973 K, the only identifiable vapor species were $K(g)$, $CO(g)$, and $CO_2(g)$, suggestive of carbothermic reduction of the inorganic salt:

$$K_2CO_3(s) + C(s) = 2K(g) + CO_2(g) + CO(g) \qquad 6)$$

$$K_2CO_3(s) + 2C(s) = 2K(g) + 3CO(g) \qquad 7)$$

The temperature dependence of vapor pressures for $K(g)$, $CO(g)$, and $CO_2(g)$ is given in Table 2. The vapor pressures of $K(g)$ above the K_2CO_3-char sample and the pure K_2CO_3 sample are plotted in Figure 1 along with the equilibrium lines calculated from JANAF data (5) for Reactions 2, 6, and 7. The pressures of $K(g)$ above the mixture of salt with char are intermediate between those for the pure salt and for the two reduction reactions.

In a similar manner the vaporization behavior of pure Cs_2CO_3 and mixtures with Spheron-6 and coal char were investigated. A sample of Cs_2CO_3 admixed with Spheron-6 (25 wt% Cs, mole ratio Cs/C = 0.033) was studied in the temperature range 729-1059 K. The major species observed were Cs(g), CO(g), and CO_2(g), but the CO_2^+ and the CO^+ signals decreased continuously with time (Table 3). CsOH(g) was also observable in the vapor at very low partial pressures. The temperature dependence of partial pressures of the observed species above the mixture is given in the order in which data were taken in Table 3. Successive points at the same temperature demonstrate the time behavior of the signals for each species. The material removed from the Knudsen cell at the conclusion of this experiment was pyrophoric.

To provide a clue to the composition of the solid that remained in the cell, another sample of the Cs_2CO_3-Spheron-6 mixture was heated in a separate vacuum system at 800 K overnight. A portion of this vacuum-heated mixture was transfered into a capillary tube under an argon atmosphere and analyzed by X-ray diffraction. A crystalline diffraction pattern was observed but could not be identified.

In separate experiments, the equilibrium pressure of Cs above pure Cs_2CO_3, 8 wt% Cs_2CO_3 in char, 25 wt% Cs_2CO_3 in char, and 25% Cs_2CO_3 in Spheron-6 was observed. The results of these experiments are plotted in Figure 2, along with the calculated values for vaporization of the pure solid and for a possible carbothermic reduction reaction. The pressure of Cs above the Spheron-6 samples is observed to be approximately one order of magnitude higher than that above the pure salt, while the Cs pressure over the 8 wt% mixture with char is two orders of magnitude lower than that of the pure salt. Increasing the weight loading of Cs in the sample to 25% is accompanied by an increase of the Cs vapor pressure by an order of magnitude. X-ray diffraction analysis of the residual solid removed from the Knudsen cell revealed the presence of cesium aluminum silicate, $CsAlSiO_4$, among other unidentified lines.

In marked contrast to the results for the carbonate-carbon systems, samples of pure KBr and KBr admixed with Spheron-6 (4 wt%K; mole ratio K/C = 0.014) behaved identically with respect to the vaporization of K-containing species; KBr sublimation was the only observable reaction involving potassium in both samples.

Effect of Added Gases

The effects of added H_2O, CO , and CO_2 upon vapor pressure of K(g) above a Spheron-6 admixture with K_2CO_3 was investigated in the graphite Knudsen cell. Effects on the K^+ signal level were studied in the temperature range 900-1100 K. During addition of the reactant gas the total pressure in the mass spectrometer was increased by a factor of 10 to approximately 1×10^{-4} Pa. Substitution of Ar(g) for the reactive gases had no effect on the K^+ signal, indicating that there was no dynamic flow effect on the performance of the Knudsen cell. Addition of CO(g) caused an immediate, completely reversible K^+ signal depression by 10-20%. This behavior would be expected by the effect of the law of mass action on Reactions 6 and 7. CO_2(g) addition resulted in immediate depression of the K^+ level by 10% followed by a slower decrease as flow continued. When CO_2 input was discontinued, only partial recovery of the K^+ signal level occurred. A similar pattern in K^+ signal depression was observed upon addition of H_2O(g). A blank run, with pure K_2CO_3 in the graphite cell at 1000 K, exhibited measurable pressures of K(g) and CO(g), indicative of some interaction between K_2CO_3 and the cell. However, the addition of H_2O or CO_2 had no effect on levels of CO^+ and H_2^+. The K^+ signal level was depressed by about 15% during H_2O flow, but returned to the same level after the flow was terminated. The depression of K^+ during H_2O flow is accounted for in part by the appearance of KOH^+ in the effusate at about 1% of the intensity of K^+.

As mentioned above, KBr(g) was the only K-containing vapor species detected over an admixture of KBr and Spheron-6. The addition of H_2O to the Knudsen cell gradually depressed the pressure of KBr(g); over a period of 1800 s the KBr^+ signal dropped to 50% of its initial value. At T = 945 K in the presence of H_2O, a K^+ peak, associated with K(g) by its appearance potential, appeared in the mass spectrum and began to grow steadily. Termination of the H_2O supply caused this peak to decrease.

DISCUSSION

Comparison of the equilibrium pressures of K(g) and Cs(g) over the respective carbonates with those observed over admixtures of the carbonates and Spheron-6 or char, indicates that there is a strong chemical interaction between the salts and the carbon at elevated temperature. This interaction is not simply carbothermic reduction of the salt, as evidenced by the disparity between the calculated and the measured vapor pressures of K(g) (Figures 1 and 2). It seems likely that, in the observed temperature range, a discrete chemical compound is formed with a thermodynamic activity of the alkali metal greater than that of the carbonate but substantially below that of the pure element. The Knudsen cell data give no direct clue to the structure of this solid or liquid phase, but they do suggest that oxygen is a component because oxygen-containing gaseous species (CO and CO_2) are observed to be in equilibrium with the substance. The suppression of the pressure of molecular KBr(g) coupled with the appearance of K(g) over a KBr-Spheron admixture upon the addition of H_2O, is further evidence of an essential role of oxygen in the formation of the compound. The clear X-ray diffraction pattern obtained from the Cs_2CO_3-Spheron sample that had been heated under vacuum is indicative of a crystalline material. This pattern could not be associated with a specific chemical structure, but it was definitely not produced by Cs_2CO_3, CsOH, Cs_2O, nor by a Cs-graphite intercalation compound. Such structures have been suggested as intermediates in the alkali-metal catalyzed steam gasification of coal chars (2).

At high temperatures in the absence of an external source of oxygen, the alkali metal Spheron admixtures exhibit a gradual loss of oxygen as evidenced by the diminution in CO and CO_2 partial pressures (Tables 2 and 3). Accompanying this process, the alkali metal partial pressures increase slightly, indicative of an increase in activity with the change in oxygen stoichiometry. An opposite change occurs when the mixture is exposed to an oxidizing gas (steam or CO_2).

Based on these considerations, we propose that the chemical species formed by the interaction of alkali metal carbonates and carbon at high temperatures is a non-stoichiometric oxide that contains an excess of the metal as ions and also in a dissolved state. Metal-rich Cs-O compounds, with stoichiometries corresponding to Cs_4O and Cs_7O, have been characterized as crystalline solids at room ambient temperatures (6). At high temperatures they melt into liquid phases comprised of a higher oxide containing excess Cs (7). Information on the K-O system is available only for higher oxygen stoichiometries (8), but, by analogy, we would expect all alkali metal-oxygen systems to behave similarly.

The role of the alkali metal additive as a gasification catalyst is probably critically dependent on the formation and action of such an oxide phase. We suggest that during gasification the catalyst forms a liquid oxide film distributed over the surface of the char or carbon. (There is considerble evidence that catalyst melting does occur (10)). The composition of the film is determined by a dynamic balance between a reducing process at the carbon interface and an oxidizing process at the surface in contact with the gaseous reactant, H_2O or CO_2. At the catalyst/char interface, the anions in the catalyst react with the carbon to form an intermediate, such as a phenolate (11) that subsequently splits out CO. The anions are replenished by reaction between the oxidizing gas and the oxide at the gas/catalyst

interface. Net transport of oxygen from gas to carbon occurs by diffusion of the species in the molten catalyst film.

The presence of mineral constituents (typically SiO_2) in most coal chars complicates this picture by providing an alternative reaction path for the alkali metal salt additives. The interaction of these minerals with an alkali metal is illustrated strikingly in the case of the Cs_2CO_3-char admixture. The equilibrium partial pressure of Cs(g) over this sample is significantly lower than over pure Cs_2CO_3. Thus, the Cs activity in the solid phase is highly suppressed, as would be the case if it were chemically combined in a very stable compoud, such as the $CsAlSiO_4$ detected in the X-ray pattern of the residue. However, the low intensity of this pattern considered together with the variation in equilibrium Cs(g) pressure with the Cs content of the sample (Figure 2), suggests that all the Cs is not tied up as a discrete crystalline compound of fixed composition. It is more likely that the Cs is dissolved in an amorphous mineral glass, in which its activity is a function of its concentration.

ACKNOWLEDGMENT

This work was supported by the U.S. Department of Energy, Morgantown Energy Technology Center. The X-ray diffraction measurements were made by Eldon Farley.

REFERENCES

1. D. W. McKee, Chem. Phys. Carbon, 16, 1 (1981).
2. W-Y. Wen, Catal. Rev.-Sci. Eng., 22, 1 (1980).
3. D. L. Hildenbrand, J. Chem. Phys. 48, 3657 (1968); 52, 5751 (1970).
4. K. H. Lau and D. L. Hildenbrand, J. Chem. Phys., 71, 1572 (1979).
5. JANAF Thermochemical Tables, NSRDS-NBS 37, Second Edition, U.S. Government Printing Office, Washington, D.C. (1971).
6. A. Simon, Struct. Bonding, 36, 81 (1979).
7. C. F. Knights and B. A. Phillips, J. Nucl. Mat., 84, 196 (1979).
8. A. J. Leffler and N. M. Wiederhorn, J. Phys. Chem., 68, 2882 (1964).
9. D. W. McKee, Carbon, 20, 59 (1982).
10. B. J. Wood, K. M. Sancier, D. R. Sheridan, B. L. Chan, and H. Wise, "The mechanism of Catalytic Gasification of Coal Char," Quarterly Report No. 4, Dept. of Energy Contract No. DE AC21-80MC14593, SRI International, Menlo Park, CA, November 15, 1981.
11. C. A. Mims and J. K. Pabst, ACS Div. Fuel Chem. Preprints, 25 (3), 258 (1980).

Table 1

APPEARANCE POTENTIALS AND RELATIVE INTENSITIES OF IONS IN MASS SPECTRUM OF K_2CO_3

Ion	AP(eV	Temperature (K)	Neutral Precursor	I^+(AP + 3 eV) at 1153 K
K^+	4.3 ± 0.3	1121	K	1035
CO_2^+	13.7 ± 0.3	1121	CO_2	285
$C_2CO_3^+$	6.1 ± 0.3	1153	K_2CO_3	0.3
K_2O^+	7.8 ± 0.5	1068	K_2CO_3	2.0
K_2O^+	5.2 ± 0.5	1153	K_2O	0.03[a]
O_2^+	11.9 ± 0.3	1153	O_2	33

[a]Measured at AP + 2 eV to eliminate the fragment contribution from K_2CO_3.

Table 2

PARTIAL PRESSURES OF GASEOUS SPECIES ABOVE K_2CO_3-CHAR ADMIXTURE AT VARIOUS TEMPERATURES

Temperature (K)	Partial Pressures (kPa x 10^4) K(g)	CO(g)	CO_2(g)
720	0.001	0.5	0.06
788	0.015	0.24	0.2
871	0.19	1.9	1.56
909	1.2	38.	15.1
952	5.17	53.1	2.43
978	9.68	-	-
875	0.63	1.5	0.22

Table 3

PARTIAL PRESSURES OF GASEOUS SPECIES ABOVE Cs_2CO_3-SPHERON-6 ADMIXTURES

Temperature (K)	Partial Pressure (kPa x 10^3) Cs(G)	CO(g)	CO_2(g)	(CsOH(g)
397	0	0	0.16	0
421	0	0	8.01	0
549	0	0	5.22	0
727	0	0	18.4	0
727	0	0	5.3	0
729	<0.001	0.25	1.56	0
826	0.002	3.14	14.5	0
857	0.002	3.00	4.42	0
886	0.005	3.92	2.13	0
886	0.014	1.73	0.36	0
935	0.065	9.35	1.43	0.001
936	0.33	3.77	0.11	0.001
936	0.31	1.80	0.09	0.001
992	1.41	7.96	0	0.003
1059	4.98	15.50	0	0.005
972	0.76	0.36	0	0.002

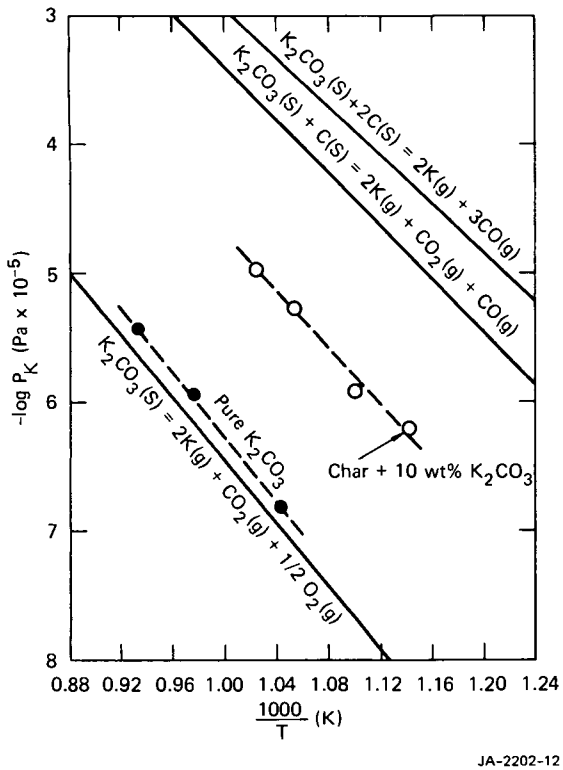

FIGURE 1 COMPARISON OF THE CALCULATED K VAPOR PRESSURES WITH EXPERIMENTAL DATA

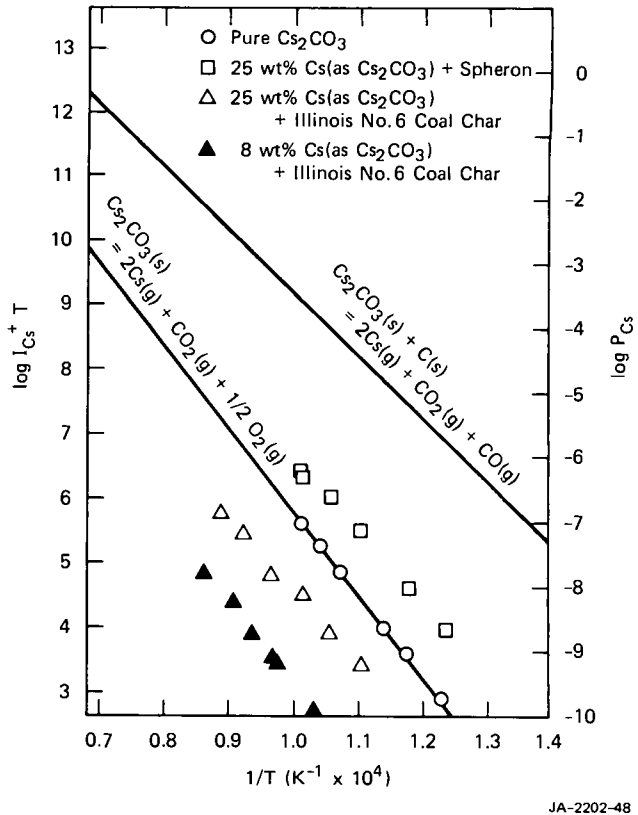

FIGURE 2 COMPARISON OF CALCULATED EQUILIBRIUM Cs PRESSURES WITH EXPERIMENTAL DATA

EFFECTS OF CATALYSTS AND CO_2 GASIFICATION ON THE ESR OF CARBON BLACK. II.

Kenneth M. Sancier

SRI International
Menlo Park, CA 94025

INTRODUCTION

In a previous paper, we reported some preliminary results of an in situ esr study of a K_2CO_3-carbon black mixture as a function of temperature and steam gasification.[1] We found that (1) heating the mixture in helium above 600 K produced irreversible broadening of the esr line, which did not occur for carbon black alone, (2) the broadened line had a shape broader than Lorentzian, and (3) under steam gasification conditions, the esr line width decreased in proportion to the steam concentration.

In the present paper, we report further results from in situ esr studies of (1) the thermal interaction between carbon black and various salts and (2) effect of CO_2 gasification conditions. Also, we used the esr technique[2] to provide information on changes in the electrical conductivity of a sample that may relate to the mechanisms of the thermal and gasification reactions.

EXPERIMENTAL

The specifications of the carbon black (Spheron-6, Cabot Corporation) and the esr apparatus have been described.[1] The samples consisted of a mixture of 3 wt% carbon black in a given salt that was mechanically ground with a mortar and pestle. The only diluent of the carbon black was a given salt. All the salts were of reagent quality. The amount of sample mixture examined by esr was adjusted so that a known mass of carbon black was present, between 3 and 6 mg.

Carbon dioxide gasification was performed by using premixed gases containing and 0, 4.1, 7.9, and 15.8 vol% CO_2 in helium. A switching valve was used to select the desired gas mixture to flow over the sample in the quartz reactor mounted in the high temperature esr sample heater.

The techniques for measuring changes in the relative electrical conductivity of a sample resulting from temperature changes or chemical changes have been described elsewhere.[2] Briefly, a change in electrical conductivity of a sample is approximately proportional to two electrical conductivity parameters, ΔI_P^{-1} and ΔI_D, that can be measured during an esr measurement. I_P is the peak height of the resonance signal of a reference sample (0.1% pitch in KCl, Varian), which was situated in the auxiliary cavity of a dual rectangular cavity (TE_{104}); the sample was situated in the other cavity, which has the sample heater accessory. ΔI_P^{-1} calculated from the differences in the values of I_P^{-1} referring to two different conditions of the sample, e.g., temperature. I_D is the bias current of the crystal diode detector of the microwave bridge, and ΔI_D is the change in this current resulting from a change in the electrical conductivity of the sample. By connecting a recorder to the crystal diode current meter, it was possible to record ΔI_D as a function of time during gasification experiments. The parameter

ΔI_p^{-1} is suitable for measuring relatively large changes in electrical conductivity, such as those arising from heating a sample. The parameter ΔI_p is useful for following smaller changes in the electrical conductivity of a sample, e.g., arising from a chemical change associated with CO_2 gasification.

Free radical concentrations were measured by using a computer to store the esr data and to calculate the first moments of the first derivative curves. The results were normalized for cavity sensitivity using I_p, gain, rf modulation amplitude settings (typically 0.1 mT), and mass of carbon. Microwave power incident on the sample cavity was 1 mW.

RESULTS

For convenience, the results of the *in situ* esr measurements made on several salt-carbon black mixtures will be subdivided into two parts: thermal effects and CO_2 gasification effects.

Before each series of esr measurements with a given sample, oxygen was desorbed from the carbon by heating the sample in the esr reactor cell at about 500 K for 5 min while helium flowed through the cell. The value of the esr line width measured at room temperature was about 7.0 mT (70 gauss) before the desorption and about 0.15 mT after the desorption. The esr line was symmetric for all the salt-carbon black mixtures.

Various samples were tested for microwave power saturation, and none was detected for sample temperatures examined in the range from 290 to 800 K and for microwave power levels incident on the sample in the range of 0.1 to 40 MW; the upper value was limited by the electrical conductivity of the samples.

Thermal Effects

The thermal interaction between a salt and carbon black heated in helium were investigated by studying a series of potassium halide-carbon black mixtures. Alkali metal halides are less active catalysts than K_2CO_3 for gasification of carbonaceous materials.[3,4] For comparison, a K_2CO_3 carbon black mixture was included. Also included was a mixture of carbon black with CaO which is expected to be a relatively poor gasification catalyst[3,5] and has relatively low electrical conductivity at elevated temperatures. Hence, the CaO serves as a diluent to decrease microwave skin depth effects so that the esr properties of carbon black alone can be studied.

To determine the effects of heating the mixtures in helium we measured three esr parameters simultaneously: variations in the free radical concentration, line width, and ΔI_p^{-1}. Measurements were made at successively higher temperatures (Figures 1a and 2a), but before progression to each next higher temperature, a measurement was made at 290 K (Figures 1b and 2b).

The free radical concentrations uncorrected for Curie's law were essentially independent of both the measurement temperature and the type of salt, within the accuracy of these measurements The values of I_p, which were used to normalize the free radical concentrations for changes in cavity sensitivity, varied by a factor of about 10 over the temperature range studied, indicating the importance of such a correction.

The esr line width began to increase at temperatures above 850 K, and the magnitude of the increase was strongly dependent on the anion of the salt (Figure 1a). When the sample was cooled to room temperature the line width decreased. An irreversible effect is evident by the fact that a significant fraction of the line broadening produced at higher temperatures was retained upon cooling the samples (compare Figures 1a and 1b). In general, the effect on line width and the magnitude of the irreversible effects for the salts decreased in the following order: KBr ≈ KCl ≈ KI > K_2CO_3 ≈ KF > CaO.

The electrical conductivity parameter, ΔI_p^{-1}, generally increased with heating temperature, and with few exceptions was almost independent of the type of salt mixed with carbon black (Figure 2a). The results of the measurements at 290 K, after cooling from a given higher temperature, also indicate that an irreversible increase in the electrical conductivity for some salts had been produced thermally (compare Figures 2a and 2b). Measurements on two salts, K_2CO_3 or KCl, in the absence of carbon black show that the ΔI_p^{-1} parameter has a very small temperature dependence, increasing less than 10% as the temperature was raised from 300 to 1200 K.

Comparison of Figures 1 and 2 suggests that there is a qualitative similarity in the way the heating temperature affects the two parameters, line width and ΔI_p^{-1}. A test of the relationship between line width and ΔI_p^{-1} is shown in Figure 3, which is a replot of the results in Figures 1a and 2a. The curves drawn in Figure 3 indicate that line width has a monotonic relationship to ΔI_p^{-1}, but that the functional dependence may be different for different salts.

CO_2 Gasification Effects

At elevated temperatures when He gas passing over a sample was switched to He containing CO_2 (15.8%), the line width decreased and the free radical concentration increased as shown in Figures 4 and 5, respectively. Before the CO_2 gasification measurements, the sample was thermally equilibrated at a given temperature for about 20 min. However, the line width and free radical concentration continued to change slowly, probably the result of slow irreversible changes caused by CO_2 as discussed above. Therefore, to separate the slow thermal changes from the rapid changes produced by CO_2, we switched the gas flowing over the sample at a given temperature, 800 or 850 K, back and forth between He and He containing CO_2. The sequence of the measurements is indicated by the numbers beside the data points in Figures 4 and 5. These results show that CO_2 had a greater effect at the higher temperature for both line width and free radical concentration. Also, at a given temperature the magnitude of the effect tended to become limited at concentrations of CO_2 greater than about 4%; e.g., see the line width dependence at 850 K in Figure 4. This behavior is probably due to a diffusion-limited process.

It was of interest to determine whether CO_2 gasification conditions altered the electrical conductivity of the sample, but the electrical conductivity parameter, ΔI_p^{-1}, exhibited a very small and almost imperceptible response. Therefore, the more sensitive electrical conductivity parameter, ΔI_D, was used. The recorded value of ΔI_D is shown in Figure 6, which shows the changes that occurred as the gas passing over the sample at 855 K was switched between He and 15.8 % CO_2 in He. Although the sample was initially in He the positive slope of ΔI_D indicates that the sample was not stable although it had been thermally equilibrated. However, it is clear from the recording that CO_2 caused the value of ΔI_D

to decrease (electrical conductivity decrease) and that subsequent exposure to He caused the value of ΔI_D to increase.

The observed values of the line width are marked in Figure 6 at three points in time. The results show that the line width changed reversibly when the sample was alternately exposed to He and CO_2. Also, the decrease in line width correlates with the decrease in the electrical conductivity of the sample, as was the case in the study of thermal effects discussed earlier.

When carbon black alone and mixtures of carbon black with the potassium halides or with CaO were exposed to CO_2 gasification conditions at 850 K, very small or no changes were observed to occur in line width, free radical concentration, or in electrical conductivity (ΔI_D).

The correlation between an increase in the value of ΔI_D and an increase in electrical conductivity was established by noting that both ΔI_D and ΔI_P^{-1} changed in the same way for large enough changes in electrical conductivity, e.g., as produced by an increase of sample temperature.

DISCUSSION

In the previous paper[1] some suggestions were made to account for those changes occurring in the esr spectra due to a thermal interaction between carbon black and K_2CO_3 and due to steam gasification. The additional experimental information obtained in the present esr study, pertaining to various other salts and a study of CO_2 gasification, provides a broader basis for interpreting the mechanisms of the thermal and gasification reactions.

Thermal Effects

Two mechanisms were suggested[1] to account for the esr line broadening resulting from heating a mixture of salt and carbon black: (1) increased electrical conductivity and (2) unresolved hyperfine splitting (hfs) due to an interaction between the magnetic moment of the unpaired electron and that of the nucleus of the cation of the salt. The current results suggest that the increase in line width is related to the increase in the electrical conductivity because of the observed proportionality between the line width and the change in the electrical conductivity parameter for a series of salt-carbon black mixtures heated to various temperatures (Figure 3). In the following discussion, the relationship between these two parameters is examined in detail.

We postulate that some sort of complex is formed between certain salts and carbon black to account for the increase in the electrical conductivity and esr line width resulting from heating mixtures of salts and carbon black being significantly greater than the increase when the individual components are heated. Generally, an increase in electrical conductivity is due to an increase in the concentration or mobility of the charge carriers. Since the free radical concentration of the salt-carbon black mixtures was insensitive to temperature, it appears that charge carriers (conduction electrons or holes) are mainly responsible for the observed esr signal, whereas π-electrons would obey Curie's law. If the esr measurements detect all the charge carriers, then the observed increase of the electrical conductivity with increase in temperatue is due mainly to an increase in charge carrier mobility.

We propose a series of reactions to account for the effect of the electronic properties of the solid. First, elemental metal atoms are produced by carbon reduction of the cation of the salt (e.g., K^+);[6] Second, an extended aromatic structure develops by loss of hydrogen and polymerization of the carbonaceous material,[7,8] and this polymerization could possibly be catalyzed by a salt or a metal atom. Third, a complex is formed between an aromatic structure and the ions or atoms of the salt. For example, such a complex could involve metal ions or atoms which (1) substitute for the hydrogens of CH or OH groups of the aromatic structure,[9] (2) interact electrostatically with the π-orbitals of the extended aromatic structure,[10] or (3) form a kind of intercalation compound with the available graphite-like structures, although such compounds are usually not expected to be stable at gasification temperatures.

For most salts studied, the changes in the esr parameters are largely irreversible, indicating that the salt-carbon black complex is stable. The greater effects produced by the alkali metal salts than by CaO or Al_2O_3[1] are probably due to the greater ease with which carbon can reduce the alkali metal cations.

Based on the concepts suggested above, we propose that the observed line broadening results from relaxation effects that occur in the salt-carbon black complex when the unpaired electrons observed by esr experience the inhomogeneous fields developed near the sites at which a salt (e.g., the metal atom or cation and the anion) interacts with the aromatic carbon structure. Since these sites are nonuniformly distributed, the unpaired electrons in a conduction band or in π-orbitals experience different environments, resulting in inhomogeneous broadening of the esr line. The observed line shape, which is broader than Lorentzian, probably results from a superposition of two or more Lorentzian lines representing different environments.

Gasification Effects

Gasification by either steam[1] or CO_2 of a salt-carbon black sample results in the same qualitative changes in the three esr parameters: a decrease in the line width, a decrease in the electrical conductivity, and an increase in the free radical concentration. Therefore, it appears that a single mechanism could account for the changes in the esr spectra that occur during gasification conditions.

We suggest that steam or CO_2 reacts with the salt-carbon complex and fragments carbon-carbon bonds of aromatic rings. As a result, the unpaired electrons will experience a decreased resonance path and less interaction with the atoms or ions of the salt that were associated with the aromatic ring before fragmentation. In other words, the unpaired electron will experience fewer regions with inhomogeneous fields, and therefore the esr line width should decrease.

Also as a result of the fragmentation of the aromatic rings the steady-state concentration of free radicals will be increased. Although these free radicals are probably unstable and will react with CO_2 or polymerize to produce a more stable structure, other radicals will be produced continuously by the gasification reaction.

The *in situ* esr results clearly indicate that for a salt to promote catalytic gasification, both the cation and anion of a salt must interact with the carbon structure. That is, switching to CO_2 gasification conditions caused changes in

the esr parameters only for salts with catalytic activity, e.g., salts with an alkali metal cation and a non-halide anion. Evidently, the character of the salt-carbon complex determines catalytic activity.

However, the changes in the esr parameters produced by thermal effects do not appear to correlate with the catalytic activity of the salts. For example, large increases in both line width and electrical conductivity occurred upon heating mixtures of carbon black with either of two salts, K_2CO_3 or KCl, which have widely different catalytic activities.

To elucidate the mechanism of catalytic gasification, we plan to consider the information developed by esr along with that obtained by other techniques being pursued in our laboratory.

ACKNOWLEDGMENTS

The author is grateful to his colleagues Bernard Wood and Henry Wise for valuable discussions and to Steven Leach and Robert Brittain for computer programming for the esr studies. He also acknowledges valuable discussions with L. S. Singer and J. Uebersfeld. The research was supported by the U. S. Department of Energy under Contract No. DE AC21-80MC14593.

REFERENCES

1. K. M. Sancier, Fuel, in press.

2. M. Setaka, K. M. Sancier, and T. Kwan, J. Catal. 16, 44 (1970).

3. M. J. Veraa and A. T. Bell, Fuel, 57, 194 (1978).

4. D. W. McKee, C. L. Spiro, P. G. Kosky, and E. J. Lamby, ACS Fuel Division Reprints, 27(1), 74 (1982).

5. E. J. Hippo, R. G. Jenkins, and P. L. Walker, Jr., Fuel, 58, 338 (1979).

6. D. A. Fox and A. H. White, Ind. Engng. Chem., 23, 259 (1931).

7. S. Mrozowski, Carbon, 6, 841 (1968).

8. L. S. Singer and I. C. Lewis, Appl. Spectroscopy, 36, 52 (1982).

9. C.A. Mims and J. K. Pabst, Proc. International Conf. Coal Science, Dusseldorf, 730 (1981).

10. N. L. Holy, Chem. Rev., 74, 243 (1974).

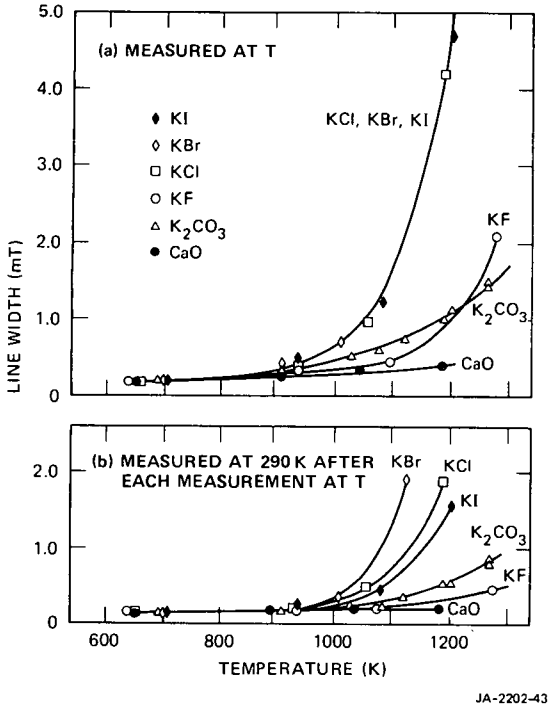

FIGURE 1 EFFECT OF TEMPERATURE ON ESR LINE WIDTH OF SALT-CARBON BLACK MIXTURES

3 wt% carbon; heated in helium.

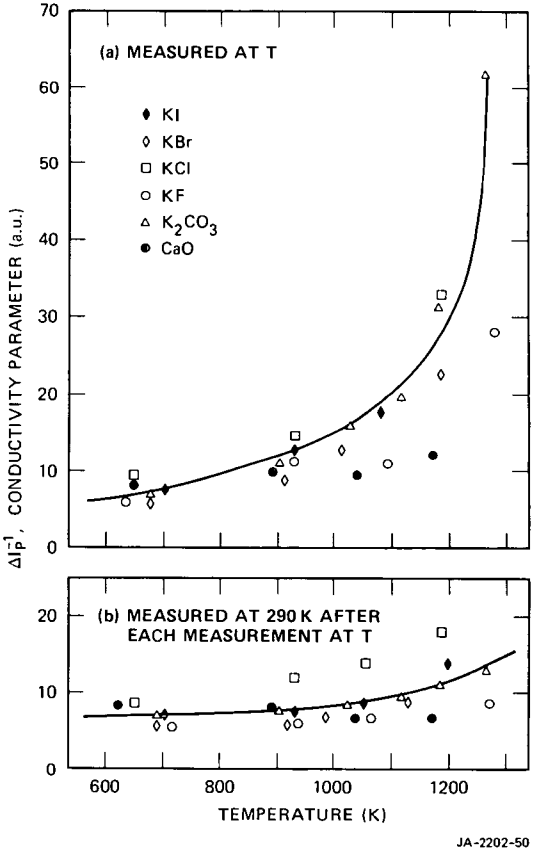

FIGURE 2 EFFECT OF TEMPERATURE ON ESR ELECTRICAL CONDUCTIVITY PARAMETER OF SALT-CARBON BLACK MIXTURES

3 wt% carbon; heated in helium.

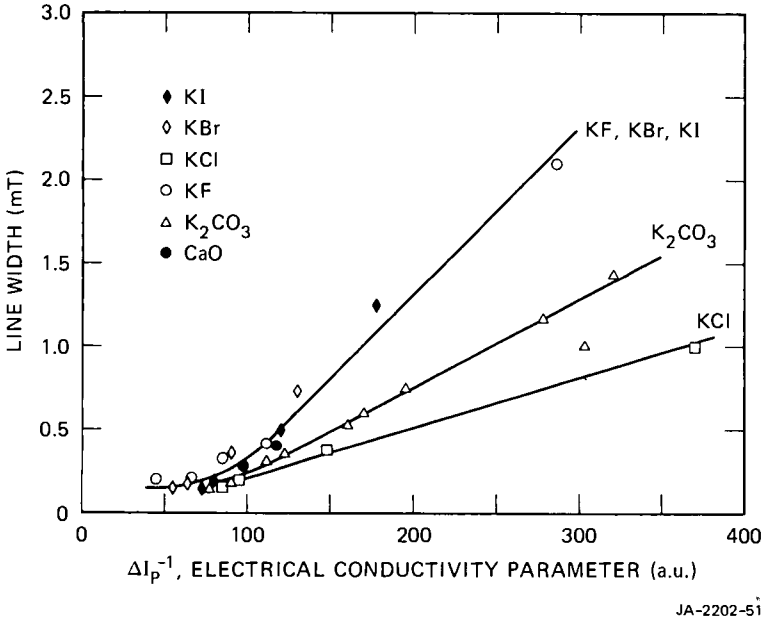

FIGURE 3 RELATIONSHIP BETWEEN ESR LINE WIDTH AND ESR ELECTRICAL CONDUCTIVITY PARAMETER OF POTASSIUM SALT-CARBON BLACK MIXTURES

3 wt% carbon; heated in helium. Replot of Figures 2a and 3a.

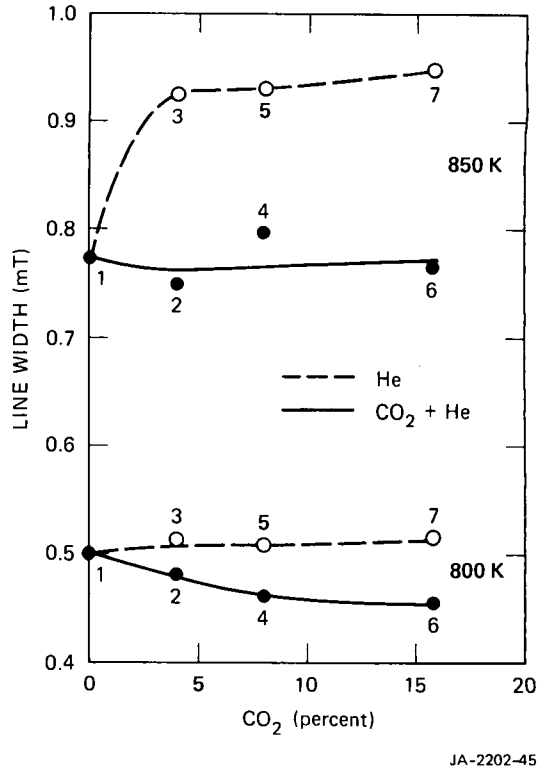

FIGURE 4 EFFECT OF CO_2 ON ESR LINE WIDTH OF K_2CO_3-CARBON BLACK MIXTURE

3 wt% carbon; numbers identify sequence of measurements.

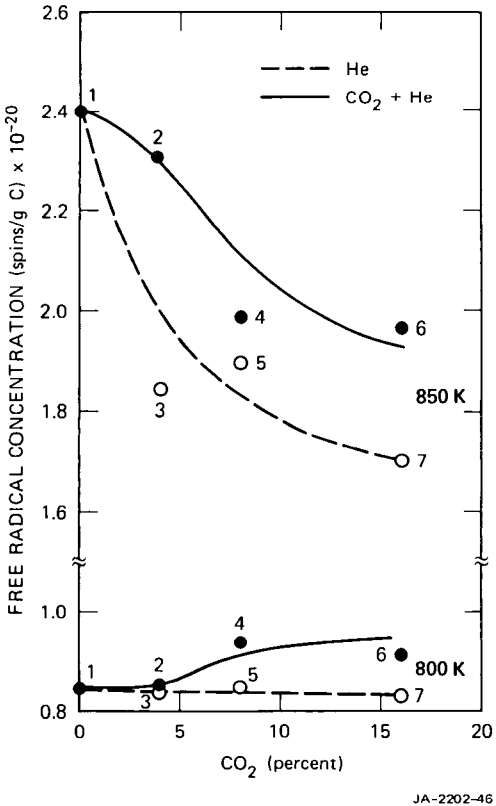

FIGURE 5 EFFECT OF CO_2 CONCENTRATION ON FREE RADICAL CONCENTRATION IN K_2CO_3-CARBON BLACK MIXTURE

3 wt% carbon; numbers identify sequence of measurements.

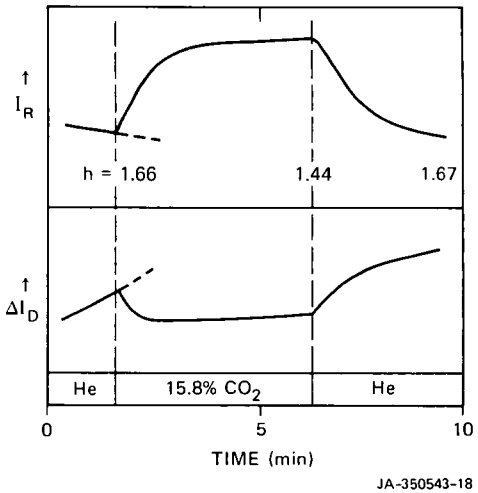

FIGURE 6 EFFECT OF CO_2 GASIFICATION ON ESR PARAMETERS OF CARBON — K_2CO_3 (8 wt% K) MIXTURE AT 855 K

I_R – Peak intensity of radical signal

I_D – Detector current

h – Line width (mT)

CONTROLLED ATMOSPHERE ELECTRON MICROSCOPY STUDY OF THE K_2CO_3 - CATALYZED GRAPHITE - H_2O REACTION

C. A. Mims, R. T. K. Baker, J. J. Chludzinski,

Exxon Research and Engineering Co.
P.O. Box 45, Linden, NJ 07036

and

J. K. Pabst

Exxon Research and Engineering Co.
P.O. Box 4255, Baytown, TX 77520

Controlled atmosphere electron microscopy has provided unique insight into the details of the mode of catalytic attack of carbons by reactive gases (1). Many of the systems investigated show graphite gasification to occur at the interfaces between discrete catalyst particles and edges of the graphite layer planes. Graphite is removed in these cases by the formation of channels through the graphite sheets. Some catalysts (e.g. Mo (2)) display increased tendency to wet the reactive graphite surface and therefore exhibit a stronger interaction.

Alkali salts are perhaps the best known catalysts for gasification of carbon and have been extensively studied. Several investigators have provided evidence that potassium salts react readily with the carbon substrate to form surface salt complexes (3). We undertook this study in part to see if the morphology of K_2CO_3 - catalyzed attack would reflect this strong surface bonding.

EXPERIMENTAL METHOD

All experiments were performed in the controlled atmosphere microscope (4). Pure, thin specimens of Ticonderoga graphite were mounted on heating stages and impregnated by a fine mist of 0.1% K_2CO_3 solution. Water vapor was admitted to the controlled atmosphere cell from a wet argon stream. The behavior was monitored as the sample was taken by steps through heating and cooling cycles to temperatures as high as 800°C. Higher temperatures than this were avoided to minimize the amount of catalyst vaporization. Several successful runs on different samples make up the data base.

RESULTS

Initial heating cycle in H_2O

We paused for sufficient time (15 min) at each temperature during the initial heating program to detect slow changes in the specimen and catalyst morphology. Up to temperatures of 550°C the only change noticed was the gathering of particles of K_2CO_3 on the edge of the specimen (see Figure 1a). The particles generally had liquid-like shapes with contact angles sugestive of attractive (wetting) interaction. When the temperature was raised above 550°C the particles slowly, or more rapidly at higher temperature, disappeared from the graphite edge. The sequence of photographs in Figure 1 shows this occurrence over the span of approximately 2 minutes at 670°C. That catalyst remained on the specimen after the particles disappeared was shown by the subsequent gasification behavior of the graphite. Therefore we believe that the disappearance of the particles reflects spreading of the salt to a thin film on the graphite surface rather than evaporation.

Onset of gasification

Almost simultaneously with the disappearance of the catalyst particles, attack of the edges of the graphite specimen became evident. The edges began receding at many places along the entire edge, at first showing as a series of irregular notches. Soon the notches took on a hexagonally facetted appearance (see Figure 2). The rate of edge recession at 550°C was too slow to be readily apparent in real time but increased with increasing temperature. The rates were much faster than the uncatalyzed rate at the same conditions, reflecting the fact that catalyst had remained on the sample. The edge recession eventually involved the entire specimen edge with hexagonal faceting throughout.

We analyzed films of the experimental runs to derive rates of edge recession. Reactive edges exhibit a reproducible and characteristic recession rate which is general for all features on a given sample. These rates for one run are plotted in Figure 3. Data are shown for both increasing temperature sequence and decreasing temperature sequence. We observed no hysteresis in the rates for a complete cycle of temperature.

DISCUSSION

The morphology of the K_2CO_3 catalyst during gasification is striking confirmation of strong interaction betwen the catalyst and the edges of the graphite lattice. The interfacial bonding is strong enough to compete with the cohesive bonding within the bulk salt and effectively disperse the catalyst along the active edge. Surface salts groups such as phenoxide analogs have been identified on less ordered carbons impregnated with alkali catalysts and quenched from gasification conditions (3c). These surface salts are though to be responsible for the high dispersion of alkali catalysts on carbons such as coal char and also explain the reproducibility of the catalytic effect of potassium salts on these materials.

Hexagonal faceting of the gasifying graphite edge reflects a preferential reaction of one crystallographic orientation over another. J. M. Thomas exploited this feature very elegantly in optical microscopy (5). The facets in this study are aligned parallel to the <1120> set of crystal directions. This can be determined by noting the orientation of the facets with respect to twin bands along the <1010> direction which are usually present in graphite specimens. One such twin boundary appears in Figure 2. The K_2CO_3 catalyzed reaction thus exposes the "zig zag" presentation of the surface. This orientation must be less reactive than other orientations, for example the "armchair" or 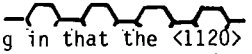 configuration. This is perhaps not surprising in that the <1120> orientation presents one uncondensed carbon atom per ring exposed at the edge whereas the <1010> orientation presents two uncondensed carbons together. The latter might a priori be expected to be the more reactive and would explain the results obtained here. Thomas did see a dependence of the orientation of etch pits in the graphite-O_2 reaction on reaction conditions.

The activation energy derived from the edge recession data (35 kcal/mol) is lower than that observed by McKee and Chatterji for K_2CO_3 on graphite (52.2 kcal/mol (6)). Direct comparison is difficult because in neither study is the reactant gas composition (particularly the H_2 partial pressure) well characterized. Furthermore very different pressures were used in the two studies.

CONCLUSIONS

We have seen microscopic evidence of strong interaction between potassium catalyst and the reactive edges of graphite. This interaction is thought to be driven by the formation of surface salt bonds. The spreading of the catalyst which results from this strong interaction provides high dispersion and efficient use of the catalyst. The hexagonal facetting provides additional insight into the reactivity of proposed surface ensembles.

REFERENCES

1 R. T. K. Baker, to be published.

2 R. T. K. Baker, P. S. Harris, D. J. Kemper and R. J. Waite, Carbon 12, 179 (1974).

3 a. F. J. Long and K. W. Sykes, J. Chem. Phys. 47, 361 (1950).

b. C. A. Mims, and J. K. Pabst, Proc. Int. Conf. on Coal Sci. 1981 p. 730 (verlag Gluckauf GmbH, Essen).

c. C. A. Mims and J. K. Pabst, J. Am. Chem. Soc. to be published.

4 R. T. K. Baker and P. S. Harris, J. Sci. Instrum. 5, 793 (1973).

5 J. M. Thomas in Chemistry and Physics of Carbon (P. L. Walker, ed.) vol. 1 p. 122, Marcel Dekker (NY) (1965).

6 D. W. McKee and D. Chatterji Carbon 16, 53 (1978).

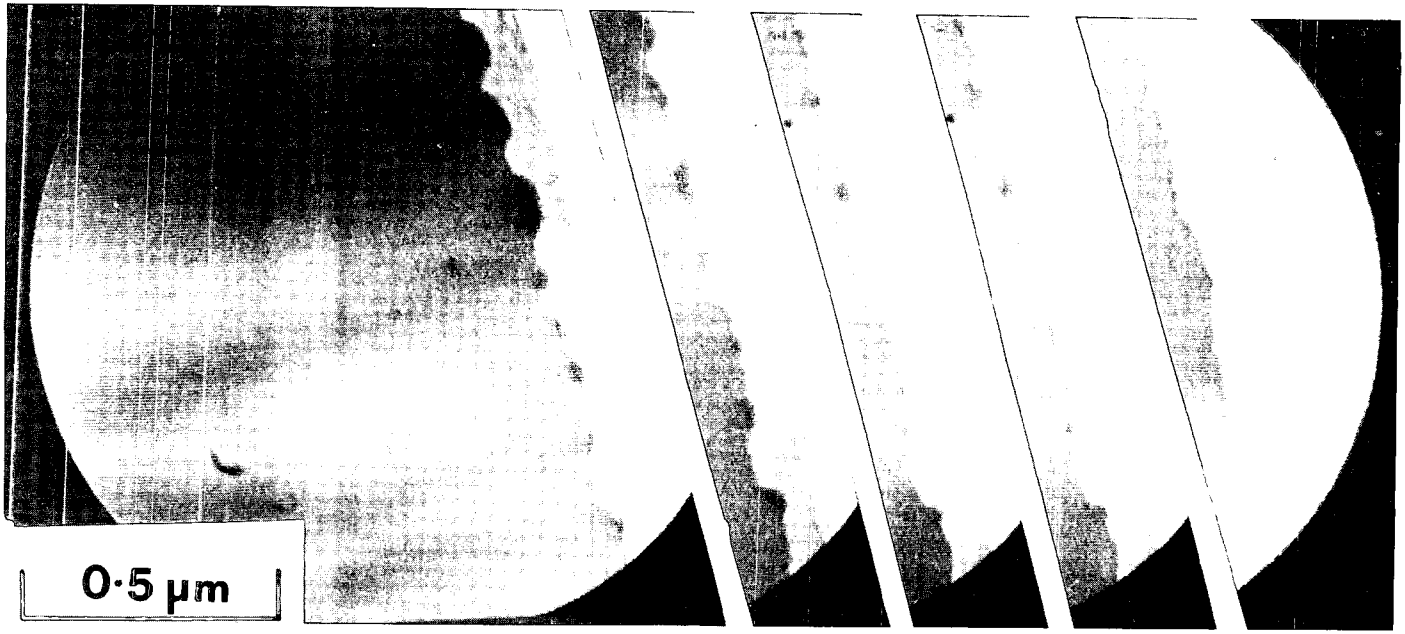

Figure 1. Sequence of photographs taken from the CAEM video display showing the progressive disappearance of droplet-like particles of K_2CO_3 on the edge of graphite at 670°C in water vapor. The sequence spans 120 seconds.

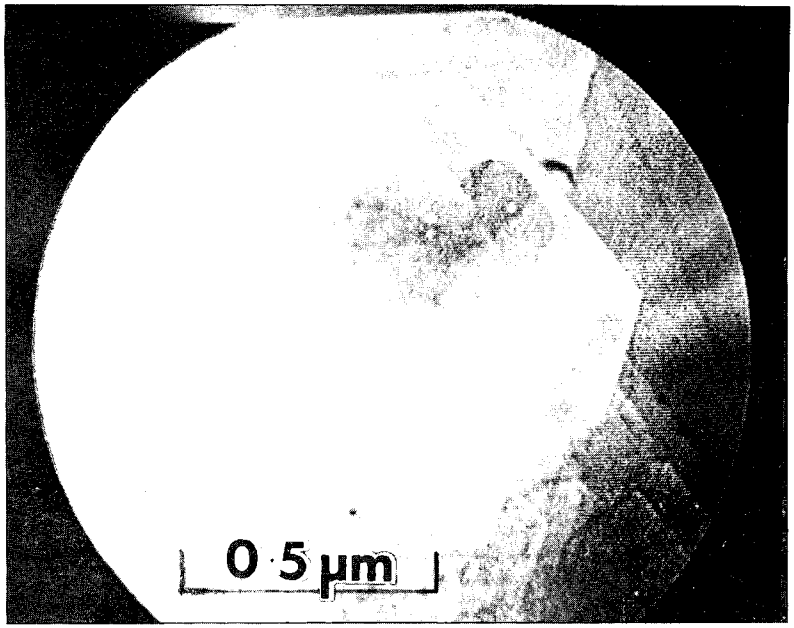

Figure 2. Photograph of video display showing active edge of graphite while reacting at 715°C in H_2O. General motion of features was from left to right. The remnant of the original edge (E) can be seen as well as a twin band (T).

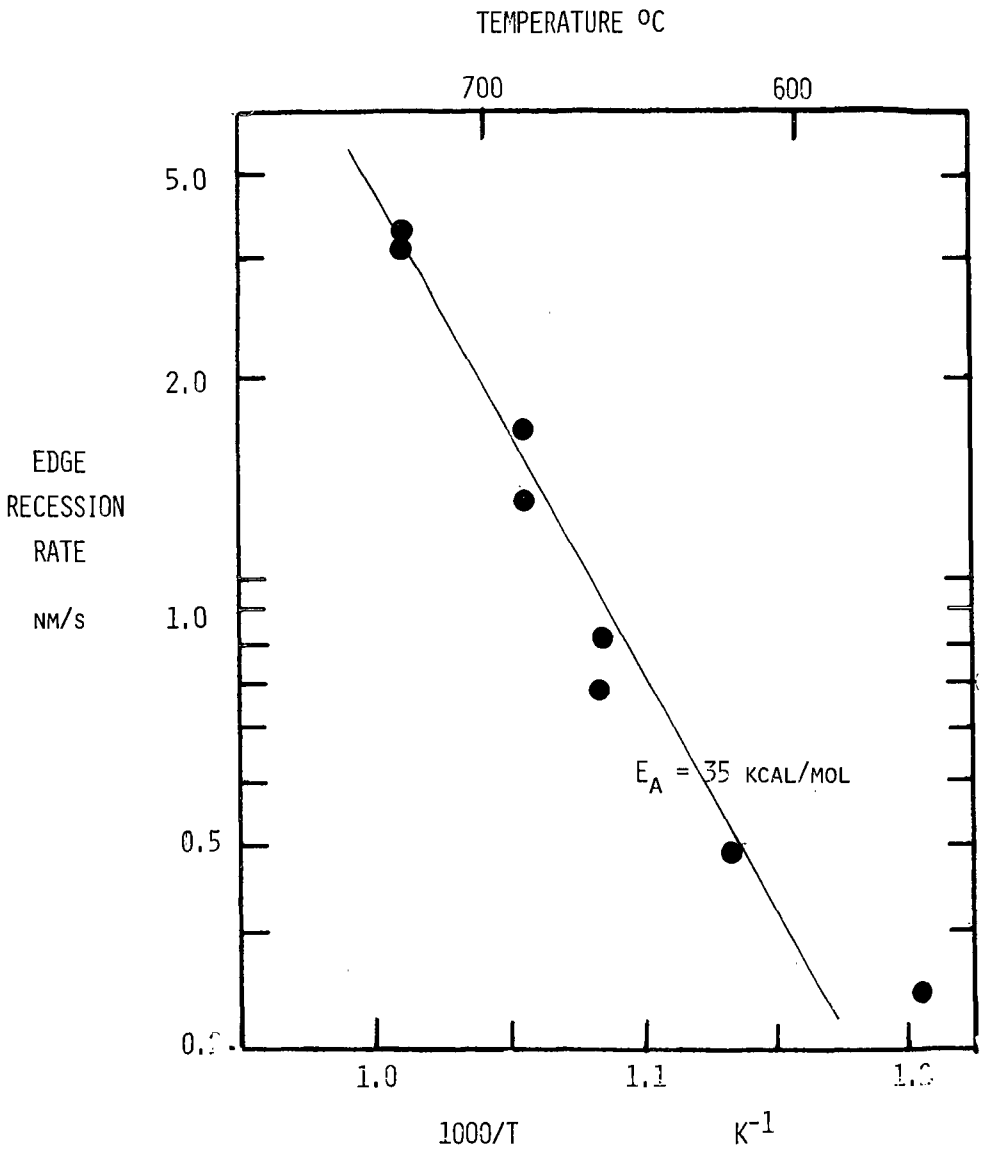

Figure 3. Arrhenius plot of catalyzed edge recession rates measured on a single graphite sample. Data points are the average of many features. Data for ascending and descending temperature sequence are shown at several temperatures

LOW TEMPERATURE METHANE PRODUCTION BY THE CATALYZED REACTION OF GRAPHITE AND WATER VAPOR

F.Delanny, W. T Tysoe, G. Yee, R. Casanova, H. Heineman and G. Somarjai

Materials & Molecular Research Division
Lawrence Berkeley Laboratory
and
Department of Chemistry
University of California
Berkeley, California 94720

The gasification of carbon (coal) by reaction with water vapor is usually conducted at a temperature higher than 1200K. This reaction exhibits an apparent activation energy of the order of 50 kcal/mole. It is catalyzed by various salts of alkali metals, especially potassium [1,2]. At these high temperatures, the main products are CO and H_2, according to the reaction

$$C + H_2O \longrightarrow H_2 + CO \qquad (1)$$

The simultaneous production of CH_4 has also been reported [3] especially when the reaction temperature is lowered. The relatively high temperature would, however, facilitate the decomposition of most hydrocarbons that could have been produced.

Our research is focussed on finding suitable catalysts for the low temperature production of low molecular weight hydrocarbons from the reaction of carbon (coal) with water vapor. It has been reported recently that potassium hydroxide, potassium carbonate and several other alkali metal hydroxides catalyze the production of methane in the temperature range from 500 to 600K with an apparent activation energy of about 11 kcal/mole [4]. In order to gain more insight into the mechanism of this production, this study has been extended by

i) using two different reactors to accomodate either graphite single crystals or graphite powder,

ii) extending the temperature range up to 1075K,

iii) varying of the reactor vapor pressure, and

iv) investigating other catalysts: calcium oxide and transition metals.

Graphite single crystals were obtained by cleavage from a larger piece of highly oriented pyrolytic graphite (HOPG) from Union Carbide Corporation. They were mounted on the manipulator of a UHV system, in firm contact with a gold foil that could be heated resistively. The sample was accessible to surface analysis by AES, XPS, ion sputter cleaning and mass spectrometry. It could also be isolated within a high pressure cell where it was exposed to water vapor and/or other gases for chemical reaction. The products were analyzed by gas chromatography. This apparatus has been described in more detail elsewhere [4].

---

*On leave from the Groupe de Physicachimie Minerale et de Catalyse, Universite Catholique de Lauvoin, Belgium.

Pure graphite powders were reacted with water in a fixed bed reactor made of a quartz tube 4 mm. ID containing about 0.4 g of sample fixed between two glass wool plugs. A carrier gas (usually nitrogen) was saturated with water vapor by bubbling through a water container where the temperature could be adjusted from 30°C to 95°C in order to vary the water vapor pressure. The flow rate could be varied between 4 and 20 ml/min. At the outlet of the reactor, the water vapor was condensed in a copper coil maintained at the melting ice temperature. Care was taken to avoid the condensation of water in other parts of the apparatus. The products were analyzed by gas chromatography.

The potassium hydroxide catalyzed reaction was studied from 525 to 1075K under a water vapor pressure ranging from 20 to 600 torr. The production of methane exhibited the same apparent activation energy of about 12 kcal/mole within the whole temperature range. This suggests that the catalytic mechanism involved remains the same at high temperature and has no relation to the (simultaneously occurring) reaction (1). The methane production appeared also to be first order with respect to the water vapor pressure.

Calcium oxide was also tried as catalyst in the temperature range 623-873K [5]. Single crystal graphite samples were impregnated with 1M solution of $Ca(NO_3)_2$ and dried in air. CaO was obtained from the decomposition of $Ca(NO_3)_2$ at the temperature of the reaction. No methane was detected when the sample was exposed only to 22 torr of H_2O and 730 torr of helium. XPS analysis showed, however, the appearance of a new peak at a binding energy of 290 eV. Methane was readily detected when the sample was subsequently exposed to 1 atm H_2 at the same temperature. The intensity of the peak at 290 eV decreased simultaneously with increasing time of reaction with hydrogen. We tentatively attribute this peak to a new form of active carbon that is hydrogenated to CH_4 by H_2. A steady rate of production of methane was obtained when reacting the sample in a mixture of 22 torr of H_2O and 32 torr of H_2. This reaction had an apparent activation energy of 16.3 kcal/mole and exhibited a first order dependence on the hydrogen pressure.

Alkali and calcium catalysts do not produce organic molecules other than methane under our experimental conditions. Studies are now in progress to determine if the combination of these catalysts with transition metal compounds could be utilized to produce higher molecular weight hydrocarbons.

This work is supported by the Director, Office of Energy Research, Office of Basic Energy Sciences, Materials/Chemical Sciences Division of the U.S. Department of Energy under Contract DE-AC03-76SF00098.

REFERENCES

1. Wen-Young Wen, Catal. Rev. Sci. Eng. 22, 1 (1980).

2. D.W. McKee, Chemistry & Physics of Carbon (P.L. Walker, Jr. and P.A. Thrower), Vol. 16, pg. 1, Marcel Dekker, New York (1981).

3. C.A. Mims and J.K. Pabst, Amer. Chem. Soc. Preprints, Div. of Fuel Chemistry, Vol. 25, 3, pg. 258 (1980).

4. A.L. Cabrera, H. Heinemann and G.A. Somorjai, J. Catalysis 75, 7 (1982).

5. R. Casanova, A. Cabrera, H. Heinemann and G.A. Somorjai, to be published.

CHARACTERIZATION OF COAL MACERALS ON THE BASIS OF THEIR FLUORESCENT SPECTRA

John C. Crelling* and David F. Bensley**

*Department of Geology, Southern Illinois University at Carbondale, Carbondale, Illinois, 62901
**Coal Research Section, The Pennsylvania State University, University Park, Pennsylvania, 16802

INTRODUCTION

One of the major problems of coal science is that very little is known about the basic properties of the various macerals that make up coal. Two of the main reasons for this lack of knowledge about the properties of coal macerals is that they are extremely difficult to separate from coal and that they are non-crystalline organic compounds and, therefore, not good subjects to analyze with such standard methods as x-ray diffraction or electron-microprobe analysis. Some of the most successful characterization of coal macerals to date has been by petrographic methods, in which the individual macerals do not have to be separated. In the steel industry, for example, petrographic techniques have proven so successful in allowing the prediction of the coking properties of coal that most major steel companies have now established petrographic laboratories. Another petrographic technique that has only recently been applied to coal analysis is qualitative and quantitative fluorescence microscopy. With this technique, the visible fluorescent light excited from the macerals reveals shapes, textures and colors not visible in normal white-light viewing. The technique also yields quantitative spectra that are characteristic of both the individual maceral type and the rank of the coal. It is now also well established that all of the liptinite macerals (derived from the resinous and waxy parts of plants) and some of the vitrinite macerals will fluoresce, and that some recently discovered liptinite macerals can only be identified by their fluorescence properties. Some of the first measurements of the absolute intensity of fluorescence of coal macerals at specific wavelengths were made by Jacob (1,2). Relative intensity measurements of fluorescent spectra of modern plant materials, peats and coals have been reported by van Gijzel (3,4,5). Teichmuller (6,7,8) described three new members of the liptinite group of macerals in part by demonstrating their distinctive spectral properties. Ottenjann, Teichmuller and Wolf (9) illustrated the correlation of changes in fluorescence spectra of sporinite with rank, and Crelling and others (10) and Crelling (11) have demonstrated the use of fluorescence spectra to discriminate macerals. In addition, Ottenjann, Wolf, and Wolff-Fischer (12) have been able to relate the fluorescence spectra of vitrinite macerals to the technological properties of coal. These studies have shown the potential of using fluorescence measurements in the study of liptinite and vitrinite macerals.

EQUIPMENT AND METHODS

The fluorescence microscopy system used in the SIUC Coal Characterization Laboratory is a Leitz MPV II reflectance microscope which is fitted with a 100 watt mercury arc lamp, a Ploem illuminator and a Leitz oil immersion 40X objective with a 1.3 numerical aperture. For spectral measurements the light from the mercury arc passes through a UG1 ultra-violet filter to a TK400 dichroic mirror which reflects light less than 400 nm to the sample. The fluorescent light excited from the sample is passed through a 430 nm barrier filter to a motorized interference wedge in front of the photometer. The interference wedge controls the wavelength of the fluorescent light hitting the photometer so that the intensity variations from 430 to 700 nm can be scanned and recorded in about 40 seconds.

The spectral data are then fed into a computer from the microscope system and digitized, corrected and analyzed. Each spectrum is corrected for the effects of background fluorescence and for the effects of the microscope system, especially the sensitivity of the photo-multiplier tube, following correction procedures described by van Gijzel (13). For comparison the various spectra are normalized and reduced to a number of parameters such as: 1) the wavelength of maximum intensity peak (λmax); 2) the red/green quotient (Q) where Q = relative intensity at 650 nm/relative intensity at 500 nm; 3) the area below λmax; 4) the area above λmax; 5) area blue (430 to 500 nm); 6) area green (500 to 570 nm); 7) area yellow (570 to 630 nm); and 8) area red (630 to 700 nm).

RESULTS AND DISCUSSION

In coals of the Illinois Basin, standard white-light petrographic methods generally reveal three types of liptinite macerals, resinite, sporinite and cutinite. These macerals are identified on the basis of their petrographic properties such as reflectance, size, shape and texture. When qualitative fluorescence analysis is used, the fluorescence colors and intensity commonly reveal an additional maceral, fluorinite. When fluorescence spectral analysis is used, the spectral data distinguish these four types of liptinite macerals plus additional varieties of resinite, sporinite and cutinite. Also, altered or weathered varieties of these macerals can be distinguished in some coals. For example, spectral analysis of the various liptinite macerals in samples of the Herrin (No. 6) coal seam with a reflectance of 0.65% (in oil at 546 nm) showed distinctive spectra for the macerals fluorinite, resinite, sporinite and cutinite. In this case, the spectra were assigned to maceral groups on the basis of the petrographic identification of macerals from which the spectra were obtained. When the groups of spectral data for each maceral type were subjected to discriminant function analysis of the eight different parameters for each spectrum, the maceral types were well separated. From this analysis it was easily seen that there were two different groups of resinite macerals. Thus, the statistical analysis of the spectral parameters of the macerals revealed two varieties of the resinite maceral group that could not be readily distinguished by normal petrographic means. The average spectra of the various maceral types distinguished by the discriminant function analysis are plotted in Figure 1. The combined results of maceral analyses in both white-light and fluorescent light as well as the reflectance value for the Herrin (No. 6) coal are given in Table 1.

Table 1.

RESULTS OF COMBINED WHITE-LIGHT
AND FLUORESCENT LIGHT PETROGRAPHIC ANALYSES

Coal Seam	Herrin (No. 6)	Brazil Block	Hiawatha
Reflectance (in oil at 546 nm)	0.65	0.58	0.52
Vitrinite	65.1	56.3	73.7
Pseudovitrinite	19.8	8.7	7.8
Fluorinite	0.3	0.2	0
Resinite	0.1	0.7	6.9
Sporinite	3.0	14.1	0.5
Cutinite	0.4	2.0	0.8
Amorphous Liptinite	1.8	4.2	1.0
Semi-fusinite	5.7	4.9	4.2
Fusinite	2.1	3.4	1.3
Micrinite	1.7	5.5	3.8

In a study on the fluorescence properties of the Brazil Block seam, a somewhat different approach was used. In this case, about a hundred individual spectra were taken on all fluorescing liptinite macerals. Although the macerals from which the spectra were taken were not identified at that time, photomicrographs in both normal white-light and fluorescent light were taken for documentation. The spectral parameters for each spectrum were calculated and these data were subjected to cluster analysis to generate groupings of spectra on the basis of the spectral parameters. When these groups were identified they were subjected to discriminant function analysis to test degree to which the groups could be separated on the basis of their spectral parameters. It was found that seven groups could be distinguished. The basic petrographic data for the Brazil Block coal seam are given in Table 1 and the average spectral parameters for each group are given in Table 2. When the macerals from which the spectra were taken were identified from the photomicrographs, it was found that each group corresponded to a separate maceral type or a variety of a maceral type. There was one type of fluorinite, one type of resinite, three types of sporinite and two types of cutinite. While this correspondence of maceral types and varieties to statistical groupings of spectral data was not unexpected, it is further confirmation that the spectral parameters of macerals are unique to maceral type and variety.

Table 2.

SPECTRAL PARAMETERS OF AVERAGE SPECTRA
OF THE BRAZIL BLOCK COAL SEAM

Parameter	Fluorinite	Resinite	Sporinite I	Sporinite II	Sporinite III	Cutinite I	Cutinite II
Peak (nm)	480	520	550	590	690	610	650
Red/Green Quotient	0.32	0.58	0.85	1.00	1.22	1.47	2.27
Area Blue (%)	37	19	16	14	13	12	7
Area Green (%)	38	43	36	34	31	32	29
Area Yellow (%)	15	23	25	28	26	28	29
Area Red (%)	10	15	23	24	30	28	35
Area Left of Peak (%)	21	33	40	53	93	59	60
Area Right of Peak (%)	79	67	60	47	7	41	40

An interesting result of this analysis is that one of the sporinite varieties and one of the cutinite varieties distinguished by statistical means showed petrographic evidence of alteration (weathering). Because the coal sample itself was collected from a fresh exposure at an active mine, it appears as if the weathered maceral varieties were weathered before they were incorporated into the peat that was later coalified.

The results of these two studies show that fluorescence spectral analysis can distinguish on a quantitative basis the various types of liptinite macerals and, indeed, even varieties of each type. That the various spectra are unique to the individual macerals is further indicated by the recurrent order of the spectral parameters, especially the wavelength of maximum intensity (λmax) and the red/green quotient in any given coal. For example, as shown in Figure 1 for the Herrin (No. 6) seam and in Table 2 for the Brazil Block seam the order of the maceral types on the basis of increasing λmax and Q is fluorinite, resinite, sporinite and cutinite. It should be noted, however, that as the rank of coal increases, all of the spectral peaks shift toward longer wavelengths and diminish in intensity and are thus difficult or impossible to distinguish from each other. Weathering of the macerals has a similar effect.

However, even when macerals have been altered by increases in rank, or weathering, or other processes, fluorescence microscopy can sometimes still be quite useful in characterizing coal macerals. For example, in some coal seams in the western U.S. there is an abundance of resinite. In fact, the resinite is being extracted from some of these coals and commercially exploited as a chemical raw material. In these seams the resinite most often occurs as a secondary material, filling fissures and voids in the coal. Numerous flow textures, inclusions of coal in resinite veinlets, and intrusive relationships throughout coal seams indicate that the resinite was mobilized at some point in its history. These secondary resinites are often difficult to detect in normal white-light viewing, however, they all tend to fluoresce strongly in a variety of colors and are therefore, quite amenable to fluorescence analysis. When samples of the Hiawatha seam from Utah are so examined, four types of secondary resinites, each with a different fluorescence color -- green, yellow, orange, red-brown -- are seen. Each type has a spectra that is distinctive and the various types can also be statistically separated on the basis of their spectral parameters. The average spectra of the four resinite types are shown in Figure 2 and the basic petrographic analysis of the sample from the Hiawatha seam is given in Table 1. It should be noted that at this time the only way to distiguish the various types of secondary resinite is with fluorescence microscopy. Work is now underway to separate these various resinite types and chemically characterize them.

SUMMARY

Although the characterization of coal macerals on the basis of their fluorescence spectral is a recent innovation, it has already proven to be an excellent fingerprinting tool for the various macerals. In some cases, it is even more sensitive than normal petrographic analysis. The initial results of fluorescence spectral studies show that the various fluorescent macerals in single coals can be statistically separated on the basis of their spectral parameters and that even varieties of one type of maceral can be so separated. Although the spectra obtained at this time are rather broad and not suitable for chemical structure analysis, the potential for structural analysis exist and may be realized with improvements in instrumentation.

REFERENCES

1) Jacob, H., (1964), Neue Erkenntnisse auf dem Gebiet der Lumineszensmikroskopie fossiler Brennstoffe. -Fortschr. Geol. Rheinl. u Westf, v. 12, p. 569-588.

2) Jacob, H., (1972), Mikroskop-Photometrie der organischen Stoffe von Boden I. Organopetrographische Nomenklatur und mikroskop-photometrische Methodik.- Die Bodenkultur, v. 23, p. 217-226.

3) van Gijzel, P., (1967), Autofluorescence of fossil pollen and spores with special reference to age determination and coalification. Leidse Geol. Meded., v. 50, p. 263-317.

4) van Gijzel, P., (1971), Review of the UV-fluorescence microphotometry of fresh and fossil exines and exosporia. In: Brooks et al.: Sporopollenin, p. 659-685, London, New York (Academic Press).

5) van Gijzel, P., (1975), Polychromatic UV-fluorescence microphotometry of fresh and fossil plant substances with special reference to the location and identification of dispersed organic material in rocks. In: Petrographic Organique et Potential Petrolier (Ed. by B. Alpern), p. 67-91, CNRS, Paris.

6) Teichmuller, M., (1974a), Uber neue Macerale der Liptinit-Gruppe und die Entstehung von Micrinit: Fortschr. Geol. Rheinld. u. Westf., v. 24, p. 37-64.

7) Teichmuller, M., (1974b), Entstehung and Veranderung bituminoser Substanzen in Kohlen in Beziehung zur Enstehung and Umwandlung des Erdols: Fortschr. Geol. Rheinld. u. Westf., v. 24, p. 65-112.

8) Teichmuller, M., (1974c), Generation of petroleum-like substances in coal seams as seen under the microscope. In: Advances in Organic Geochemistry 1973 (Ed. by B. Tissot and F. Bienner), p. 379-407, Editions Technip, Paris.

9) Ottenjann, K., Teichmuller, M. and Wolf, M. (1975), Spectral fluorescence measurements in sporinites in reflected light and their applicability for coalification studies. In: Petrographie Organique et Potentiel Petrolier (Ed. by B. Alpern), p. 49-65, CNRS, Paris.

10) Crelling, John C., Dutcher, Russell R. and Lange Rolf V., (1982), Petrographic and fluorescence properties of resinite macerals from wester U.S. coals: Proceedings of the Fifth Symposium on the Geology of Rocky Mountain Coal - 1982: ed. Klaus D. Gurgel, Bulletin 118, Utah Geological and Mineral Survey, p. 187-191.

11) Crelling, John C., (1982), Current uses of fluorescence microscopy in coal petrology: Journal of Microscopy (in press).

12) Ottenjann, K., Wolf, M. and Wolf-Fischer, E., (1981) Beziehugen zwurischen der Fluoreszenz von Vitriniten und den technologischen Eigenschaften von Kohlen: Proceedings of International Conference on Coal Science - Dusseldorf, IEA, p. 86-89.

13) van Gijzel, P., (1979), Manual of the techniques and some geological applications of fluorescence microscopy. Workshop sponsored by Am. Assoc. of Strat. Palynologist, Core Laboratories, Inc., Dallas.

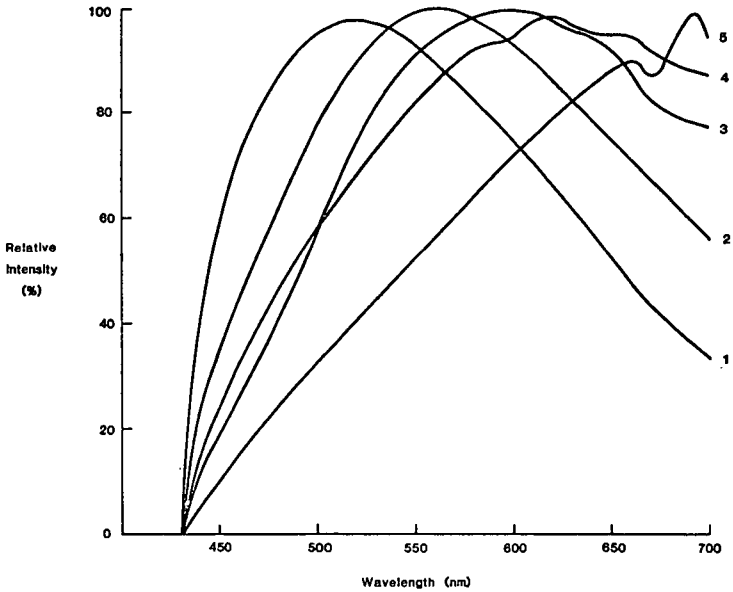

Figure 1. Average fluorescence spectrum for various macerals in the Herrin (No. 6) coal seam: 1) fluorinite; 2) low-peaking resinite; 3) high-peaking resinite; 4) sporinite; 5) cutinite. Vitrinite reflectance of the seam is 0.65%.

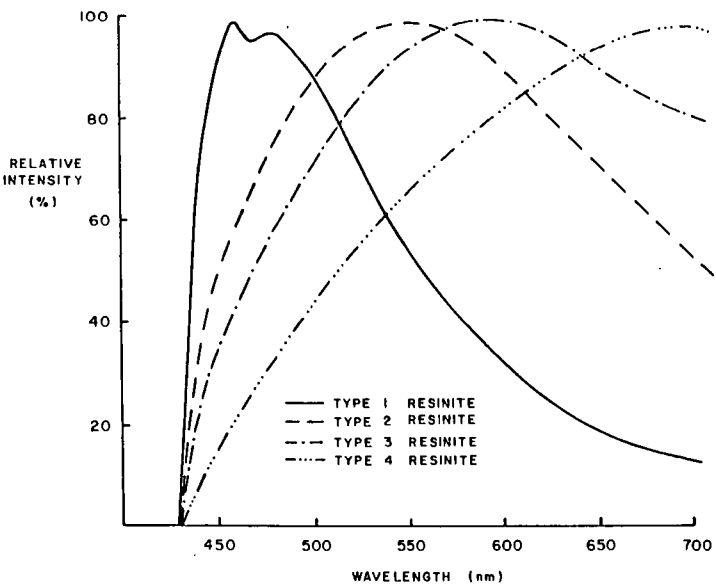

Figure 2. Average fluorescence spectra of resinite macerals in the Hiawatha seam, Utah after Crelling, et al. (10)

MICROSCOPIC INFRARED SPECTROSCOPY OF COALS

D. Brenner

Exxon Research and Engineering Company
P.O. Box 45
Linden, New Jersey 07036

Introduction

Most IR (infrared) spectroscopy of coal involves the use of finely crushed particles. Techniques in common use include incorporating the particles in potassium bromide disks (1) or slurrying them in a hydrocarbon oil such as Nujol (2). Such particulate samples generally include a wide range of types of vitrinite and other macerals which are derived from different plants (such as trees, bushes, and grasses) and from various parts of each plant (such as trunks, stems, roots, leaves, etc). In addition, inorganic substances of various types and degrees of dispersion are generally mixed in. Because of their different derivations, the various organic plant remnants are likely to have different physicochemical characteristics; however, because of the intimate mixing of these subcomponents, which usually occurs on a microscopic scale, it is difficult to separately characterize the different maceral components. In particular, IR spectra obtained on pulverized coal samples give averaged information rather than being characteristic of any individual component in the coal. A few techniques have been utilized in the past to overcome this problem. These include the hand separation of macerals (3,4), sink-float techniques, and the recently developed method of centrifugal separation of very finely pulverized coal (5). These preparation techniques provide a mixture of material which is highly enriched in a selected maceral type. These maceral concentrates can then be analyzed by a variety of chemical procedures. The averaged properties of a maceral type can be characterized using these procedures, but they do not enable the IR analysis of individual microscope macerals.

The particulate samples of coal used for infrared analysis must be finely ground because of the high absorbance of the coal. The particles must be less than roughly 20 micrometers thick (depending on the rank) for substantial transmission of the IR radiation in the more absorbing regions of the spectrum. The small particles of coal cause considerable scattering to appear in the IR spectrum. Other complications are the differences in the thicknesses of the various particles of the sample, and the variations in thickness along each particle. For example, the thinner edges (with respect to the illuminating beam) of the particles will be more transparent than the central regions, so the volume of the particles may not be sampled uniformly. This can be a problem for a heterogeneous material such as coal. Thin section samples of coal having a relatively uniform thickness of 20 micrometers or less have been used occassionally in the past (6). However, the difficulties in preparing these thin section samples and problems of contamination with the adhesives used in the preparation of the sections (7) has limited their usage. Also, because the cross sectional area of the samples must be several square millimeters or more for analysis with most IR spectrometers, microscopic components of the thin sections can not be individually analyzed.

In this paper a technique for the IR spectroscopic analysis of individual microscopic components in coal is described. This method combines new procedures for preparing uncontaminated thin section specimens of coal with a sensitive IR microspectrophotometer which has recently become commercially available. Details of this new technique are discussed and some representative spectra are described.

Experimental

The coal used in this study was Illinois No. 6 which is a high volatile C bituminous coal. To prepare thin sections, a chunk of coal about 1.5 cm across was cut perpendicular to the bedding plan to produce a roughly flat surface. This surface was ground smooth on a 20 cm diameter wheel using 600 grit and then 8 micrometer silicon carbide on disks. The flat surface was cemented to a glass slide with a thermoplastic hydrocarbon-based adhesive (Paraplast, manufactured by the Lancer Company) which is soluble in hexane. A temperature of about 70°C was used in melting and applying the adhesive. The coal was exposed to this temperature for only about a minute before cooling was started. The coal on the slide was ground to a thickness of 15 micrometers using the abrasives described above. The sample was then soaked in hexane at room temperature until the thin specimen floated off of the slide. The sample came off as a number of small pieces of various sizes from less than a millimeter across to several millimeters long. Although no residual adhesive could be observed on the pieces of coal, to insure complete removal of the adhesive the samples were immersed in a large excess of fresh solvent for several days. Then the hexane was decanted off and the specimens were stored in nitrogen at room temperature until they were used.

The microscopic infrared spectrophometer used in this work (NanoSpec/20IR manufactured by Nanometrics Inc.) operates in transmission and contains reflecting lenses. Because of the reflecting optics, the visual and IR images of the sample correspond and the region of the sample being analyzed can readily be identified visually while it is in place in the IR microscope. This enables unambiguous correlation of visual microscopic characterization and IR analysis for the same area of the sample. The condenser and the objective of the microscope are both 15 power, 0.28 numerical aperature reflecting lenses. The part of the sample to be IR analyzed is optically delineated by an adjustable aperature at the image plane of the objective, so no masking is needed at the sample itself to define the analyzed area. The useful IR range of the instrument is from about 4000 to 700 cm^{-1} (2.5 to 14 micrometers). The IR monochromator is a variable interference filter. The resolution is only about 1% of the wave number value over the IR range; however, this should be adequate for many applications with coal because of the breadth of most of the absorbances. The IR source is a Nerst Glower and the detector is a liquid nitrogen cooled mercury cadmium telluride photodetector having high sensitivity. The operation of the spectrometer is computer-controlled and the data, which is stored digitally, can be automatically averaged and difference spectra can be obtained.

Results

In this preliminary study, spectral characteristics of vitrinite and exinite macerals in Illinois No. 6 coal were examined to evaluate the utility of this new technique for microscopic IR analysis of coals. In Figure 1, a photomicrograph of a thin section specimen consisting of a megaspore (a form of liptinite) surrounded by relatively homogeneous vitrinite is shown. The thin section was placed on a barium fluoride disk on the stage of the IR microscope. The megaspore and a region of the vitrinite lying close to the megaspore on the same specimen were analyzed with the IR microscope. The analyzed regions are indicated by rectangles drawn on the photograph of the sample; they are each about 55 micrometers wide by 180 micrometers long. Spectra of the two regions were taken in air at room temperature; they are compared in Figure 2. The spectra are displaced vertically to avoid overlapping. The displayed spectra actually involve a reference scan which was taken without the sample present but with all other conditions the same. The subsequent sample spectra are automatically normalized with respect to the reference spectrum. Each of the two sample spectra in Figure 2 are 2 minute scans.

A number of differences between the liptinite and vitrinite spectra are apparent. Note that since the thicknesses of the liptinite and vitrinite regions are the same and since scattering is minimal, these spectra can be directly compared quantitatively on a per unit volume basis. Some of the more prominent of the differences are as follows. The broad hydroxyl peak around 3350 cm^{-1} is much deeper for the vitrinite. This probably is caused chiefly by a much larger number of phenols in the vitrinite, but it may also indicate more water absorbed on the vitrinite. Between 2800 and 2975 cm^{-1} the liptinite shows a much stronger absorption than the vitrinite. This indicates much more aliphatic hydrogen in -CH, $-CH_2$, AND $-CH_3$ groups in the liptinite. Also, at about 2850 cm^{-1} the liptinite shows a substantially larger peak than the vitrinite on the side of the larger absorption. At about 1600 cm^{-1} the vitrinite peak is much larger than the liptinite peak probably indicating much more aromatic character in the vitrinite. Conversely, the CH_2, CH_3 peak around 1440 cm^{-1} is much more pronounced for the liptinite. The spectra clearly contrast the more aromatic and hydroxyl-containing structure of the vitrinite to the more aliphatic structure of the liptinite.

Mention should be made of some artifacts which appear in the spectra of Figure 2. At about 2350 cm^{-1} there is a peak caused by CO_2 in the air. (This peak could be eliminated, if desired, by sealing the region of the beam path and maintaining a nitrogen atmosphere). At about 2250 cm^{-1} and 1230 cm^{-1} are peaks caused by changes in the IR filters. Three filters are used to obtain the full spectrum, and small peaks occur where the second and third filters are brought into use. Another artifact is broad peaks seen around 2100 cm^{-1} in the liptinite spectrum, 1950 cm^{-1} in the vitrinite spectrum and in some other areas. These peaks are caused by interference fringes which arise from the IR radiation being internally reflected from the top and bottom surfaces of the sample. The fringes can be misleading if they are not correctly identified.

The applicability of this technique for "in situ" IR analysis during chemical treatments and the ability to perform kinetic measurements was tested by observing the effect of applying deuterated pyridine to a thin section of vitrinite and then allowing it to dry. An area 40 X 180 micrometers was analyzed. First a spectrum was taken of the untreated sample. Then the solvent was placed on the sample and repetitive scans were made to monitor changes in the IR spectrum as the deuterated pyridine evaporated. Figure 3 shows spectra of the untreated sample, the sample wet with pyridine, and the sample after drying for about 20 minutes. For the latter spectrum, peaks characteristic of deuterated pyridine are still prominent, such as those at about 950 and 820 cm^{-1}. Later scans showed no appreciable lessening of the peaks. The retention of some of the pyridine is consistent with the results of Collins et. al. (8).

Tests were made to determine the minimum area of analysis which could be conveniently used with thin sections of coal in this technique. Figure 4 shows spectra of regions of a tiny roughly 30 X 30 micrometer piece of vitrinite. One spectrum was taken using a 21 X 21 micrometer analyzing area, and the other spectrum was taken using a 20 X 30 micrometer analyzing area. Four minutes were used for each scan. For this scan time, the smaller area gives quite a noisy spectrum, but the 20 X 30 micrometer spectrum is much better. By using a longer scanning time or by accumulating repetitive scans this spectrum could probably be made quite respectable. The spectral region having the greatest problem in the analysis of such very small areas is beyond 1000 cm^{-1} where the sensitivity of the spectrometer falls off. Subcomponents or macerals in the coal which are somewhat less than 25 micrometers across can probably be IR analyzed by using long data accumulation times. Preferably such small subcomponents should be physically separated from the surrounding material. Alternatively, the spectrum of a region including the subcomponent as well as some of the surrounding material could be substracted (using an appropriate normalization factor) from a spectrum only of the surrounding

material in order to isolate the contribution of the subcomponent. Note, however, that for subcomponent sizes near the wavelength of the IR radiation the possibility of interference effects from the edges of the sample must be considered. Such effects ought to be made apparent by comparing spectra from subcomponents having different sizes or shapes.

Discussion

Infrared spectra of good quality have been obtained on uncontaminated individual microscopic macerals and microscopic subregions in coal. This development enables the infrared characterization of microsocpic individual subcomponents of coals and other solid fossil fuels as opposed to obtaining statistically averaged data on complex mixtures. In addition, variations in functionalities over microscopic distances can be studied. The technique should also be applicable for the analysis of virtually any chemical process or chemical treatment of coal which causes changes in the IR spectrum and in which the area of interest is identifiable after the treatment. For example, the initial chemical functionality of an individual microscopic maceral or subregion can be determined with the microspectrometer; the maceral can be reacted; and the effect of the treatment on that same microscopic subregion can be determined.

In Figure 2 the IR spectrum of a subregion of vitrinite about 0.010 mm^2 in area is compared with the IR spectrum from an equal area which is within a single megaspore. The two regions of analysis are on the same piece of thin section and they are separated by only about 160 micrometers. The two minute scans of the 15 micrometer thick samples give excellent signal to noise. As described in the results section, these spectra clearly contrast the more aromatic and hydroxyl-containing structure of the vitrinite to the more aliphatic structure of the megaspore. The ability to analyze closely lying regions having identical preparation, equal areas being analyzed, and the same thickness, facilitates quantitative comparisons of the regions. Thus, while these data are generally consistent with the results of Bent and Brown (9) taken on maceral concentrates, the present technique enables a more direct quantitative comparison of the spectra.

The spectra in Figure 3 demonstrate the "in situ" treatment of an uncontaminated thin section of coal. One operational difficulty is the possibility of movement of the sample during treatment which would make analysis of the same microscopic region before and after treatment difficult. For example, application of a drop of solution to the coal is likely to cause movement. Movement can be avoided by securing the sample, but this may be difficult for small samples or it may affect the sample. Alternatively, if the region under analysis is carefully recorded, such as on a photograph, then during or after treatment the sample can be accurately repositioned on the stage.

Figure 4 demonstrates that isolated samples of coal less than 30 micrometers across can be satisfactorily IR analyzed and that delineated regions of a sample less than 25 micrometers across can be characterized by IR. Signal to noise levels which are improved over those shown in Figure 4 can be obtained by using longer data accumulation times. Alternatively, if better quality data is required only for some small regions of the spectrum, then those regions alone can be scanned to shorten the time needed to obtain an acceptable signal to noise level. The ability to analyze small regions of a coal sample is important even for a single maceral type such as vitrinite. For example, substantial variations occur in the structure (10,11) and swellability (12) of different microscopic areas of vitrinite from the same coal.

In the IR microscope the region of the sample being analyzed is delineated by a variable aperature at the image plane of the objective. Therefore, no spacial

restrictions are placed around or near the sample itself. Since the image of the sample has been substantially magnified at this image plane, it is relatively easy to accurately define even very small subregions of the sample for analysis with the aperature. However, the geometrical region delineated by the variable aperature which is observed visually is not nearly so well defined for the infrared radiation because of diffraction effects. The spacial uncertainty is proportional to the wavelength, so the resolution is considerably poorer near the long wavelength end of the IR range. The divergence or angular spread of the IR beam passing through the sample, which is determined by the numerical aperature, will further diminish the spacial specificity of the delineated area. This, of course, becomes more of a problem for thick samples. For analysis of a very small subregion in the coal, the most unambiguous way to avoid contributions from contiguous material is to physically remove the subcomponent from the surrounding material.

The 15 micrometer thickness for the Illinois No. 6 coal is quite satisfactory since the percent transmissions of a number of the larger peaks are below 40 percent, but without saturation. Also, at this thickness the thin sections can be conveniently manipulated without fracturing. Using the described grinding technique for preparation, samples containing any maceral types and even substantial amounts of mineral matter can be prepared. A wide range of coals (with the possible exception of very low or very high ranks) can be handled by these techniques.

The interference peaks which occur in the spectra of Figure 2 can be misleading when trying to interpret the spectra. These fringes occur when some of the IR radiation reflects from the top and bottom surface of the sample and then interferes with the unreflected beam. The fringes are particularly a problem where the top and bottom surfaces are nearly parallel and where the thickness of the sample is comparable to the wavelengths of the radiation such as for the thin section specimens used in the technique described here. However, the intensity of the interfering beam is not large since it is reflected twice and it passes through the sample three times instead of once. Thus, as seen in Figure 2, the fringes are most prominent in the spectral regions having low absorbance. The fringes can be partially compensated for by determining their position and intensity in a low absorbance region and then calculating and subtracting out their contribution to other parts of the spectrum where their presence is less obvious. Alternatively, tilting the sample, or using samples of different thicknesses and of higher adsorbance can be used to identify the effects of the fringes on a spectrum so that they can be compensated for.

Summary and Conclusions

Microscopic macerals and subregions in coal have been characterized by infrared spectroscopy using a new technique. Individual macerals or subregions of the coal as small as 25 micrometers across can be analyzed. The technique utilizes new procedures for preparing uncontaminated thin sections of coal in combination with a recently available microscopic IR spectrometer.

Because the thin section specimens are not contaminated with adhesives or embedding materials, and because the samples are readily accessible on the stage of the IR microscope, this technique is well suited for "in situ" treatments of the coal. Alternatively, since the 15 micrometer thick specimens of coal can ordinarily be handled and transported without damage (if proper care is taken), an untreated sample can be initially analyzed, then it can be removed from the instrument for chemical or thermal treatment, and finally, the same specimen can be returned to the microspectrometer for determination of the changes in the IR spectrum. The analysis of the same spectrum before and after treatment is highly desirable for micro-heterogeneous substances such as coal.

The microscopic IR spectroscopy technique described here differs from and complements prior IR work on maceral concentrates in being able to spacially delineate an individual subcomponent being IR analyzed and to characterize it visually in the context of its surroundings.

Preliminary IR measurements on microscopic subregions of individual macerals of homogeneous-appearing vitrinite and of megaspores in Illinois No. 6 coal clearly demonstrate quantitative as well as qualitative chemical differences between these macerals. This work demonstrates that good quality IR spectra of microscopic subregions of coal can be obtained.

Acknowledgement

The author wishes to acknowledge the excellent technical assistence of Mark S. Beam in the preparation of the samples for these studies.

References

1. Gordon, R. R., Adams, W. N., Pitt, G. J., Watson, G. H., Nature, 174, 1098 (1954).

2. Brooks, J. D., Durie, R. A. and Sternhell, S., J. Appl. Sci., 9, 63 (1958).

3. Fenton, G. W. and Smith, A. H. V., Gas World, 149 (1959).

4. van Krevelen, D. W. and Schuyer, J., Coal Science, p. 240, Elsevier, Amsterdam (1957).

5. Dyrkacz, G. R., Horwitz, E. P., Fuel, 61, 3 (1982).

6. Cannon, C. G. and Sutherland, G. B. B. M., Trans. Faraday Soc., 41, 279 (1945).

7. Mackowsky, M.-Th., "Stach's Textbook of Coal Petrology," p. 243, Gebruder Bontraeger, Berlin (1975).

8. Collins, C. J., Hagaman, E. W., Jones, R. M., and Raaen, V. F., Fuel,. 60, 359 (1981).

9. Bent, R. and Brown, J. K., Fuel, 40, 47 (1961).

10. Taylor, G. H., Coal Science, Advances in Chemistry Series 55, p. 274, edited by Given, P. H., Am. Chem. Soc., Washington D.C. (1966).

11. Brenner, D., Proceedings of the International Conference on Coal Science, p. 163, Verlag Gluckauf GmbH, Essen (1981).

12. Brenner, D., Preprints of the Division of Fuel Chemistry, ACS National Meeting, Vol. 27, No. 3-4, 244 (1982).

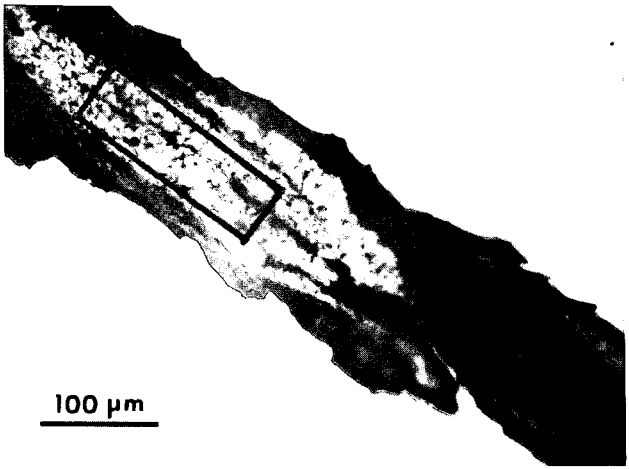

Fig. 1. Thin Section Sample of Illinois No. 6 Coal Containing Regions of Vitrinite and Liptinite

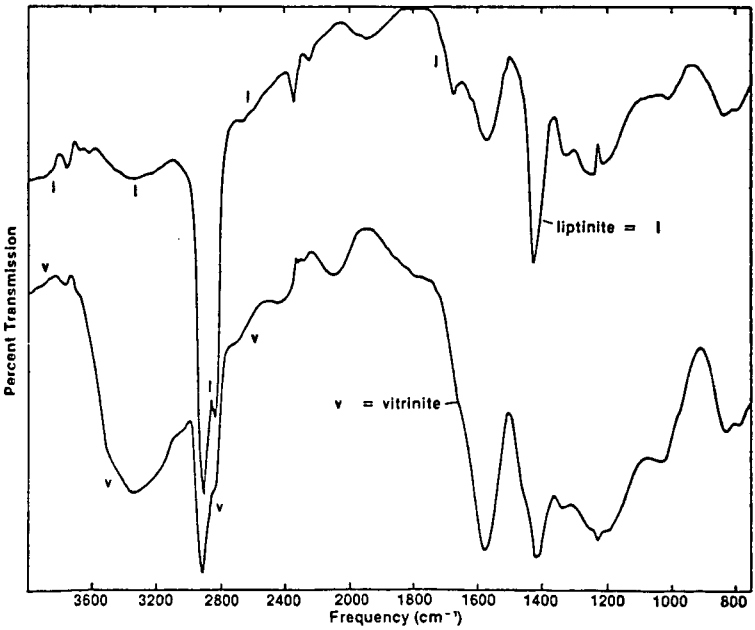

Fig. 2. IR Spectra of Microscopic Regions of Vitrinite and Liptinite in the Same Thin Section Sample of Illinois No. 6 Coal

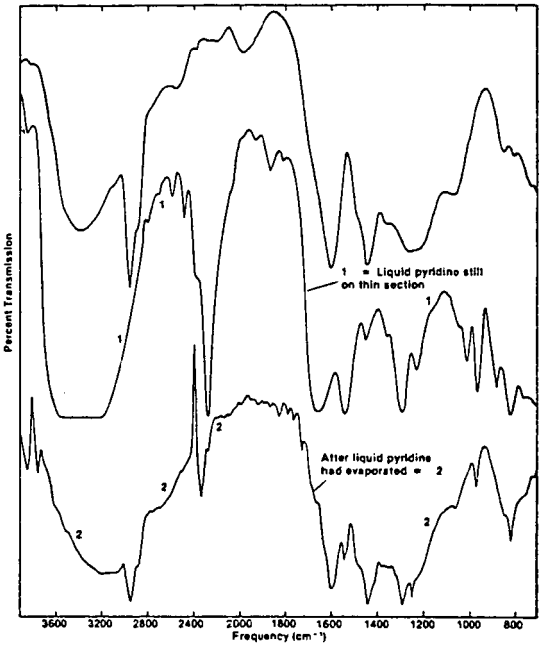

Fig. 3. IR Spectra of a Microscopic Region of Vitrinite in a Thin Section of Illinois No. 6 Coal
Top ----- Untreated Sample
Middle -- Liquid Deuterated Pyridine on the Sample
Bottom -- After Pyridine has Evaporated

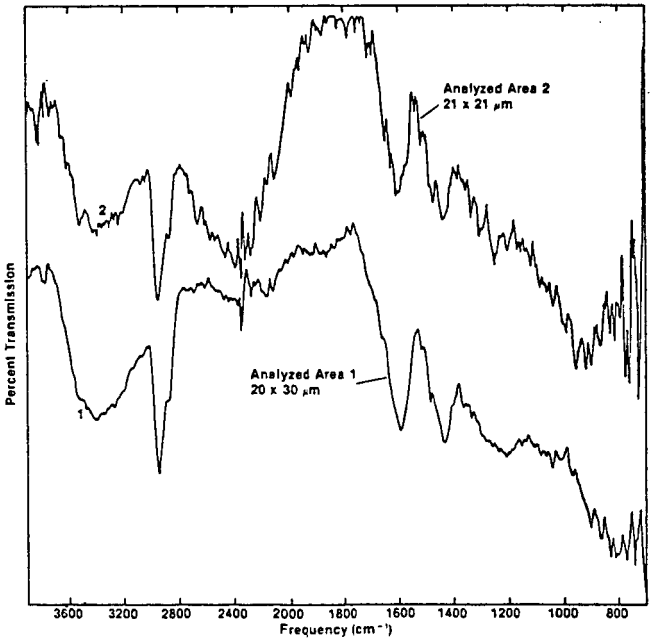

Fig. 4. IR Spectra of a Thin Section Sample of Illinois No. 6 Coal having an Area of 30μmX30μm
Top ----- Delineated Area is 21μmX21μm
Bottom -- Delineated Area is 20μmX30μm

SOME VARIATIONS IN PROPERTIES OF COAL MACERALS ELUCIDATED BY DENSITY GRADIENT SEPARATION*

Gary R. Dyrkacz, C. A. A. Bloomquist, L. Ruscic, and E. Philip Horwitz

Chemistry Division, Argonne National Laboratory
Argonne, Illinois 60439

INTRODUCTION

Our recent development of a new procedure for the density separation of macerals offers a method for obtaining high resolution separation of the maceral groups: exinite, vitrinite, and inertinite, and can further resolve individual maceral types, e.g., sporinite (1,2). The procedure utilizes well-known techniques of density gradient centrifugation (DGC) to separate the coal into its components in a continuous aqueous CsCl density gradient. This results in a series of bands representing the density variations in maceral groups and maceral types. The gradient is then divided into convenient size fractions, the coal in each fraction is isolated and micropetrographic analyses are performed on selected fractions. In addition to providing pure materials for further work, a density fingerprint of a coal is produced. The observed changes in density are related in a complex way to the chemical structure of the coal or maceral (3). In order to better understand the chemical variations occurring in coal macerals we have examined the ultimate analysis of selected density fractions separated from the same coal.

EXPERIMENTAL

Separation

The basic procedures for DGC separation of macerals with advantages and disadvantages has been discussed previously (1,2). To summarize, the coal is ground to ~3 micron average particle size, chemically demineralized and separated on a density gradient. The gradient is then divided into fractions of ~0.01 g/cc range and each fraction is then filtered, washed, and dried.

Analysis

Because of the small samples often generated, ultimate analysis of selected density fractions was performed with a Perkin-Elmer 240 C, H, N Analyzer using a modified burn procedure which includes increasing the time of burn and the amount of O_2 used in the burn. Good correlation (r^2 = .98) with ASTM methods was found for a range of coals from sub-bituminous to anthracites.

RESULTS AND DISCUSSION

All the coals used here were obtained from the Pennsylvania State University Coal Data Base. The data for the coals are given in Table I. The separation of all these coals was performed in the same way and all the coals were resolved to the same degree. We have previously published detailed separation data on the high volatile B bituminous coal, PSOC-106, which gave good yields of all three maceral groups (1,3). The exinite in this coal is mainly sporinite, while the inertinite is mainly semi-fusinite. Figure 1a shows the distribution of the pure maceral particles as a function of density for PSOC-106. Pure maceral particles refer to those particles which by optical microscopy are composed of only one maceral species. Figure 1b shows the corresponding atomic ratios H/C, S/C, N/C,and O/C.

*Work performed under the auspices of the Office of Basic Energy Sciences, Division of Chemical Sciences, U. S. Department of Energy, under Contract W-31-109-Eng-38.

The selected fractions analyzed represent density fractions consisting of at least 88% (vol.) of a single maceral species. The lines connecting sets of points between maceral groups must not be taken literally. These intermediate regions consist of particles with two or more macerals composing a single particle or two distinct populations of pure maceral particles. Thus, whether or not the connecting lines between maceral groups represent the atomic value in that region, their only purpose for this discussion is to aid the eye in following trends between maceral groups.

The H/C ratio exhibits a very large range of values over the entire coal: from 1.13 at the lowest density monitored to 0.48 at the highest density. The S/C ratios follow a similar trend: with the highest sulfur values in exinites and the lowest in inertinites. These sulfur values represent almost all organic sulfur since pyritic sulfur has been eliminated by the separation procedure. The S/C data is consistent with data found by an 'in situ' method of sulfur analysis in coal (4). Because of the nature of the separation method we can also see significant variations not only between maceral groups, but within each maceral group. Figure 2 is an attempt to provide some idea of the magnitude of variation that exists in the H/C ratio in the three maceral groups. The distributions are incomplete because of overlapping of maceral bands or composite maceral particles which give unreliable data. Table II represents the range of H/C values for each band and combined with previous ^{13}C with solid probe nmr data for f_a, shows the ring index or number of rings per 100 carbon atoms. The data for 50% of the coal refers to the coal centered around the peak value. The ring index includes all aromatic, aliphatic, and heterocyclic rings. The number of rings per 100 carbons is roughly the same for all the maceral groups and indicates, as expected, that they are all highly condensed species. However, the ratio of aromatic to aliphatic rings increases dramaticallly from exinites to inertinites. Exinite tends to exhibit wide variations in its composition, while vitrinite and inertinite are somwhat less variable. In all cases, though, the indications are that substantial variations in each maceral group are being observed by the density separation method. The oxygen and nitrogen data also show strong variations within the exinites and vitrinites, while inertinites do not.

In Figure 3 we have used the graphical densimetric method to show how the ring index varies with the density of the macerals (5). As can be seen the data parallels the increase in aromaticity.

The change in atomic ratios are not unique to the particular coal PSOC-106. Figures 4a and 4b show data on three more bituminous coals which contain substantial amounts of all three maceral groups. (The very high H/C value of 1.4 for PSOC-297 is due to alginite in this coal.) Although all the coals exhibit their own character in the magnitude and range of the H/C values, they all show significant chemical changes across each maceral band in a similar manner to PSOC-106. Similar data also holds for coals that contain ±95% vitrinite.

What do these variations represent? There are a number of factors which can be invoked to explain the changes observed. Each of the three major maceral groups is composed of sub-macerals (maceral types). Exinite is composed of the maceral types: sporinite, resinite, alginite, cutinite. Since the source materials for each maceral type had different chemical structures some artifact of these differences would be expected to remain. This is one source of variation. Moreover, within a single maceral type itself significant petrographic changes can be observed. For example, different spore species show different fluorescence color, and collinite and semi-fusinite can have broad reflectance ranges within a coal. All these microscopically observable changes suggest differences in chemical structure. Qualitatively, we do see regular variations in fluorescence and reflectance across the maceral bands. It is apparent that density gradient centrifugation can, to some extent, isolate these physical and chemical variations and, in a sense, provide more

homogeneous materials. However, the chemical variations we see by DGC have to be considered as lower limits of the chemical heterogeneity expected for coal. Since we are still dealing with discrete particles, its density may still be a weighted average of the maceral variants comprising the particle, even though these variants are below optical resolution. Further grinding may separate these variants, but problems of mechanochemistry and surface problems may then become significant.

CONCLUSIONS

Substantial variation in the chemical behavior of macerals has been shown for a number of coals. Density gradient techniques can provide better defined, more homogeneous materials as well as provide a lower limit on the heterogeneity.

REFERENCES

1. Dyrkacz, Gary R. and Horwitz, E. Philip, Fuel, 61, 3 (1982).
2. Dyrkacz, Gary R., Bloomquist, C. A. A., and Horwitz, E. Philip, Separation Science and Technology, 16, 1571 (1981).
3. Van Krevelen, D. W., 'Coal', Elsevier, 1961, p. 315.
4. Raymond, R., International Conference on Coal Science, Proceedings, Dusseldorf, 1981, p. 857.
5. Van Krevelen, D. W. and Chermin, H. H. G., Fuel, 33, 338 (1954).
6. Pugmire, R. J., Zilm, K. W., Woolfenden, W. R., Grant, D. M., Dyrkacz, G. R., Bloomquist, C. A. A., and Horwitz, E. P., Jour. Org. Geochem., in press.

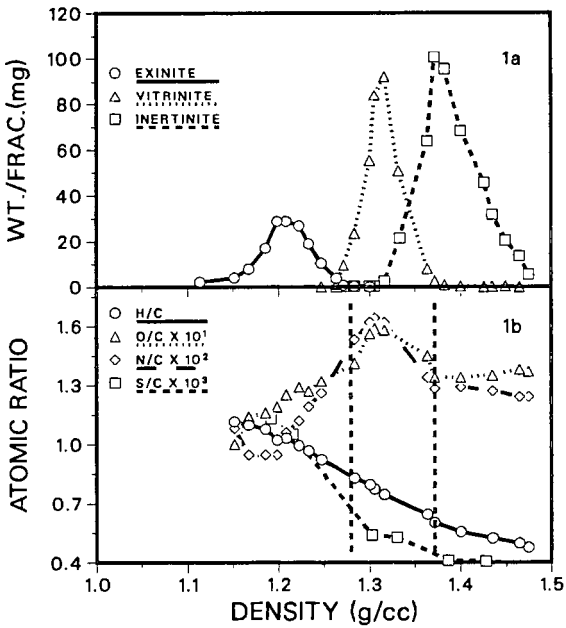

Figure 1a. Pure maceral distribution of PSOC-106.
1b. Variations of atomic parameters.

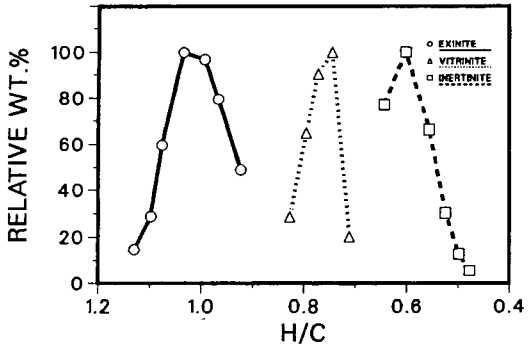

Figure 2. Distribution of coal macerals in PSOC-106 as a function of H/C ratio.

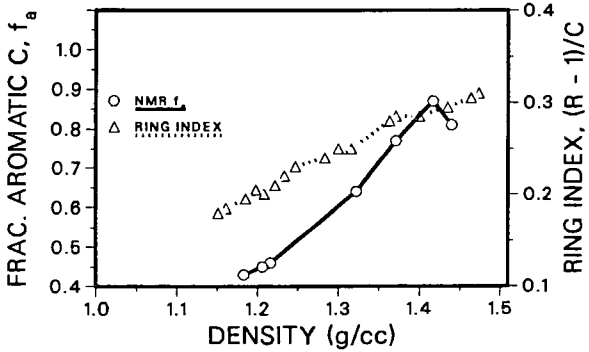

Figure 3. Variation of f_a and ring index with density in PSOC-106.

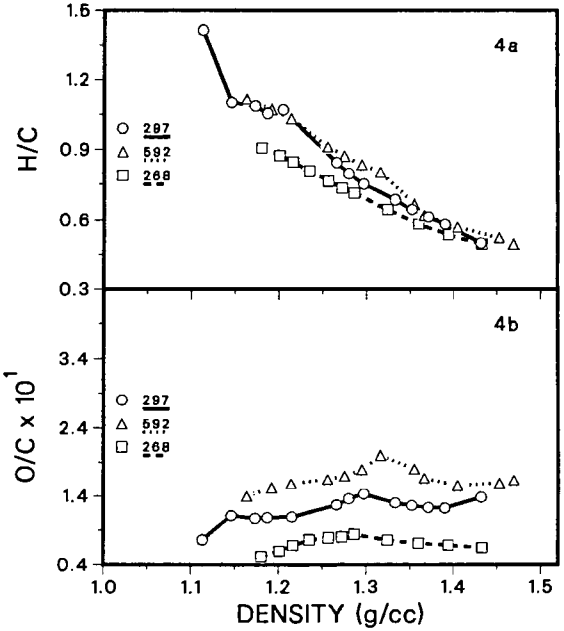

Figure 4a. Variation of H/C ratio with density.
4b. Variation of O/C ratio with density.

COMPUTERIZED PYROLYSIS MASS SPECTROMETRY OF COAL MACERAL CONCENTRATES

Henk L.C. Meuzelaar, Alice M. Harper and Ronald J. Pugmire

University of Utah, Salt Lake City, Utah 84112

INTRODUCTION

A few pyrolysis mass spectra of purified coal maceral concentrates have appeared in the literature [1-4] showing the presence of more or less pronounced differences between the spectra of vitrinites, fusinites, sporinites and alginites. However, these studies did not attempt to distinguish between the possible effects of rank or depositional environment on the spectra and the more basic structural differences between maceral types.

Recently, the feasibility of distinguishing between these effects was demonstrated by Meuzelaar *et al.* [5,6] in a study of over 100 Rocky Mountain coal samples by Curie-point pyrolysis mass spectrometry (Py-MS) in combination with computerized multivariate statistical analysis of the data. In the present study, the same analytical approach is used to characterize a set of 30 selected maceral concentrates.

EXPERIMENTAL

The maceral concentrates analyzed are listed in Table I. Seventeen samples originated from the maceral collection of the British National Coal Board and had been prepared by the sink/flotation method. Most of these were obtained through Dr. Given at Penn State University who redistributed these samples to different groups as part of a cooperative study [7]. Thirteen maceral concentrate fractions were prepared from two US coals by the cesium cloride gradient centrifugation method [8].

Samples were ground to 300 mesh under liquid nitrogen and 4 mg aliquots were suspended in 1 ml of methanol. Two 5 microliter drops of this suspension were coated on the ferromagnetic filaments used in Curie-point pyrolysis. A detailed description of the sample preparation and Curie-point Py-MS methods has been given elsewhere [4,6]. The Py-MS system used was an Extranuclear 5000-1 Curie-point pyrolysis MS system based on a quadrupole mass spectrometer. Experimental conditions were as follows: sample weight 20 μg, Curie-point temperature 610°C, temperature rise time 5 s, total heating time 10 s, electron impact ionization energy 12 eV, mass range m/z 20-260, scanning speed 1000 amu/s, total scanning time 25 s. All samples were analyzed in triplicate. Data processing involved the use of computerized signal averaging followed by spectrum calibration, normalization and scaling procedures. Multivariate statistical analysis, e.g. factor analysis, procedures involved the use of SPSS [9] and ARTHUR [10] program packages.

RESULTS AND DISCUSSION

Three pyrolysis mass spectra averaged over all vitrinites, inertinites and exinites (sporinites) respectively are shown in Figure 1. The overall pattern of each maceral group agrees quite well with the spectra published by other authors [1-4], with vitrinites showing prominent phenolic series, fusinites being dominated by aromatic hydrocarbon signals and sporinites showing marked alkene peaks. More subtle differences - the significance of which can only be appreciated with the help of computerized data analysis techniques - will be discussed later.

Figure 2 shows a scatter plot of m/z 110 *vs.* 124, two peaks known to provide a direct measure of rank in high volatile bituminous coals [5,6] and believed to represent dihydroxybenzenes and methyldihydroxybenzenes respectively. The peak intensities in Figure 2 indeed appear to correspond more or less directly with

carbon content and to be largely independent of maceral type. In other words, if carbon content is accepted as a measure of the rank of whole coals then a plot of m/z 110 *vs.* 124 will reflect this rank measure in spite of possible differences in maceral composition. However, it hardly needs to be pointed out that the large differences in carbon content between macerals from the same coal (see Table I) illustrate the inadequacy of using carbon content as a coalification parameter for coals with markedly different maceral compositions.

Figure 3 shows a scatter plot of the peak intensities of m/z 34 vs. 122, two peaks known to be influenced strongly by differences in depositional environment [5,6] and thought to represent hydrogen sulfide and C_2-alkylphenols respectively. In a previous study of whole coals from the US Rocky Mountain coal province the ion intensity at m/z 34 was found to correlate strongly with organic sulfur content. However, in this study insufficient data were available on organic sulfur content to attempt such a correlation. Nevertheless a crude correlation appears to exist with total sulfur content. In agreement with Py-MS studies on whole coals [5] the alkylphenol peak intensities at m/z 122 show a rough negative correlation with rank. Nevertheless, four of the British vitrinites show much higher peak intensity values at m/z 122 than the US vitrinites of comparable rank. This is not surprising, since differences in hydroxyl content between coals from different depositional environments have also been reported [11].

Finally, the high intensity of m/z 122 in the Dunsil seam inertinite, compared to the other inertinites should be noted. This is probably due to the relatively low rank of the Dunsil inertinite as well as to the fact that this sample is composed largely of semifusinite. All semifusinite-rich samples included in this study (see Table I) exhibit mass spectral patterns which tend to be intermediate between fusinites and vitrinites (compare also the two Ballarat seam samples in Figure 3) which is in agreement with presently accepted views on the origin of semifusinites from partly charred wood [12].

In view of the presence of strongly correlating series of homologous ions in all maceral spectra, as shown in Figure 1, factor analysis was performed to reduce the apparent dimensionality of the data and to bring out the major underlying chemical tendencies. The K-L plot in Figure 4 was obtained while using 80 mass peaks with highest ratio's for "between category" and "within category" variance (with each set of three replicate spectra per sample serving as a separate category). Figure 4 shows a clear separation between the three different maceral groups, with vitrinites occupying an intermediate position between fusinites and exinites. The density gradient centrifugation samples of the two US coals blend in amazingly well with the corresponding British macerals. Moreover, factor I appears to show a positive correlation with differences in sample density.

To help explain the differences in chemical composition between the three maceral groups causing the separation in Figure 4 a spectrum of the first factor, calculated according to a procedure described by Windig *et al.* [13], is shown in Figure 5. The positive component of this factor spectrum is explained by peaks with relatively high intensities in inertinites (compare with Figure 4) and is thought to represent polynuclear aromatic series with rather pronounced degrees of alkyl substitution, e.g. biphenyls and/or acenaphthenes, phenanthrenes and/or anthracenes, fluorenes, etc. The high intensity of the residual methanol solvent peak groups at m/z 30-33 in inertinites may well reflect the long known correlation between the methanol absorption capacity of a coal and its degree of coalification [14]. The negative component of the factor spectrum - largely explained by peaks with relatively high intensities in the sporinite samples - shows a distinct peak pattern which we interpret as representing (poly)isoprenoids and/or related polyenic compounds. This pattern is found in all five sporinites, in spite of differences in origin, coalification stage and preparation technique. Moreover, in contrast with the more or less completely saturated or aromatized isoprenoid skeletons reported in the extractable fractions of coals and shales [15], these isoprenoid fragments liberated by Curie-point pyrolysis appear to possess a degree of unsaturation consistent with that found in many naturally occurring isoprenoids. Whether these polyenic signals are derived from carotenoid moieties in sporopollenin

[16] or perhaps from some type of fossilized natural rubber, remains open to speculation at this point. Selected peak intensities at m/z 122 and 288, representing the positive (inertinite) and negative (sporinite) components of factor I respectively, are shown in Figure 6.

Although the positive portion of the factor spectrum of factor II (not shown) might be expected to provide peak patterns characteristic of vitrinites, few if any such peaks are found. In fact, factor II is dominated by an as yet unexplained series of peaks loading on the negative component and thus representing compounds which are characteristically low in vitrinites as compared to inertinites and exinites.

It may be concluded that Curie-point pyrolysis mass spectrometry in combination with multivariate statistical analysis provides valuable information on the specific chemical characteristics of coal maceral concentrates as well as on the influence of depositional environment and coalification processes. The results obtained appear to agree well with generally accepted views on the chemical nature and origin of coal macerals. Perhaps the most important new finding of this study is the presence of distinct peak patterns in sporinites which appear to represent more or less intact (poly)isoprenoid and/or related polyenic hydrocarbon moieties. More detailed accounts of these studies are being published elsewhere [6].

TABLE I
MACERAL CONCENTRATES ANALYZED

NCB SINK/FLOTATION CONCENTRATES										
Sample			Maceral Composition (%)			Elemental Composition				
#	Code	Seam (Colliery)	VITRIN	INERT	LIPT	% C	% H	% O	% N	% S_t
1	T	Dunsil (Teversal)	98	1	1	81.5	5.1	10.8	2.1	1.4
2	T	ibid	6	93*	tr.	87.7	3.9	6.9	1.1	1.6
3	M	Barnsley (Markham)	3	9	88	82.2	7.4	7.3	1.1	1.9
4	M	ibid	98	2	tr.	82.2	5.5	9.3	1.9	1.3
5	M	ibid	6	92**	1	91.6	3.6	4.1	0.4	1.2
6	W	Wheatley Lime (Woolley)	96	1	3	87.9	6.9	3.0	1.1	1.2
7	W	ibid	3	9	88	86.5	5.6	4.9	1.8	1.4
8	A	Silkstone (Aldwarke)	0	5	95	87.2	7.4	3.6	1.2	0.7
9	A	ibid	98	1	1	86.9	5.4	4.2	1.8	1.1
10	A	ibid	5	96*	-	92.1	3.7	3.1	0.7	0.4
11	R	Ballarat (Roddymoor)	96	3	1	88.8	5.3	3.6	1.7	0.7
12	Ra	ibid	2	97	-	93.9	3.5	1.4	0.5	0.8
13	Rb	ibid	14	85*	1	91.9	4.3	3.1	0.3	0.5
14	C	Gellideg (Coegnant)	89	11	0	91.4	4.6	1.9	1.6	0.6
15	C	ibid	34	66	0	92.3	4.2	1.9	1.1	0.6
16	P	Beeston (Peckfield)	"exinite"; density 1.22 g/cm^3							
17	P	ibid	"inertinite"; density 1.44 g/cm^3							

U OF U DENSITY GRADIENT FRACTIONS				
Sample				
#	Code	Seam (Coal Field)	Density (g/cm^3)	Maceral Type
18	E1	Upper Elkhorn (E. Appalachian)	1.17	SPORIN
19	E2	ibid	1.26	VITRIN
20	E3	ibid [PSOC 2	1.29	VITRIN
21	E4	ibid 85.6 %C]	1.30	VITRIN
22	E5	ibid	1.32	INERT***
23	E6	ibid	1.36	INERT***
24	S1	Dakota (San Juan River)	1.23	VITRIN
25	S2	ibid	1.25	VITRIN
26	S3	ibid	1.26	VITRIN
27	S4	ibid [PSOC 858	1.27	VITRIN
28	S5	ibid 84.2 %C]	1.30	VITRIN
29	S6	ibid	1.32	SFUSIN
30	S7	ibid	1.38	SFUSIN

* semifusinite
** equal amounts of fusinite and semifusinite
*** the parent coal (PSOC 2) contains approximately equal amounts of fusinite, semifusinite, macrinite and micrinite.

ACKNOWLEDGEMENTS

The generous help of the British National Coal Board and the Pennsylvania State University in obtaining well characterized maceral samples is gratefully acknowledged. Furthermore, the authors are indebted to Dr. J. Karas for preparing the gradient centrifugation samples and to D.J. Davis and K.H. Wong for performing these analyses. The research reported here was sponsored by DOE grant DE FG22-80PC30242 and by matching funds from the State of Utah.

REFERENCES

1. Van Graas, G., de Leeuw, J.W. and Schenck, P.A., in *Advances in Organic Geochemistry*, A.G. Douglas and J.R. Maxwell, eds., Pergamon Press (Oxford), 1979, p. 485.
2. Larter, S.R., Ph.D. Thesis, University of Newcastle upon Tyne, England, 1978.
3. Allan, J. and Larter, S.R., Proc. 10th Int. Meeting on Organic Geochemistry, Bergen (Norway), September 1981 (in press).
4. Meuzelaar, H.L.C., Haverkamp, J. and Hileman, F.D., *Curie-point Pyrolysis Mass Spectrometry of Recent and Fossil Biomaterials; Compendium and Atlas*, Elsevier, Amsterdam, (1982).
5. Meuzelaar, H.L.C., Harper, A.M. and Given, P.H., Proc. 5th ROMOCO Symp., UGMS Bulletin 118, 1982, p. 192.
6. Meuzelaar, H.L.C., Harper, A.M., Hill, G.R., Futrell, J.H., Davis, D.J.and Metcalf, G.S., Final report to DOE (Grant #DE-FG22-80PC30242) 1982.
7. Given, P.H., in *Organic Geochemistry and Chemistry and Coal Macerals for Advances in Chemistry Series*, J.W. Larsen (ed.) to be published.
8. Dyrkacz, G.R., Bloomquist, C.A.A., Winans, R.E. and Horwitz, E.P., Proc. Int. Conf. Coal Science, Dusseldorf, Verlag Gluckauf GmbH, Essen, 1981, p. 34.
9. Nie, N.H., Hull, C.H., Jenkins, J.G., Steinbrenner, K. and Bent, D.H., *Statistical Package for the Social Sciences* (2nd Ed.), McGraw-Hill, N.Y., 1975.
10. Harper, A.M., Duewer, D.L., Kowalski, B.R., Fasching, J.L., in *Chemometrics: Theory and Application*, B.R. Kowalski (ed.), Washington, D.C., ACS Symp. Series No. 52, 1977, p. 14.
11. Yarzab, R.F., Abdel-Baset, Z., and Given, P.H., *Geochem. et Cosmochim. Acta*, 43:281 (1979).
12. Teichmuller, M., Teichmuller, R., in *Stach's Textbook of Coal Petrology*, E. Stach, G.H. Taylor, M-Th Mackowsky, D. Chandra, M. Teichmuller and R. Teichmuller (eds.), Gebruder Borntraeger, Berlin, 1975, p. 5.
13. Windig, W., Kistemaker, P.G., Haverkamp, J. and Meuzelaar, H.L.C., *J. Anal. Appl. Pyrol.*, 2:7 (1980).
14. Van Krevelen, D.W., *Coal*, Elsevier, Amsterdam, 1961.
15. Gallegos, E.J., in *Developments in Petroleum Science*, Vol. 5, T.F. Yen and G.V. Chilingarian (eds.), Elsevier Scientific Pub. Co., Amsterdam, 1976.
16. Brooks, J. and Shaw G., in *Sporopollenin*, J. Brooks, P.R. Grant, M. Muir, P. van Gijzel and G. Shaw (eds.), Academic Press, London, 1971, p. 351.

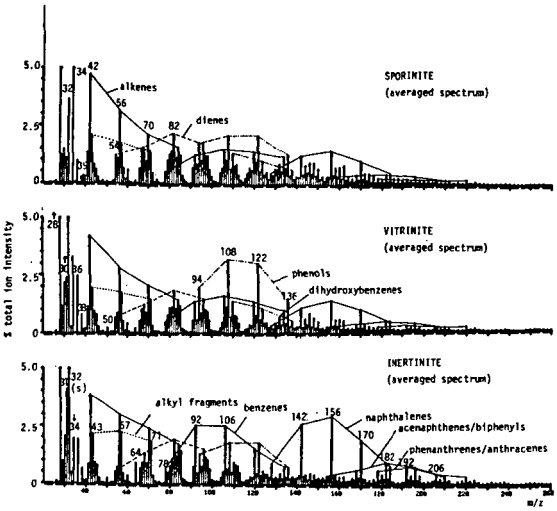

Figure 1. Averaged pyrolysis mass spectra of the three maceral types analyzed. Homologous ion series connected by solid or broken lines. Arrows indicate markedly higher or lower peaks. Chemical identifications are tentative. For conditions see text.

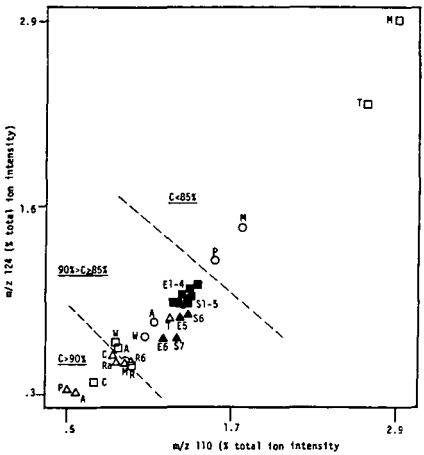

Figure 2. Scatter plot of ion intensities at m/z 110 and 124, believed to represent dihydroxybenzenes and methyldihydroxybenzenes respectively. Exinites (sporinites), vitrinites and inertinites are represented by circles, squares and triangles respectively. Index code is identified in Table I. Solid black symbols indicate US gradient centrifugation samples. Note that carbon content boundaries have not been confirmed for US samples (Table I).

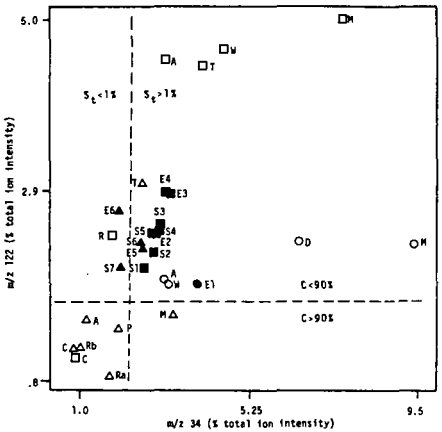

Figure 3. Scatter plot of ion intensities at m/z 34 and 122, believed to represent hydrogen sulfide and C_2-alkyl phenols respectively. For explanation of symbols, codes and markings see Figure caption 2 and Table I. Note crude positive correlation of m/z 34 with total sulfur content and negative correlation of m/z 122 with carbon content.

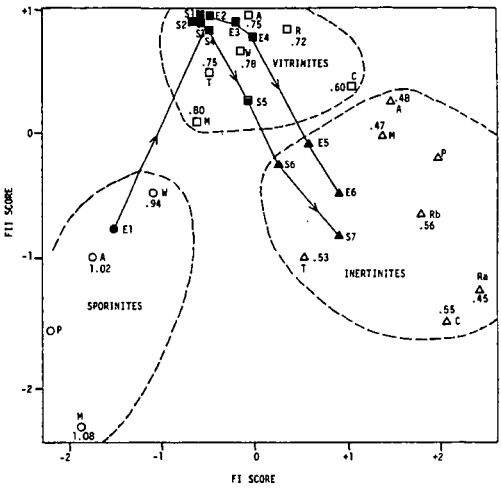

Figure 4. Karhunen Loeve plot of the first two factor scores. For explanation of symbols and codes see Figure caption 2 and Table I. US density gradient fractions are connected by arrows in order of increasing density. Numerical values ranging from .45 (Ballarat inertinite a) to 1.08 (Barnsley exinite) represent atomic H/C ratio's. Note positive correlation of factor I with density and negative correlation with H/C ratio.

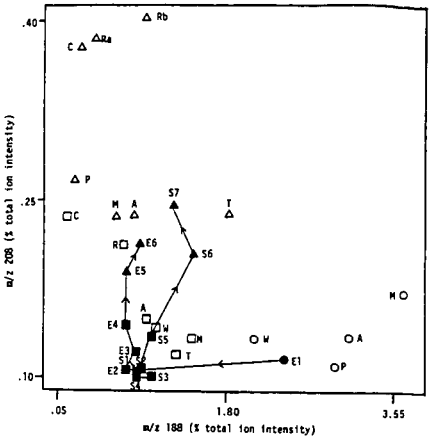

Figure 6. Scatter plot of ion intensities at m/z 188 and 208 believed to represent $C_{14}H_{20}$ polyenic and $C_{16}H_{16}$ polynuclear aromatic hydrocarbon compounds respectively. For explanation of symbols and codes see Figure caption 2 and Table I. Comparison with Figure 5 shows that m/z 208 is prominent in the positive component of Factor I whereas m/z 188 is one of the highest mass peaks in the negative component.

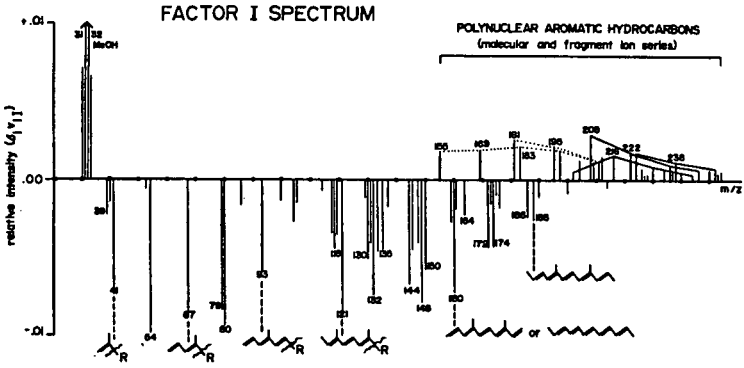

Figure 5. Factor spectrum representing factor I in Figure 4. Note marked simplification of spectral patterns as compared to Figure 1. Chemical labels are examples of possible structures only.

APPLICATION OF 2-D AND DIPOLAR DEPHASING ^{13}C NMR TECHNIQUES TO THE STUDY OF STRUCTURAL VARIATIONS IN COAL MACERALS

Ronald J. Pugmire, Warner R. Woolfenden, Charles L. Mayne
Jirina Karas, and David M. Grant

University of Utah
Salt Lake City, Utah 84112

INTRODUCTION

Coal has been described as an organic rock. In order to better utilize coal supplies, however, the chemical structure of coal needs to be known in much greater detail so that methods can be developed to convert coal to a clean burning liquid or gaseous fuel.

Coal is known to be a physically heterogeneous substance with inorganic mineral matter mixed randomly in the organic material. The organic matter is further subdivided into maceral groups which reflect the floristic assemblages available at the time of the formation of the coal measures. The chemical structural detail of the organic components of these materials is not well known, even though researchers have been working for decades on structure analysis. Of interest is the nature of the carbon skeleton including the aromatic and aliphatic groups; the level, type and role of oxygen, nitrogen, and sulfur; the type and extent of cross-linking; and the molecular weight distribution of the macromolecules.

Useful reviews and monographs published on coal structural analysis include works by Van Krevelan (1), Ignasiak (2), Tingey and Morrey (3), Davidson (4), Larsen (5), and Karr (6). These reports indicate the following: Coal is a highly aromatic substance (65-90% aromatic carbon, variable with rank but with few coals having aromaticities lower than 50%), with clusters of condensed rings (up to approximately four rings); the aliphatic part of the coal appears to be mostly hydroaromatic rings and short aliphatic chains connecting the aromatic clusters; the oxygen has been found in the form of phenols, quinones, ethers, and carboxylic acids, but less detail is known about the nature of the organic sulfur or nitrogen.

The study of the aromaticity of coal has included infrared spectroscopy (7) and various chemical methods (8,9), but the most promising analytical tool appears to be cross-polarization magic angle sample spinning nuclear magnetic resonance spectroscopy (CP/MAS C-13 NMR). This technique, initially developed by Pines, et al (10), has been successfully applied to coals by several workers in order to obtain aromatic-to-aliphatic ratios (11-14) (f_a). There is evidence that further structural information on coals and coal macerals can be gained from the CP/MAS C-13 NMR experiments (15-19). The aliphatic part of coal has also been characterized by a novel chemical method involving a trifluoroacetic acid/aqueous hydrogen peroxide oxidation of the aromatic rings to yield aliphatic acids and diacids (20). Chemical test results may be spurious, however, due to the severity of the reaction conditions and the insoluble and heterogeneous nature of coals.

CP/MAS ^{13}C NMR offers a powerful non-destructuve tool for the analysis of carbonaceous solids. Depending on the nature of the carbonaceous material and the concomitant resolution obtainable, a wide range of structural information can be obtained. In complex organic sediments, the diversity of structural components leads to broad bands that frequently lack detail. However, employing multiple pulse techniques, it is possible to obtain additional structural information. The dipolar dephasing technique reported by Opella (26,27) discriminates protonated from nonprotonated carbons in a CP/MAS spectrum on the basis of the ^{1}H-^{13}C dipolar interaction. Hagaman and Woody (28) have reported the spectra of Illinois No. 6 coal.

We wish to report data on a series of whole coals and coal macerals using conventional CP/MAS, dipolar dephasing, and 2-D dipolar dephasing techniques. These data provide a wealth of new structural information and demonstrate that multiple pulse and 2-D spectroscopic techniques can be utilized on complex carbonaceous materials. We also report data obtained on maceral samples separated by the density gradient centrifugation method which separates coal maceral groups according to density.

EXPERIMENTAL

All ^{13}C NMR CP/MAS spectra were obtained on a Bruker CXP-100 instrument equipped with a Z32DR ^{13}C-MASS superconducting magnet probehead for proton enhanced magic angle spinning experiments (CP/MAS). Samples were packed in carefully prepared rotors machined from boron nitride (body material) and Kel-F (spinner head material) in Andrew-Beams type rotors (22). Boron nitride is used as the body material because of its good tensil strength and its resistance to deformation at high spinning speeds, whereas the Kel-F material is used for the rotor head material because of its better resistance to wearing as it comes into occasional contact with the stator assembly during start ups and stops. Both materials are free of carbon and hydrogen which would cause extraneous resonance signals and decoupler heating problems. The spinning speed was slightly in excess of 4 KHz to avoid complications due to overlapping of spining side bands with other spectral components. The carbon-proton cross polarization time was 1.5 msec and the cycle time was 0.3 seconds. Experiments performed at this laboratory have shown that such short cycle times are indeed feasible with coals because of the inherent free radical induced short relaxations times (23). Each spectra resulted from averaging 10,000 repetitions on samples of approximately 100 mg size. The dipolar dephasing experiments involved a 40 μsec delay inserted between the contact time and the acquisition period. It is well known that this delay period will decrease the signal intensities of <u>all</u> carbon peaks compared to their intensities in the normal CP/MAS spectrum due to T_2 relaxation effects; however, no effort has been made to correct for this decrease in intensity to effect a material balance between compared spectra since it is assumed that the decrease in intensity of the nondipolar dephased carbon-13 peak is small. Chemical shifts are reported referenced to TMS. Hexamethyl benzene was used as an external referencing material. A rotor of the reference solid is used to adjust the magic angle and the carbon/proton power levels for the Hartman Hahn condition such that the aromatic and aliphatic carbon peaks are of essentially equal intensities. The coal samples were then substituted using the same rotor without changing any resolution or referencing parameters. The upfield peak of hexamathylbenzene is presumed to be at 18 ppm from TMS.

COAL MACERALS AND MACERAL SEPARATION

The coals designated as PSOC-2 and PSOC-858 were obtained from the Coal Data Bank at the Pennsylvania State University. The maceral groups from this coal were separated by the density gradient centrifugation technique described by Dyrkacz (24,25). The samples designated by PSMC-67, -19, -34, -43, -47, and -53 were vitrinite concentrates obtained from Professor Alan Davis at Penn State and the analytical and CP/MAS data have been previously reported (16). The British maceral concentrates designated as Aldwarke, Silkstone, Teversil, Dunsil, Woolley, Wheatley Lime, Markham Main, and North Celyen were obtained from Professor Peter Given at Penn State and the analytical data on these coals are given in Table III. The samples were provided to Professor Given by the British National Coal Board and were stored under nitrogen since their preparation.

RESULTS AND DISCUSSION

We have recently established in our laboratory the capability to separate coal macerals by the density gradient centrifugation technique (DGC) described by Dyrkacz (24,25). The DGC fractogram of PSOC-2 is presented in Figure 1 indicating the density delineation of the three maceral groups. The mean densities indicated in the Figure correspond to the liptinite (largely sporinite, see Table I) vitrinite and inertinite maceral fractions. The actual density ranges for the six different samples studied are used as labels for each spectrum illustrated in Figure 2 along with the separate f_a values. This coal contains essentially no liptinite and hence exhibits only two peaks corresponding to vitrinite and inertinites (semi-fusinite and fusinite). The stacked CP/MAS spectra of the PSOC-2 whole coal and the sporinite, three vitrinite, and two inertinite fractions separated by the DGC technique are given in Figure 2. Note the variation in the band shapes in the aliphatic regions of the vitrinite and inertinite maceral groups. These data clearly indicate that additional structural information is obtainable from studies of coal maceral groups which have been separated from a given coal as previously reported (17,18). Even within the three vitrinite samples, large variations in spectral characteristics indicate structural differences among macerals of small density variance. Similar structural changes are observed in the vitrinite maceral group for PSOC-858.

Additional structural information can be obtained by means of the dipolar dephasing technique reported by Opella (26,27) which discriminates protonated from nonprotonated carbons in a CP/MAS spectrum on the basis of the ^{1}H-^{13}C dipolar interaction. Hagaman and Woody (28) have reported the spectra of Illinois No. 6 coal by employing this technique. In model compounds, Alemany (29) has observed that a 40-μs interruption in the proton decoupling will cause all of the CH and CH_2 resonances to vanish, while the intensity of the nonprotonated carbons experience only minor attenuation (ca. 10-20%). The dephasing of a methyl group is more complex but approximately 50% of the methyl carbon signal is still observed after a 40 sec dephasing delay. Hence, by appropriately varying the interruption of the decoupler one can differentiate among methine/methylene, methyl and nonprotonated carbons. Typical results are given in Figure 3 for the Aldwarke Silkstone exinite. The fraction of the carbon in the sample which is aromatic and nonprotonated, f_a^N, is obtained by comparing the relative intensities of the aromatic region of the spectra with decoupler pulse delays of 0 and 40 sec before data acquisition. The fraction of protonated aromatic

carbon is then f_a^H; thus $f_a^H + f_a^N = f_a$. Using a solvent refined coal tar for which high resolution ^1H and ^{13}C NMR data were taken, Wilson (30) has obtained values of f_a, and f_a^H in the solid tar. These values agree nicely with those corresponding values obtained for the dissolved tar. (f_a = 0.62, 0.62; f_a^H = 0.24, 0.23 for the solid and dissolved solvent refined coal, respectively).

Dipolar dephasing data (26,17) have been acquired on 36 coal and maceral samples and some of the results are given in Table II. The data are indicative again of the highly variable structure found in coal samples. The values designated as f_s^S and f_a^B are the fraction of aromatic carbon atoms which are substituted and those which are bridgehead carbons respectively. This separation is based strictly on the chemical shift range of the nonprotonated aromatic carbons; i.e., in the dipolar dephasing spectrum, it is assumed that nonprotonated carbon resonance shifts greater than 133 ppm are substituted while those with chemical shifts less than 133 ppm are bridgeheads. This arbitrarily chosen chemical shift value has, of course, been assigned from previous experience using the spectral assignments of known compounds. The values found in the last column of Table II reflect the fraction of the aliphatic region which is both nonprotonated carbons and methyl group carbons and has been designated as f_s^*. If the carbon resonances due to these two differing types of species are distinctive, they can be further identified with the use of 2-dimensional dipolar dephasing techniques based on their differing dephasing rates. Carbon-13 data obtained on a series of British maceral concentrates are also expressed in Table II. Further analytical data for these concentrates are found in Table III. The data found in this table has been supplied by the Coal Survey National Coal Board. The Woolley Wheatly Lime sample is 93% fusinite while the Teversal Dunsil concentrate is 80% semifusinite with 13% fusinite. The Aldwarke Silkstone sample contains 43% semifusinite and 43% fusinite. The petrographic analysis of PSOC-2 reveals nearly equivalent amounts of fusinite, semifusinite, micrinite, and macrinite (6.8, 8.1, 7.5 and 8.5% respectively in the whole coal). The differences in f_a^H values for these samples are greater than the experimental error and these differences suggest that NMR techniques may be useful in characterizing the chemical structural differences between inertinite macerals.

The use of 2-D ^{13}C NMR techniques in liquids has progressed from a novelty to a very useful analytical tool. Even though the use of 2-D pulse techniques on solids is not as advanced, experiments on simple organic compounds have appeared in the literature (31). The principal value of 2-D spectroscopy in solid CP/MAS studies of coal and related macerals lies in the ability of such methods to separate spectral information which in the typical one dimensional case appears as a single resonance. Figure 3 is a 2-D contour plot of the Aldwarke Silkstone exinite maceral exhibiting chemical shift along the F_2 axis. It should be emphasized here that those carbon resonances which extend further along the F_1 axis have larger dipolar dephasing effects working upon them. Such effects can then be graphically used to differentiate between carbons of similar chemical shift but differing proton environments. Figure 5 is a stack plot of the same information found in Figure 3. Spectral traces differ from each other by 977 Hz starting with the top spectrum at zero Hz dipolar dephasing rate.

The capability of measuring directly the fraction of aromatic carbon, f_a relative to total carbon via solid ^{13}C NMR has stimulated considerable interest. The f_a values previously found (32,33) for coal macerals have been consistent with the order fusinite > micrinite > vitrinite > exinite given by Dormans et al (34) for macerals of a specific rank. For the sample set of PSOC-2 and its separated maceral groups, the f_a values found in this study are in the order inertinite > vitrinite > exinite as expected. An interesting observation is that f_a^H, the fraction of the total carbon in the coal that is aromatic and protonated, decreases in that same order for this series of six macerals. These data imply that there is a significant diversity in the amount of ring substitution and/or cross linking among the aromatic carbons in the various macerals as seen in the estimated values for the fraction of aromatic substituted and bridgehead carbons, f_a^S and f_a^B. An examination of the pure vitrinite series PSMC-67, -19, -34, -43, -47, and -53, which is a suite of samples from a common depositional environment but of varying rank, reveals a similar trend in samples of increasing rank. The CP/MAS data reported earlier (16) exhibited a decrease in functionality with progressing rank (i.e., loss of alkyl and aromatic oxygen groups). The dipolar dephasing data of this report indicate that this loss of functionality leads to a net increase in the fraction of protonated aromatic carbons. Ring condensation reactions alone cannot explain these results as ring condensation would produce an opposite effect. It appears that reactions associated with vitrinite maturation in these samples must also include some ring protonation reactions accompanying ring defunctionalization and the data suggests that these protonation reactions are preferred to ring condensation reactions.

Data on the set of British maceral concentrates, Table I, exhibit trends similar to those noted above. Comparing the f_a^H data on the inertinite fractions from PSOC-2, Woolley Wheatley Lime, Teversal Dunsil, and Aldwarke Silkstone reveals some significant differences between these samples from coals of high volatile bituminous rank (albeit, perhaps from quite different environments).

Carbon resonances arising from both nonprotonated and protonated aromatic carbons may appear at the same frequency under proton decoupling. Yet these two resonances could possess very different relaxation behavior and in a solid could evolve very differently due to local proton dipolar fields which attenuate with the carbon proton distances as $1/r_{CH}^3$. When the spin locking pulse for proton nuclei is turned off, carbons with directly bound protons such as methines and methylenes rapidly dephase in the local proton fields and their spectral response is rapidly diminished. The rapid internal motion of CH_3 groups greatly decreases the effectiveness of methyl protons. Nonprotonated carbons are only dephased by remote and therefore much weaker magnetic fields. This type of response is given in Figure 2 using the pulse sequences first proposed by Rybaczewske et al (31) and popularized by Opella (26,27) for powders. These two spectral traces demonstrate how carbon atoms with protons are significantly attenuated following a 40μsec dephasing time. Thus, the upfield portion of the aromatic peak due to protonated carbons and essentially all of the aliphatic region are attenuated leaving primarily the nonprotonated aromatic carbons and methyl carbons (the two high field peaks in the lower trace which have chemical shift values for aliphatic and aromatic CH_3 carbons). The small vestigial remnant of the once very strong methine/methylene peak appears as the lowest field peak of the three distinct aliphatic peaks. Thus, this spectral response is limited to a subportion of the total spectrum contained in the upper trace.

Thus, otherwise overlapping spectral information has been obtained by employing in a subtle way the differing dipolar properties of the different types of carbons. If this spectral feature is made the basis of a two dimensional, 2-D, FT spectrum, one may simultaneously obtain spectral information on both nonprotonated and protonated carbons directly. Figures 3 and 4 contain such a 2-D spectrum for the Aldwarke Silkstone exinite. In Figure 4 a contour plot of the spectral intensities is given for the rate of dipolar dephasing along the y-axis vs. chemical shift along the x-axis. Thus, the nonprotonated and methyl carbons show steep fall off in the intensity contours while protonated carbons are represented by much broader (along y-axis) spectral responses. Vertical cuts through the 2-D surface along the chemical shift axis are given in Figure 5. Hence, we observe in a more typical format the spectral respose as a function of a dipolar dephasing frequency. For a solid powder the C-H dipole-dipole vectors span all possible orientations and thus zero frequency responses are found for all resonances, albeit the spread in aliphatic response is distributed over such a much greater range of dephasing frequencies as to reduce this part nearly to the noise level. The successive slices in Figure 5 leaves the CH_2 peak persisting to higher dephasing frequencies as would be expected from the data in Figure 3. There is an inverse relationship between the time slices in Figure 3 and the frequency slices in Figure 5. Short times contain information corresponding to larger dephasing frequencies. The three dimensional plot (Figure 6) of the aromatic portion of Figures 4 and 5 helps one to appreciate the above point. Note in the plot sharp peaks corresponding to nonprotonated carbons. This feature is graphically shown in the 3-D portrayal. A single chemical shift slice through the aromatic region, also shown in Figure 5, emphasized the dual nature of the spectral response with a sharp peak resting on a broad base peak. Curve fitting techniques can easily resolve the true components.

Thus, using very sophisticated spectral resolving techniques, important structural information on coal is now available from these techniques for the first time. Hence, multiple pulse/multidimensional spectroscopy offers an exciting new analytical tool for the study of complex materials such as coal and coal macerals.

ACKNOWLEDGMENT

This work was supported by the Department of Energy Office of Energy Research under Contract No. DE-AS02-78ER05007 and the Office of Basic Energy Sciences, Division of Chemical Sciences, U. S. Department of Energy under Contract No. 31-109-ENG-38. We are indebted to Professor Peter Given for supplying the British maceral concentrates which were obtained from the British National Coal Board.

REFERENCES

1. P. W. Van Krevelan, "Coal" Elsevier Publishing Company, New York, 1961.

2. B. S. Ignasiak, T. M. Ignasiak, and N. Berkowitz, Reviews in Analytical Chemistry, 1975, 2, 278.

3. G. L. Tingey, and J. R. Morrey, "Coal Structure and Reactivity", TID-16627 Batelle Pacific Northwest Labs, Richland Washington, 1973.

4 R. M. Davidson, "Molecular Structure of Coal" IEA Coal Research, London, 1980.

5. J. W. Larsen, "Organic Chemistry of Coal" ACS Symposium Series 71, Washington, D.C. 1978.

6. C. Karr, "Analytical Methods for Coal and Coal Products", Vol. I-III, Academic Press, New York, 1978.

7. H. L. Retcofsky, Applied Spectroscopy, 1977, 31, 166.

8. S. K. Chakrabartty, and H. O. Kretschmer, Fuel, 1974, 53, 132.

9. J. L. Huston, et al, Fuel, 1976, 55, 281.

10. A. Pines, H. G. Gibby, and J. S. Waugh, J. Chem. Physics, 1973, 59, 569.

11. D. L. VanderHart, and H. L. Retcofsky, Fuel, 1976, 55, 202.

12. V. J. Bartuska, G. E. Maciel, J. Schaefer, and E. O. Stejskal, Fuel, 1977, 56, 354.

13. V. J. Bartuska, G. E. Maciel, and F. P. Miknis, "C-13 NMR Studies of Coals and Oil Shales," American Chemical Society, Division of Fuel Chemistry, Preprints, 1978, 23.

14. K. W. Zilm, R. J. Pugmire, D. M. Grant, W. A. Wiser, and R. E. Wood, Fuel, 1979, 58, 11.

15. K. W. Zilm, R. J. Pugmire, S. R. Larter, J. Allen, and D. M. Grant, Fuel, 1981, 60, 717.

16. R. J. Pugmire, D. M. Grant, S. R. Larter, J. Allen, A. Davis, W. Spackman, and J. Sentfle, New Approaches in Coal Chemistry, ACS Symposium Series No. 169, 1981, p 23.

17. R. J. Pugmire, K. W. Zilm, W. R. Woolfenden, D. M. Grant, G R. Dyrkacz, C. A. A. Bloomquist, and E. P. Horwitz, Proceedings of the International Conference on Coal Science, Dusseldorf, Germany, September 7-9, 1981, p. 798-806.

18. R. J. Pugmire, K. W. Zilm, W. R. Woolfenden, D. M. Grant, G. R. Dyrkacz, C. A. A. Bloomquist, and E. P. Horwitz, Carbon-13 NMR Spectra of Macerals Separated from Individual Coals, in press.

19. A. Pines and D. E. Wemmer, "Developments in Solid State NMR and Potential Applications to Fuel Research", ACS Division of Fuel Chemistry, Preprints, 1978, 23, 15.

20. N. C. Deno, B. A. Greigger, and S. G. Stroud, Fuel, 1978, 57, 455.

21. P. H. Given W. Spackman, A. Davis, and R. G. Jenkins, Coal Liquefaction Fundamentals, D. D. Whitehurst, Ed. ACS Symposium Series No. 139, Washington, D.C., 1980, p. 334.

22. K. W. Zilm, D. W. Alderman, and D. M. Grant, J. Mag. Res., 1978, 30, 563.

23. K. W. Zilm, R. J. Pugmire, and D. M. Grant, ^{1}H and ^{13}C Relaxation in Coals: Effects on Quantitation, manuscript in preparation.

24. G. R. Dyrkacz and E. P. Horwitz, Fuel, 1982, 61, 3.

25. G. R. Drykacz, C. A. A. Bloomquist and E. P. Horwitz, Sep. Sci. and Tech., 1981, 15, 1571.

26. S. J. Opella, and M. H. Fry, J. Amer. Chem. Soc., 1979, 101, 5854.

27. S. J. Opella, M. H. Fry, and T. A. Cross, J. Amer. Chem. Soc., 1979, 101, 5856.

28. E. W. Hagaman and M. C. Woody, Proceedings of the International Conference on Coal Science, Dusseldorf, September 7-9, 1981, pp 34-38.

29. L. B. Alemany, R. J. Pugmire, D. M. Grant, T. D. Alger, and K. W. Zilm, Cross Polarization and Magic Angle Spinning NMR Spectra of Model Organic Compounds III. The Effect of Dipolar Interaction on Cross Polarization and Carbon-Proton Dephasing, manuscript in preparation.

30. M. A. Wilson, R. J. Pugmire, N. J. Russell, and D. M. Grant, Structure of Australian Oil Shales and Solvent Refined Coal as Revealed by ^{13}C CP/MAS Studies, manuscript in preparation.

31. E. F. Rybaczewski, B. L. Beff, J. S. Waugh, and J. S. Sherfinski, J. Chem. Phys., 1977, 67, 1231.

32. R. E. Richards and R. W. York, J. Chem. Soc., (London), 1960, 2489.

33. H. Tschamler and E. deRuiter, Coal Science, R. F. Gould, Ed., Advances in Chemistry Series 55, American Chemical Society, Washington, D.C., 1966, p 332.

34. H. N. M. Dormans, F. J. Hutjens, and D. W. Van Krevelen, Fuel, 1957, 36, 321.

TABLE I

Elemental Analysis and Maceral Composition of Coal PSOC-2 Separated by Density Gradient Centrifugation Techniques

Petrographic Analysis (Volume %)	COAL PSOC-2
Liptinites	
Alginites	0.0
Resinite	1.2
Cutinite	1.4
Sporinite	33.6
Vitrinite	29.6
Inertinites	
Micrinite	8.7
Semifusinite	8.3
Fusinite	7.0
Macrinite	7.7
Total Liptinites	36.2
Total Vitrinite	32.1
Total Inertinites	31.7
Elemental Analysis (DMMF %)*	
C	85.49
H	5.56
N	1.46
S	0.62
O (by difference)	6.79
Mineral Matter Content of Coal* (Before Demineralization)	3.82
Vitrinite Reflectance* (Mean maximum)	0.89
Class*	HVAB
Coal Type	Channel Lithotype

* Values reported by Penn State on different samples of the same coal.

TABLE II

Structural Parameters of Coals and Coal Macerals

	H/C	%C (DMMF)	f_a	f_a^H	f_a^N	f_a^B	f_a^S	f_s^H	f_s^*
PSOC-2	0.79	86.61	0.60	0.39	0.21	0.11	0.10	0.36	0.05
E	-	-	0.34	0.24	0.10	0.02	0.07	0.59	0.06
V-1	-	-	0.61	0.41	0.20	0.07	0.13	0.33	0.06
V-2	-	-	0.70	0.45	0.25	0.10	0.15	0.26	0.04
V-3	-	-	0.67	0.47	0.20	0.11	0.09	0.26	0.07
I-1	-	-	0.75	0.59	0.17	0.06	0.11	0.21	0.04
I-2	-	-	0.76	0.63	0.13	0.05	0.08	0.19	0.07
PSMC-67	0.80	82.2	0.73	0.29	0.44	0.23	0.21	0.22	0.05
-19	0.86	84.4	0.77	0.35	0.33	0.18	0.15	0.20	0.03
-34	0.75	83.9	0.77	0.42	0.35	0.19	0.16	0.20	0.03
-43	0.78	87.0	0.78	0.44	0.34	0.20	0.14	0.19	0.03
-47	0.73	88.0	0.86	0.43	0.43	0.26	0.16	0.12	0.02
-53	0.63	89.1	0.85	0.48	0.38	0.22	0.16	0.13	0.01
Aldwarke Silkstone									
Exinite	1.02	87.2	0.53	0.26	0.27	0.14	0.13	0.40	0.07
Vitrinite	0.75	86.9	0.80	0.38	0.42	0.21	0.21	0.15	0.05
Inertinite	0.48	92.1	0.89	0.59	0.30	0.17	0.13	0.10	0.01
Teversil Dunsil									
Vitrinite	0.75	81.5	0.78	0.30	0.48	0.23	0.25	0.18	0.04
Inertinite	0.53	87.7	0.86	0.37	0.49	0.21	0.28	0.12	0.02
Woolley Wheatley, Lime									
Exinite	0.95	87.9	0.47	0.29	0.18	0.09	0.09	0.46	0.07
Vitrinite	0.78	86.6	0.77	0.48	0.29	0.12	0.17	0.20	0.03
Inertinite	0.37	93.7	0.89	0.53	0.36	0.21	0.15	0.09	0.02
Markham Main									
Exinite	1.08	82.6	0.45	0.25	0.20	0.09	0.12	0.48	0.07
Vitrinite	0.80	82.2	0.76	0.33	0.41	0.23	0.18	0.21	0.06
Inertinite	0.47	91.6	0.82	0.51	0.31	0.18	0.13	0.15	0.03
North Celyen									
Exinite	0.65	90.6	0.84	0.40	0.44	0.27	0.17	0.14	0.02
Vitrinite	0.67	89.9	0.83	0.46	0.37	0.24	0.13	0.16	0.01
Inertinite	0.61	91.3	0.85	0.47	0.38	0.24	0.14	0.14	0.01
PSOC-1108	0.65	68.0	0.43	0.29	0.14	0.06	0.08	0.46	0.11
PSOC-1110	0.93	72.5	0.16	0.03	0.13	0.06	0.07	0.65	0.19
Beluga Lignite	0.94	65.7	0.64	0.17	0.47	0.07	0.40	0.25	0.11

$$f_a = f_a^H + f_a^N = f_a^H + f_a^S + f_a^B \qquad f_s = f_s^H + f_s^*$$

$$f_a + f_s = 1$$

f_s^* = Non-protonated aliphatic carbon plus methyl carbons.

Table III. Analytical Data for British Maceral Concentrates

Colliery	Woolley			Markham Main			Teversal			Aldwarke			North Celynen		
Seam	Wheatley Lime			Barnsley			Dunsil			Silkstone			Meadow Vein		
	V	E	I	V	E	I	V	E	I	V	E	I	V	E	I
H_2O, as anal., %	1.6	0.7	0.5	6.9	2.0	1.8	9.2	-	4.1	1.7	0.7	0.8	1.0	0.6	0.7
VM dmmf	36.1	57.8	9.0	40.1	73.7	18.1	35.1	-	21.5	33.2	66.5	15.4	24.4	22.2	19.4
C dmmf	86.6	87.9	93.7	82.2	82.6	91.6	81.5	-	87.7	86.9	87.2	92.1	89.9	90.6	91.3
H	5.6	6.9	2.9	5.5	7.4	3.6	5.1	-	3.9	5.4	7.4	3.7	5.0	4.9	4.6
N	1.8	1.1	0.4	1.9	1.1	0.4	2.0	-	1.1	1.8	1.2	0.7	1.6	1.4	1.2
S	1.1	1.1	0.2	1.1	1.6	(0.3)	0.6	-	0.4	0.73	0.6	0.4	0.68	(0.6)	(0.5)
O (diff.)	4.9	3.0	2.8	9.3	7.3	4.1	10.8	-	6.9	5.17	3.6	3.1	2.82	2.5	2.4
Rank	HVA	-	-	HVB	-	-	HVB	-	-	HVA	-	-	MVb	-	-
MM	1.4	2.8	4.9	1.4	0.9	6.0	0.4	-	2.9	0.8	0.3	5.0	2.9	4.5	8.87*
Vitrinite	96.0	10.0	4.0	98.0	3.0	6.0	98.0	-	6.0	98.0	0.0	4.0	86.0	40.0	15.0
Exinite	3.0	79.0	tr	tr	88.0	1.0	1.0	-	tr	1.0	95.0	-	3.0	30.0	11.0
Inertinite	1.0	11.0	96.0	2.0	9.0	92.0**	1.0	-	93.0*	1.0	5.0	96.0	11.0	30.0	71.0

* semifusinite

** equal amounts fusinite and semifusinite

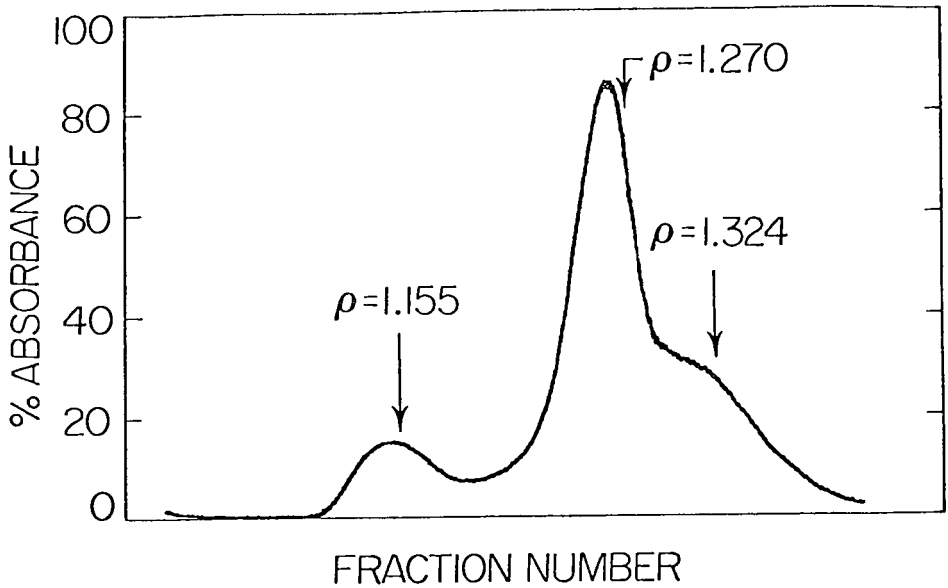

Figure 1. Fractogram for analytical DGC separation run on PSOC-2. The densities indicate the separation of the liptinite, vitrinite, and inertinite maceral groups.

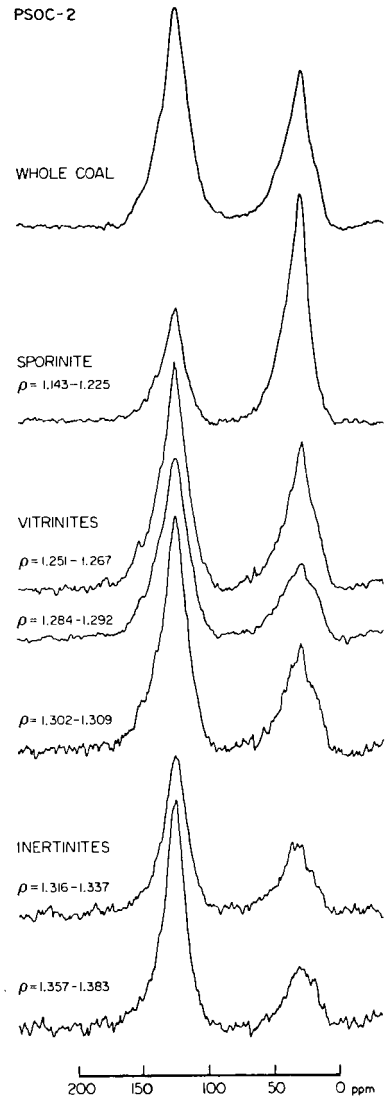

Figure 2. CP/MAS spectra of PSOC-2 whole coal and the maceral groups separated from the coal by density gradient centrifugation. The density ranges represent the range of densities for samples employed. f_a values are given for each sample.

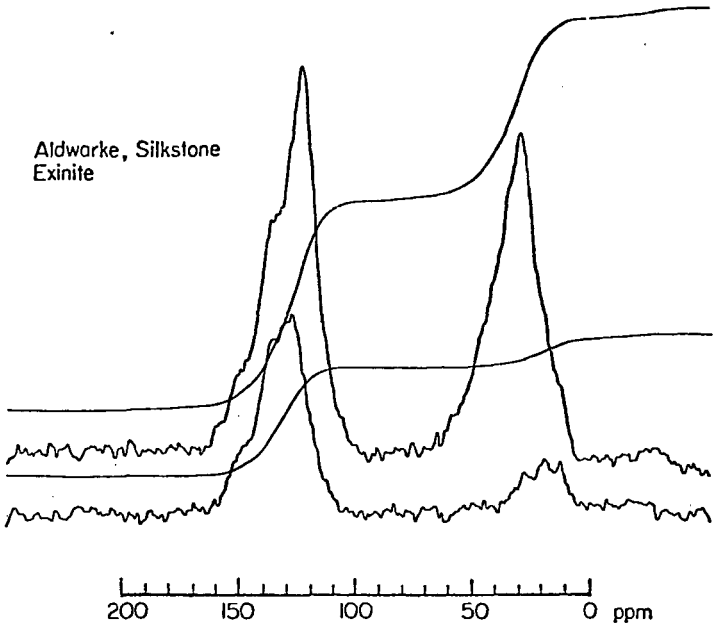

Figure 3. CP/MAS (top) and dipolar dephasing data with lower trace acquired following 40 μ sec. pulse delay. Note three separate peaks in the aliphatic region due to methyls and CH_2's.

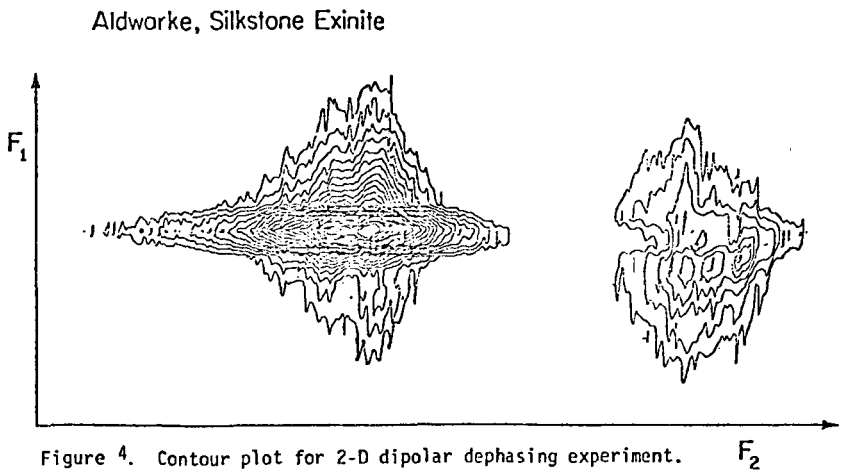

Figure 4. Contour plot for 2-D dipolar dephasing experiment.

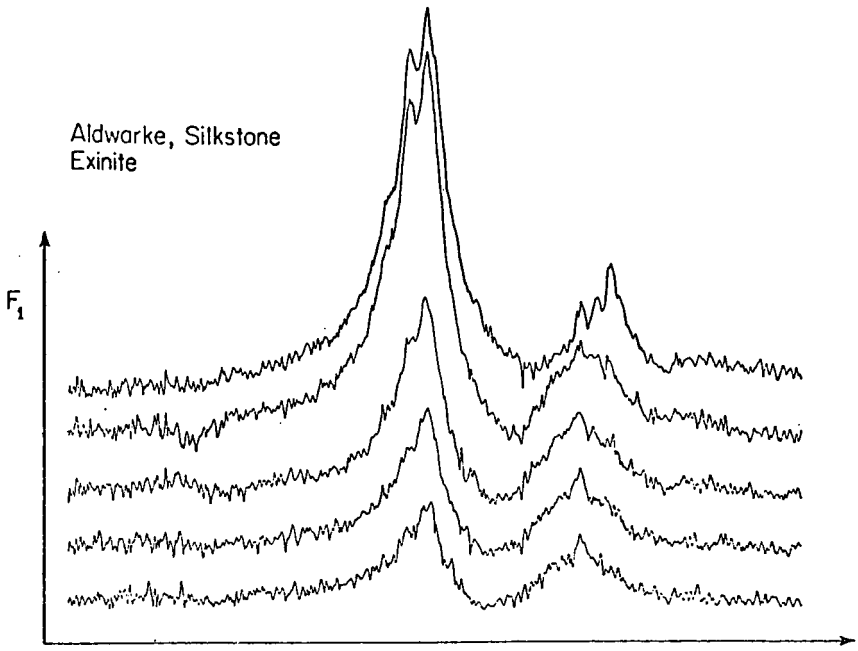

Figure 5. Spectral slices at 977 Hz intervals taken from Figure 3.

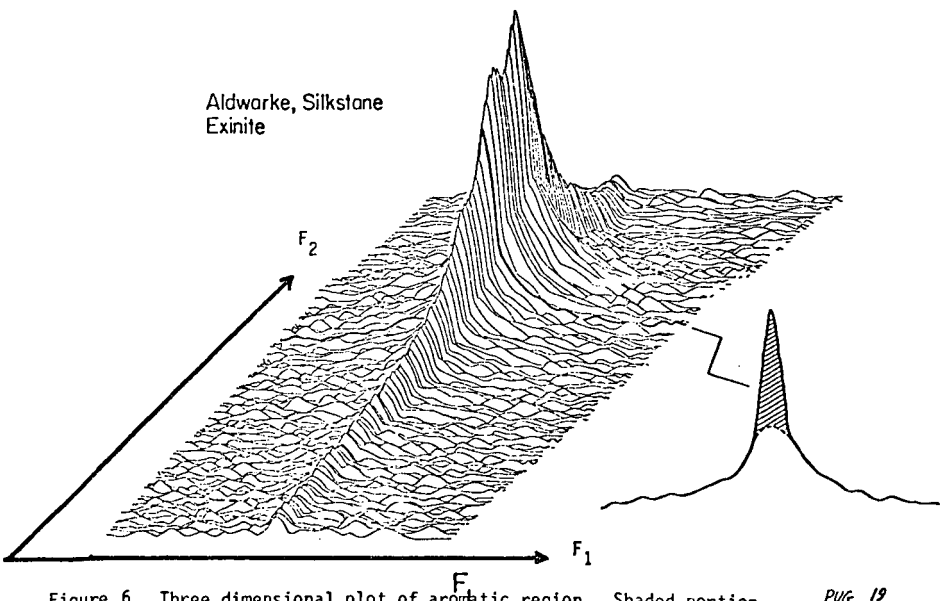

Figure 6. Three dimensional plot of aromatic region. Shaded portion is non-protonated carbon on top of resonance from protonated aromatic carbon.

PUG 19

ELECTRON SPIN RESONANCE OF ISOLATED COAL MACERALS: A PRELIMINARY SURVEY

B. G. Silbernagel and L. A. Gebhard
Corporate Research - Science Laboratories
Exxon Research and Engineering Company
Linden, New Jersey 07036

G. R. Dyrkacz
Chemistry Division - Argonne National Laboratory
Argonne, Illinois 60439

INTRODUCTION

While there have been a large number of electron spin resonance (ESR) studies of coal and coal products,[1] previous interpretations were based on the "average" properties of coals due to the chemical heterogeneity of the coal samples examined. The recent evolution of maceral separation techniques permits detailed ESR observations on coals of different rank, for which maceral type, and maceral density can be discriminated simultaneously. The present ESR survey of carbon radicals in separated macerals shows that each maceral type exhibits characteristic carbon radical properties. Furthermore, the properties of carbon radicals change within a given maceral type as the density varies.

EXPERIMENTAL PROCEDURES

A total of 37 samples from 16 coals of the Pennsylvania State University coal data base (PSOC) were examined. Separate fractions were obtained by isopycnic density gradient centrifugation of small (~3 μm) coal particles in a aqueous CsCl density gradient.[2] The individual samples are listed by PSOC numbers, maceral type, and density, in Table 1. After separation, the samples were kept under dry nitrogen until they were transferred to ESR tubes and sealed under helium gas. Typical ESR sample weights were approximately 10 mg. The ESR observations were conducted at 9.5 GHz in a Varian E-line ESR spectrometer with variable temperature capabilities from 90K-300K. The g-value, linewidth (defined as the splitting between peaks of the derivative curve of the ESR absorption - ΔH_{pp}) and the intensity of the carbon radical signal were observed in each case.

Before discussing the correlation of these properties, it is useful to note a significant difference in the response of carbon radicals in different maceral types to the applied microwave field. At sufficiently low microwave powers, the radical intensity varies linearly with microwave field strength, or equivalently varies as the square root of the microwave power. At higher powers, this response is less than linear, a phenomenon known as saturation, when the microwave power absorbed by the carbon radicals exceeds the radicals' ability to dissipate it to their environment. This process is illustrated in Figure 1, where the radical intensity, divided by the square root of the microwave power, is plotted as a function of the logarithm of the microwave power. The flat response at low power indicates the linear behavior; the fall-off at higher microwave

powers indicates the onset of saturation. It is clear from Figure 1 that vitrinite saturates at low powers, a fall-off being noted already at ~10μ Watts of microwave power. A similar departure from linear behavior does not occur in inertinite until powers of ~10^4 μW are applied. Exinite is intermediate in behavior. To avoid saturation-related problems, all samples were run at microwave powers of 3μW, indicated by the arrow and dashed-line in the figure.

EXPERIMENTAL RESULTS

Examination of the ESR linewidth and the maceral density show clear distinctions between different maceral types. Figure 2 shows that exinite macerals have low densities and a narrow range of ESR linewidths, ΔH_{pp}~6.5 G. While vitrinite and inertinite show considerable overlap in maceral densities, the inertinite linewidths are dramatically smaller, ~1-2 G, as opposed to ~5.5-7.5 G for the vitrinites. This significant linewidth difference may assist in the discrimination of maceral types. As Figure 2 indicates, two macerals which petrographic analyses indicated to be inertinite, fall into the vitrinite maceral field. Since the small particle size required for separation (~3μm) complicates the petrographic analysis, combined ESR and petrographic examinations may prove useful in future maceral type determinations. It is also interesting to note a weak trend in the vitrinite of decreasing ΔH_{pp} with increasing maceral density. Such a decrease might be anticipated if the increased maceral density resulted from a larger fraction of aromatic species, reducing proton broadening of the carbon radical linewidth .

The relationship between ESR intensity and maceral density is far less obvious, as Figure 3 indicates, Exinite samples have relatively low densities and radical intensities, as might be anticipated for aliphatic-rich macerals. Vitrinite and inertinites exhibit intensity variations in excess of an order-of-magnitude, and there is no clear variation of intensity with the physical density of the macerals. This suggests that a variety of factors, including the nature of the organic species and the details of the coalification process may serve as determinants of the number of carbon radicals.

A direct comparison of ESR linewidth and intensity, shown on Figure 4, shows a significant dependence on the type of coal sample being examined. In this case, open-circle symbols designate PSOC 106 samples, open-squares - PSOC 297, and open-triangles PSOC 1005. Solid-circles designate the balance of the vitrinite samples examined. No obvious clustering of vitrinite samples of a single type is observed. The fact that ΔH_{pp} is nearly independent of ESR intensity suggests that unresolved hyperfine interactions with adjacent protons, rather than dipole interactions between carbon radicals, are responsible for the observed linewidth.

The ESR linewidth variation with density for vitrinite macerals of different coals is presented in Figure 5. The open-symbols designate the three PSOC coals mentioned in Figure 4. As suggested in Figure 1, there is a general tendency for linewidth to decrease with increasing density. For PSOC 106 and 297, there is little density or linewidth variation observed for the vitrinites from each coal. Conversely, PSOC 1005 shows a broad range of density variations, and the linewidth increases. The source of this different behavior is still under investigation.

The isolated inertinite macerals provide an opportunity to examine their distinctly different properties. While strikingly narrower than the exinite and vitrinite ESR signals, the ESR absorption is still symmetric. The linewidth varies dramatically, from H_{pp} = 0.89 - 2.00 Gauss, and the linewidth is temperature independent. The intensity of the resonance absorption varies approximately as I/T, the Curie-like susceptibility expected for simple magnetic spins. Motion of these radical species could account for the relatively narrow linewidth.

CONCLUSION

We have successfully examined a suite of very small (∿10 mg) samples by ESR. Different maceral types have strikingly different saturation behavior and are readily distinguished in a H_{pp}/density analysis. Radical intensities vary widely and are not related to physical density. Surveys of vitrinites from three of the PSOC coals suggest that intensities are reasonably similar within a given coal, but can vary significantly from one coal to the next.

At present, we are correlating these results with microanalysis of elemental composition and solid state ^{13}C NMR estimates of carbon aromaticities. These studies will be reported elsewhere.

ACKNOWLEDGMENT

We wish to express our gratitude to M. L. Gorbaty for his encouragement of this research activity and helpful comments.

REFERENCES

1. H. L. Retcofsky, "Magnetic Resonance Studies of Coal" in Coal Science and Technology, Vol.I, M. L. Gorbaty, J. W. Larsen and I. Wender, eds. (New York, Academic Press, 1982), pp. 43-82.

2. G. R. Dyrkacz and E. P. Horwitz, Fuel 61, 3 (1982).

TABLE I: MACERAL RESUME

(Indicated numbers are the maceral densities in gm/cm^3)

PSOC #/Maceral Type	Vitrinite	Exinite	Inextinite
1	1.257	-	-
81	WHOLE COAL	-	-
106	1.291	1.191	1.413
	1.330	-	1.447
	1.334	-	1.475
	1.371		
151	1.385		
236	1.278		
240	1.407		
268	1.272		
285	1.276		
297	1.264	1.040	1.384
	1.271	1.149	1.436
	1.305	1.165	
	1.340	1.200	
		1.207	
317	1.317		
409	1.302		
592	1.306		
594	1.332		
852	1.314		
975	1.408		
1005	1.345		
	1.382		
	1.420		
	1.455		
	1.486		

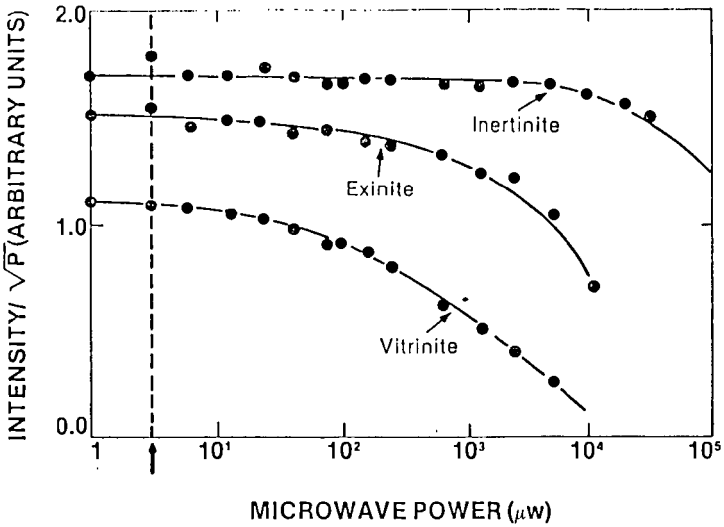

FIGURE 1: The various maceral types exhibit distinctly different microwave saturation properties.

FIGURE 2:

ESR linewidth, maceral density plots discriminate maceral types:

▲ = Exinite

● = Vitrinite

■ = Inertinite

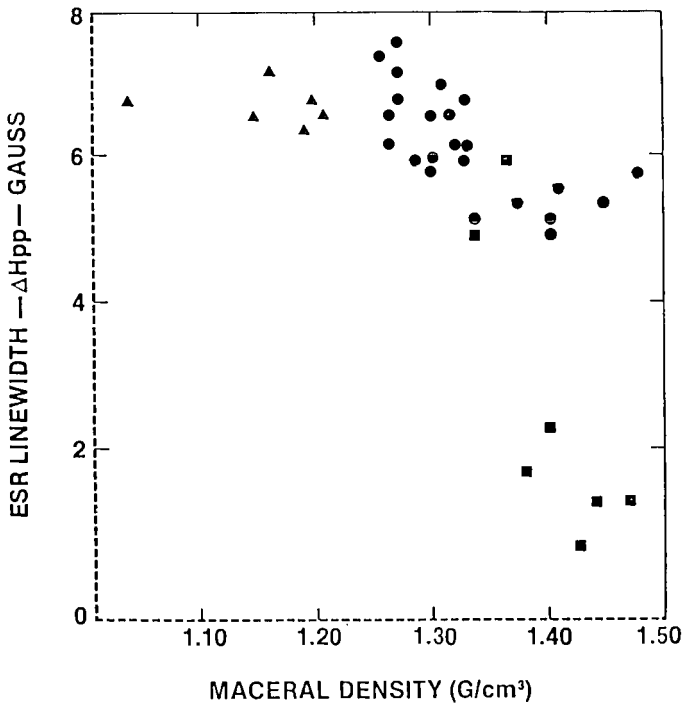

FIGURE 3: Carbon radical intensities do not depend explicitly on maceral type or maceral density.

▲ = Exinite

● = Vitrinite

■ = Inertinite

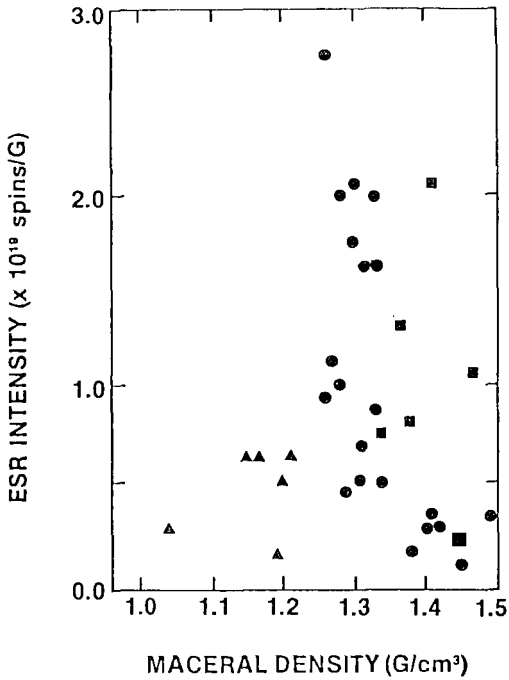

FIGURE 4: A weak variation of ESR linewidth on ESR radical intensity is observed.

○ = PSOC 106

□ = PSOC 297

△ = PSOC 1005

● = All other Vitrinites

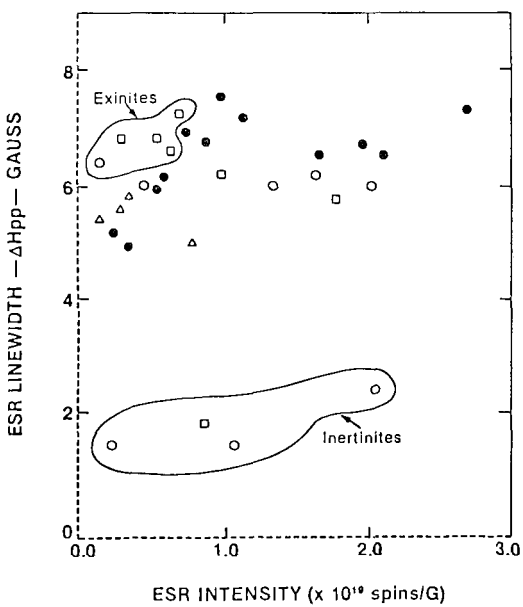

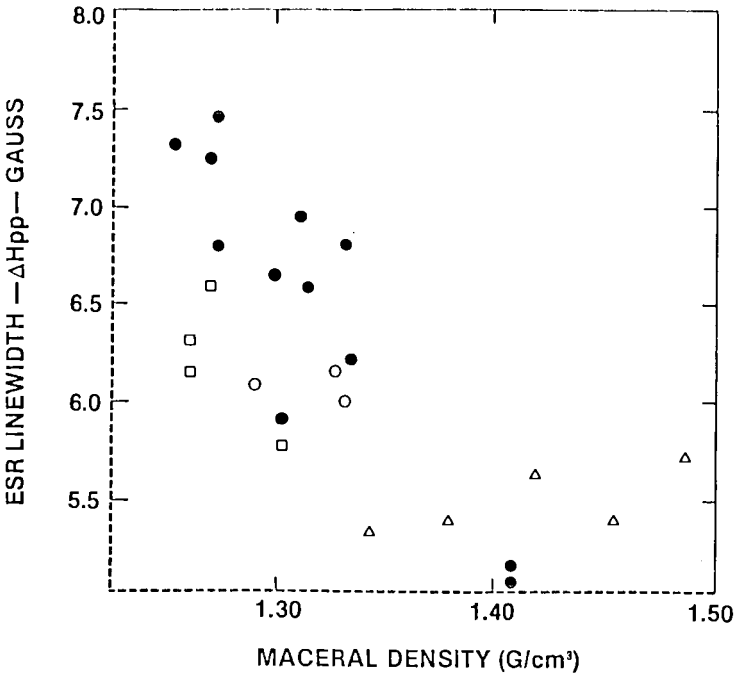

FIGURE 5: A weak decrease in ESR linewidth with maceral density is observed for vitrinite macerals. Little systematic change is observed for macerals from a given coal.

○ = PSOC 106

□ = PSOC 297

△ = PSOC 1005

● = All Other Vitrinites

PREMACERAL CONTENTS OF PEATS CORRELATED WITH "PROXIMATE AND ULTIMATE ANALYSES"

A. D. Cohen* and M. J. Andrejko

Department of Geology
University of South Carolina, Columbia, South Carolina 29208
*(presently at Los Alamos National Laboratory
Earth and Space Sciences Division, MS K586
Los Alamos, New Mexico 87545)

I. Introduction

In a number of publications, peat types have been defined petrographically by their botanical and "premaceral" compositions (1, 2, 3, 4). "Premacerals" are the organic components in the peats which, due to their color, opacity, shape, and fluorescence, can be projected as the probable progenitors of particular corresponding macerals in coals. Although the petrographic characterization of peats constitutes an important "first step" in understanding the origin and in predicting the general composition of the resultant coals, it is important that premaceral types and amounts in peats be correlated with various coal-quality tests (such as "proximate" and "ultimate" analyses). With these results it then becomes possible to develop a series of models with which to predict more precisely the chemical and physical composition of the resulting theoretical coals. These predictive characterizations can be applied not only to the projected seam-wide variability in coal quality for coals produced in similar depositional settings as that of the studied peats, but also to the prediction of the variations in industrial properties of the peats themselves, such as for gasification, liquifaction, soil conditioning, organic chemical production and so forth.

It is for these reasons that we have initiated this correlative study of peat petrography and peat industrial-chemical (coal quality) properties. Note that the information reported herein represents preliminary results based on a limited number of different types of peats that were analyzed for only a few "coal quality tests" (i.e., proximate analysis, ultimate analysis, and BTU content). Future studies will involve measurement of other petrographic parameters and include other industrial analyses (such as, gas and liquid yields, physical properties, organic chemical yields, and so forth).

II. Objectives

The objectives of this study are to:

A. Determine the variations in premaceral types and proportions within a wide variety of peat types.
B. Correlate premaceral contents with corresponding proximate (fixed carbon, moisture, ash, volatile matter), ultimate (C, H, O, N, S) and heating value (BTU) analyses.
C. Predict the probable variations in the proximate and ultimate makeup and BTU levels for coals which formed in similar vegetational and depositional settings to those of the peats studied in this project.

III. Methods

Carefully extracted samples of peat were slowly dehydrated in a series of alcohol solutions and then embedded in paraffin. After embedding, thin-sections (15 microns in thickness) were cut from these samples with a sliding microtome and mounted in Canada Balsam. Details of the procedure for the embedding and sectioning of peats have previously been described by Cohen.(2,3).

Premaceral identification was made in transmitted white light, in polarized light (birefringence) and fluorescent light. Premaceral proportions were determined by area point-counting at 200 X. Proximate and ultimate analyses and BTU were obtained from commercial testing laboratories and also from the Department of Energy's Energy Technology Center at Grand Forks, North Dakota.

IV. Results and Discussion

A. Botanical Composition

Figure 1a shows the relative abundances of plant groups observed in microtome sections of the peats. Note that these peats varied considerably in their botanical compositions. The Minnesota peat consisted predominantly of Sphagnum (peat moss) debris with some grasses and conifers. The Maine peat was composed mostly of algal material with some Sphagnum and Nymphaea (water lily) debris. The North Carolina peat was dominated by bay tree (Magnolia, Persea, Gordonia) and gum tree (Nyssa) debris; while the Georgia Nymphaea peat consisted predominantly of Nymphaea debris.

Figure 1b shows the abundance of plant organs comprising the peat. Again the differences between peat types are pronounced. The Minnesota peat is dominated by roots but with lesser but equal amounts of stem and leaf debris. On the other hand, the Maine peat has the highest concentration of leaves; the North Carolina peat has the highest wood content (stems) and lowest leaf content, while the Georgia (Nymphaea) peat has the highest proportion of roots.

B. Premaceral Types and Proportions

One simplified but useful means of displaying petrographic composition of peats in thin section is by graphing the area percentages of ingredients of different colors. Figure 2 shows such a point-count for four representative types of peat from this study. Note that the Minnesota Sphagnum and Georgia Nymphaea peats have approximately the same range of colors (peaking between light-yellow and light-brown) but that the Maine peat peaked in the clear to light-yellow range while that of the North Carolina peat had peaks in the light-yellow to red-brown range and also in the dark-brown and black categories.

The Georgia Nymphaea and Minnesota Sphagnum peats tended to have the highest previtrinites while the North Carolina and Georgia Taxodium peat (not shown) had the highest prephlobaphenites (and precorpocollinites) and also the highest preinertinites (premicrinites, prefusinites, and presclerotinites).

Figures 3 and 4 give the area percentages of birefringent premacerals found in the samples studied. Since birefringence has been equated with cellulose content, it might therefore be expected that birefringence would decrease with depth in a deposit as a result of cellulose decomposition. However, as can be seen in Figure 3 (representing two cores from the Okefenokee Swamp of Georgia), birefringence may increase or decrease with depth depending on successions of peat types and moisture conditions during initial deposition. Figure 4 shows that Georgia Nymphaea and Minnesota Sphagnum peats have the highest proportions of birefringent constituents.

The concentration of fluorescent premacerals tended to correlate slightly with the proportion of birefringent premacerals. However, different plant types were found to produce different fluorescent colors and intensities. Furthermore, natural "staining" (i.e., darkening or coloring by natural impregnation or chemical alteration) of cell walls tended to effect birefringence and fluorescence in very different ways. Natural staining tended to correlate strongly with birefringence (i.e., the darker the staining the less the birefringence), but did not correlate well with overall fluorescence properties. For example, some tissues that were highly stained tended to have higher fluorescence intensities than those that were unstained.

C. Proximate and Ultimate Analyses and BTU

Figure 5 shows the results of proximate and ultimate analyses and BTU measurement. Note that the peat from North Carolina (a lower-coastal-plain, woody, dark, more inertinite-rich sample) had the highest fixed carbon, elemental carbon and sulfur content. Woody Taxodium peats from Georgia (not shown) and South Carolina (not shown)

were similar in character to the North Carolina samples. The Georgia Nymphaea peats, which had the highest previtrinites, can be seen to have the highest oxygen, hydrogen, and volatile matter contents. Note that BTU values tended to correlate more strongly with ash contents than with maceral contents.

V. Summary and Conclusions

Preliminary correlations of petrographic characteristics of peats (i.e., peat types, premaceral proportions, and premaceral types) with proximate and ultimate analyses suggest the following trends:

A. Peats with the highest proportions of birefringent macerals tend to have the highest volatile matter (and H and O contents).
B. Fluorescence of macerals, on the other hand, seems to correlate only slightly with proximate and ultimate analyses.
C. Higher previtrinite contents tend to correlate with higher volatile matter contents.
D. Peats with higher preinertinites, prephlobaphenites (and pre-corpocollinites), and presclerotinites have the highest fixed carbon.
E. BTU correlates strongly with ash content and only slightly with maceral content.

VI. Acknowledgments

This work was funded in part by Grant #EAR-79-26382 from the National Science Foundation and in part by funding from the Office of Basic Energy Sciences of the Department of Energy.

References

1. Cohen, A. D. (1968). The Petrology of Some Peats of Southern Florida (with Special Reference to the Origin of Coal), Ph.D. Thesis: Penn. State Univ., 352 p.
2. Cohen, A. D., and Spackman, W. (1972). Methods in Peat Petrology and Their Application to Reconstruction of paleoenvironments: Geol. Soc. Amer. Bull,, v. 83, 129-142.
3. Cohen, A. D. (in press). Obtaining More Precise Descriptions of Peats by Use of Oriented Microtome Sections, In Proceedings of ASTM Symposium for Testing of Peats and Organic Soils. Toronto, Canada. ASTM, Philadelphia, PA.
4. Corvinus, D. A., and Cohen, A. D. (in press). Petrographic Characteristics of Carbonaceous Sediments from the Snuggedy Swamp of South Carolina. Compt. Rendu. IX Inter. Carb. Cong.

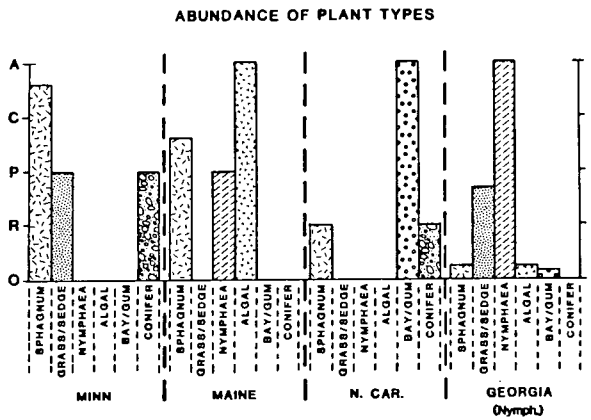

FIGURE 1a

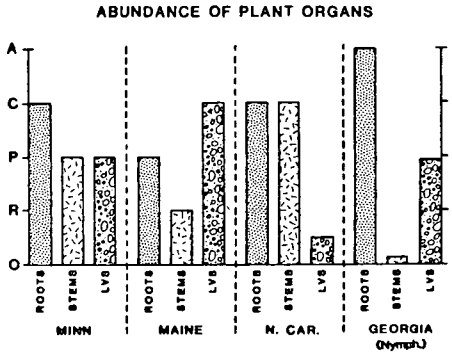

FIGURE 1b

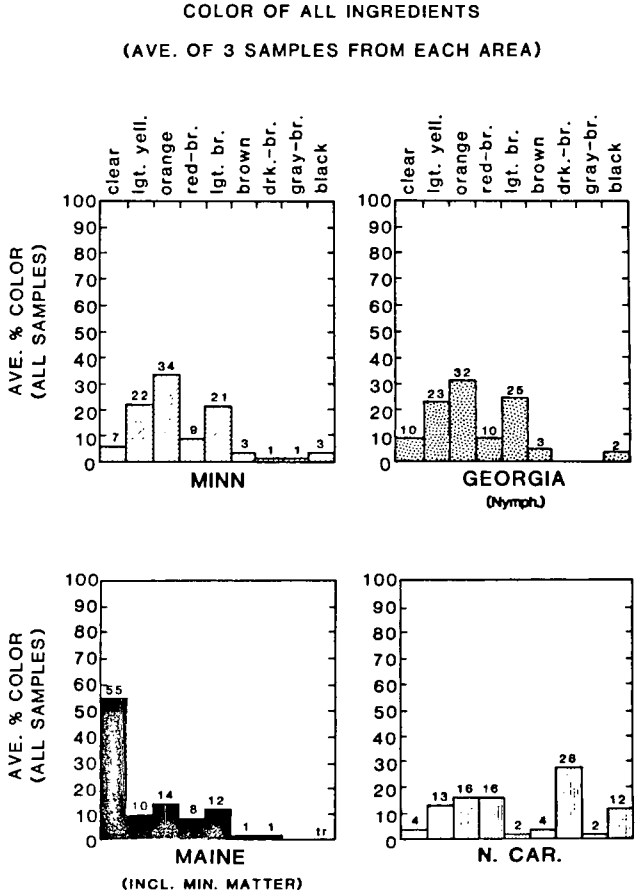

FIGURE 2

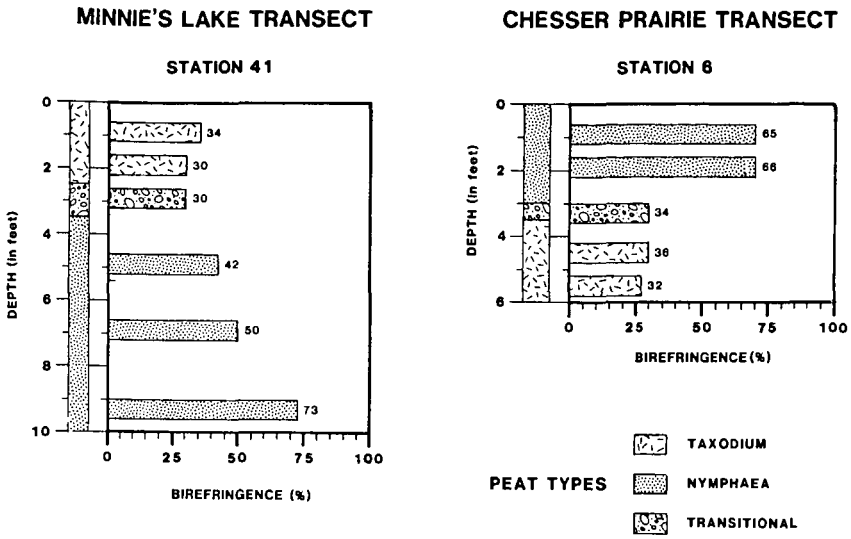

FIGURE 3

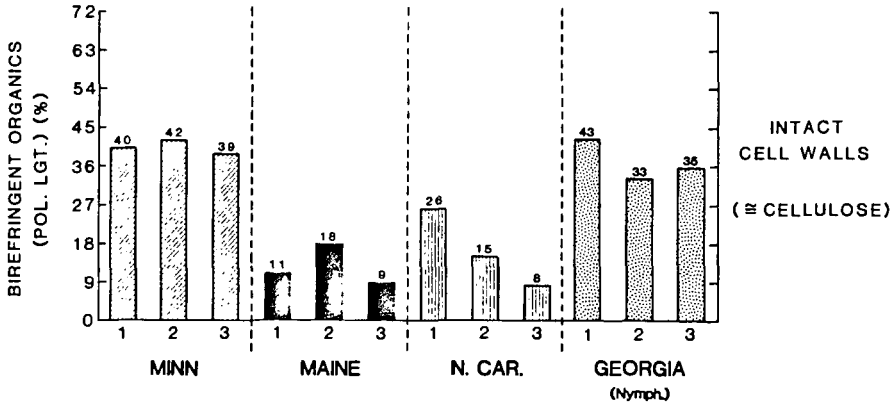

FIGURE 4

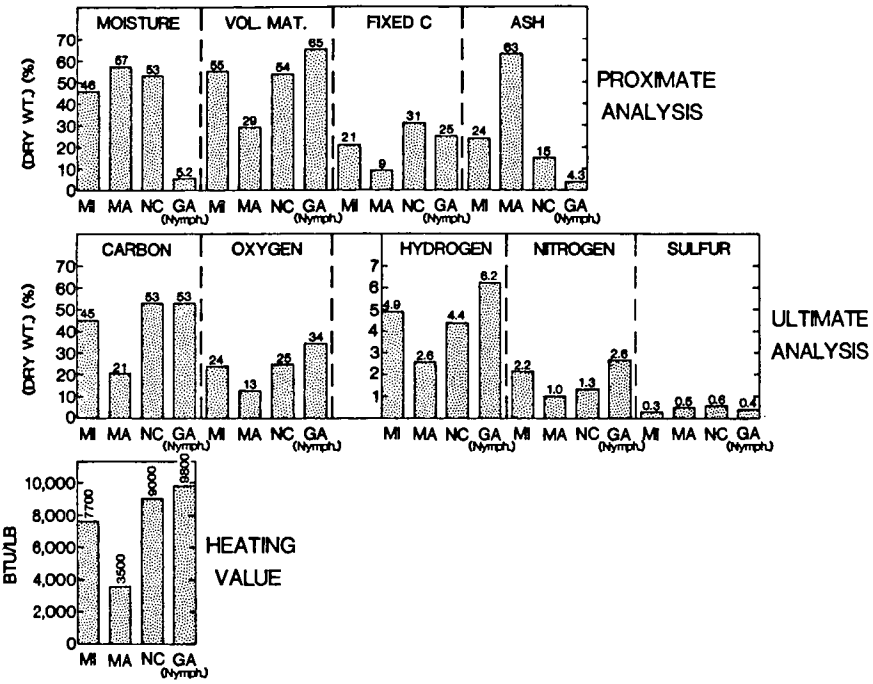
MOISTURE
VOL. MAT.
FIXED C
ASH
(DRY WT.) (%)
46
57
53
5.2
55
29
54
65
21
9
31
25
24
63
15
4.3
PROXIMATE ANALYSIS
MI MA NC GA (Nymph)
CARBON
OXYGEN
HYDROGEN
NITROGEN
SULFUR
45
21
53
53
24
13
25
34
4.9
2.6
4.4
6.2
2.2
1.0
1.3
2.6
0.3
0.5
0.6
0.4
ULTIMATE ANALYSIS
BTU/LB
7700
3500
9000
9800
HEATING VALUE

FIGURE 5

Reactivity and Characterization of Coal Macerals

Randall E. Winans, Ryoichi Hayatsu, Robert G. Scott, and Robert L. McBeth

Chemistry Division
Argonne National Laboratory
Argonne, IL 60439

In a study of the organic structures in coals and their reactivity in chemical and thermal processes, it is desirable to reduce the complexity of the material with some sort of physical separation. One such approach is the separation of the coals into their maceral groups, which are the microscopically identifiable organic portions of coal which have different origins, chemical and physical features, and reactivity. Two bituminous coals have been separated into their three main maceral groups: exinite, vitrinite, and inertinite, using a modified float-sink technique which uses analytical density gradient centrifugation (DGC) to determine the appropriate density ranges. The DGC technique which exploits the differences in densities has just recently been reported (1,2).

The chemistry of macerals separated by DGC, float-sink and hand picking has been investigated recently by several techniques including: solid ^{13}C nmr (3,4), oxidation (5,6), and mass spectrometry (5,6,7,8). Early work focused on chemical properties (9) and esr spectroscopy (10). In the approach taken in this study the maceral concentrates were pyrolyzed in a vacuum and the resulting products collected and then characterized by gas chromatography mass spectrometry and by GC microwave plasma emission spectroscopy. The vacuum technique was chosen over the typical on-line pyrolysis-GCMS method for two reasons. First, experiments in this laboratory have shown that with the vacuum technique, secondary reactions such as aromatization of alicyclics is less likely to occur. Second, better quantitative data can be obtained with a batch type reaction scheme.

In addition to characterization of thermal products, the chemical reactivity of these concentrates has been studied. Reactive hydrogens such as benzylic types have been determined from the reaction of the macerals with pyridine and iodine to form pyridinium iodides:

$$\text{Coal-ArCH}_2^- \xrightarrow[I_2]{\text{pyridine}} \text{Coal-ArCH}\underset{\underset{Py^+I^-}{|}}{-} + \text{HI} \qquad 1)$$

It has been shown that the number of pyridinium iodides per 100 carbon atoms in the original coal decreases with increasing rank (11). Further studies have shown that these derivatized coals are activated toward oxidative solubilization using a reagent, alkaline silver oxide, which normally is quite ineffective in dissolving raw coals. In the results from the thermal and chemical reactions, similarities and differences have been noted which will be discussed later. Also, it should be emphasized that in this study we are examining maceral concentrates from the three main groups which are derived from the same coal. These coals were chosen to be representative of bituminous coals and not to be sapropelic coals where the chemistry may be more unusual due to the typically large exinite content.

EXPERIMENTAL

Two of the coals used in this study were obtained from the Penn State Coal Sample Bank. They were an HVA bituminous coal (PSOC 1103) from the Upper Elkhorn #3 seam in Eastern Kentucky and an HVA bituminous coal (PSOC 828) from the Brazil Block seam in Indiana. A third coal from which vitrinite and fusinite were hand picked was an Illinois No. 2 seam HVC bituminous coal from Northern Illinois. All

of the elemental analyses, petrographic analyses, and yields of the samples are presented in Table 1. The details of the sink-float technique have been reported previously (1). Typically, 3 micron particle size demineralized coal is centrifuged in aqueous $CsCl_2$ solution of the appropriate density with a small amount of surfactant added to disperse the coal particles. The exinites in the float are collected and the sink fraction is further separated into vitrinite and inertinite fractions by repeating the procedure at a higher density. The process yielded gram quantities of concentrates. The density cutoff points were determined from analytical DGC of coals of similar origin and rank. The technique used for petrographic analysis has also been reported earlier (2).

In the pyrolysis experiment, typically 30 mg of sample was heated in a quartz tube at 400°C for 24 hrs at $2x10^{-3}$ torr. Tars were trapped at room temperature and the more volatile products at liquid nitrogen temperature. These two fractions were analyzed by GCMPES (MPD-850) using a 25m x 0.25 mm i.d. OV-101 fused silica column and by GCMS (Kratos MS25) using a 30m x 0.25 mm i.d. DB-5 column.

The pyridinium iodide coals were prepared by refluxing 1 g of coal or maceral concentrate in 60 ml of pyridine with 4 g of iodine for 70 hrs. The reaction mixture was poured into 10% aqueous $NaHSO_3$ and the solution filtered. The derivatized coal was washed free of pyridine, dried, and analyzed. Portions of the activated coal were oxidized with freshly prepared silver oxide in refluxing aqueous NaOH. The oxidation products, which were soluble in alkaline solution, were acidified and then extracted with a series of organic solvents. The major products were only soluble in alkaline solution or polar solvents.

RESULTS AND DISCUSSION

Of particular interest in this study is the nature of the non-aromatic structures in the three main maceral groups. It should be noted that the exinites in both these coals are 90% sporinite. It has been theorized that small molecules, especially the aliphatics, are fairly mobile at some period during the formation of coal (5,6). The studies which support this theory were done on coals that were very rich in exinites and some contained alginite. The two coals chosen in the present work have a more normal distribution of macerals and yet the pyrolysis results indicate that migration of molecules from the exinites to vitrinite and then incorporation into the macromolecular structure might have occurred.

Chromatograms from the GCMPES carbon channel of the tars from two exinites and a vitrinite are shown in Figure 1. Long chain normal alkenes and alkanes dominate the compounds in the tar along with a series of triterpenes which are slightly altered hopanes. A general structure for hopane is shown in the upper right of the figure. Several points should be made concerning these results. First, we believe that these compounds were derived from the macromolecular structures in these macerals. During the preparation of the concentrates most of the soluble molecules are removed. Evidence for this is found from examination of the extracts of the whole, untreated coals. One of the major compounds isolated is the biomarker pristane which has been identified many times previously in extracts (11) and coal liquids (12). However, this compound is absent from the pyrolysis products, although it is stable under the conditions used. At least a portion of the macromolecular structures in the exinite and vitrinite could be similar. As one would expect, the yields of these aliphatic and alicyclic compounds are less in the vitrinites. The yields follow inversely the fraction of aromatic carbons (4) in these three maceral groups. The exinite concentrate for the Kentucky coal is quite impure (50% vitrinite) which is reflected in the pyrolysis yields.

Another similarity between vitrinite and the exinite is the existence of 5 member ring triterpenes in the pyrolysates. These compounds, which show the base peak at m/z = 191 in their mass spectra, have been found in pyrolysis MS of alginite

(5), coal extracts (6,13), and oil shales (14) and are usually associated with some type of algal origins. It is surprising that they were found in these coals and probably more importantly, that they were not aromatized. From the GCMS it appears that only one of these peaks may represent a species containing one aromatized ring. Again these results suggest that there could have been a significant amount of molecular mobility during the early stages of the formation of this coal.

There is a much larger variation between pyrolysis product volatile fractions for the exinites and vitrinites. The sporinite yielded mostly normal alkanes and alkenes up to approximately C19 with C16 being the most abundant product. The very low molecular weight hydrocarbons such as methane and ethane were not analyzed. Also, benzene and phenol derivatives were found as minor products. The vitrinite products were dominated by aromatics such as alkylbenzenes, alkylnaphthalenes, phenols, and naphthols. The smaller alkane/alkenes were also found. These results are more consistent with what was found in pyrolysis MS of sporinites and vitrinites (5,7).

Pyrolysis results for the inertinite concentrates are fairly inconclusive due to the high concentration of vitrinite except for the Ill #2 fusinite which was quite unreactive. Pyrolysis MS of this fusinite shows mostly alkylated naphthalenes and phenanthrenes. What may be interesting is the Kentucky inertinite fraction which is thought to contain ∿50% pseudo-vitrinite. This maceral which is usually categorized with vitrinites was placed in the inertinite column due to its low reactivity both in pyrolysis and in the pyridine-iodine reaction.

In the formation of the pyridinium salts the vitrinites were the most reactive and gave similar results to those found for a series of vitrinite rich coals of various ranks. If the sporinites had a highly cross linked aliphatic structure similar to that found in Type I or Type II oil shale kerogens one would expect these exinites to be unreactive. However, they have been found to be only slightly less reactive than vitrinite. Apparently, the yields in this reaction cannot explain the difference in reactivity between sporinites and vitrinites in pyrolysis and SCT liquefaction (15), but do reflect the lower reactivity of inertinites.

A tentative conclusion is that sporinites and vitrinites of the same rank have very similar structures but vary in the mix of aliphatics and aromatics while the structures in inertinites are very different.

ACKNOWLEDGEMENTS

This work was performed under the auspices of the Office of Basic Energy Sciences, Division of Chemical Sciences, U.S. DOE under contract W-31-109-ENG-38. The authors thank K.L. Stock for the maceral separations, G.R. Dyrkacz for the petrographic analysis and helpful discussion, and W. Spackman, Penn. State University for choosing and providing the coal samples.

REFERENCES

1. G.R. Dyrkacz, C.A.A. Bloomquist, and E.P. Horwitz, Sep. Sci. Technol. 16, 1571 (1981).

2. G.R. Dyrkacz and E.P. Horwitz, Fuel 61, 3 (1982).

3. K.W. Zilm, R.J. Pugmire, S.R. Larter, J. Allan, and D.M. Grant, Fuel, 60 717 (1981).

4. R.J. Pugmire, K.W. Zilm, W.R. Woolfenden, D.M. Grant, G.R. Dyrkacz, C.A.A. Bloomquist, and E.P. Horwitz, J. Org. Geochem. (in press).

5. R.E. Winans, G.R. Dyrkacz, R.L. McBeth, R.G. Scott, and R. Hayatsu, Proceedings Inter. Conf. Coal Sci., Dusseldorf, Verlag Gluckauf, Essen, p. 22 (1981).

6. J. Allan and S.R. Larter, Proceedings of 10th International Meeting on Organic Geochemistry, Bergen, Norway (1982) (in press).

7. G. van Graas, J.W. de Leeuw and P.A. Schenck, Adv. in Org. Geochemistry 1979, A.G. Douglas and J.R. Maxwell, Eds., Pergamon Press, Oxford, p. 485 (1980).

8. H.L.C. Meuzelaar, A.M. Harper, and R.J. Pugmire (this volume).

9. P.H. Given, M.E. Peaver, and W.F. Wyss, Fuel 39 323 (1960); Fuel 44, 425 (1966).

10. A.G. Sharkey and J.T. McCartney, in "Chemistry of Coal Utilization," M.A. Elliot, Ed., Wiley-Interscience, NY p. 241 (1981).

11. R. Hayatsu, R.E. Winans, R.G. Scott, L.P. Moore, and M.H. Studier, Fuel 57 541 (1978).

12. C.M. White, J.L. Schultz, and A.G. Sharkey, Nature 268, 620 (1977).

13. D.W. Jones, H. Pakdel, and K.D. Bartle, Fuel 61, 44 (1982).

14. B.P. Tissot and D.H. Welte, "Petroleum Formation and Occurrence," Springer-Verlag, N.Y. (1978).

15. H.H. King, G.R. Dyrkacz, and R.E. Winans (submitted to Fuel).

TABLE I. Sample Characterization and Reaction Yields

Sample	Elemental Analysis (DMMF %) C	H	N	S	O[1]	Ash	Maceral Composition % Exinite	% Vitrinite	% Inertinite	Vacuum Pyrolysis Yields Volatiles	Tar	Char	Pyridine/I_2 Yields Wt % Increase	Py^+I^-/ 100 C	Ag_2O Oxidation Solubles (Wt%)
Indiana (PSOC 828) Brazil Block															
Whole	74.3	5.9	1.5	1.0	17.3	<1.0	15.1	61.8	23.1	29.6	8.4	62.0	23.4	3.1	48.4
Exinite[2]	78.6	7.5	1.1	1.6	11.2	<1.0	91.0	9.0	~0	23.3	48.4	28.3	19.4	2.6	59.0
Vitrinite	76.4	5.6	1.5	0.9	15.6	<1.0	4.0	89.8	6.2	16.3	16.9	67.8	24.8	3.3	60.3
Inertinite	77.1	5.0	1.3	0.7	15.9	<1.0	0.0	62.5	32.5	16.9	13.4	69.7	19.4	2.6	45.5
Kentucky Upper Elkhorn #3 (PSOC 1103)															
Whole	72.0	5.6	1.4	2.3	18.7	<1.0	7.4	74.2	18.4	12.2	24.5	63.3	28.6	3.8	50.3
Exinite[2]	80.9	6.4	1.5	1.1	10.1	<1.0	45.5	49.6	4.9	14.8	35.2	50.0	25.8	3.4	41.5
Vitrinite	80.4	5.6	1.8	1.0	11.2	<1.0	2.5	92.5	5.0	20.2	22.7	57.1	28.8	3.9	62.5
Inertinite	70.9	3.8	1.2	8.8	15.3	?	1.5	16.2	82.3[3]	8.3	5.9	85.9	14.1	1.8	45.8
Illinois No. 2															
Whole	73.1	5.3	1.3	2.2	18.1			88.6					37.5	5.0	
Vitrinite	73.9	5.3	1.1	1.6	18.1	<1.0		>95		18.3	5.4	76.3			
Inertinite[4]	79.3	3.2	.5	4.0	13.0	4			>90	10.7	1.8	87.5			

[1]By difference; [2]Mostly sporinite; [3]Contains 49.8% pseudo-vitrinite; [4]Mostly fusinite, hand picked; pyrolysed at 500°C.

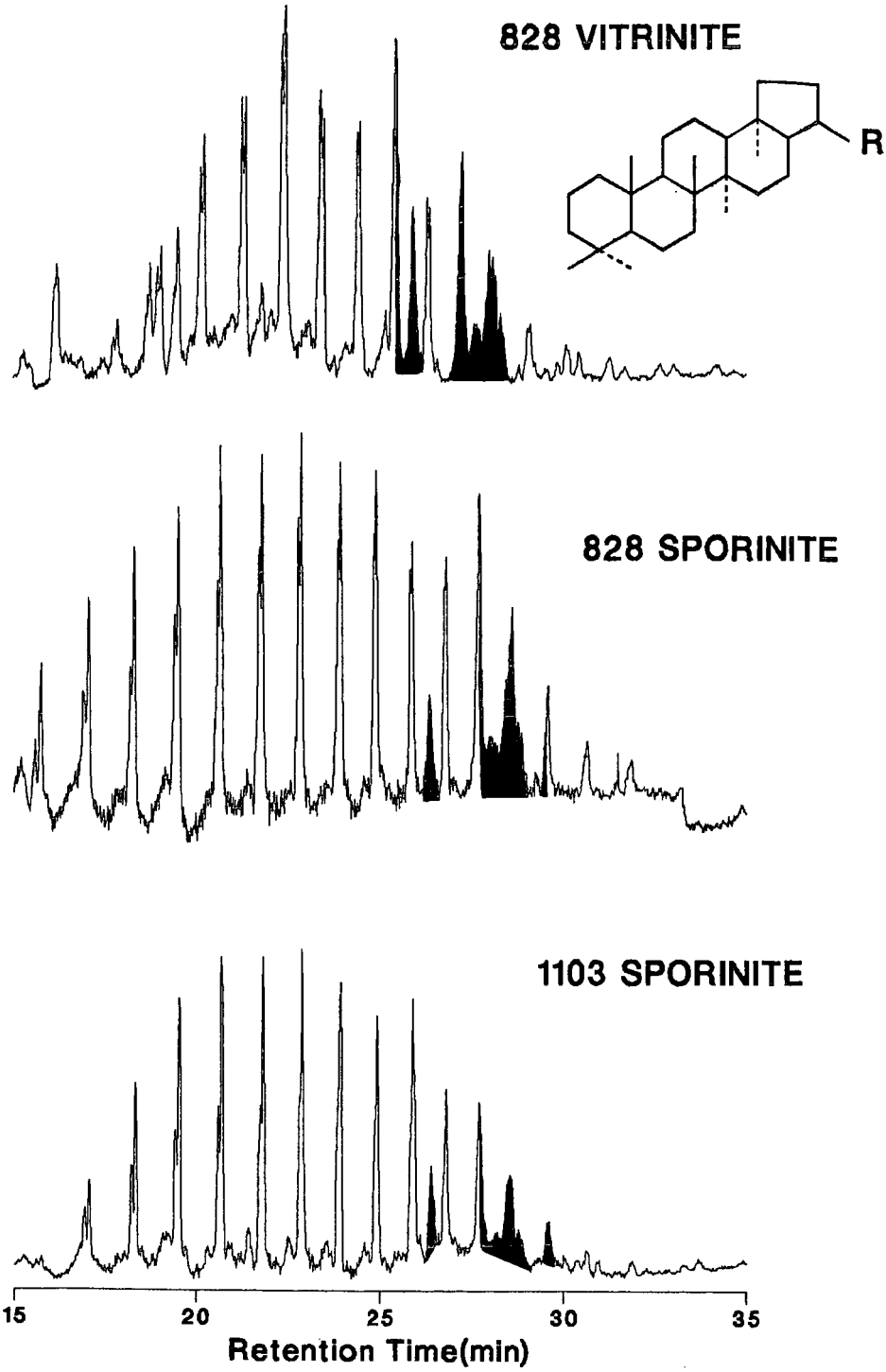

Figure 1. Partial gas chromatograms of vacuum pyrolysis tars. The shaded peaks are compounds derived from triterpenes.

THE INFLUENCES OF MACERALS ON THE HYDROGEN-DEUTERIUM EXCHANGE REACTION BETWEEN TETRALIN AND DIPHENYLMETHANE

Chol-yoo Choi and Leon M. Stock

Department of Chemistry
University of Chicago
Chicago, Illinois 60637

INTRODUCTION

The concept that free radical reactions predominate during coal dissolution reactions is quite widely accepted (1). Recent findings concerning the selective and reversible abstraction reactions of hydrogen atoms from tetralin by radicals formed during the thermal decomposition of Illinois No. 6 coal at 400°C support this interpretation (2). The fact that weak organic acids and bases have only a modest influence on the rates of the exchange reactions of aromatic, aliphatic, and benzylic hydrogen atoms under these conditions whereas compounds such as benzyl phenyl ether, benzyl phenyl sulfide, thiophenol, the BDPA radical, anthraquinone, anthrone, tetracene, and acridine actively promote the benzylic exchange reactions are also in accord with the view that radical processes dictate the outcome of coal dissolution (2). Indeed, benzyl phenyl sulfide and thiophenol significantly enhance the rate of dissolution of Illinois No. 6 coal (3). The interactions between coals and donor molecules such as tetralin have been examined in several laboratories to improve the understanding of these reactions (2,4-6). However, no information concerning the reactivity of coal macerals in such situations has been available. Accordingly, we have compared the influences of maceral concentrates of some selected coals on the exchange reactions between tetralin-d_{12} and diphenylmethane.

EXPERIMENTAL PART

The macerals used in this study were obtained from G. R. Dyrkacz and R. E. Winans of the Argonne National Laboratory. Some of the samples were prepared by density gradient centrifugation and others were prepared by float-sink techniques. The coal particles in all these samples were milled to three micron diameter and the separations were conducted in the presence of a surface active agent, polyoxyethylene (23) lauryl ether, in cesium chloride solutions (7).

The exchange reactions were conducted using a degassed solution of diphenylmethane (0.376 mmole) and tetralin-d_{12} (0.376 mmole) and the maceral material (25 mg) in a sealed glass vessel under an argon atmosphere at 400°C. The reactions were carried out for different times depending upon the reactivity of the maceral.

The products were isolated and analyzed using high field nmr spectroscopy as previously described (2). However, the macerals incorporate deuterium during the reactions and the change in the deuterium content of tetralin-d_{12} is emphasized in this report rather than the degree of incorporation of this isotope into diphenylmethane. Control experiments indicated that neither polyoxyethylene (23) lauryl ether nor cesium chloride altered the rate of the exchange reactions between tetralin-d_{12} and diphenylmethane.

The compositions of the macerals were determined by G. R. Dyrkacz. As already reported (7), the PSOC 106 maceral concentrates were greater than 90% pure. For PSOC-828, separation I, it was found that the exinite concentrate contained 91% exinite and 9% vitrinite; the vitrinite concentrate contained 4% exinite, 90% vitrinite and 6% inertinite; the inertinite concentrate contained 62.5% vitrinite and 32.5% inertinite. For PSOC-1103, separation II, it was found that the exinite concentrate contained 46% exinite, 50% vitrinite, and 5% inertinite; the vitrinite concentrate contained 3% exinite, 93% vitrinite and 5% inertinite; the inertinite concentrate contained 2% exinite, 16% vitrinite, 33% inertinite, and 50% other material--either semifusinite or pseudovitrinite. The data provided by the sample bank strongly suggest that this material is semifusinite.

RESULTS AND DISCUSSION

The exchange reactions of the macerals isolated from two hvB bituminous coals, PSOC-106 and PSOC-828, are presented in Tables 1 and 2, respectively.

Table 1. The influence of the macerals from PSOC-106 on the deuterium-hydrogen exchange reaction of tetralin-d_{12} and diphenylmethane at 400°C [a]

Maceral (mg)	Deuterium Content of Tetralin (%)		
	Aromatic Positions	Benzylic Positions	Aliphatic Positions
None	95.1	92.3	92.3
Exinite (25.3)	94.7	79.6	89.1
Exinite (24.9)	95.6	83.8	90.1
Vitrinite (25.6)	95.4	84.9	89.9
Vitrinite (25.4)	95.3	84.2	89.7
Inertinite (25.1)	95.1	86.7	89.3
Inertinite (25.2)	94.7	86.9	88.6

[a]Diphenylmethane (0.376 mmole) and tetralin-d_{12} (0.376 mmole) were reacted for 60 minutes in the presence of these macerals. The tetralin-d_{12} used in these experiments contained 96.1, 96.8 and 93.7% deuterium at the aromatic, benzylic, and aliphatic positions.

Table 2. The influence of macerals from PSOC-828 on the deuterium-hydrogen exchange reaction of tetralin-d_{12} and diphenylmethane at 400°C [a]

Maceral (mg)	Deuterium Content of Tetralin (%)		
	Aromatic Positions	Benzylic Positions	Aliphatic Positions
Experimental Series A			
None	94.7	91.3	93.0
Demineralized coal (25.6)	94.1	82.5	90.8
Exinite (25.4)	94.3	75.9	90.6
Vitrinite (25.4)	94.1	80.0	90.9
Inertinite (25.8)	94.7	82.4	90.3
Experimental Series B			
None	95.7	92.2	92.7
Raw whole coal	95.0	75.8	89.2
Demineralized coal	95.0	80.2	89.6
Exinite	94.9	80.0	89.1
Vitrinite	95.5	81.1	88.8
Inertinite	94.9	81.5	87.5

[a]Diphenylmethane (0.376 mmole) and tetralin-d_{12} (0.376 mmole) were reacted for for 60 minutes in the presence of these macerals. The tetralin-d_{12} used in these experiments contained 96.1, 96.8 and 93.7% deuterium at the aromatic, benzylic, and aliphatic positions.

The exchange reactions of the macerals isolated from different coals are presented in Table 3.

Table 3. The influences of macerals isolated from different coals on the deuterium-hydrogen exchange reaction of tetralin-d_{12} and diphenylmethane at 400°C [a]

Source of Maceral (mg)	Deuterium Content of Tetralin (%)		
	Aromatic Positions	Benzylic Positions	Aliphatic Positions
Experimental Series C, Vitrinites			
None	94.7	91.7	92.4
PSOC-828, separation I, (25.3)	94.3	81.5	89.1
PSOC-828, separation II (25.3)	93.9	76.3	87.8
PSOC-1103, separation I (25.1)	93.9	79.2	87.4
PSOC-1103, separation II (25.4)	93.5	77.9	88.1
Illinois No. 2, undemineralized (25.2)	94.1	78.7	90.2
Illinois No. 2, demineralized (25.2)	94.0	78.0	89.5
Experimental Series D, Exinites			
PSOC-828, separation I (25.1)	94.7	78.0	89.2
PSOC-828, separation II (25.1)	93.9	78.4	88.6
PSOC-1103, separation II (25.0)	94.1	77.9	87.4
Experimental Series E, Inertinites			
PSOC-828, separation I (25.4)	94.9	81.7	89.7
PSOC-828, separation II (25.4)	94.5	80.8	88.9
PSOC-1103, separation II (25.2)	94.3	76.5	89.4

[a]Diphenylmethane (0.376 mmole) and tetralin-d_{12} (0.376 mmole) were reacted for 60 minutes in the presence of these macerals. The tetralin-d_{12} used in these experiments contained 96.1, 96.8 and 93.7% deuterium at the aromatic, benzylic, and aliphatic positions.

Collins and his coworkers reported that Illinois No. 6 coal reduced benzophenone to diphenylmethane (8,9). We have used this reaction to assay the reactivities of the macerals. The results are summarized in Table 4.

Table 4. The effectiveness of macerals isolated from different coals for the reduction of benzophenone at 400°C for 60 minutes [a]

Reducing Agent (mg)	Reduction (%)
Experimental Series F, PSOC-828, Separation I	
Tetralin (51)	1.0
Demineralized whole coal (5.2)	2.0
Exinite (5.2)	3.6
Vitrinite (5.1)	2.1
Inertinite (5.1)	1.9
Experimental Series G, PSOC-1103, Separation II	
Tetralin (51)	1.2
Demineralized whole coal (5.8)	3.9
Exinite (5.7)	3.5
Vitrinite (5.6)	3.2
Inertinite (5.8)	1.5

[a]The reaction solutions in glass vessels were degassed prior to the introduction of argon and sealing.

The highly purified macerals obtained from PSOC-106 selectively enhance the rate of the exchange reaction at the benzylic position of tetralin-d_{12}. The order of reactivity, exinites > vitrinites > inertinites, is clearly established for the macerals of this coal. The macerals also enhance the exchange reactions at the aliphatic positions of tetralin, but to a lesser degree. No significant exchange occurs at the aromatic positions of tetralin or diphenylmethane under the conditions of these experiments. It is notable that the ratio of benzylic to aliphatic exchange decreases as the degree of benzylic exchange decreases. The finding is combatible with the view that the radicals produced from the macerals of lesser reactivity, the inertinites in this instance, are less selective.

The observations for the exchange reactions of the somewhat less pure macerals obtained from PSOC-828 and PSOC-1103 have some features in common with the results for the pure macerals of PSOC-106. In all cases, the reaction occurs selectively at the benzylic positions. In addition, the same reactivity sequence, exinite > vitrinite >inertinite, is also observed for PSOC-828. However, the differences in reactivity are somewhat less sharply defined, possibly because the inertinite concentrate contains a large amount of vitrinite. In contrast, the inertinite fraction obtained from PSOC-1103 exerts a greater accelerating influence on the exchange reaction than does the vitrinite obtained from the same coal. Analytical data indicate that this inertinite fraction is expecially rich in sulfur. Consequently, the high reactivity is not unexpected (3).

The results obtained in the reduction of benzophenone, although not without anomalies, are more regular than the results obtained in the exchange reactions. The reactivity sequence, exinite > vitrinite > inertinite, is observed for both PSOC-828 and PSOC-1103. Moreover, the inertinite concentrates from these coals are both moderately more reactive than tetralin.

This preliminary series of observations reveal that there are differences in the hydrogen donor capacity of the different macerals obtained from three different coals, however, the differences in reactivity in the test reactions used in our study are not highly pronounced.

ACKNOWLEDGEMENT

We are indepted to G.R. Dyrkacz and his collaborators and to R.E. Winans and K.L. Stock for the preparation of the macerals used in this study. The research was supported by a contract (DE-AC22-80PC30088) from the Department of Energy. The whole coal samples were provided by W. Spackman from the Penn State Coal Bank.

REFERENCES

1. Whitehurst, D. D., Mitchell, T. O. and Farcasiu, M. "Coal Liquefaction," Academic Press, New York, 1980

2. King, H. H. and Stock, L. M. Fuel, 1982, **61**, 257

3. Huang, C. B. and Stock, L. M. Am. Chem. Soc., Div. Fuel Chem., Preprints 1982, **27**(3-4), 28

4. Franz, J. A. Fuel, 1979, **58**, 405

5. Ratto, J. J., Heredy, L. A. and Skowronski, R. P. Am. Chem. Soc. Div. Fuel Chem., Preprints 1979, **24**(2), 155

6. Cronauer, D. C., McNeil, R. I., Young, D. C. and Ruberto, R. G. Fuel 1982, **61**,610

7. Dyrkacz, G. R., and Horwitz, E. P. Fuel, 1982, **61**, 3

8. Collins, C. J., Benjamin, B. M., Raaen, V. F., Maupin, P. H. and Roark, W. H. "Organic Chemistry of Coal", (Ed. J. W. Larsen), Am. Chem. Soc., Washington DC, 1978, p. 165

9. Raaen, V. F. and Roark, W. H. Fuel, 1978, **57**, 650

Effect of Thermal Alteration on Petrographic Constituents of the Hanna No. 1 Coal

F. J. Rich
Department of Geology and Geological Engineering
South Dakota School of Mines and Technology
Rapid City, South Dakota 57701

A. D. Youngberg
U. S. Department of Energy,
Laramie Energy Technology Center
P.O. Box 3395, University Station
Laramie, Wyoming 82071

INTRODUCTION

The United States Department of Energy, Laramie Energy Technology Center, (LETC) has conducted numerous underground coal gasification (UCG) experiments. DOE recognizes the great potential value of UCG as a means of extracting energy from coal beds which cannot otherwise be utilized. Many beds are too deeply buried to be strip-mined, or are unsuitable for underground mining, yet constitute a vast energy reserve. We are currently developing UCG technology which should lead to an energy- and cost-efficient means of utilizing such coal beds.

LETC has chosen the Hanna No. 1 coal for experimental UCG work. The Hanna No. 1 lies within the Paleocene Hanna Formation and is confined to the Hanna Coal Basin of Wyoming (Figure 1). The No. 1 coal has been classified as a high-volatile C bituminous coal (1).

Various approaches have been used to improve the efficiency of the UCG process at the Hanna site. While these include proper installation and use of surface facilities, LETC personnel have also recognized the need for a complete understanding of the coal itself. Through careful analysis of the coal, improved systems for conversion to high quality gaseous fuel can be designed. Various types of analyses have been performed on samples of altered and unaltered coal and carbonaceous shales from the Hanna site. This report details the results of one aspect of those analyses.

PURPOSE OF THE STUDY

The purpose of the study has been to construct a geothermometer based upon visible thermal alterations in the organic constituents of Hanna No. 1 coal and carbonaceous shale samples. Youngberg, at LETC, and Rich, at the South Dakota School of Mines and Technology (SDSM&T) agreed that a correlation might be made between discrete alteration temperatures and unique petrographic compositions produced by alteration. If such a correlation could be made, then samples of coal and/or carbonaceous shale taken from UCG sites could be observed microscopically and determinations made as to the maximum temperatures to which the sediments had been subjected. The organic constituents of the samples, termed macerals, were observed, described, and quantified as changes occurred in their appearances during heating at progressively higher temperatures.

LABORATORY METHODS

Sample Preparation

Crushed bulk samples of coal and carbonaceous shale from the Hanna 170 sample site were sent to SDSM&T. One sample from 277-278 feet depth was chosen for a low ash sample (12.7% dry basis), while the sample interval 279.7-280.7 feet was

chosen for a high ash sample (63% dry basis). A third sample interval, 284.2-285.2 feet was added to the work schedule about midway through the project. Its unusual petrographic composition indicated it might actually perform better as an indicator of thermal alteration than the original samples.

Five gram samples were placed in a previously weighed crucible, and their combined weight was recorded. The furnace, meanwhile, had been heated to the desired temperature and thoroughly flushed with helium. Helium was chosen because it is totally inert and would not cause alterations in the samples in and of itself. Heating was done at 50°C intervals between room temperature (~20°C) and 600°C.

After being heated for 1 hour, the crucible was removed from the furnace as quickly as possible and weighed to record any weight change. Each sample was mixed immediately with APCO adhesive #5823. This is a low viscosity epoxy-type embedding medium which is commonly used for coal pellet preparation. The mixture of coal or shale and epoxy was divided between two steel 1-inch internal diameter steel molds, and compressed at 7000 psi for 2 minutes. After each sample hardened (~18 hours) it was labeled, then ground and polished on a Jarret Automatic Grind-Polisher.

Furnace Construction

The furnace apparatus consisted of two Parr oxygen bombs connected by a length of teflon-lined steel mesh hose (Figure 2). Only one bomb was used as a furnace. The furnace bomb was wrapped with Samox-insulated heating tape, which was then covered with several windings of Glaspun fiberglass insulating tape. The heating tape was plugged into a variable transformer which provided current for heat generation.

The lid of a Parr oxygen bomb is equipped with several fixtures, including one-way gas valves which allow flow either into or out of the bomb, and two electrical terminals which, under ordinary oxygen bomb operation, provide a heat source for sample ignition. The inlet gas valve on the furnace bomb was connected to a helium tank, while the exit valve was connected to the steel mesh hose. The hose was also connected to the second bomb, as previously mentioned. The stream of helium, then, flowed into the furnace bomb, out through the hose, and into the second bomb. From there, gases were exhausted into a fume hood. The second bomb served as a barrier to atmospheric gases which might have accidentally entered the furnace bomb, and therefore helped to prevent unwanted or dangerous combustion of samples.

One of the two electrical terminals in the furnace bomb lid was removed, and a thermocouple inserted in its place. The thermocouple was wrapped with fiberglass insulation to provide a tight seal against the air outside the bomb. The end of the thermocouple was inserted to a level just above and to the side of the crucible (Figure 2) in order that the heat sensor would measure the furnace temperature at the sample location within the bomb. Accurate temperature monitoring was provided by an Omega digital centigrade thermometer which was attached to the thermocouple.

The crucible was placed within a circular loop of wire which is designed to hold more conventional oxygen bomb samples. The crucible rested in about the middle of the furnace chamber and was, presumably, heated evenly from all sides.

A typical sample run consisted of the following steps:

1. heating of furnace bomb to preselected temperature

2. flushing of both bombs with helium

3. recording of sample weight

4. insertion of crucible into furnace bomb

5. securing furnace bomb lid

6. heating in a helium stream for 1 hour

7. removal of furnace bomb lid and sample

8. weighing of sample

9. immediate mixing of sample with epoxy

10. pellet pressing and polishing

Sample Analysis

Methods of analyzing polished pellets, or briquettes of coal are fairly well established. Stach (2) presents a concise review of techniques. The method of microscope analysis employed in this studied involved incident illumination of polished pellet surfaces and observation at 500 X magnification in oil immersion. Blue-light (actually blue-and ultraviolet wavelengths) was employed initially, though one typically observes samples using incident "white" light. Such "white" light analyses were provided by LETC, however, and so were not duplicated by Rich for unheated samples. The average maceral compositions of 108 unaltered samples of Hanna No. 1 coal are shown in Table 1.

TABLE 1. Average Maceral Composition (mineral-matter free basis) of 108 Unaltered Coal Samples from the Hanna UCG site (1).

MACERAL GROUP	VOLUME %	MACERAL	VOLUME %
Vitrinite	91.8	Vitrinite	90.3
		Pseudovitrinite	1.5
Liptinite (Exinite)	6.1	Exinite	5.5
		Resinite	0.6
Inertinite	2.1	Semi-Fusinite	1.0
		Semi-Macrinite	0.1
		Fusinite	0.3
		Macrinite	0.1
		Micrinite	0.5
		Sclerotinite	0.1

The application of blue-light was done at first merely to see how many of the macerals in the Hanna 170 samples would fluoresce. Incident blue-light causes liptinite macerals (waxes, resins, spores, etc.) to fluoresce brightly, especially in low-rank coals. As the liptinites fluoresce they can be easily identified and quanitifed.

Sample surveys revealed a particular type of liptinite, exudatinite, to be unusually common in the Hanna 170 core samples. Exudatinite is a mobile or semi-mobile oil- or resin-like liptinite which has been recognized only in recent years (3). It occupies open spaces within the coal, and therefore tends to be found in fractures or

the lumens of coalified cells. Exudatinite in the Hanna 170 samples is especially common in structured woody tissue (telinite) and fungal bodies (sclerotinite). Inasmuch as exudatinite is rather mobile, and may actually migrate out of samples into the immersion oil (4) Rich decided to emphasize exudatinite analyses. The rationale was that, if any substances in the Hanna samples would react quickly to thermal alteration, exudatinite would certainly be among them. Exudatinite is confidently identified only in blue-light, as it fluoresces brightly, but is nearly invisible in "white" light. In view of those facts, and because exudatinite is believed to be of great potential value in geothermometry, Rich concentrated on blue-light analyses.

Two pellets from each sample interval were counted to determine relative abundances of macerals. Each pellet was attached to a glass slide with modeling clay and pressed onto the clay so that the observed surface lay parallel with the microscope stage. Counts were performed along parallel transects which did not overlap. Pellets were moved laterally by discrete units so that no adjacent fields of view overlapped. One point was counted per field of view, that point lying at the intersection of an ocular cross-hair reticle. Five hundred points were counted per pellet, and both pellets per sample were observed, providing 1000 points per sample.

TABLE 2

CHANGES IN LIPTINITE COMPOSITION FOR SAMPLES FROM 277-278 FEET

Temperature°C	% Liptinites	# Exudatinite	# Liptodetrinite & Bituminite	# Exinite
19	4.4	10	17	10
50	4.9	12	22	8
100	3.6	14	14	4
150	2.8	8	8	5
200	3.7	8	22	5
250	4.0	5	17	5
300	2.8	1	13	6
350	1.0	1	7	0
400	0.0	0	0	0

TABLE 3

CHANGES IN LIPTINITE COMPOSITION FOR SAMPLES FROM INTERVAL 284.2-285.2 FEET

Temperature°C	% Liptinites	# Exudatinite	# Liptodetrinite & Bituminite	# Exinite
21	7.7	1	58	10
50	8.5	3	67	9
100	11.5	4	87	12
150	9.3	7	68	14
200	8.3	4	69	5
250	8.5	2	67	7
300	5.2	1	38	8
350	0.8	0	6	2
400	0.0	0	0	0

RESULTS

Tables 2 and 3 illustrate several of the changes which took place during heating of samples from the 277-278 and 284.2-285.2 foot levels respectively. The following observations may be made:

1) In samples from both levels there was a gradual decrease in percentages of total liptinites as temperatures increased.

2) At both sample intervals, fluorescence essentially ceased at 400°C.

3) Reaction vesicles developed within vitrinite particles between 250-300°C. Vitrinite which contained spores or pollen, resin bodies, etc. became especially vesicular. Exudatinite showed distinct reactivity with consequent evacuation from sclerotinite bodies and interstices among crystals in pyrite framboids. Cracks developed in vitrinite.

4) Between 300-350°C vitrinite became obviously cracked and vesicular. Resinites clearly showed alteration rims as they reacted.

5) Between 350-400°C vitrinite became increasingly vesicular, with vesicle size and abundance increasing. Glassy or pitchey appearing deposits occurred in many vesicles. Exudatinite and resinite nearly vanished.

6) Within the 400-500°C range reflectivity of vitrinite particles appeared to be much more uniform. Resinite, exinite, cutinite, etc. were no longer visible in either "white" or blue light.

7) At 500-600°C, every coal particle developed a multitude of vesicles, and many were intensely cracked, almost brecciated. Coal particles were of uniform color and composition except for the vesicles and cracks.

Samples from the 279.7-280.7 foot interval were not point counted in blue light. The abundant clay particles were filled with detrital liptinites and were saturated with bituminite. Bituminite is another semi-mobile maceral, similar in some respects to exudatinite, which frequently infiltrates the layers of clay minerals. It thus causes the clays and interstices among clay particles to fluoresce. It is almost impossible to get an accurate quantification of bituminte in such clayey samples as virtually everything fluoresces, yet clearly the samples are not pure bituminite. Alteration in shale samples proceeded as listed for the other samples, however.

DISCUSSION AND CONCLUSIONS

Distinct petrographic changes did take place in the Hanna No. 1 samples as they were heated. Decreasing abundances of fluorescence macerals, increasing vesicularity and cracking in vitrinites, and eventual elimination of all macerals except vitrinite can be correlated with temperature ranges. It should, then, be feasible to take samples of carbonaceous shale and coal from UCG burn sites and determine the thermal gradiant away from the sites.

This work has also shown that macerals in the Hanna No. 1 coal react at quite different rates when heated. Liptinites are altered before vitrinites and intertinites, though eventually all the macerals become involved in the physical alterations. The fact that liptinites react earlier than vitrinites may carry important implications as far as maintaining optimum gas composition and production are concerned.

Liptinites, for example, are enriched in hydrogen as compared to the other maceral groups. As liptinites decompose thermally, then, one would expect gases with a high hydrogen/carbon ratio to be produced. In a coal, such as the Hanna No. 1 which contains an abundance of easily altered liptinites (e.g. the resinite-rich Blind Canyon seam of Utah) conversion of coal to gas could occur at a comparatively low temperature and yet yield a gaseous product enriched in hydrogen. On the other hand, coals which do not have such an abundance of liptinites might require higher conversion temperatures which would involve more vitrinite in the conversion reactions in order to produce gases with a high hydrogen content.

An additional observation is that at higher temperatures, i.e., 400°C and above where particles become vesicular and fractured the reactive surface area within coal fragments is much greater than at cooler temperatures. The abundance of vesicles and the eventual brecciation of the particles should allow the coal to react more readily with hot gases within the gasification chamber. Brecciated coal particles would, of course, also allow product gases to move more readily through the coal bed than if the coal fragments were less extensively broken.

We believe the results of the work show that the most successful UCG operations will be those where careful consideration has been given to the petrographic composition of the coals. Petrography can be used both as a geothermometer and as a technique to predict coal reactivity during underground gasification.

References

1. Youngberg, A. D., 1981, Petrographic Analysis of Unaltered and Thermally Metamorphosed Coal from the Hanna, Wyoming, Gasification Area: Seventh Underground Coal Conversion Symp., Fallen Leaf Lake, Calif., Sept. 8-11, p. 402-415.

2. Stach, E., 1975, Coal Petrology: Gebruder Borntraeger, Berlin, 428 p.

3. Teichmuller, M., 1974, Uber neue Macerale der Liptinit-Gruppe und die Entstehung des Micrinits: Fortschr. Geol. Rheinld. u. Westf., v. 24, p. 37-64.

4. Spackman, W., A. Davis, and G. D. Mitchell, 1976, The Fluorescence of Liptinite Macerals: Brigham Young Univ. Geol. Studies, v. 22, pt. 3, p. 59-75.

Figure 1
Location of Hanna Basin

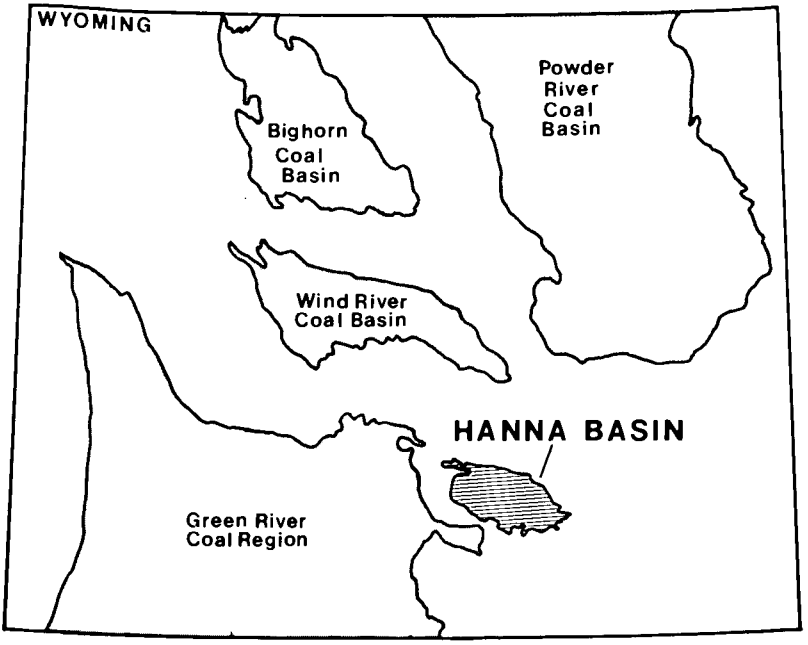

Figure 2
Bomb Assembly

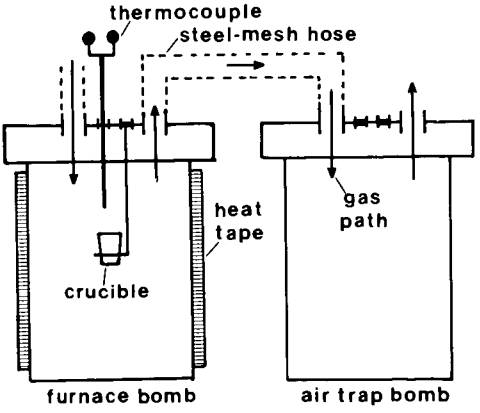

HYDROUS METAL OXIDE ION EXCHANGERS AS HYDROGENATION CATALYSTS FOR DIRECT COAL LIQUEFACTION*

H. P. Stephens, R. G. Dosch and F. V. Stohl

Sandia National Laboratories, Albuquerque, NM 87185

INTRODUCTION

Interest in efficient conversion of coal to liquid fuels has encouraged exploration of promising catalytic systems for direct coal liquefaction. We have identified a group of hydrous oxide ion exchange compounds of Ti, Zr, Nb, and Ta which can be used to prepare hydrogenation catalysts by a novel synthesis route involving exchange of active metals into these compounds. Hydrous oxide ion exchange compounds have previously been investigated at Sandia National Laboratories for use in decontamination of aqueous nuclear waste (1,2) and as precursors for ceramic materials (3). A number of properties of the compounds suggested their use as substrates for catalyst preparation: 1) any metal or mixture of metals can be atomically dispersed in the materials over a wide concentration range by a simple process; 2) the materials have high surface areas; 3) they exhibit good chemical stability; 4) solution chemistry or high temperature reactions can be used to provide active metal oxidation state control; and 5) acidity and basicity of the substrate can be modified by ion exchange.

Although these properties suggested hydrous oxide ion exchangers may exhibit wide versatility for catalyst preparation, it was not known if catalysts synthesized by exchanging ions of active metals into the material would exhibit hydrogenation activity. The purpose of the experiments reported here was to explore the hydrogenation activity of these materials for slurry phase catalysis of direct coal liquefaction. It is also possible that hydrous metal oxide ion exchangers may be used to prepare multifunctional catalysts and catalysts for other reactions such as oxidation or dehydrogenation.

EXPERIMENTAL

Preparation and Characterization of Catalysts

The titanate system, the best characterized and least expensive of the hydrous oxides, was chosen for exploratory testing. Titanate catalysts were prepared by exchanging the sodium ions of a hydrous oxide titanium compound, generically called sodium titanate (ST), with the desired metal ions in aqueous solution. ST was prepared by reacting tetraisopropyl titanate with sodium hydroxide in methanol, hydrolyzing the solution in a water acetone mixture and drying the resulting precipitate at ambient temperature under vacuum. The preparation steps may be illustrated as follows:

(1) $Ti(OC_3H_7)_4 + NaOH \xrightarrow{CH_3OH}$ Soluble Intermediate

(2) Soluble Intermediate $\xrightarrow{\text{acetone}\quad H_2O} [NaTi_2O_5H]_x$

(3) $2[NaTi_2O_5H]_x + XNi(aq) \longrightarrow 2xNa + [Ni(Ti_2O_5H)_2]_x$

* This work supported by the U. S. Dept. of Energy, Contract No. DE-AC04-76DP00789.

A typical ST product is an amorphous fluffy powder, which contains approximately 20% residual volatile constituents, predominately water and minor amounts of alcohols. The titanates of other metals, formed by exchange of the sodium ions, were found to have the same morphology and volatile content as the starting ST material. Drying the titanates at elevated temperature resulted in loss of volatiles. Approximately 90% of the volatiles were removed at 200°C and greater than 95% were removed after heating to 400°C. X-ray diffraction and SEM work indicated that a transition from an amorphous to a crystalline form (rutile) occurs at approximately 600°C. This is supported by DTA and TGA studies, which showed a large exotherm with no corresponding weight change at the same temperature.

Surface areas and pore volumes for several titanates have been measured by nitrogen BET and adsorption-desorption techniques. Surface areas for the material ranged from 150 to 300 m^2/g and the desorption pore volumes from 0.24 to 0.41 cc/g. All of the titanates had bimodal pore volume distributions similar to the distribution illustrated for Ni titanate (total pore volume = 0.31) in Figure 1. For comparison, the unimodal pore volume distribution for a Ni/Mo on alumina catalyst, Shell 324, (total pore volume = 0.44) is also shown.

Materials, Apparatus and Procedure

Liquefaction reactions were performed with Illinois No. 6 (Burning Star) coal, SRC-II heavy distillate solvent from the Ft. Lewis Pilot Plant (1:2 coal:solvent, by weight) and high purity hydrogen. Shell 324, a 2.7% Ni/13.2% Mo on alumina catalyst, currently used in integrated two stage liquefaction pilot plant studies (4), was ground to -200 mesh and used as a reference for comparison of catalytic activity. Control experiments were also performed without catalyst addition.

As a result of screening liquefaction experiments with a number of titanates, including Cr^{+3}, Fe^{+3}, Fe^{+2}, Ni^{+2}, Pd^{+2}, Mo*, Rh^{+3}, Ru^{+3}, Co^{+2}, Mn^{+2} and Eu^{+3}, three were chosen to test the effects of active metal, metal loading and post-preparation treatment on catalytic activity.

A randomized factorial experimental plan (3 x 2 with duplication) was used to test the effect of active metal and metal loading on liquefaction activity. For these experiments, Ni, Mo and Pd titanates with metal loadings of 1% and 10%, by weight of titanate, were used. Catalyst weight added to the reactor was adjusted so that liquefaction reactions with the 1% titanates were performed with 4×10^{-5} moles of active metal and reactions with the 10% titanates with 4×10^{-4} moles. To test the effects of catalyst post-preparation treatments, which result in loss of volatiles and surface area, and oxidation or reduction of the Ni, duplicate experiments were performed with the 10% Ni titanate heated for two hours at six conditions--300, 450 and 700°C in air and hydrogen. Reference experiments with Shell 324 were performed with the same number of moles of active metal (Ni + Mo) as the 10% loading experiments.

All liquefaction reactions were performed in 40 cm^3 microreactors which were charged with 2.67 g of coal, 5.33 g SRC-II,

* Oxidation state not determined.

and powdered catalyst, pressurized to 800 psig (cold) with hydrogen, then heated to 425°C for 30 minutes and shaken at ∿150 cycles/min. during the heating period. Temperatures and pressures were accurately recorded with a digital data acquisition system during the course of the experiments. Following the heating period of each experiment, the reaction vessel was quenched to ambient temperature, the resulting pressure was recorded, a gas sample was taken, and the product slurry was subsampled for analysis.

Product Analyses

Gas samples were analyzed for mole percentages of CO, CO_2, H_2S and C_1-C_4 hydrocarbons with a Hewlett-Packard 5710A gas chromatograph, which was calibrated with standard mixtures (Matheson Gas Products) of hydrocarbon gases in hydrogen. Hydrogen in the samples was obtained by difference as the remainder of the product gas mixture. The quantity of each gas produced was calculated from the mole percent in the gas sample and the post-reaction vessel temperature and pressure using an ideal gas law calculation. Hydrogen consumed during the reaction, obtained as the difference between the initial charge and hydrogen remaining after the reactor was quenched, was reported on a percent dmmf coal basis.

The reaction product slurry was analyzed for insols, high molecular weight (mw) product, intermediate mw product and low mw product by tetrahydrofuran (THF) solubility and high performance liquid chromatography (HPLC). A 0.2 g subsample was mixed with about 50 ml of THF, filtered to obtain the weight of insols, and brought to 100 ml with additional THF. Chromatograms of 5 μℓ aliquots of the filtrate were obtained with a Waters Assoc. Model 6000A solvent delivery system, a 100 Å microstyragel gel permeation column, and a Model 440 uv absorbance detector. The uv absorbance response factors for the product groups were determined using calibration samples prepared by dissolving known weights of high (∿ 1000 g/mole), intermediate (∿ 500 g/mole) and low (250 g/mole) mw coal-derived products obtained by preparative scale liquid chromatographic (gel permeation) separation of whole liquid product from liquefaction reactions performed under similar conditions with the same coal and solvent. Chromatogram area measurements and response factors were used to calculate the percentages of high, intermediate and low* mw products for the THF soluble product. Conversion data were calculated on a dmmf coal basis, and included corrections for the conversion of the pyrite content of the coal to pyrrhotite and the loss of volatiles, if any, from the catalyst.

RESULTS AND DISCUSSION

Previous statistical analysis of experiments with oil soluble catalysts (5) has shown that hydrogen consumption and conversion to low mw product may be used as quantitative measures of catalyst activity for coal liquefaction. Figures 2 and 3 illustrate the conversion to low mw product and hydrogen comsumption for the experiment with the 1 and 10% Ni, Mo and Pd titanates without post-preparation treatments. The values represented in the figures are the averages of duplicate experiments. Standard deviations were statistically determined to be 1.4% for conversion

* % conversion to low mw product is approximately equivalent to pentane soluble product.

to low mw product and 0.13% for hydrogen consumption. As can be seen from Figures 2 and 3, the ranking for metals effect with respect to both low mw conversion and hydrogen consumption is Pd > Mo > Ni and with respect to metals loading is 10% > 1%.

Results of a two way analysis of variance were used to make a quantitative comparison of performance. The effect of active metals (1 and 10% loadings averaged), were as follows:

low mw product:
Pd (47.7%) > Mo (45.3%) > Ni (43.0%) $F = 10.8$, $P < .01$;

hydrogen consumption:
Pd (1.86%) > Mo (1.65%) > Ni (1.35%) $F = 22.4$, $P < .005$,

where F is the variance ratio and P is the probability of a chance occurrence of the result. These values may be compared with the results of experiments without catalyst addition (low mw product = 26.8% and hydrogen consumption = 0.69%) and experiments with Shell 324 (low mw product = 42.8% and hydrogen consumption = 1.88%). It was found that the 10% titanates averaged 3.2% greater conversion ($F = 10.8$, $P < 0.01$) and 0.37% greater hydrogen consumption ($F = 35.0$, $P < .005$) than the 1% titanates.

Only one post-preparation treatment of the 10% Ni titanates was found to have a significant effect on catalytic activity. Experiments with the titanate heated to 700°C in air produced a conversion of 33.6% to low mw product and had a hydrogen consumption of 0.71% which was significantly lower than the values for the other treatments (45.2 ± 1% and 1.5 ± 0.2%). X-ray diffraction analysis of the post-preparation treated materials shows formation of $NiTiO_3$ for only the material heated to 700°C in air. The $NiTiO_3$ formed probably cannot be reduced to Ni under liquefaction conditions and therefore is not available for catalysis of hydrogenation reactions. This has been supported by preliminary oxygen chemisorption experiments which show that the 700°C/air treatment produces a catalyst that has less than half the active nickel of the other materials.

Although this preliminary study was brief in its scope, the results indicate that catalysts prepared using hydrous metal oxide exchange compounds show promise for potential application to coal liquefaction processes. The initial activities of the titanates appear to be at least comparable to a commercial catalyst currently used in pilot plant liquefaction studies. Considering the versatility of the hydrous oxide ion exchangers with respect to their potential for preparation of multi-metal loadings and adjustment of substrate acidity or basicity, it is possible that these materials can be used to produce improved catalysts for direct coal liquefaction and other hydrogenation processes.

REFERENCES

1. R. G. Dosch, "The Use of Titanates in Decontamination of Defense Waste", SAND-78-0710, Sandia National Laboratories, Albuquerque, NM, June 1978.
2. R. G. Dosch, "Final Report on the Application of Titanates, Niobates, and Tantalates to Neutralized Defense Waste Decontamination - Materials Properties, Physical Forms, and Regeneration Techniques", SAND-80-1212, Sandia National Laboratories, Albuquerque, NM, January 1981.

3. D. L. Hankey, W. F. Hammetter and R. G. Dosch, "Preliminary Investigations on Microstructure Development in PZT Ceramics", Abstract, 34th Pacific Coast Regional Meeting of American Ceramic Society, October 1981.
4. H. P. Schindler, J. M. Chen, M. Peluso, and J. D. Potts, Proceedings of the Seventh Annual EPRI Contractor's Conference, Palo Alto, CA, May 1982.
5. K. P. Johnston, A. W. Lynch, H. P. Stephens, F. V. Stohl and M. G. Thomas, "Coal Liquefaction Process Research Quarterly Report for January 1 - March 31, 1982", SAND-82-1924, Sandia National Laboratories, Albuquerque, NM, October 1982.

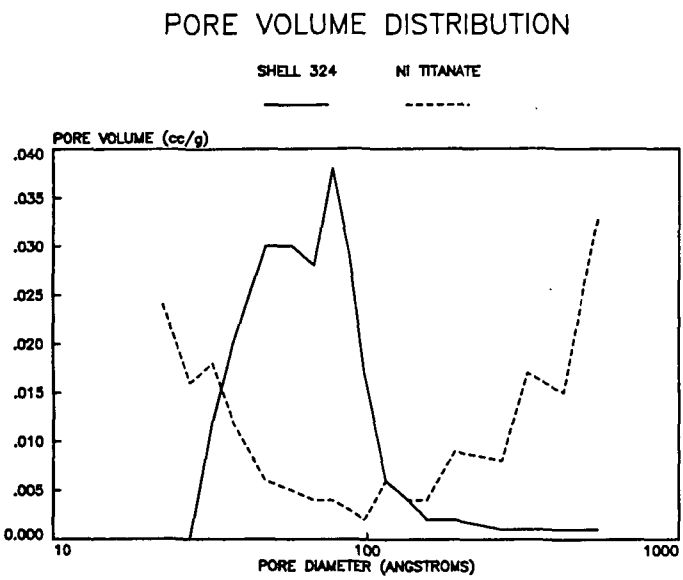

Figure 1

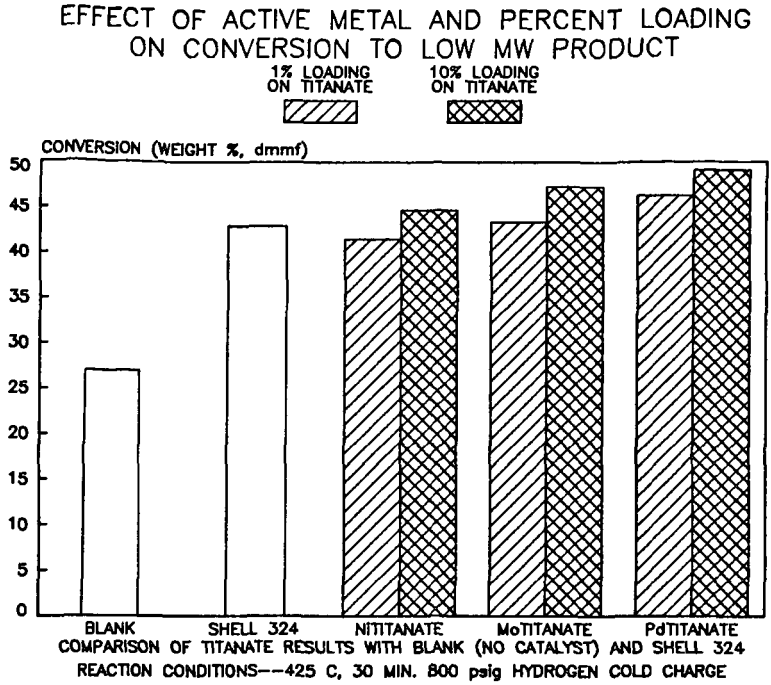

Figure 2

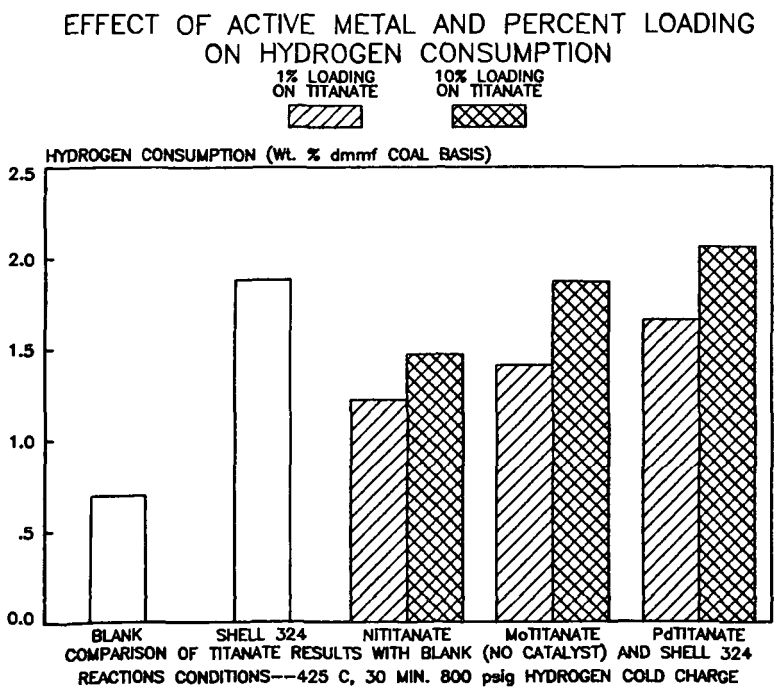

Figure 3

INTEGRATED TWO-STAGE LIQUEFACTION PROCESS - SOLVENT QUALITY EFFECTS

Eneo C. Moroni, Frank P. Burke*, Richard A. Winschel* and Bary W. Wilson**
U.S. Department of Energy, Fossil Energy/Coal Liquefaction Technology Division, FE-34, E-338 Germantown, Washington, D.C. 20545
*Conoco Inc., Coal Research Division, Library, PA 15129
**Pacific Northwest Laboratory, Battelle, Richland, Washington 99352

Introduction

For the majority of the developed coal liquefaction processes the solvent is a portion of a selected liquefaction process stream, and not supplied from external sources, consequently a strict process control is needed to produce the required solvent balance and desired solvent quality.

Problems in maintaining both solvent balance and solvent quality has been particularly associated with the development of the SRC I process. With the introduction of the Two-Stage Liquefaction process in which SRC I is upgraded and converted to a distillate product the solvent balance does not constitute a problem anymore and the solvent quality has been improved.

Several modifications to the Two-Stage Liquefaction, which were dictated by important experimental results involving both the dissolution/hydrogenation of coal and the upgrading of the coal extract, led to a new process configuration in which first and second stages are interlocked in one integrated processing scheme. The major experimental results leading to these modifications are listed below:

- o Coal extract produced at lower operating severity than SRC I is more responsive to subsequent catalyzed reactions.[1]
- o Coal extracts produced at low severity can be upgraded to fuel products and a recycle process solvent of consistantly high quality.
- o Hydrogenated high boiling polyaromatics are superior hydrogen "donors" than compared to lower molecular weight tetralins.[2]
- o Nitrogen compounds inhibit catalytic hydrogenation of aromatics and deoxygenation of oxygen containing compounds in coal.[3]
- o Phenols inhibit catalytic denitrogenation of nitrogen compounds in coal or coal extracts.[4]
- o Heteroatom compounds, are not easily recovered since they form strong "adducts" with coals.
- o Hydrogenated polyaromatics, which also form "adducts" with coals are readily produced in the course of coal liquefaction/coal extract upgrading operations, providing a constant supply of steadily high quality recycle process solvent.

The first Integrated Two-Stage Liquefaction (ITSL) process configuration included Short Contact Time (SCT) coal extraction to maximize low severity operation in the first stage and LC-Fining using Shell 324 NiMo supported catalyst to provide extensive removal of heteroatom compounds. Further modifications of the ITSL process operating conditions were prompted by data obtained during actual

operation in the 3/4 ton coal/day ITSL process development unit at C-E Lummus, Engineering Development Center in New Brunswick, N.J., and by computed data and refining requirement as ascertained by upgrading coal-derived distillates from other processes. The major conclusions from all these sources can be summarized as follows:

- In a continuous operation the solvent fraction below 340-360°C is in vapor phase and participate little, if any, in the liquefaction of coal and also depresses the hydrogen partial pressure. Computed Vapor/Liquid equilibrium data confirm this fact.
- The -340°C fraction constitutes the most valuable refinery feedstock, being within the boiling range of gasoline, jet and diesel fuels.
- The +340°C fraction constitutes the best solvent quality for both dissolution of coal and hydrogen "shuttling."

The most recent ITSL process configuration, which is described below, attempts to exploit modifications indicated by these experimental results.

ITSL Process Flow Sheet

The current flow scheme of the ITSL operation is shown in Figure 1. Coal, hydrogen and recycle solvent (the +343°C fraction) react in the SCT reactor which is actually the SRC I preheater operated at higher outlet temperature (450°C). The gases and light oil are flashed off and the heavy oil (+343°C solvent/coal adduct) goes to the deasher. The deasher underflow containing virtually all of the ash and insoluble organic matter (IOM) goes to a vacuum flash, where the distillate portion goes overhead and combines with the deasher overflow. The ash/IOM containing flashed bottoms are drummed. Commercially this stream would go to a gasifier to generate the hydrogen for the process. The deasher overflow (cleaned +343°C solvent/coal adduct) combines with the vacuum flash overhead as feed to a continuous distillation column where the antisolvent is recovered overhead and the bottoms constitute the feed to the LC-Finer (LCFF) along with make-up hydrogen. The LC-Finer product (Total Liquid Product:TLP) is atmospherically flashed to collect the -343°C high quality product, and the +343°C bottoms are recycled to the SCT solvent pool. In this manner, the only product leaving the process is the -343°C fraction which has petroleum refinery feedstock quality superior to some petroleum crudes (Table 1).

Table 1
ITSL - PRODUCTS AND RECYCLE SOLVENT
Elemental Analysis

	C	H	O	N	S
Naphtha (C_5-177°C)	86	13	0.4	0.08	Traces
Fuel Oil (177-343°C)	88	11	0.3	0.08	0.01
Recycle Solvent (+343°C)	86	8	3.0	0.50	0.50

Phenols and nitrogen compounds are minor constituents of the process solvent compared to the level of polyaromatic hydrocarbons and they do not appear to

provide much contribution to the process solvent quality. Data examination of several ITSL recycle operations, as the coal-derived solvent replaces the hydrogenate creosote oil initial solvent, reveal the decrease of heteroatom compounds and at the same time the increase of the solvent quality. It is difficult to correlate these two experimental evidences since the more powerful the solvent becomes the more phenols and nitrogen compounds, present in the coal, are dissolved and in turn they can contribute to further the dissolution of the coal.

Bench-scale vacuum fractionation of the +343°C fraction of the recycle process solvent revealed that the heteroatom compounds, particularly nitrogen, are heavily concentrated in the +560°C distillation bottoms.

Boiling Point versus Solvent Quality (Conoco Inc.)

Relationship between boiling point and solvent quality was studied on a sample of ITSL recycle process solvent taken during steady state operation and in material balance. Twenty-two distillate fractions of ca. 100 ml. each were collected and analyzed by ^{1}H-NMR for proton distribution. Every third fraction was used for kinetic and equilibrium microautoclave tests.

Proton distribution of the distillate fractions are given in Table 2 along with the weight percent hydrogen for those fractions used in the microautoclave tests.

Table 2
Proton Distribution of Distillate Fractions

Fraction	Boiling Point °C	H_2 Wt %	Condensed Aromatics	Cyclics α + β	Alkyls α + β	Alkyl γ
1	203	10.26	9.6	30.4	36.3	15.0
4	323	9.33	15.7	34.3	29.7	12.6
7	349	8.86	20.8	36.4	26.9	10.8
10	383	8.20	26.8	34.4	24.3	9.4
13	410	7.81	31.0	31.0	23.6	8.9
16	423	7.32	35.8	29.3	21.7	7.7
19	498	7.20	36.6	30.4	21.0	6.5
22	514	6.70	36.2	30.6	20.5	5.5

As the boiling point of the fractions increases the concentration of condensed aromatics increases from 8 to 39 percent. The results of the concentration of uncondensed aromatics are not shown since it decreases from 10 to 6 percent by the third fraction then remains fairly constant. The concentration of cyclic alpha and beta (naphthenic) protons, which provide one measure of donor concentration, increases for the first ten fractions, then decreases continuously to 31 percent. The concentration of alkyl alpha, beta and gamma protons which provide a measure of paraffins content decreases over the range with boiling point. Weight percent hydrogen decreases monotonically with increasing boiling point.

Microautoclave tests were carried out at 1000 psig (cold) nitrogen pressure, and are shown in Figure 2. At kinetic conditions, conversion increases sharply with boiling point to approximately 350°C (fraction 7) then the rate of increase lessens to 514°C (fraction 22).

The increase in kinetic conversion is attributed to the increase in aromaticity of the solvent with increasing boiling point as the ^{1}H-NMR data have shown. At the equilibrium conditions, conversions increase with boiling point to about 87 percent at 400°C, then decrease to 83 percent at 500°C. The equilibrium test is designed to give a measure of donor content of the solvent and the ^{1}H-NMR data on the cyclic/alkyl aliphatic proton ratio gives a relative measure of donor content in solvents with comparable hydrogen contents. The cyclic/alkyl ratio increases from 0.56 to 1.18 as the boiling points of the solvents increase. On the other hand the total hydrogen contents of the fractions decrease from 10.26 to 6.70 percent (Table 2). The shape of the curve of equilibrium test conversions vs. boiling point is caused by two opposing factors, i.e., increasing cyclic/alkyl ratio and decreasing total hydrogen content. The net effect of these opposing factors is to produce a maximum conversion at about the 375-425°C boiling point range.

ITSL Process Solvent Components (Battelle PNL)

Total ion GCMS chromatograms show the unusual configuration of the ITSL recycle process solvent at steady state operation. The chromatogram of the deashed SCT extract which is also known as LC-Finer feed (LCFF) represented in Figure 3 shows that the solvent has donated a large portion of his hydrogen to the coal, as few large peaks of distinguishable aromatic compounds have appeared. Among major peaks identified were phenanthrene, pyrene, chrysene and also benzo(a) pyrene and anthathrene. These compounds seem to grow dominant as the solvent recycles and its hydrogen donor quality improves. The LCFF stream is hydrotreated in the second stage LC-Finer and converted to Total Liquid Product (TLP). The GCMS chromatogram of TLP is shown in Figure 4 in which the major peaks disappear, more likely due to conversion of the parent hydrocarbons to a variety of hydrogenated derivatives, except for the pyrene peak, which is only slightly hydrogenated.

Conclusion

The peculiar behaviour of polyaromatic hydrocarbons under catalytic hydrogenation/hydrocracking condition, leads to a variety of speculative thoughts on the role of each individual variety in coal liquefaction.

On the basis of preliminary data some tentative statements and speculative thoughts are presented below with the particular objective of guiding further experimental studies on the nature of the ITSL process recycle solvent at equilibrium:

- The ITSL equilibrium process solvent is largely constituted by a few major polyaromatic hydrocarbons and related hydrogenated moieties.
- The possibility exists now to reproduce the ITSL equilibrium process solvent by using few model compounds, i.e., hydrogenated phenanthrenes, chrysene and perhaps pyrene and their alkyl derivatives.
- Reacting the above model solvents of different hydrogen contents with aromatic model compounds representing coal as hydrogen acceptor e.i., anthathrene and pyrene and their alkyl derivatives, a researcher can better simulate the reaction between the actual solvent and the coal.
- Practically all the hydrogen is very rapidly donated by the process solvent and very little, if any, via hydrogen gas. Consequently, the SCT coal extraction should not be affected by gas-slurry flow-dynamics and in turn bench-scale and scale-up operations should have excellent correlation, as one of the major differences is removed.

Acknowledgment

The authors appreciate the technical support of Dr. Harvey Schindler of The Lummus Company, Mr. John Potts of Cities Service Research and Development Company and Dr. Martin Neuworth of Mitre Corporation.

References

1/ This experimental evidence was indipendently discovered by Mobil R&D Co.- F. J. Derbyshire and D. D. Whitehurst - Private Communication.

2/ F. J. Derbyshire et al. "Fundamental Studies in the Conversion of Coals to Fuels of Increased Hydrogen Content" EPRI AP-2117, Project 1655-1 November 1981.

3/ D. O'Rear - Chevron R&D Company - Private Communication.

4/ E. J. Hollstein, E. J. Janoski, E. G. Scheibel, A. Schneider and A. F. Talbot, Sun Tech, Inc. Research and Development of an Advanced Process for the Conversion of Coal to Synthetic Gasoline and Other Distillate Fuels - Final Report DOE/FE 2306-23, In Print.

Figure 1
Integrated Two Stage Liquefaction PDU
Current Process Flowscheme

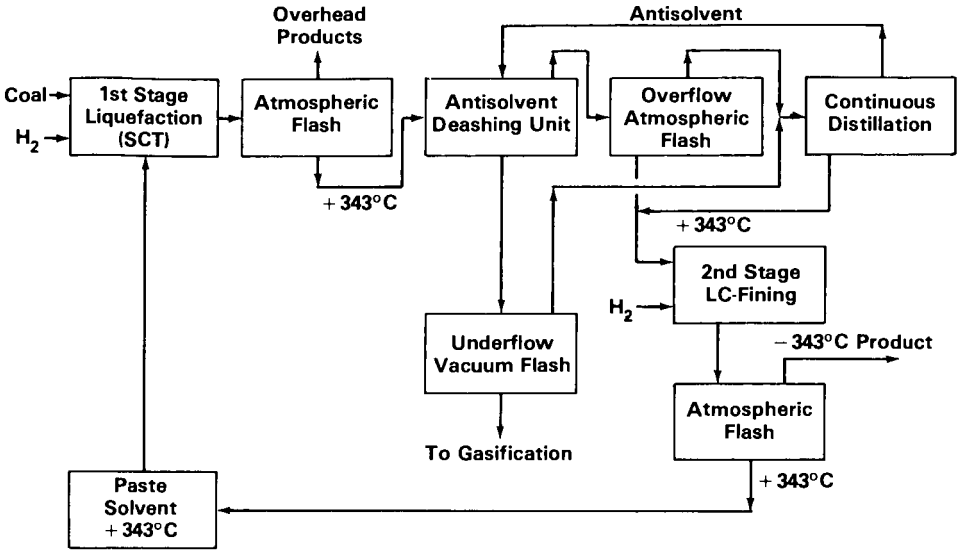

Figure 2
Microautoclave Tests with Fractions

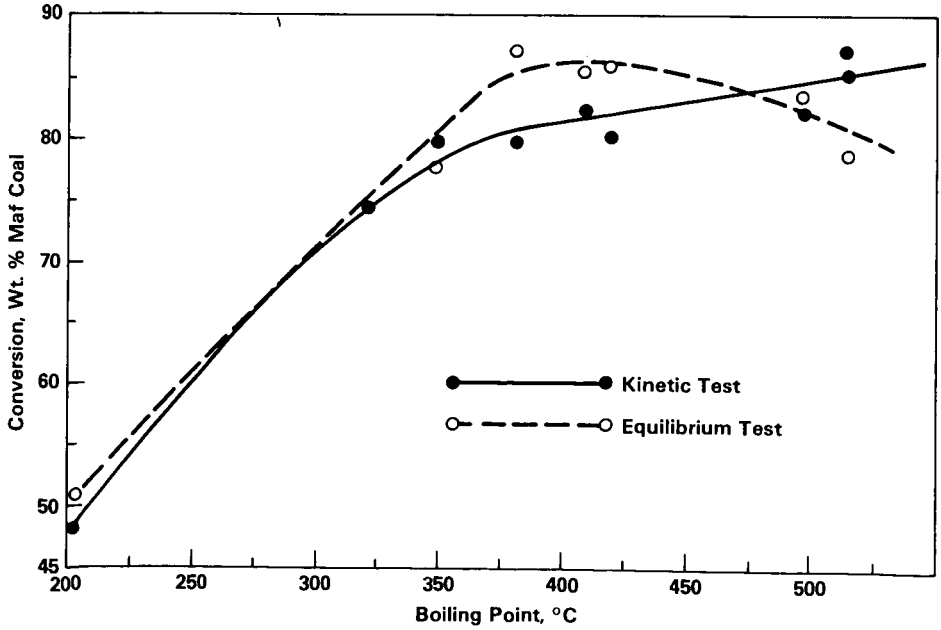

Figure 3

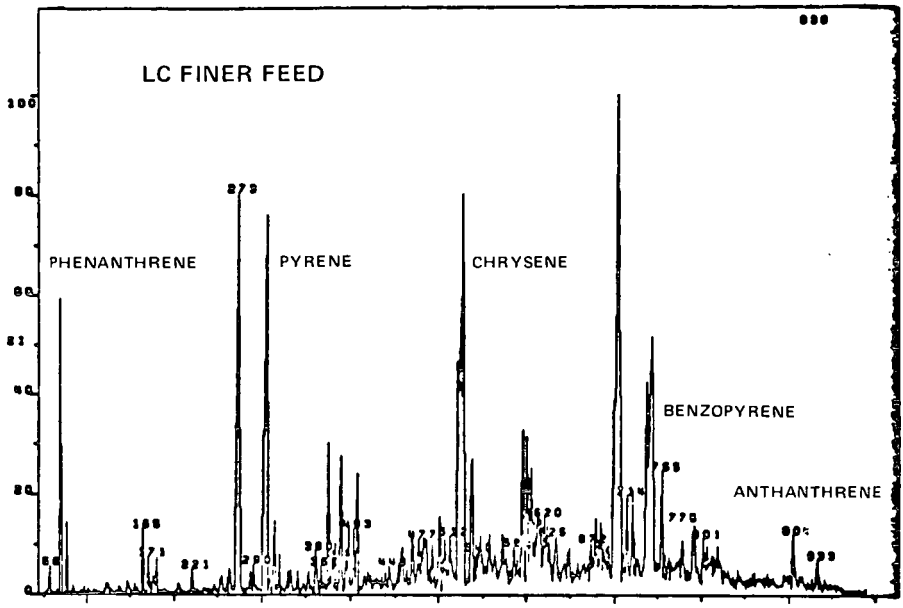

Figure 4

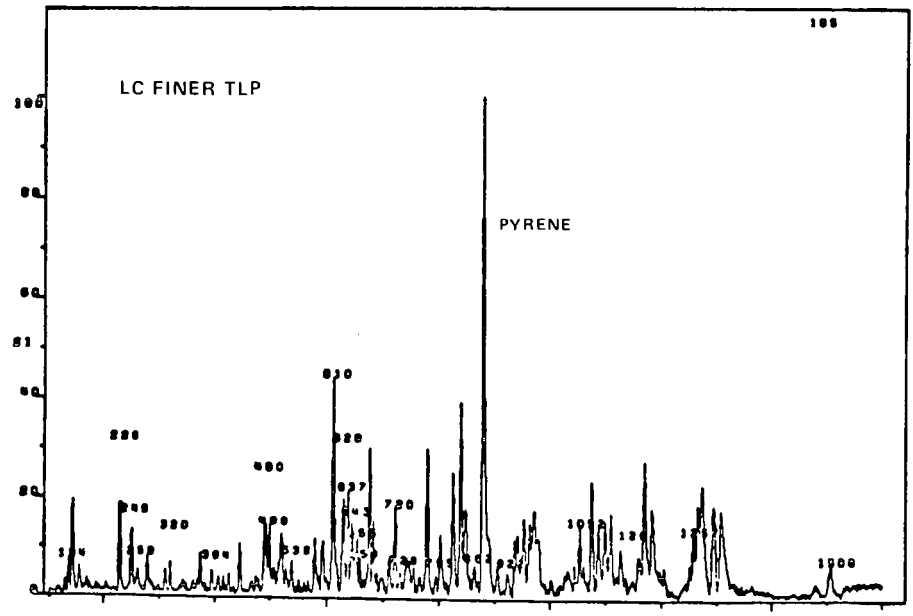

THE EFFECT OF SOLVENT PRETREATMENT ON COAL LIQUEFACTION

Nand K. Narain, Herbert R. Appell, and Bruce R. Utz

U. S. Department of Energy
Pittsburgh Energy Technology Center
P. O. Box 10940
Pittsburgh, PA 15236

This paper describes research on the chemical and physical phenomena occurring between coal and solvents prior to the onset of the major liquefaction (bond breaking) step. This report is limited to those phenomena that occur readily at temperatures near 200°C and have an effect on the subsequent liquefaction reactions.

A series of microautoclave experiments with Bruceton Coal and W. Kentucky 9/14 Coal, using creosote oil or SRC-II heavy distillate as solvents, showed that small but experimentally significant increases in conversion can be obtained by heating the coal-solvent slurry for one hour at 200°C prior to a short contact time liquefaction test (Table 1). (The presence of hydrogen at 200°C did not appear to be essential for this increase to occur.)

In order to obtain a better understanding of the factors that cause this increase in conversion, and thus propose a means to enhance the effect, several experiments were conducted with coal and model solvent compounds. Quinoline, 1-methylnaphthalene, and blends of these two compounds were chosen as solvent models. The results of these experiments show that these compounds are incorporated into the coal with pretreatment at 200°C, but no incorporation occurs with similar pretreatment at room temperature.

A tetrahydrofuran (THF) soluble-cyclohexane insoluble fraction was isolated from the quinoline treated coal and purified by three successive dissolution and reprecipitation steps in THF and cyclohexane. Nitrogen analysis of the products showed that the original value of 3.3 percent was reduced to 1.9 percent after three reprecipitation steps. Further reprecipitation resulted in no further decrease in the amount of nitrogen present. Comparing these values with the 1.5 percent nitrogen in the original coal shows two-thirds of the original quinoline incorporated into the coal was removed by the dissolution/precipitation steps. This fraction of the initially retained quinoline is considered to be physically incorporated into the pore structure of the crude quinoline-coal adduct. This quinoline is not readily removed by extraction but is removable by dissolution followed by reprecipitation in excess cyclohexane.

The quinoline remaining in the thrice-reprecipitated product is believed to be bound by hydrogen bonds to acidic sites, presumably phenolic. A comparison of the microautoclave liquefaction behavior of this adduct with a corresponding fraction of the coal obtained by analogous treatment of the coal with 1-methylnaphthalene did not show any significant difference. Inasmuch as the 1-

methylnaphthalene treatment of coal at 200°C could not result in acid-base adduct formation it was concluded that the coal quinoline adduct has no significant effect on subsequent liquefaction.

The possibility of a beneficial effect of the physically incorporated solvent was considered. Physical incorporation of the 1-methylnaphthalene as well as quinoline and blends of these compounds occurs readily at 200°C. These physically incorporated solvents are not removable by extraction, apparently because they enter the fine pore structure of the coal when the coal swells and are then locked into the pores when cooling of the coal solvent slurry causes the pore structure to shrink to near its original dimensions.

The beneficial effect of the solvent pretreatment is therefore believed to be a result of a greater extent of solvent aided liquefaction in contrast to the pyrolytic decomposition of some of the coal that reaches liquefaction temperatures before it is contacted by solvent.

Table 1. Effect of Solvent Pretreatment

(1g coal, 5g solvent, 2000 psig, 425°C)

Coal	Solvent	Pretreatment Time	Pretreatment Temperature	Run Time	THF Solubles (%)
Bruceton	Creosote Oil	None	--	15 min.	61.5
Bruceton	Creosote Oil	1 hour	200°C	15 min.	66.7
Bruceton	SRC-II, H.D.[a]	None	--	15 min.	75.6
Bruceton	SRC-II, H.D.	1 hour	200°C	15 min.	78.2
W. KY 9/14	SRC-II, H.D.	None	--	5 min.	85.7
W. KY 9/14	SRC-II, H.D.	1 hour	200°C	5 min.	88.1
W. KY 9/14	SRC-II, H.D.	15 min.	320°C	5 min.	88.2
W. KY 9/14	Creosote Oil	None	--	5 min.	79.5
W. KY 9/14	Creosote Oil	1 hour	200°C	5 min.	81.8

[a]H.D. = Heavy Distillate

ANALYSIS OF LIGNITE LIQUEFACTION PRODUCTS PROCESSED WITH SYNGAS AND HYDROGEN SULFIDE

Bruce W. Farnum, Sylvia A. Farnum
and Edward F. Bitzan

Grand Forks Energy Technology Center
Box 8213, University Station
Grand Forks, ND 58202

The Grand Forks Energy Technology Center has successfully processed low-rank coals in their continuous processing unit (CPU) in the bottoms recycle mode both with and without added H_2S. The addition of H_2S has been shown to enhance operability and to increase the yield and improve the quality of the distillable oils (1-3).

Products from four runs which compared the effect of added H_2S and different startup solvent were analyzed for H-donor content as a measure of recycle liquid quality and for incorporation of sulfur into organic compounds. The coal processed was a Beulah North Dakota lignite (B3).

The run conditions are shown in Table I and the coal analysis in Table II. Startup solvents included a hydrogenated anthracene oil distillate (HAODI), and surrogate recycle solvent (SS) formulated from an anthracene oil and SRC II middle distillate (4). Syngas was a 1:1 mole mixture of CO and H_2.

TABLE I

CONTINUOUS PROCESS UNIT-SLURRY RECYCLE TEST
RUN CONDITIONS

CPU Run No.	41	65	72	79
Start Up Solvent	HAOD1	SS	SS	SS
Coal	B3	B3	B3	B3
Gas	Syngas	H_2	Syngas	H_2
Temperature, °C	460	460	460	460
Pressure, psi	4000	2600	2600	2600
Added H_2S	No	No	Yes	No

TABLE II

ANALYSIS OF BEULAH NORTH DAKOTA LIGNITE (B3)

Proximate Analysis As-received		Ultimate Analysis Moisture-free	
Moisture	28.84	Ash	16.44
Volatile matter	28.99		
Fixed carbon	30.76	Moisture and ash-free	
Ash	11.70		
Heating value		Carbon	69.49
Btu/lb	6,731	Hydrogen	4.43
		Nitrogen	0.99
		Oxygen (diff)	22.26
		Sulfur	2.81

RESULTS AND DISCUSSSION

Separations of the light oils and recycle slurry ASTM D-1160 distillates were carried out by extraction and silica gel column chromatography as described previously (5). The extraction fractions included two phenolic fractions, a basic fraction and a hydrocarbon fraction. The hydrocarbon fractions were analyzed by quantitative ^{13}C NMR spectroscopy (6) and the phenols were determined by capillary gas chromatography on a 60m DB5 fused silica column (7). No significant differences in concentrations of phenols were noted, and no sulfur was detected in the phenolic fractions.

All of the extracted fractions were tested for mutagenicity (Ames test). The results showed no detectable response to the hydrocarbon and phenolic fractions from either Run 72 (with H_2S) or Run 79 (without H_2S). The activity of the basic fractions was within the expected response region usually associated with coal-derived liquids.

An additional separation of the light oils and recycle slurry ASTM D-1160 distillates was effected by silica gel column chromatography (5). The twelve fractions were analyzed by capillary GC (DB5 60m column) using a post-column splitter with a flame ionization detector (FID) and a flame photometric detector (FPD) specific for sulfur compounds. The concentration of the main sulfur-containing organic compound, dibenzothiophene was essentially the same for the D-1160 ASTM distillates for two of the runs (Runs 72 and 79) which were carried out with and without H_2S, 0.28 and 0.31% respectively. A typical chromatogram is shown in Figure 1. The presence of dibenzothiophene and two C_1-dibenzothiophene isomers was confirmed by capillary GC-MS analysis. The comparative analyses of the light oil column fractions from Runs 72 and 79, with and without H_2S, showed that the light oil from Run 72, to which H_2S was added contained a much larger variety of organic sulfur compounds and also contained elemental sulfur. Elemental sulfur elutes from the silica gel column with pentane in fractions 3 and 4 and gives an excellent response with the FPD but no response with the FID.

Analyses of the ASTM D-1160 distillate column fractions for H-donors indicated that the distillates obtained from Run 72 (H_2S added) yielded the same or higher levels of H-donors even though the partial pressure of hydrogen, P_H , was only about half that of Run 79 without H_2S. Since there is usually a strong dependence of H-donor concentrations on the P_{H_2}, (Table III), this result is apparently due to the presence of H_2S.

TABLE III

COMPARISON OF H-DONOR CONCENTRATIONS AT VARIOUS P_{H_2} WITH AND WITHOUT H_2S, 450°C, P_T = 2600 PSI, (% IN RECYCLE SLURRY ASTM D-1160 DISTILLATE). LIQUEFACTION OF BEULAH (B3) LIGNITE.

Run No.	65	79	72
H_2S	No	No	Yes
P_{H_2} (psi)	2582	1986	1199
H-Donors (%)			
Tetralin	0.85	0.17	0.10
6-Methyltetralin	0.65	0.10	0.64
Dihydrophenanthrene	0.41	0.25	0.40
Tetrahydrophenanthrene	0.19	0.09	0.28
Octahydrophenanthrene	0	0	0.06
Dihydropyrene	0.12	0.02	0.09
Tetrahydropyrene	not determined	0.20	0.34

The presence and variety of organic sulfur compounds present in the products depends on sulfur compounds present in the starting solvent during the first 12-14 passes. Two CPU runs with B3 coal started up with different solvents showed different amounts and varieties of organic sulfur compounds in their distillable oils. Run 40 started up with AOD1 (1.4%S) gave a much more complex FPD sulfur trace for many of the silica gel column fractions than fractions from CPU runs started up with SS (0.4%S). The pattern noted is reproduced in the coal liquids formed (Figure 2).

CONCLUSIONS

1. A method for monitoring the presence of elemental and organic sulfur compounds in distillable low-rank coal liquefaction products utilizing column chromatography and dual detection (FID/FPD) capillary GC has been developed.

2. The addition of H_2S to the continuous processing of Beulah, North Dakota lignite does not increase the amount or variety of sulfur-containing organic compounds in the recycle slurry ASTM-D1160 vacuum distillate products. It does, however, introduce sulfur and a variety of volatile sulfur-containing organics into the light oils condensed from the vapor phase in the reactor.

3. The presence and variety of sulfur compounds after 12-14 reactor passes reflects the introduction of these components in the startup solvent.

4. No increased mutagenicity was observed with the coal liquids processed with H_2S.

5. The production of H-donors in the recycle slurry ASTM D-1160 distillates was enhanced by the presence of H_2S.

BIBLIOGRAPHY

1. Stenberg, V.I., W.G. Willson, D.E. Severson, G.G. Baker, C.L. Knudson, T.C. Owens and J.R. Rindt. GFETC Preprint, Synfuel Tech I. Colorado Springs, CO, 1982.

BIBLIOGRAPHY (Cont'd)

2. Willson, W.G., V.I. Stenberg, D.E. Severson, G.G. Baker, C.L. Knudson, T.C. Owens and J.R. Rindt. Proceedings of the Low-Rank Coal Science Workshop, Houston, TX, 1981.

3. Sondreal, E.A., W.G. Willson, and V.I. Stenberg. Proceedings of the Joint US-Australian Workshop on the Science of Coal Liquefaction, Melbourne, Australia, May 1982.

4. Farnum, S.A., Farnum, B.W., Bitzan, E.F., Willson, W.G. and G.G. Baker, Fuel (in press).

5. Farnum, S.A., and B.W. Farnum, Anal. Chem. 54, 979 (1982).

6. Farnum, S.A., and B.W. Farnum, Preprints ACS Div. of Fuel Chem. 27 (3) 6 (1982).

7. Olson, E.S., S.A. Farnum, B.W. Farnum, D.J. Miller, J.W. Diehl and E.F. Bitzan. Proc. of DOE-OHER Workshop, Chemical Characterization of Hazardous Substances in Synfuels, Seattle, WA, Nov. 1981.

ACKNOWLEDGMENT

We thank Dr. Christopher Reilly of Argonne National Laboratory for the bacterial mutagenesis assays, and David Miller of GFETC for GC-MS analyses. The assistance of Bruce Gebhardt under an Associated Western Universities Student Research participantship is also acknowledged.

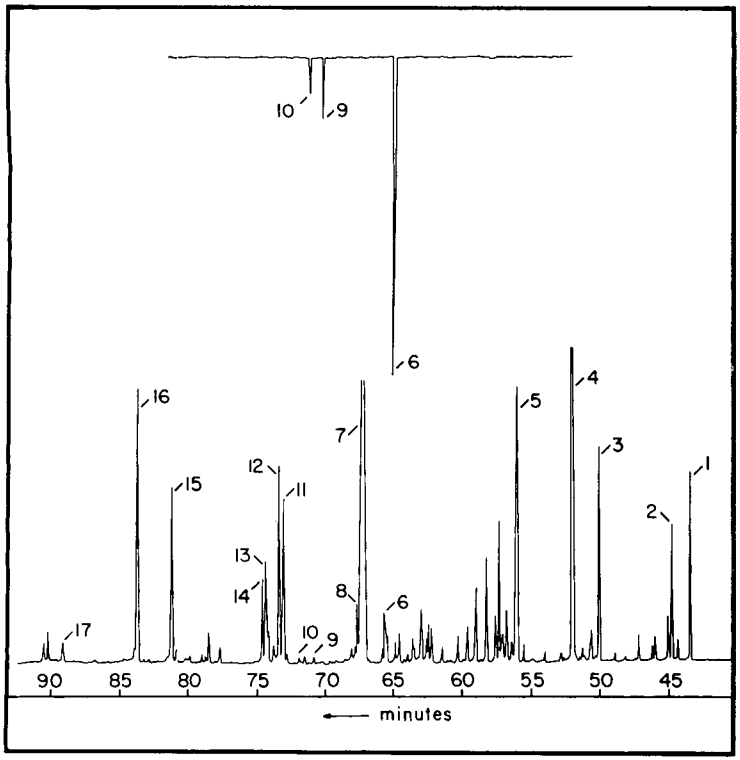

FIGURE 1. Capillary gas chromatography of light oil silica gel chromatographic fraction 7, Run 79, top trace sulfur detection by FPD, bottom trace, FID. 1. biphenyl, 2. 2-methylbiphenyl, 3. 3-methylbiphenyl, 4. dibenzofuran, 5. fluorene, 6. dibenzothiophene, 7. phenanthrene, 8. anthracene, 9. C, dibenzothiophene, 10. C, dibenzothiophene, 11. 3-methylphenanthrene, 12. 2-methylphenanthrene, 13. 4-methylphenanthrene, 14. 1-methylphenanthrene, 15. fluoranthene, 16. pyrene and 17. 2-methylpyrene

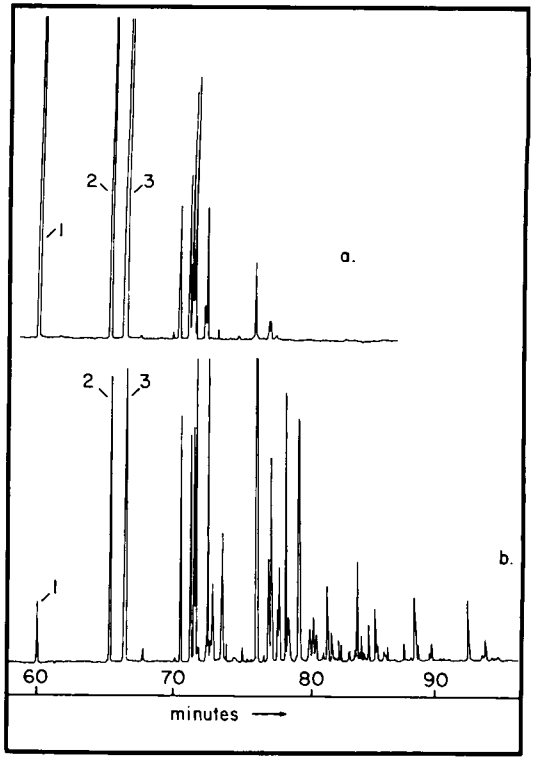

FIGURE 2. Capillary gas chromatography a). FPD trace of silica gel column fraction7 of light oil from Run 41 b). FPD trace of silica gel column fraction 7 of anthracene oil AOD1 startup solvent. (1. dibenzothiophene, 2. Cl-dibenzothiophene and 3. Cl-dibenzothiophene).

ANALYSIS OF THE n-HEPTANE SOLUBLE FRACTION OF COAL HYDROGENOLYSIS PRODUCTS BY HPLC

David M. Bodily, Jason W. Miller and Mark J. England

Department of Fuels Engineering, University of Utah, Salt Lake City, Utah 84112

Liquid products from the hydrogenolysis of coal are very complex and time and cost constraints limit the detail to which they can be characterized. Methods have been developed to separate the complex liquids into classes of chemical compounds and average properties of such fractions are often reported. Many of the separation schemes are adapted from methods applied to petroleum. Solvent extraction has been widely used to separate the liquid into hexane-soluble oils, asphaltenes and pre-asphaltenes (1). Liquid chromatography using ion exchange and clay columns has been used to separate coal liquids(2,3). Neutral oils were further fractionated on columns packed with silica and alumina to produce saturate, 1-ring aromatic, 2-ring aromatic and polynuclear aromatic fractions. Sequential elution by solvents allows separation into a larger number of fractions (4,5).

High performance liquid chromatography (HPLC) offers the potential for detailed yet rapid separation of complex liquid mixtures. Both solvent and column packing can be varied to give the desirable separation. In this research, the heptane soluble fractions from the heavy oil produced by hydrogenolysis of coals have been separated by HPLC and characterized by various analytical methods.

Experimental

The coal-derived liquid samples were obtained from the hydrogenolysis of coals in an entrained-flow reactor (6,7). The reaction was catalyzed with 6% $ZnCl_2$ at approximately 500° C and 12.4 MPa hydrogen pressure. The residence time varied from 20 seconds to 12 minutes depending on the properties of the coal. Seven samples from the study of Garr (6) were selected, as well as one medium volatile bituminous coal. Properties of the coals are listed in Table 1 (6,8). Coals were selected which showed a range of reactivity during hydrogenolysis. The yield of products and the properties of the heptane-soluble fraction are found in Table 2. Conversion is defined as one minus the toluene insoluble fraction. The heavy oil is defined as the material collected in the first condenser of the liquefaction reactor. It consists of the liquids transported in the vapor phase from the hot catch tank, boiling above approximately 100° C. The heavy liquid was extracted in Soxhlet apparatus to obtain the heptane soluble fraction.

The heptane soluble fraction was separated by two HPLC schemes. A Waters modular HPLC system was used with two solvent delivery systems, a solvent programmer, an automated sample injector, a UV absorbance detector, a differential refractometer detector, and a data module. The first scheme employed an NH_2 - μBondapak column. Saturates and non-polar aromatics were eluted with heptane at a flow rate of 2.0 ml/min. After 15 minutes, flow was reversed and a polar fraction was eluted. After 45 minutes, a 90/10 mixture of CH_2Cl_2/C_2H_5OH was introduced to elute a more polar fraction. This method is similar to that employed by Dark and McFadden (9). The second scheme employed a phenyl-μBondapak column and a non-linear gradient. The initial solvent was n-heptane. The gradient involved a 90/10 mixture of CH_2Cl_2/C_2H_5OH mixed with the heptane up to 75% over 36 minutes. A non-polar fraction was eluted by the heptane and a polar fraction was eluted by the gradient.

The heptane-soluble fractions were analyzed by carbon, hydrogen and nitrogen analysis and by vapor pressure osmometry (VPO). A Perkin-Elmer Model 240 CHN analyzer was used for elemental analysis. The VPO measurements were performed in dilute pyridine solutions.

The fractions collected by HPLC separations were analyzed by gas chromatography/ mass spectrometry. A 3% Dexsil 300 on Supelcoport was used for the separation. Approximately 300 mass spectral scans were recorded for each sample. Total ion chromatograms were obtained. Mass chromatograms were obtained for selected fragment masses. The fractions were also analyzed by Fourier Transform infrared techniques.

Results and Discussion

The conversion of the coal to toluene-soluble liquids, water and gases varies from 26% to 86%. The low conversion sample 7 is a lower rank coal and the conversion is mostly due to pyrolysis rather than hydrogenolysis. The residence time of this sample was only 20 seconds, indicating that the sample was blown through the reactor with little reactions. Samples which soften and agglomerate are retained in the reactor for longer times and show greater conversion. A sample with high conversion will pass through the reactor in 2-5 minutes while sample 6 required 12 minutes.

The molecular weight of the heptane-soluble fractions is about 285 and is independent of the degree of conversion or the properties of the starting coals. The hydrogen-to-carbon ratios vary from 1.08 to 1.41. The lower number corresponds to the medium volatile coal, which has a lower H/C ratio than the other coals. These values are averages for the entire fraction and do not indicate the range covered by the sample. More detailed analysis of a sample similar to No. 3 indicated a range of molecular weights of from 200 to 700 and the H/C ratio varied from 0.8 to 1.5 (10).

HPLC separation with the NH_2-μBondapak column produces a non-polar fraction that is eluted with heptane, a polar fraction that is adsorbed on the column and is eluted with heptane by reversing the direction of flow and a more strongly adsorbed fraction that is only removed by a polar solvent. Only the first fraction shows chromatographic separation. The elution pattern for each of the eight samples is very similar, differing only in the relative amounts of the three fractions.

HPLC separation with the phenyl-μBondapak column produces a non-polar fraction which elutes with heptane and a solar fraction that elutes with the increasingly polar solvent gradient. Samples 4, 6 and 8 showed considerable material eluting between the two fractions. The other samples showed only the two, rather distinct peaks. The phenyl-μBondapak column offers the potential for improved separations of the liquids.

The infrared spectra of all non-polar fractions are similar. They show moderate OH stretching near 3400 cm^{-1} and some C=O stretching at 1700 cm^{-1}. The aromatic C-H stretch is weak but there are bands due to aromatic species at 1600 cm^{-1} and 800 cm^{-1} and aliphatic compounds at 1455 cm^{-1}. The polar compounds show a stronger OH absorption and lower carbonyl intensities. The spectra of all polar fractions are similar.

The GC/MS results demonstrate that the non-polar fractions contain alkyl aromatics. The aromatic systems are highly substituted with alkyl chains and saturated rings. The polar groups contain phenols and diphenols in addition. These results agree with previous structural characterization of coal liquids (10, 11,12).

The HPLC separation offers the potential for separating and characterizing coal-derived liquids. However, the samples analyzed in this study did not show major differences, even though they were produced from different coals with different degrees of conversion.

References

1. M. J. Mina, H. Schultz and W. F. McKinstry, Analytical Methods for Coal and Coal Products, Vol. 1, C. Karr, Jr., Ed., Academic Press, New York, 1978, p. 557.

2. J. E. Dooley, G. P. Sturm, Jr., P. W. Woodward, J. W. Vogh and C. J. Thompson, "Analyzing Syncrude from Utah Coal," Bartlesville Energy Research Center, Rept., BERC/RI 7517, August 1975.

3. S. W.Holmes, P. W. Woodward, G. P. Sturm, Jr., J. W. Vogh and J. E. Dooley, "Characterization of Coal Liquids Derived from the H-Coal Process," Bartlesville Energy Research Center Rept., BERC/RI 7610, November 1976.

4. M. Farcasiu, Fuel, 56, 9 (1977).

5. M. Farcasiu, T. O. Mitchell, D. D. Whitehurst, Am. Chem. Soc., Fuel Chem. Div., Preprints, 21(7), 11 (1976).

6. G. Garr, "The Quality of Utah Coals for Synthetic Fuels Production," M.S. Thesis, University of Utah, 1978.

7. G. T. Garr, J. M. Lytle and R. E. Wood, Fuel Proc. Tech., 2, 179 (1979).

8. R. E.Wood and D. M. Bodily, Am. Chem. Soc., Fuel Chem. Div., Preprints, 24(2), 364, (1979).

9. W. A. Dark and W. H. McFadden, J. Chromatogr. Anal., 16, 289 (1978).

10. S. Yokoyama, D. M. Bodily and W. H. Wiser, Am. Chem. Soc., Div. Fuel Chem., Preprints, 21(7) 84 (1976). Accepted for publication in Fuel.

11. S. Yokoyama, D. M. Bodily and W. H. Wiser, Fuel, 58, 162 (1979).

12. S. Yokoyama, N. Tsuzaki, T. Katoh, Y. Sanada, D. M. Bodily and W. H. Wiser, in Coal Structure, M. L. Gorbaty and K. Ouchi, Eds., Adv. Chemistry, Series 192, Am. Chem. Soc., Washington, D.C., 1981, p. 257.

Table 1

Properties of Coals[a]

Sample No.	Coal, Field	Volatile matter, % mafb	H/C	Vitrinite reflectance, %	Inert macerals, %	Rank
1	Beehive, Wasatch Plateau	53.6	0.93	0.556	8.5	HVAB
2	Swisher, Wasatch Plateau	52.3	0.90	0.533	4.5	HVAB
3	Hiawatha, Wasatch Plateau	50.3	0.93	0.547	4.1	HVAB
4	Kaiser, Book Cliff	43.9	0.84	0.714	6.7	HVAB
5	Soldier Creek, Book Cliff	49.2	0.82	0.658	20.7	HVAB
6	Convulsion Canyon, Salina	45.3	0.85	0.502	35.5	HVAB
7	Morby Seam, Coalville	59.0	0.84	0.527	18.1	HVCB
8	Coal Basin (Colorado)	26.0	0.71	--	--	MVB

[a] Data for Samples 1-7 from Reference 6.
Sample 8 from Reference 8.

Table 2

Hydrogenolysis Products

Sample	Conversion,[a] % coal	Heavy oil,[a] % coal	Heptane Soluble Fraction		
			% of Heavy oil	Molecular weight	H/C
1[b]	86.2	67.4	59.0	298	1.34
2	71.0	53.4	47.1	280	1.32
3	79.6	55.3	71.3	289	1.30
4	73.5	60.0	43.3	284	1.39
5	37.3	20.3	49.7	293	1.28
6	53.3	37.8	65.8	280	1.22
7	26.3	7.1	66.7	286	1.41
8	47.5	28.9	53.9	273	1.08

[a] Data from Reference 6.

[b] 3% $ZnCl_2$.

IRON CARBONYL CATALYZED REDUCTIONS OF MODEL COAL CONSTITUENTS UNDER WATER GAS SHIFT CONDITIONS

Thomas J. Lynch, Mahmoud Banah, Herbert D. Kaesz

Department of Chemistry and Biochemistry
University of California, Los Angeles, CA 90024
and
Clifford R. Porter
Pentanyl Technologies, Inc., 11728 Highway 93, Boulder, CO 80303

INTRODUCTION

Liquefaction and heteroatom removal are of importance in adapting coal into fuels and chemical feedstocks which now depend on petroleum. Soluble reagents and catalysts are needed to deal with coal solids. Iron pentacarbonyl has been found to be an economically viable reagent and/or catalyst for up-grading coal; studies of its use in desulfurization and hydrogenation have been reported (1). In fundamental studies at UCLA our objective is to elucidate the reactivity of iron carbonyl under water gas shift (WGS) conditions towards organic substrates that model coal structure. Our work is paralleled by similar studies using a variety of other metal carbonyls, (2) and is preceded by studies of Wender and Orchin and their co-workers using cobalt carbonyl (3,4).

EXPERIMENTAL

Glass reaction vessels, fitted to a 0.3 L copper lined autoclave or a 0.1 L stainless steel autoclave were used for all studies. Reactions were analyzed by extracting the glass liner contents with CCl_4, drying with $MgSO_4$ and removing solvent on a rotary evaporator. Characterization was perfomed by IR, GC, ^1H and ^{13}C NMR and mass spectral methods. Gas sampling above the reaction mixture shows both H_2 and CO_2 (by gas chromatography) indicating that the water gas shift reaction had taken place. Control experiments in which no iron complex was present were performed for all reported reactions. Acridine is the only compound that is significantly hydrogenated under the control conditions; the other substrates are unaffected unless iron carbonyl is also present.

RESULTS AND DISCUSSION

Reactions in methanol, water and base under carbon monoxide pressure were initially performed at 150°C to optimize the iron carbonyl catalyzed water gas shift reaction (5,6) see Table I. Nitrogen heterocycles are readily hydrogenated under these conditions. Quinoline, 1, is 100% hydrogenated in the nitrogen-containing ring. Isoquinoline, 3, is both hydrogenated and N-formylated to 4 (7), similarly in 100% yield. Hydrogenation of only one of the two nitrogen containing rings of the phenanthrolines, is

Table I. Reductions with Iron Carbonyl Catalyzed Water Gas Shift System

Substrate	Product		Yield[a,b]
Quinoline 1	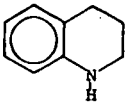	2	100%
Isoquinoline 3	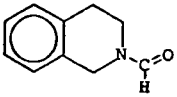	4	100%
Acridine 5	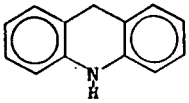	6	100%
4,7-phenanthroline 7	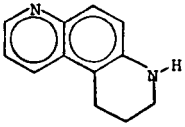	8	75%
1,10-phenanthroline 9	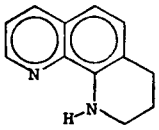	10	50%
anthracene 11	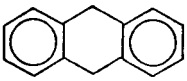	12	25%

[a]Reaction conditions are as follows: 150°C, 42 $kgcm^{-2}$, 15 h in CH_3OH (75 ml) H_2O (25 ml) KOH (4.8 g), substrate (5.0 mmol) and $Fe(CO)_5$ (2.5 mmol).

[b]Under the above conditions but without $Fe(CO)_5$, no reactions are observed.

observed. The yield of **10** is significantly reduced since it forms iron complexes as indicated by a brightly colored aqueous phase partially characterized by ^{1}H NMR of acetone-d_6 extracts. Anthracene is relatively unreactive under these conditions. We have however found ways in which its hydrogenation may be significantly increased, see below. Compounds which we found to be unaffected at 150 °C are naphthalene, phenanthrene, dibenzyl, anisole, diphenyl ether and dibenzthiophene.

In light of the 100% yields observed in the conversions of 1, 3 and 5 these reactions were performed using catalytic amounts of iron carbonyl; the results are listed in Table II. At 150 °C, 22 and 24 molar equivalents each of 3 and 5, respectively, are hydrogenated. At slightly higher temperatures, $Fe(CO)_5$ catalyzes the hydrogenation of 1 with an activity of 43 turnovers.

TABLE II

REDUCTIONS OF NITROGEN CONTAINING HETEROCYCLES USING CATALYTIC AMOUNTS OF $Fe(CO)_5$

SUBSTRATE	RATIO[A]	T/°C	PRODUCT AND TN[B]	
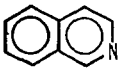	55 : 1	150	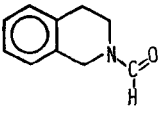	(22)
"	55 : 1	300	"	(14)
			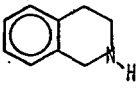	(21)
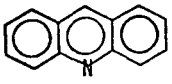	28 : 1	150	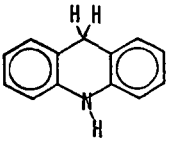	(24)
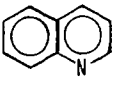	250 : 1	180	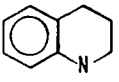	(43)

A) RATIO OF SUBSTRATE TO $Fe(CO)_5$

B) MOL OF PROD./ MOL OF $Fe(CO)_5$

Reactions were next undertaken at 300 °C to parallel coal liquefactions which are observed in higher yield at the higher temperature (8). Using catalytic amounts of $Fe(CO)_5$, isoquinoline is again N-formylated and hydrogenated with a total of 35 turnovers (Table II). Dibenzothiophene, on the other hand, remains unreactive. Other studies at 300 °C are summarized in Table III. The first entry shows that anthracene, when treated by itself is less converted (19%) than it was at 150 °C. It occurred to us that some of the constituents in coal, itself, might affect the catalytic properties of $Fe(CO)_5$. We therefore carried out experiments in which the reduction of anthracene was investigated in the presence of the substances listed in the next four entries in Table III. With these a greater degree of conversion of anthracene to 12 is observed. The

TABLE III

NITROGEN HETEROCYCLES ENHANCING THE HYDROGENATION OF ANTHRACENE TO 9,10-DIHYDROANTHRACENE, 1, AT 300°C. [A]

HETEROCYCLE	YIELD OF 1/ MOL $Fe(CO)_5$
NONE	19%
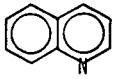	25%
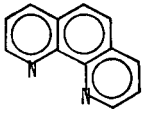	37%
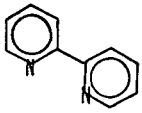	62%
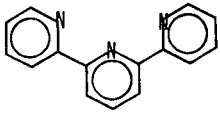	296% (461%)[B]

A) REACTION CONDITIONS AT 300°C : CO, 70 $KGCM^{-2}$, 1 H IN H_2O (2.5 ML), KOH (2.8G), SUBSTRATE (3.0 MMOL), HETEROCYCLE (3.0 MMOL) AND $Fe(CO)_5$(3.0 MMOL).

B) CO, H_2O AND KOH AS ABOVE BUT WITH PHASE TRANSFER CATALYST ADDED: Me_4NCl (1.5 MMOL); OTHER CONSTITUENTS, $Fe(CO)_5$ (1.5 MMOL); TERPYRIDINE (1.5 MMOL); ANTHRACENE (15 MMOL).

nitrogen heterocycles are thus beneficial to reductions catalyzed by iron pentacarbonyl while quinoline and phenathroline are themselves undergoing conversion to partially hydrogenated (and/or N-formylated) products. Notably, the nitrogen heterocycles phenathroline, dipyridyl and terpyridyl which may participate as chelating ligands on iron were more effective for hydrogenation of anthracene than quinoline.

The effect on the reduction of anthracene of a phase transfer catalyst added either by itself or together with dipyridyl is summarized in Table IV. In such additions, dramatic increases are observed in the reduction. Such results at 300°C contrast the work of Alper and co-workers who at room temperature observed no benefit of a phase transfer agent in the reduction of aromatic nitro compounds by $Fe(CO)_5$ (or $Fe_2(CO)_9$) (9). The presence of tetrabutylammonium iodide increases the yield of 9,10-dihydroanthracene 44 times. Combining Bu_4NI and dipyridyl with $Fe(CO)_5$, gives the greatest reduction of anthracene, 17.1 turnovers.

The role of the phase transfer catalysts is most likely to increase the base concentration in the vicinity of the iron catalyst and further, to solubilize the anionic iron intermediates in the organic phase. The last entry in Table IV represents an experiment where the tetraalkylammonium phase transfer catalyst and the base are combined in the form of Me_4NOH. With this reagent the product yield is comparable to that originally achieved with 42 equivalents of KOH.

TABLE IV

EFFECT OF PHASE TRANSFER AGENTS AND PHASE TRANSFER AGENTS WITH DIPYRIDYL FOR ENHANCING THE HYDROGENATION OF ANTHRACENE TO 9,10-DIHYDROANTHRACENE, 1[A]

PHASE TRANSFER AGENT	TURNOVER[B]	TURNOVER W/DIPYRIDYL
NONE	0.32	0.62
Me_4NCL	1.0	3.0
$BzEt_3NCL$	-	1.3
Bu_4NI	14.2	17.1
Me_4NOH[C]	0.54	

[A]CONDITIONS AS BEFORE AT 300°C

[B]MMOL OF 1/MMOL OF $Fe(CO)_5$

[C]KOH EXCLUDED FROM THIS REACTION.

Some preliminary experiments to elucidate the principal catalyst species in solution and mechanistic features of the reductions were undertaken. To determine the principle iron carbonyl species at reaction conditions, aliquots were withdrawn from the autoclave at 175° C. IR spectra of these obtained within 3 min of sampling indicate that $HFe(CO)_4^-$ is the principal iron carbonyl species (10).

Since the principal species may not be the catalytically active species some other possible candidate complexes were tested as catalysts; these are shown in Table V. All proved inferior to $Fe(CO)_5$ even in the presence of dipyridyl. Of special significance is that cluster compounds, which are known to constitute thermal degradation products of metal carbonyls, were equally less effective as the loaded forms of the catalyst than iron pentacarbonyl.

TABLE V

COMPARISON OF IRON(0) COMPLEXES FOR THE HYDROGENATION OF ANTHRACENE TO 9,10-DIHYDROANTHRACENE, 1[A]

COMPLEX	TURNOVER[B]	TURNOVER W/DIPYRIDYL
$Fe(CO)_5$	14.2	17.1
$Fe(COT)(CO)_3$	7.1	
$Fe_3(CO)_{12}$		3.4
$(Et_3NH)[HFe_3(CO)_{11}]$		11.2

A CONDITIONS AS BEFORE AT 300°C

B MOL EQUIV OF 1/EQUIV OF IRON(0)

Finally, we tested dimethylanthracene to elucidate whether a cis-concerted addition or some other process were taking place in the hydrogenation (11). Our results are shown in reaction 1.

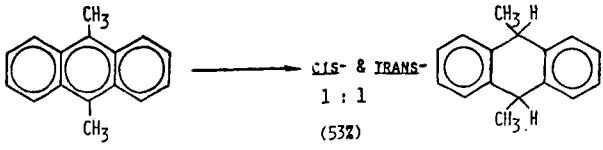

1)

We observe a 48%:52% mixture of the cis and trans isomers suggesting that either an electron transfer or hydrogen atom transfer is the initial step of reduction. The reduction potentials of a number of the compounds studied and their ability to be reduced under iron carbonyl catalyzed WGS conditions is shown in Table VI. A correlation is seen among these data, (12), supporting an electron transfer process as the initial step in the reduction of the aromatics.

TABLE VI

CORRELATION OF HYDROGENATIONS UNDER $Fe(CO)_5$ CATALYZED WGSR WITH $E_{\frac{1}{2}}$ VS SCE

SUBSTRATE		$E_{\frac{1}{2}}$/V	
	PYRIDINE	-2.52	NOT REDUCED
	NAPHTHALENE	-2.50	"
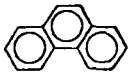	PHENANTHRENE	-2.45	"
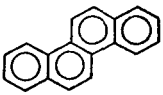	CHRYSENE	-2.32	"
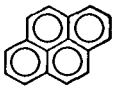	PYRENE	-2.11	"
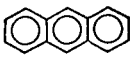	ANTHRACENE	-1.94	REDUCED IN MIDDLE RING
	QUINOLINE	-1.14	REDUCED IN NITROGEN-CONTAINING RING
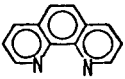	1,10-PHENANTHROLINE	1.06	"

CONCLUSION

Iron pentacarbonyl catalyzes the hydrogenation of nitrogen heterocycles regioselectively in the nitrogen containing ring and anthracene is hydrogenated in the middle ring under water gas shift conditions above 150 °C. Chelating nitrogen heterocycles activate the $Fe(CO)_5$ toward anthracene hydrogenation. Phase transfer catalysts also have a pronounced enhancement effect on all reductions. There is thus high potential in use of iron pentacarbonyl in hydrogenations when activated by appropriate synergistic agents. Preliminary studies suggest that these reductions proceed by an initial electron transfer process from $HFe(CO)_4^-$.

ACKNOWLEDGMENT

This work performed at UCLA was supported in part by a grant from the National Science Foundation (CHE-79-08406). We thank the University of Riyad, Saudi Arabia, for a Sabbatical Leave Fellowship to Prof. M. Banah.

REFERENCES

(1) C. R. Porter, H. D. Kaesz, J. L. Leto, T. J. Giordano, W. R. Haas, E. Johnson, and W. H. Berry Jr., Coal Processing Technology 1981, 7, 135; C. R. Porter and H. D. Kaesz, U.S. Patent Appl. 189,087 Sept. 22, 1980; idem. U.S.Patent Appl. 207,714 Nov. 17, 1980.

(2) R. H. Fish, A. D. Thormodsen, G. A. Cremer, J. Am. Chem. Soc. 1982, 104, 5234.

(3) S. Friedman, S. Metlin, A. Svedi and I. Wender, J. Org. Chem. 1959, 24, 1287.

(4) M. Orchin, Acc. Chem. Res. 1981, 14, 259.

(5) K. Cann, T. Cole, W. Slegeir and R. Pettit, J. Am. Chem. Soc., 100 1978 3969.

(6) A. D. King Jr., R. B. King and D. B. Yang, J. Am. Chem. Soc. 1980, 102, 1028.

(7) B. D. Dombek and R. J. Angelici, J. Catal. 1977, 48, 433.

(8) C. R. Porter, R. L. Bain, C. M. Rastle, K. L. Brownlee-Gast, M. McDougall, T. J. Lynch and H. D. Kaesz, paper presented at the International Coal Conversion Conference, Pretoria, August 16-20, 1982.

(9) H. des Abbayes and H. Alper, J. Am. Chem. Soc. 1970, 99, 98; H. Alper, Adv. Organomet. Chem. 1981, 19, 183.

(10) F. Wada and T. Matsuda, J. Organomet. Chem. 1973, 61, 365.

(11) H. C. Kang, C. H. Mauldin, T. Cole, W. Slegeir, K. Cann, and R. Pettit J. Am. Chem. Soc. 1977, 99, 8323.

(12) H. O. House, M. J. Umen J. Am. Chem. Soc. 1972, 101, 5495.

THE ORGANIC CHEMISTRY OF CALCIUM: A NEW PHENOL SEPARATION/RECOVERY APPROACH

Richard H. Schlosberg and Charles G. Scouten

Corporate Research Science Laboratories
Exxon Research and Engineering Company
P.O. Box 45, Linden, New Jersey 07036

INTRODUCTION

Phenols (e.g. phenol,cresols, xylenols) comprise a significant fraction of most coal liquids. Alkylphenols alone comprise up to 20 wt% of the liquid products from such direct coal liquefaction processes as H-Coal, Solvent-Refined Coal (SRC) and the Exxon Donor Solvent (EDS) process. The toxic, corrosive and chemically reactive nature of phenols is a potential source of problems in the direct utilization of coal liquids as synthetic fuels.

One of the more common schemes for separating phenols from coal liquids involves treatment with aqueous caustic to produce water-soluble sodium phenates. After separation of the raffinate, treatment of the sodium phenate solution with an acid, such as carbon dioxide, can be used to reconstitute the phenols.(1) One major difficulty with this method is the co-extraction of non-phenolic organic materials into the aqueous phase along with the phenols. These co-extracted organics can subsequently appear as impurities in the recovered phenols, thereby rendering the phenolic stream sufficiently impure to preclude its use as a chemical feedstock for the production of polymers or polymer intermediates. This paper describes new organocalcium chemistry which allows separation and recovery of phenols from hydrocarbon streams, and which avoids the difficulties descussed above.

EXPERIMENTAL SECTION

All manipulations were carried out under a nitrogen atmosphere to exclude carbon dioxide and oxygen. Transfers of solids were performed in a glove box. A small positive pressure of nitrogen was maintained during half-salt preparations, using a mineral oil bubbler as a pressure relief. A Perkin-Elmer Model TGS-2 Thermogravimetric System, or a comparable unit assembled from components, was used for TGA studies. Under argon, the TGA oven was programmed from ambient to 850°C at 10°C/min, then heating was continued at 850°C under air for residue combustion. Elemental analyses were performed by personnel of the ER&E Analytical and Information Division.

Materials.

Commercially obtained solvents and reagents were of analytical reagent quality and were used as-recieved. Sodium phenate and potassium phenate were prepared from phenol and the corresponding hydroxide, as described by Kornblum and Lurie.(7)

Preparation of Calcium Half-Salt of Phenol in Aqueous Slurry.

A two-liter flask was charged with 37.0 g of calcium hydroxide (0.50 mole), 47.0 g of phenol (0.50 mole) and 1 liter of carbon dioxide-free water. The flask was fitted with a magnetic stirring bar, and a condenser which was connected to a low-pressure nitrogen source. The stirred reaction slurry was heated at 85-90°C for 16 hr, then filtered while still hot. The product was isolated by evaporating the filtrate to dryness under reduced pressure, then drying the solid to constant weight under vacuum. The yield of calcium half-salt was essentially quantitative, 74.4 g (theoretical yield: 75.1 g).

The elemental composition of the product is given in Table I.

Preparation of Calcium Half-Salt of Phenol in Benzene.

The reaction of calcium hydroxide with excess phenol in benzene is described to illustrate the general procedure used to prepare half-salts in organic media.

A 500-ml Erlenmeyer flask was charged with 9.91g of calcium hydroxide (134 mmol), 25.2 g of phenol (268 mmmol, 2-fold molar excess) and 450 ml of benzene, then attached to a low-pressure nitrogen source. The reaction slurry was stirred for 72 hr at ambient temperature then filtered, washing the filter cake thoroughly with benzene to remove unreacted phenol. The resulting solid was dried to constant weight at 50°C under vacuum to give 18.8 g of the calcium half-salt (93% of the theoretical yield, 20.1 g) as a fluffy, white powder (Found: 47.39% C, 3.97% H, 25.94% Ca, 22.13% O by NAA; Calculated: 47.98% C, 4.03% H, 26.69% Ca, 21.31% O).

The TGA of this product is shown in Figure 1. An X-ray analysis (powder pattern) indicated that no significant amount of calcium hydroxide remained. No weight was lost when a 5-g sample of the solid was extracted for 72 hr with ether in a Soxhlet apparatus, and no phenol was found by GC analysis of the ether extracts.

Pyrolysis of Calcium Half-Salt of Phenol.

The pyrolysis of the calcium half-salt of phenol at 650°C for 60 min. is described to illustrate the general procedure used for pyrolyses in the minipyrolyzer (Figure 2).

In a nirogen-flushed glove box, the quartz retort was charged with 1.55 g of the phenol half-salt (10.3 mmol) and a gas bag was attached to the condenser vent. Dry Ice was added to cool the condenser, and the retort was plunged into the preheated block which was maintained at 650°C. After 1 hr, the retort was removed from the block and the condenser was allowed to warm to room temperature. The gas bag, which contained only a small amount of gas was removed and discarded. The retort contained 0.61 g of residue (39% of the charge, theoretical amount of CaO: 0.59 g). From the condenser, 0.93 g of liquids (60% of the charge, theoretical amount of phenol: 0.97 g) was recovered using a small amount of methylene chloride solvent. Analysis by GC indicated that phenol (97%) and a trace of diphenyl ether comprised the liquid products. Thus, a 94% phenol recovery and a nearly quantitative mass balance were obtained in this experiment.

Preparation of Calcium Diphenate in Toluene.

To a one-liter, round-bottommed flask was charged 7.41 g of calcium hydroxide (100 mmol), 23.5 g of phenol (250 mmol) and 700 ml of toluene. The flask was fitted with a magnetic stirring bar and a Dean-Stark trap to which was fitted a reflux condenser connected to a low-pressure nitrogen source. The stirred reaction mixture was heated under reflux for 72 hr, then filtered. Solvent was evaporated under reduced pressure, and the resulting brown solid was dried to constant weight under vacuum at 50°C. The yield of calcium diphenate was 15.14 g (70% of the theoretical yield of 22.63 g; Found: 61.86% C, 4.48% H; Calculated: 63.70% C, 4.45% H, 17.71% Ca, 14.14% O).

RESULTS AND DISCUSSION

When analytical reagent grade phenol was treated with an equimolar amount of calcium hydroxide in a water slurry at 85-90°C, a salt was formed which was not calcium diphenate, PhO-Ca-OPh, as shown in Table I. Instead, the data are consistent with formation of the calcium half-salt, PhO-Ca-OH (Eq. 1). This compound had previously been prepared by treating calcium diphenate with a mixture of carbon monoxide and hydrogen at 105 - 110°C.(2)

$$\text{Ph-OH} + \text{Ca(OH)}_2 \xrightarrow{25 - 100°C} \text{Ph-O-Ca-OH} + \text{H}_2\text{O} \qquad (1)$$

Calcium half-salts can also be prepared in organic media. The products obtained by reacting a two-fold excess of phenol with calcium hydroxide in benzene, toluene, xylene, pentane or cyclohexane slurries at 25°C were identical to those of the half-salt obtained in water. Thus, formation of calcium half-salts is a general reaction, and is not specific to the aqueous medium.

Under the mild conditions discused above, the calcium phenol half-salt is not sufficiently basic to react with additional phenol to form calcium diphenate. In a toluene slurry, calcium diphenate could, however, be obtained under forcing conditions: 72 hr under reflux with continuous separation of water (Dean-Stark trap).(3) The product was isolated by evaporating to dryness under reduced pressure. Calcium diphenate so produced was readily soluble in a variety of organic solvents including benzene, toluene, xylene and ether. In contrast, the calcium half-salt of phenol was insoluble in these solvents, and in dipolar aprotic solvents, such as tetrahydrofuran, N,N-dimethylformamide and N-methylpyrrolidone. Further support for the proposed half-salt structure was obtained from X-ray diffraction (powder pattern) experiments, which indicated the absence of calcium hydroxide in the product. Extraction of the product salt with ether in a Soxhlet apparatus failed to remove phenol, thereby ruling out the possibility of physically adsorbed phenol and confirming the half-salt structure.

The thermal chemistry of the calcium half-salt of phenol is most interesting. When the material was heated at a programmmed rate of 10°C/min in a thermogravimetric analyzer (TGA) under argon, it was stable to about 450°C (Figure 1).(1) Upon continued heating, devolatilization of the sample occurred (450-650°C) with a weight loss corresponding to the loss of phenol. An X-ray diffraction analysis of the 650°C residue revealed that calcium oxide and some calcium hydroxide were present. Further heating to 850°C in the presence of air led to a very small additional weight loss and to a residue which X-ray analysis showed to be essentially pure calcium oxide. Both at 550°C and 650°C in a small, batch pyrolysis apparatus (minipyrolyzer, Figure 2) the calcium half-salt of phenol yields phenol as the major volatile organic product (Equation 2). Table II summarizes the pyrolysis data.

$$\text{Ph-O-Ca-OH} \xrightarrow{\text{Pyrolysis at 550-650°C}} \text{Ph-OH} + \text{CaO} \qquad (2)$$

In a similar manner, the calcium half-salt of p-cresol was prepared. Thermal stability of the p-cresol half-salt is comparable to that of the phenol half-salt, but the presence of the side chain alters the distribution of products on pyrolysis, as shown in Table III. At the lower pyrolysis temperature of 550°C, cresols are the only significant products, though conversion is slow. At 650°C however, thermal cracking reactions become important. In this case, both hydrogen and methane were found in the gas product. Phenol, presumably produced by thermal dealkylation, was found in the liquids, along with the cresols.

These results are in sharp contrast to the pyrolyses of sodium phenate and potassium phenate, which under comparable conditions yield a char and gas, but essentially no volatile liquid organic products.(2,4)

The unexpected results with the organocalcium system suggested a new phenol separation and recovery approach based on the reactions shown in Equations 1 and 2. We have demonstrated phenol recovery via this half-salt technique, using both model compounds and raw naphtha from the EDS coal liquefaction process.(5,6)

CONCLUSIONS

The reaction of calcium hydroxide with phenols in aqueous or organic media provides a simple method for preparing the corresponding calcium phenol half-salts. In sharp contrast to pyrolyses of alkali metal phenates which yield gas and char, pyrolyses of calcium phenol half-salts yield calcium oxide and phenols. The unexpected results with the organocalcium system suggested a new phenol separation/recovery approach.

ACKNOWLEDGEMENTS

The authors are grateful to Drs. Martin L. Gorbaty, Daniel R. Neskora and Richard P. Rhodes for their enthusiastic support. We acknowledge the excellent technical support of H. Warren Dougherty, Constance A. Cook, Argo Kurs and Paul J. Szajowski.

REFERENCES

1. F. Fischer and U. Erhardt, Ges. Abhandl. Kenninis. Kohle., 1919, 4, 237.

2. F. Sseliwanow, J. Russ. Phys.-Chem. Soc., 1913, 45, 1535.

3. The preparation of calcium diphenate under somewhat different conditions is decribed by H. D. Kluge and K. Drake, U.S. Patent 2,870,134 (1959 to The Texas Company).

4. Key results reported in Reference 1 have been confirmed by L. Matty and by M. Siskin of this laboratory.

5. L. E. Furlong, E. Effron, L. W. Vernon and E. L. Wilson, Chem. Eng. Progr., 1976(Aug.), p.69.

6. R. H. Schlosberg and C. G. Scouten, U.S. Patent 4,256,568 (March 17, 1981).

7. N. Kornblum and A. P. Lurie, J. Amer. Chem. Soc., 1959, 81, 2710.

Table I. Elemental composition of the salt obtained from calcium hydroxide and phenol in an aqueous slurry at 85-90°C.

	$Ca(OPh)_2$	PhO-Ca-OH	Calcium Salt
Element	Calculated, Wt%	Calculated, Wt%	Found, Wt%
Carbon	63.7	48.0	46.0 (±0.4)
Hydrogen	4.4	4.0	3.89 (±0.04)
Calcium	17.7	26.7	26.8 (±0.4)

Table II. Pyrolysis of the calcium half-salt of phenol in the minipyrolyzer gives phenol and calcium oxide.

Temperature, °C	Residence Time, minutes	Product Yields, Wt% Solid	Product Yields, Wt% Liquid	Liquid Yield, % of Theoretical	Liquid Analysis, Wt% Ph-OH	Liquid Analysis, Wt% Ph-O-Ph
550	5	77 (±1)	24 (±2)	38	97 (±2)	Trace
650	5	60 (±2)	39 (±2)	62	94 (±1)	2
650	60	40 (±2)	60 (±2)	96	97 (±1)	Trace

Table III. The side chain alters product distribution in the pyrolysis of the p-cresol half-salt.

Temperature, °C	Residence Time, minutes	Product Distribution, Wt% Solid	Product Distribution, Wt% Gas	Product Distribution, Wt% Liquid	Liquid Yield, % of Theoretical	Liquid Analysis, Wt% Phenol	Liquid Analysis, Wt% Cresols
550	5	92	---	8	12	--	98
650	5	61 (±1)	4 (±3)[a]	35 (±3)	59	24 (±1)	38 (±3)

(a) Approximately 80 wt% methane and 16 wt% hydrogen by mass spectrometric analysis.

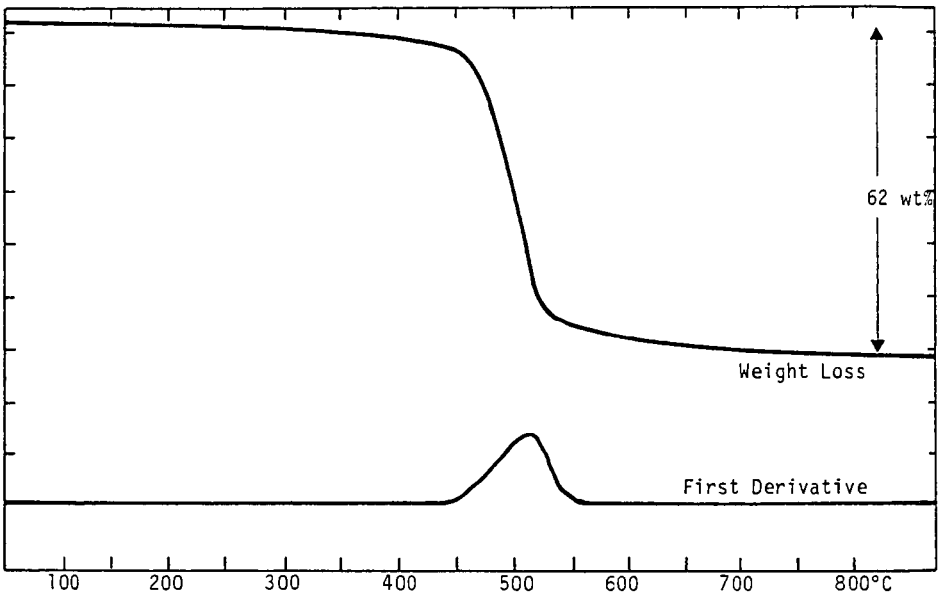

Figure 1. The weight lost during TGA of the calcium half-salt of phenol corresponds to loss of phenol.

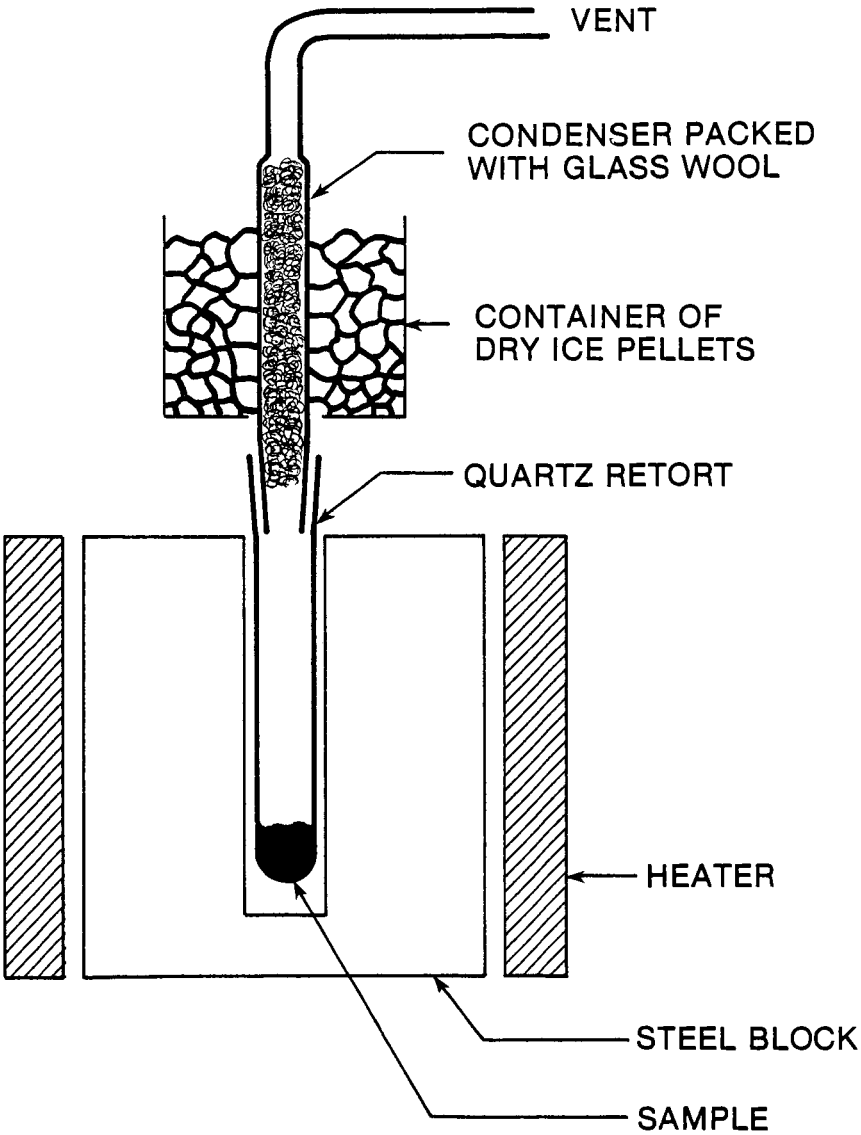

FIGURE 2. MINIPYROLYZER

Rapid Determination of Bitumen, Varsol and Other Solvents Using Proton N.M.R.

A. MAJID and J. WOODS

Division of Chemistry, National Research Council of Canada
Ottawa, K1A 0R6

Introduction

The extensive Athabasca oil sands are assuming an increasing role in supplying Canada's liquid hydrocarbon needs. One commercial plant, Suncor Inc., has operated since 1967. It extracts bitumen from the oil sands and subsequently upgrades to synthetic crude oil. Syncrude Canada Ltd. which is designed to produce 109,000 barrels of synthetic crude per day, began production in 1978. Fundamental to the successful utilization of this oil sand resource and to the economic operation of the extraction plant is a reliable analytical method for the analysis of bitumen rich froth collected from the hot water extraction process. This froth must be further treated to remove solid particles and water. The purification process consists of a diluent addition step to lighten the hydrocarbon density, two centrifuging stages to remove solids and water, and a diluent recovery step. Analytical inspection of these process streams includes analysis for bitumen, diluent, water and solids. The analyses are needed for process control and material balance calculations.

The current determination of bitumen, diluent, water and solids is performed by separating the sample into the individual components. The solvent/hydrocarbon solution must be further analyzed for diluent (naphtha) and bitumen content. Bitumen is usually determined spectrophotometrically while diluent (naphtha) is either determined by difference or by G.C. (2). The most common problems with these methods are the greater sources of errors involved (2). If the naphtha is determined by difference all the errors will accumulate in the results for this component. In the G.C. method errors will arise from dilution and the small volume required for injection (1 µl) (2). Also the adsorption of asphaltenes from bitumen on the column packaging materials limits the use of G.C. for the estimation of the diluent in the presence of bitumen.

In this paper we report the proton nmr results for the quantitative estimation of bitumen and a diluent (naphtha or varsol) in the presence of toluene, benzene or methylene chloride, three commonly used solvents for the extraction of bitumen from oil sands.

Experimental Methods

a) Proton nmr measurements were performed on a Varian EM-360 nmr spectrometer (60 MHz); 500 µl of solution was used in each case in a 5 mm internal diameter tube. Carbon tetrachloride or tetrachloroethylene was used as solvent. Gain and amplitude were adjusted to give integrations within the range of the chart paper using lowest and highest concentrations. Once adjusted all the parameters were kept constant for subsequent measurements. Integration limits for the aromatic region of benzene, CH_2-group of methylene chloride and

the CH_3-group of toluene are well defined and can be easily measured. However, it is difficult to decide the starting point for the integration for the methyl region of bitumen, varsol or naphtha at ca. 1.0 ppm downfield from tetramethylsilane. This is because of the overlap of the methylene and methyl regions. It was therefore decided to take the mid point of the two peaks (methyl and methylene) as the start for the integration. The integration limits for methyl regions were therefore as illustrated in fig. 8a. Proton nmr spectra for bitumen, varsol, bitumen + varsol, toluene, benzene, methylene chloride, bitumen + varsol + toluene and bitumen + varsol + benzene are shown in figures 6-8 to illustrate the portions integrated for calibration curves.

b) Preparation of Standard Bitumen Solution: Bitumen was extracted from a sample of high grade oil sand using toluene in a Soxhlet apparatus (2). Non-filtered solids were removed from the bitumen solution by passage through a 0.45 μm millipore filter paper. The solvent was removed in a Brinkmann rotary evaporator at 100°C under reduced pressure. The total time required to remove the solvent from a 100 gram sample was less than one hour. The residual solvent was then measured using infrared spectroscopy (3) and proton nmr.

c) Calibration Curves: (1) Bitumen: - A standard sample of the bitumen required for the calibration curve was prepared as outlined above. The amount of the residual toluene quantitatively determined by infrared and proton nmr, was applied as a correction to the bitumen content. A stock solution (35.0% w/v) of bitumen in carbon tetrachloride and another in tetrachloroethylene were prepared from the standard bitumen accurately weighed to the nearest 0.0001 gram. Serial dilutions of bitumen, ranging in concentration from 3-35%, were prepared and the areas of the methyl peaks were determined from the integration of the peaks at ca. 1.0 ppm downfield from tetramethylsilane in the proton nmr spectrum. A plot of the per cent bitumen vs area of the methyl peak produced a straight line passing through the origin, with a slope of 0.51.

$$\% \text{ Bitumen} = \frac{\text{Area of the methyl peak}}{0.51}$$

(2) Diluent: Measurements were made for two bitumen diluents, namely naphtha and Varsol (Stoddard solvent). Solutions of both naphtha and Varsol ranging in concentrations from 3-60% w/v were prepared. Areas of the methyl peaks at ca. 1.0 ppm downfield from tetramethylsilane were determined as described above for bitumen. The plots of the per cent naphtha and Varsol vs area of the methyl peak produced straight lines passing through the origin. Slopes for the two plots were 1.17 and 0.95 for % w/v concentrations and 0.85 and 0.75 respectively for % v/v concentrations. The concentration of the diluent was determined as follows:

$$\% \text{ Diluent} = \frac{\text{Area of methyl peak}}{\text{Slope}}$$

(3) Toluene, Benzene and Methylene Chloride: Carbon tetrachloride solutions of toluene, benzene and methylene chloride were prepared ranging in concentrations from 1-20% (10% in the case of benzene). Areas of the methyl peak for toluene, CH_2-peak for methylene chloride and aromatic peak of benzene were measured from their proton nmr spectra. Plots of per cent concentration vs areas were straight lines in each case. The concentrations were calculated using the following equations.

$$\% \text{ (v/v) of Toluene} = \frac{\text{Area of the methyl peak}}{5.64}$$

$$\% \text{ (v/v) of Benzene} = \frac{\text{Area of the peak from proton nmr}}{13.75}$$

$$\% \text{ (v/v) of Methylene Chloride} = \frac{\text{Area of } -CH_2 \text{ peak}}{5.64}$$

(d) Determination of Varsol/Bitumen in a mixture.

Area of the methyl peak, measured as outlined in 1 or 2 above, represents the total area due to contributions from both diluent and bitumen. Bitumen concentration was separately determined photometrically by measurements of absorption at 530 nm. Knowing the concentration of bitumen the area of the methyl peaks due to bitumen can be determined from the equation in 1 above.

$$\text{Area of the methyl peaks in bitumen} = 0.51 \times \% \text{ (w/v) Bitumen}$$

Concentration of the diluent can then be calculated as follows:

$$\frac{\text{Total Area of the methyl peak} - \text{Area due to bitumen } CH_3 \text{ group}}{\text{slope}}$$

Results and Discussion

The calibration curves for benzene, toluene, methylene chloride, bitumen and diluents (Suncor naphtha and Varsol) are shown in figures 1, 2 and 3. All plots are good straight lines with zero intercepts. This is indicative of the existence of a linear correlation between the per cent concentrations and the area of the proton nmr signals emphasising the usefulness of proton nmr in the quantitative estimation of concentrations.

The measurements involving bitumen and diluent were performed independently in two solvents, carbon tetrachloride and tetrachloroethylene. Results were found to be independent of the solvent indicating no loss due to evaporation of the carbon tetrachloride during the period of measurement. Benzene, toluene and methylene chloride were only studied in carbon tetrachloride.

Procurement of unaltered standard samples of bitumen from oil sands is a serious problem recognised by Clark in 1950 (1). Oil does not separate from the native sands and water without the use of either chemical agents, solvent, heat or extreme mechanical force, all of which may significantly alter the oil. Since no method of separation exists that can guarantee an oil sample free from alteration, the first problem encountered in obtaining a standard sample of bitumen is the development of an acceptable separation procedure. Of the various separation methods, solvent extraction of bitumen from oil sands has been recommended as the most suitable method for this purpose (3).

The major drawback of solvent extraction methods is the fact that it is not practical to completely remove all residual solvent from the bitumen. Hence analytical techniques are required to determine the residual solvent concentration. Again proton nmr is found to be very useful for determining commonly used protonated solvents such as toluene, benzene and methylene chlorides.

Concentrations of toluene, benzene and methylene chloride determined from proton nmr compare reasonably well with the actual

values. Accuracy of the nmr method is evident from the values of the standard deviations of ± 0.116, ± 0.177 and ± 0.318 respectively. A plot of Actual vs Found concentrations is shown in fig. 4. In the case of benzene or toluene the zero intercept and slope of 1 are indicative of good accuracy. In the case of methylene chloride significant errors are introduced because of the high volatility of this solvent (b.p. 39.8°C) which makes it difficult to prepare standard solutions because of evaporative losses. Hence a much higher relative standard deviation of ±1.033 with respect to least squares plots of data at different concentrations. To remedy the problem of evaporation of the solvents from the nmr tubes we find it helpful to use teflon stoppers rather than regular plastic caps. Besides reducing evaporation the teflon caps are more resistant to solvent attack, particularly by the chlorinated solvents.

Rapid and reliable determination of diluent (Varsol/Naphtha) in bitumen/diluent mixtures is essential for process control and material balance calculations both in hot water process and solvent extraction spherical agglomeration process for the extraction of bitumen from oil sands. The traditional methods for the determination of diluent do not give the required degree of accuracy. The concentrations of Varsol as determined from proton nmr measurements are shown in fig. 5 as a plot of the actual concentrations against calculated concentrations. Zero intercept and a slope of 1 indicates a very good linear co-relation. A standard deviation of ±0.281 (wt.%) was calculated for these results. This again demonstrates the accuracy of the nmr method. Advantages of the nmr method include higher precision, shorter analysis time (actual analysis time ca. 2 minutes), broader range of applicable concentrations (0.2-70%) and small quantity of the non-consumable sample needed for analysis (500 µl).

Bitumen and diluent can be determined separately by proton nmr, in all the common solvents, e.g. benzene, toluene, methylene chloride, carbon tetrachloride and other non-protonated solvents. The results are at least as accurate as obtained by other methods.

One of the peaks of the diluent spectrum overlaps with the methyl peak for toluene. Also, there is an overlap between the aromatic region of the benzene and diluent. Hence, an accurate determination of the concentrations of benzene or toluene in presence of diluent is not possible using this method. However, the presence of toluene or benzene does not effect the determinations of the concentrations of bitumen or diluent.

References:

(1) Ward, S.H. and Clark, K.A., Report No. 57. Alberta Research Council, (1950).
(2) Syncrude Analytical Methods for Oil Sand and Bitumen Processing. 1979.
(3) L.D.L. Vorndran, A.J. Serres, J.K. Donnelly, R.G. Moore and D.W. Bennion. Can. J. Chem. Eng. Vol. 58, 1980, p. 580.

Acknowledgment

Several helpful discussions with Drs. D.W. Davidson, B.D. Sparks and J.A. Ripmeester are gratefully acknowledged.

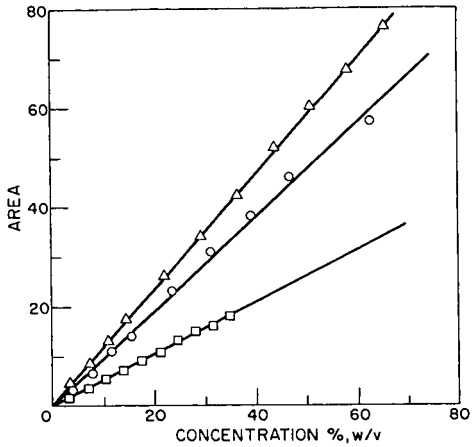

Fig. 1. Calibration Curves. Concentrations ($\frac{v}{v}$%) vs area of the ^{1}H nmr peaks. Benzene ○ ; Toluene □ ; methylene chloride △.

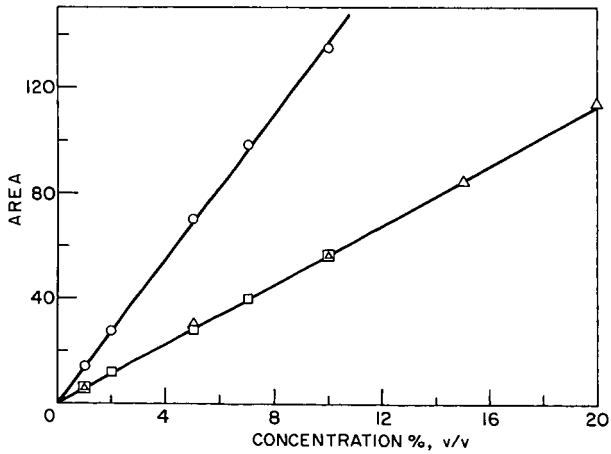

Fig. 2. Calibration Curves. Concentrations ($\frac{w}{v}$%) vs area of the methyl proton nmr peaks. Bitumen □ ; Stoddard solvent ○ ; Suncor Naphtha △ .

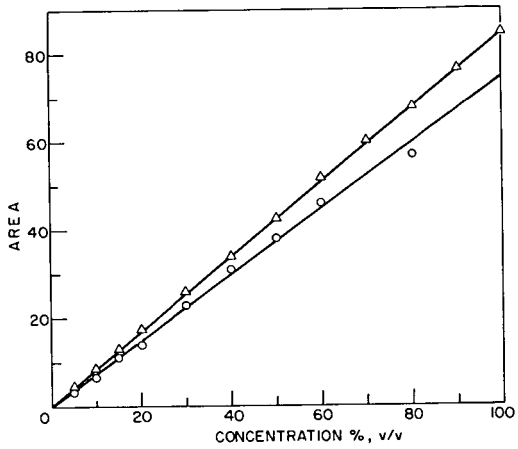

Fig. 3. Calibration Curves. Concentration ($\frac{v}{v}$%) vs area of the methyl proton nmr peaks. Varsol ○; Suncor Naphtha △.

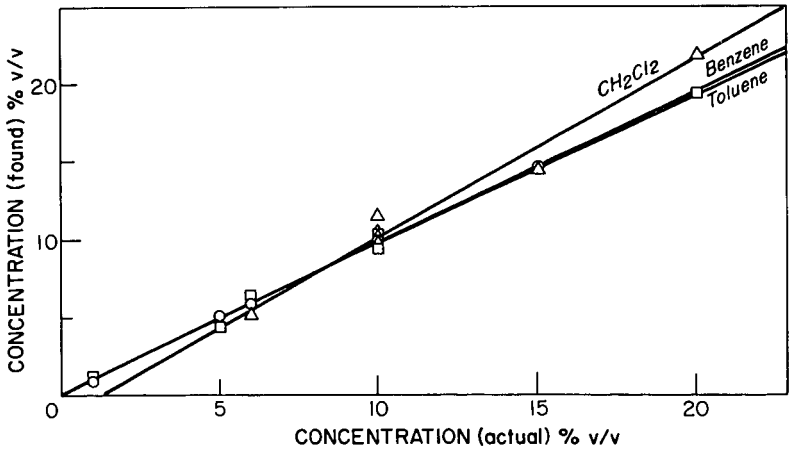

Fig. 4. Plot of the concentrations ($\frac{v}{v}$%), Actual vs Found. Benzene ○; Toluene □; methylene chloride △.

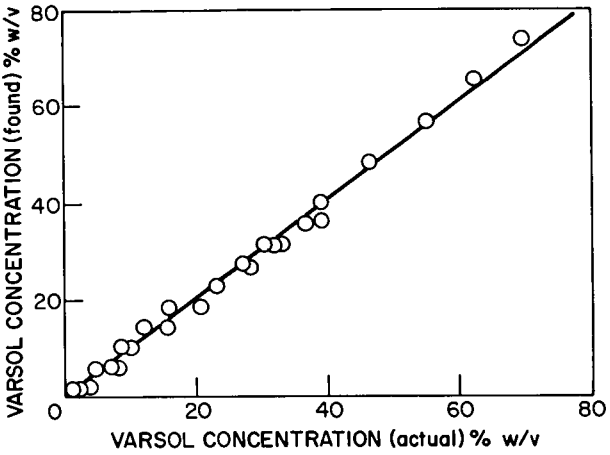

Fig. 5. Plot of the Varsol concentration actual vs Varsol concentration found.

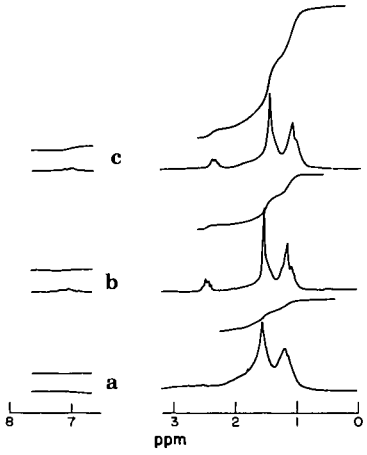

Fig. 6. ^{1}H n.m.r. spectra of a) Bitumen b) Stoddard solvent c) Bitumen + Stoddard solvent.

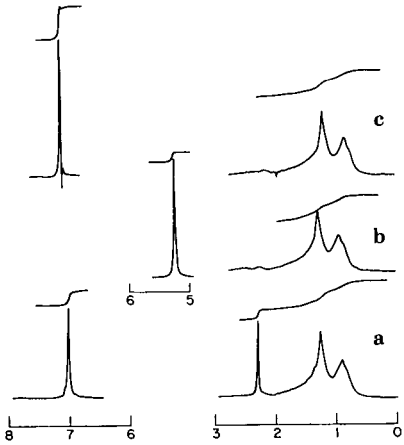

Fig. 7. ^{1}H n.m.r. spectra of a) Bitumen + Toluene b) Bitumen + methylene chloride c) Bitumen + Benzene.

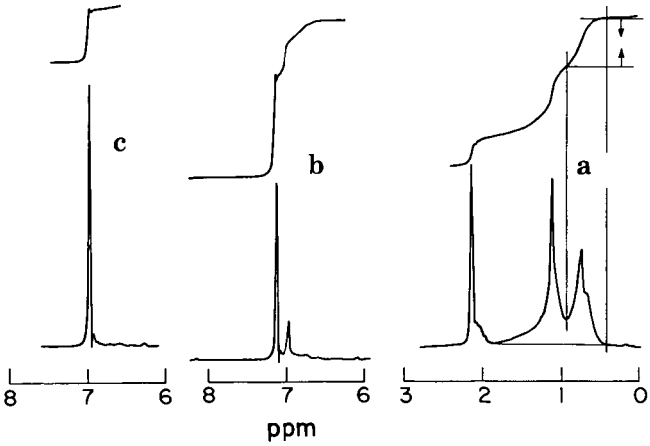

Fig. 8. ^{1}H n.m.r. spectra of a) Bitumen + Toluene + Stoddard solvent b,c) Bitumen + Benzene + Stoddard solvent.

Storage Stability Studies of Fuels Derived from Shale and Petroleum

by Laudie Jones, Robert N. Hazlett, Norman C. Li and John Ge

Naval Research Laboratory, Code 6180, Washington, D.C. 20375
and Duquesne University, Pittsburgh, PA 15282

INTRODUCTION

In considering shale oil as an alternative and complement to petroleum as a feedstock for production of liquid fuels, important compositional differences in the heteroatom components must be taken into account. Some heteroatomic compounds, containing N, S, or O, influence both the thermal stability and storage stability of the liquid fuels. Thermal stability is the resistance of a fuel to formation of deposits on surfaces within the fuel system of an operating vehicle, and storage stability is the resistance of a fuel to formation of gums (both soluble gums and insoluble sediments) under fuel storage conditions. Thermal deposits can foul fuel/lubricating heat exchangers causing decreased efficiency and storage deposits can plug filters.

The purpose of this research is to find mechanisms of storage deposit formation in jet and diesel fuels and to characterize the deposits. Insoluble sediments are the undesirable materials for these fuels since they are injected into engines as liquids. The rate of sediment formation can be determined by traditional quantitative gravimetric procedure, usually at temperatures of 43°C or higher. These procedures require storage times of weeks or months, depending on stress temperature, to develop amounts of sediments which can be measured reliably. However, fuel storage degradation can be monitored in the early stages by laser light scattering of developing particles at ambient temperature. By carrying out extensive light scattering experiments, in the presence of certain heteroatomic compounds, we hope to find out quickly which of these compounds are deleterious to fuel stability. Stability information of this kind is useful in that refining process conditions can then be selected which will minimize fuel degradation through removal of the deleterious compounds. Ultimately, it will be important to know the trade-offs betwen processes of varying severity for removing these compounds and modifying the fuel stability.

EXPERIMENTAL

Laser light scattering measurements were carried out with a photometer described by Berry (1) modified by introduction of a laser light source. Small light-scattering cells of the design by Dandliker and Kraut (2) were used. The Pyrex cells were in the form of truncated cones, in order to reduce the stray light pickup by the detector. In order to study the effects of substituted quinolines, pyridines and indoles on deposit formation, we

adapted the method of Dahlin et al. (3) of obtaining the amount of "deposited gum" from the weight gain of a glass cover slip (22 x 40 mm) placed in a 150-ml Pyrex beaker (bottom surface area 21.61 cm^2) containing 50 ml of liquid fuel.

Degradation products obtained by heat stressing (80-120°C) fuels enriched with specific heteroatomic compounds (500 ppm nitrogen concentration) were analyzed by nuclear magnetic resonance technique. For deposits which are soluble in $CDCl_3$, both 90 MHz and 600-MHz spectrometers were used. The latter instrument operates at magnetic field of 140.9 kgauss, the highest magnetic field possible today, and has been used by Hara et al. (4) to study the very complex coal-derived liquids. For deposits which are insoluble in $CDCl_3$, magic-angle spinning, solid-state carbon-13 NMR spectra were obtained on a Varian XL-200 superconducting spectrometer at 50.3 MHz. Cross polarization of the carbon nuclei was done under Hartman-Hahn matching conditions. The sample was packed into a bullet rotor and spun at approximately 2500 Hz, and sidebands were suppressed using the Dixon Sideband Suppression technique.

RESULTS AND DISCUSSION

(A) Laser Light Scattering and Deposit Formation in Liquid Fuels

Storage techniques for determining the stability of liquid fuels require weeks or months of storage, even at elevated temperatures. A technique which has greater sensitivity for initial deposit formation could shorten the storage time and/or reduce the stress temperature. We have examined one such technique, light-scattering. As a fuel ages, particles grow in size and scatter light. Figure 1 is a plot of scattering intensity at 90° scattering angle as a function of storage time at room temperature for shale II-derived JP-5 (jet fuel, sample J22) containing various concentrations of 2,5-dimethylpyrrole (DMP), while Figure 2 is a corresponding plot for petroleum-derived JP-5 (jet fuel, sample 80-8). The data indicate that in the absence of DMP, which is especially deleterious to fuel stability, the liquid fuel is stable and little light-scattering occurs. As the concentration of DMP increases, the extent of light-scattering increases, in accordance with the increase in tendency to form deposit. The use of light-scattering technique as a monitor of aging has the advantages that room temperature is adequate and that a much shorter time of experimentation is required. The small particles which are formed on aging are believed to be precursors of sediments. Comparison of Figures 1 and 2 shows that the stability of the petroleum-derived JP-5 is less than the shale-derived JP-5.

Figure 3 is a plot of scattering intensity at different angles vs. time at room temperature for petroleum JP-5. For the bottom line, where no DMP is added, the intensity remains small and constant, and independent of the measuring angle. The uper lines are for different angles for petroleum JP-5 with 105 ppm N, DMP. The data show that scattering at 45° is much greater than at 90° or 135°. As the particles get larger, they tend to scatter light more intensely in a forward direction, resulting in a larger value of I_{45}/I_{135}.

Of all the heteroatomic compounds tested, DMP is easily the most powerful promotor of deposit formation in both petroleum- and shale-derived jet fuels. Among some other nitrogen-containing compounds tested, the

deleterious effect on shale jet fuel stability, as measured by the amount of "deposited gum" (3) formed, decreases in the order: 2,6-dimethylquinoline, substituted pyridines (2-ethylpyridine, 2,4,6-trimethylpyridine, 2,6-dimethylpyridine, 2-methylpyridine), 7-methylindole. The following compounds do not form deposited gum in the shale-derived jet fuel even when stressed at 80°C for 8 weeks: 2-methylindole, 2,5-dimethylindole, and 1,2,3,4-tetrahydroquinoline. The DMP sediment is insoluble in the usual organic solvents. The gums obtained from use of other dopants are soluble in $CDCl_3$, and therefore have been studied by solution NMR and infrared techniques.

(B) Liquid State NMR

The JP-5 fuels from shale II and petroleum have essentially identical proton and carbon-13 NMR spectra. The aromaticity is 0.10 and a considerable amount of long unbranched alkyl groups is present in both. Figure 4 gives the 600-MHz PMR spectra of shale-derived JP-5 and 2,6-dimethylquinoline (DMQ), 500 ppm N, 25 days, 80°C: top spectrum, the stressed liquid phase in $CDCl_3$; bottom spectrum, the sediment dissolved in $CDCl_3$. Many NMR signals appear in the lower field regions of the aliphatic and aromatic ranges. These indicate the polycyclic nature of the sediment, 3-4 aromatic rings. Elemental analysis of the gum gives the formula: $C_6H_7O_{1.3}$. The nitrogen content is only 1%. Thus, DMQ (which has 8.9% N) does not dominate the composition of the deposit.

(C) Solid State NMR

Magic angle spinning, carbon-13 spectra of the DMP sediments formed in shale JP-5 and in shale-derived diesel, show that oxygen is incorporated in the deposit in the form of carboxylate, carbonyl and ether linkages. For both fuels, the DMP deposits have the same formula: $C_6H_7NO_{1.5}$. Since DMP is C_6H_9N, we conclude that, unlike DMQ, DMP dominates the composition of the deposits obtained in the shale derived jet and diesel fuels. The nitrogen and oxygen contents of the sediments are 11.6 and 20.1 wt.%, respectively. These values are almost twice the corresponding values of the petroleum jet fuel-DMP sediment which has the formula $C_{17}H_{28}NO_{1.5}$: N,5.1; O,8.4%.

(D) ESCA and Fourier Transform Infrared Spectroscopy

ESCA and FT-IR techniques have been used in the study of deposits formed in shale-derived jet fuel, shale-derived diesel fuel, petroleum jet fuel, and coal liquefaction products which have been subjected to severe hydrotreatment (upgraded H-coal and SRC-II liquids). The results confirm the finding that oxygen is required in formation of deposits and that oxygen is incorporated in more than one species. We are also using these techniques to study the structure of the sulfur and oxygen species of the deposit formed in the jet and diesel fuels, in the presence of DMP and thiophenol, for the purpose of studying synergism.

ACKOWLEDGEMENTS

We acknowledge support of the Naval Air Propulsion Center. The 600-MHz NMR spectrometer at Carngie-Mellon University supported by PHS Grant No. RR-00292, was used, and we thank G. Berry and E. Casassa for the use of a light-scattering instrument at CMU. We thank D. Weber and B. Strohmeier for carrying out ESCA measurements; L. Galya and D. Young for the solid-state NMR spectra taken on Varian XL-200 superconducting spectrometer; N. F. Yaggi and S. Lee for assistance with light-scattering measurements.

REFERENCES

(1) G. C. Berry, J. Chem. Phys., 44, 4550 (1966).

(2) W. B. Dandliker and J. F. Kraut, J. Am. Chem. Soc., 78, 2380 (1956).

(3) K. Dahlin, S. Daniel, and J. Worstell, Fuel 60, 477 (1981).

(4) T. Hara, K. C. Tewari, N. C. Li and F. K. Schweighardt, in "New Approaches in Coal Chemistry" (B. D. Blaustein, B. C. Bockrath, S. Friedman, eds.), ACS Symposium Series, 169, 1981, pp. 289-318.

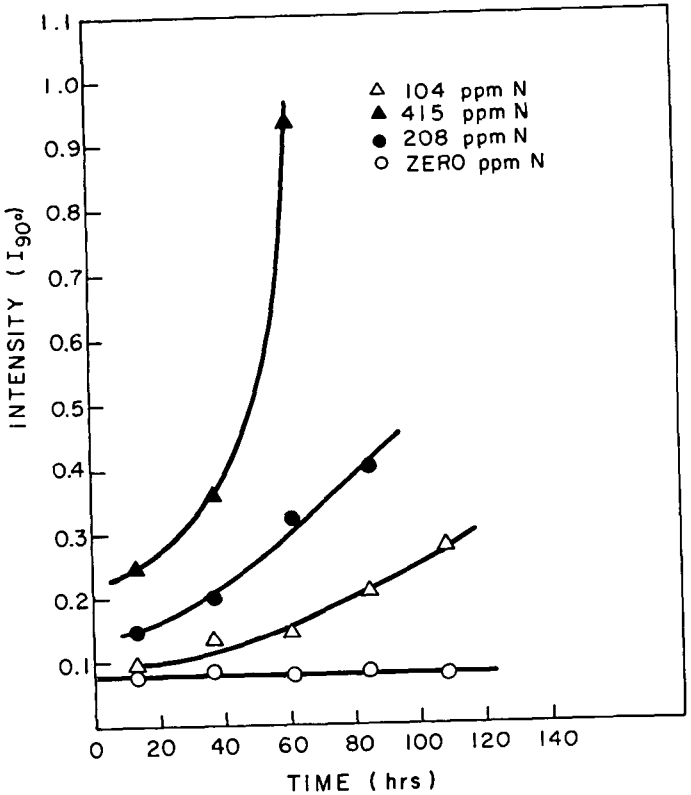

FIGURE 1. SCATTERING INTENSITY, 60°, FOR SHALE II JP-5 + DIFFERENT CONCS. DMP (ppm N) STORED AT ROOM TEMPERATURE.

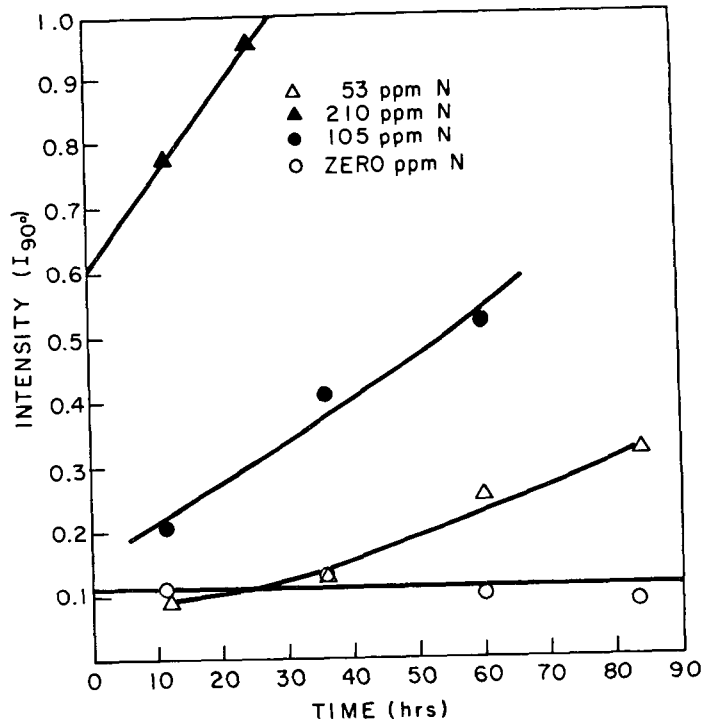

FIGURE 2. SCATTERING INTENSITY, 90°, FOR PETROLEUM JP-5 + DIFFERENT CONCS. DMP (ppm N) STORED AT ROOM TEMPERATURE.

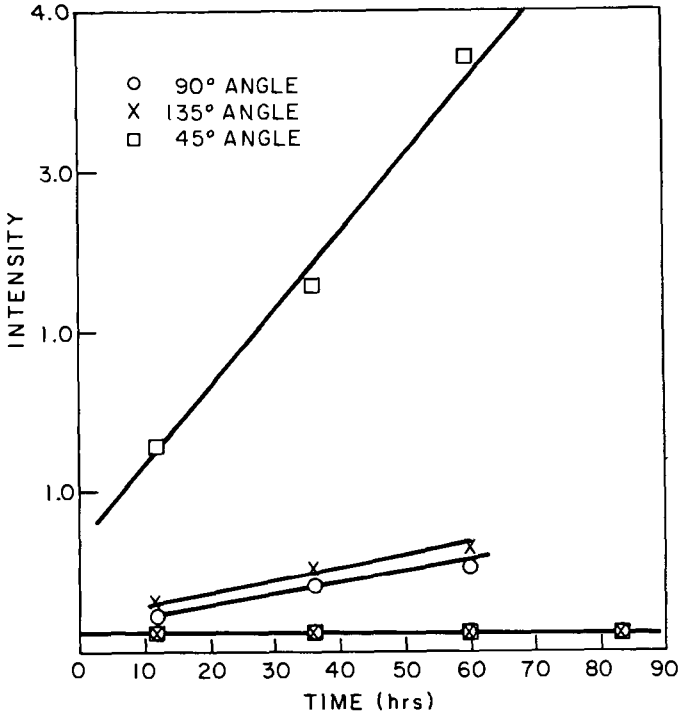

FIGURE 3. SCATTERING INTENSITY AT DIFFERENT ANGLES FOR PETROLEUM JP-5 AT ROOM TEMPERATURE. BOTTOM LINE, NO DMP; UPPER LINES, 105 ppm (N).

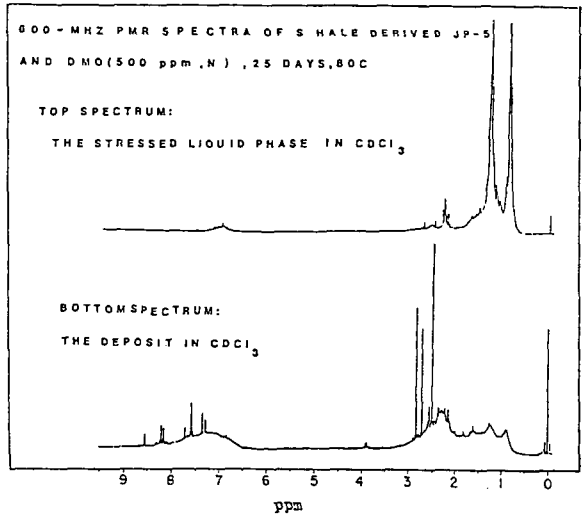

FIGURE 4.